THE ACTIVITY AND BIOSYNTHESIS OF BETA-CELL PEPTIDE HORMONES: IMPLICATIONS IN DIABETES, OBESITY, AND PANCREATIC CANCER

by

Austin James Taylor

B.Sc., The University of British Columbia, 2014

A THESIS SUBMITTED IN PARTIAL FULFILLMENT OF

THE REQUIREMENTS FOR THE DEGREE OF

DOCTOR OF PHILOSOPHY

in

THE FACULTY OF GRADUATE AND POSTDOCTORAL STUDIES

(Pathology and Laboratory Medicine)

THE UNIVERSITY OF BRITISH COLUMBIA

(Vancouver)

April 2022

The following individuals certify that they have read, and recommend to the Faculty of Graduate and Postdoctoral Studies for acceptance, the dissertation entitled:

The activity and biosynthesis of beta-cell peptide hormones: Implications in diabetes, obesity, and pancreatic cancer

submitted by Austin J. Taylor in partial fulfillment of the requirements for

the degree of Doctor of Philosophy

in Pathology and Laboratory Medicine

Examining Committee:

C. Bruce Verchere, Professor, Pathology and Laboratory Medicine, UBC
Supervisor

Francis C. Lynn, Associate Professor, Surgery, UBC
Supervisory Committee Member

Janel L. Kopp, Assistant Professor, Cellular and Physiological Sciences, UBC
Supervisory Committee Member

Brian Rodrigues, Professor, Pharmaceutical Sciences, UBC
University Examiner

William T. Gibson, Professor, Medical Genetics, UBC
University Examiner

Additional Supervisory Committee Members:

David F. Schaeffer, Associate Professor, Pathology and Laboratory Medicine, UBC
Supervisory Committee Member

Abstract

Type 1 and type 2 diabetes are characterized by hyperglycemia and loss of beta-cell mass, function, and peptide hormones. Beyond hyperglycemia, diabetes is also associated with obesity and increased risk of cancer, particularly pancreatic cancer. Islet amyloid polypeptide (IAPP) is the second most abundant beta-cell hormone, co-secreted with insulin, and reduced in diabetes. Paracrine actions of endogenous IAPP have been proposed in glycemic regulation and tumour growth suppression, but remain incompletely understood. To further characterize the effects of IAPP loss, we used an IAPP-knockout mouse fed a high-fat or control diet and assessed glycemia and adiposity. We also generated a genetic mouse model of pancreatic ductal adenocarcinoma in IAPP-knockout mice to investigate IAPP loss as a potential mechanism for the association of diabetes and pancreatic cancer. Trends in IAPP-knockout mice suggest elevated adiposity and glycemia in the absence of IAPP. We observed no effect of IAPP on pancreatic ductal adenocarcinoma survival in mice, or cancer cell proliferation, death, or glycolysis.

A reduction in the processing efficiency of beta-cell peptide prohormones is also observed in diabetes. Pcsk1 and Pcsk2 are the two major prohormone endoproteases within insulin granules, and are responsible for multiple steps in the proIAPP and proinsulin processing pathways. To determine whether impaired processing functions as a biomarker or driver of beta-cell dysfunction, we generated mouse models of beta-cell specific ($Ins1^{cre}$-driven) Pcsk1 and Pcsk2 deficiency using Cre-lox recombination. Loss of Pcsk1 in beta cells caused severe proinsulin processing impairments and increased diabetes susceptibility in male mice, while female mice remained euglycemic. In contrast, male and female beta-cell Pcsk2-deficient mice were euglycemic with minimally impaired proinsulin processing, but severely impaired proIAPP

processing. Deletion of both Pcsk1 and Pcsk2 in beta cells blocked proinsulin processing, drove hyperglycemia, increased beta-cell glucose responsiveness and mass, and reduced beta-cell maturity and proliferative capacity. In a mouse model expressing amyloidogenic human IAPP in beta cells, Pcsk1 deficiency significantly increased amyloid deposition. Collectively, these findings show that loss of beta-cell prohormone processing alters beta-cell function and drives hyperglycemia, and that endogenous IAPP does not act as a pancreatic tumour suppressor but may alter glycemia and adiposity.

Lay Summary

Pancreatic beta cells secrete insulin and fail in type 1 and type 2 diabetes, resulting in insufficient insulin and high blood sugar. Insulin is first made as a larger molecule proinsulin, which is cut by the enzymes PCSK1 and PCSK2 to make insulin. People with diabetes have increased proinsulin in their blood, suggesting that PCSK1 and PCSK2 function is reduced in diabetes. This thesis investigates how reductions in PCSK1 and PCSK2 impact the function of beta cells and control of blood sugar. It also investigates the physiological roles of another hormone from beta cells, IAPP, that is also lost in diabetes with insulin. We found that reducing PCSK1 can cause dysfunction in beta cells and increases the risk of diabetes in mice. We also found that loss of IAPP has minimal impact on blood sugar levels. This new information will help guide the development of new and existing diabetes therapies.

Preface

Initial identification of the research was by C.B. Verchere. Research experiments were designed, performed, and analyzed by A. Taylor under the guidance of C.B. Verchere. Interpretation, experimental design, and further research identification was done by A. Taylor under the guidance of C.B. Verchere. Additional interpretations, experimental design, and guidance were provided by A. Taylor's supervisory committee members J. Kopp, F. Lynn, and D. Schaeffer, and the chair A. Devlin.

Imaging in Figure 1 was assisted by E. Panzhinskiy. All animal procedures and tissue collections were assisted by G. Soukhatcheva, M. Komba, and D. Dai. Islet perifusions were performed by M. Komba. The western blot in the right panel of Figure 19 B was performed by Y.C. Chen. D. Pasula and D. Luciani assisted with initial experimental design and analysis of calcium imaging data in Figure 39. Bottom-up proteomics (Figure 41) was assisted by J. Tsui with analysis guidance from P. Lange. Immunostaining, imaging, and analysis in Figures 30, 45, 46, was assisted by D. Paterson and A. Sekhon.

Electron microscopy sample preparation and imaging was performed by M. Reid and the McMaster Electron Microscopy Facility. Support with microscope hardware was provided by J. Wang (BCCHR Imaging Core). FACS sorting of beta cells was assisted by L. Xu (BCCHR Flow Core). Animal husbandry was assisted by staff of BCCHR and MBF animal care facilities at UBC. RNA library preparation and sequencing was performed by the Biomedical Research Centre Sequencing Core (UBC). Top-down proteomics data acquisition was performed by R. Dyer (BCCHR Analytical Core for Metabolomics and Nutrition). Embedding and sectioning of tissues was performed by the BCCHR Histology Core.

Table 3 was modified from the original table drafted by A. Taylor and Y.C. Chen (co-first authors) in the following publication: Chen, Y.C., Taylor, A.J., Verchere, C.B. (2018) Islet prohormone processing in health and disease. *Diabetes Obes. Metab.* 20: 64-76.

All animal husbandry and procedures were performed according to the Canadian Council on Animal Care guidelines, and all experiments were approved by the University of British Columbia Animal Care Committee (protocols A14-0222, A16-0100, A19-0127, and A20-0073). The animal distress scoring chart (Appendix A) was generated by Dr. Janel Kopp.

Table of Contents

List of Tables

List of Figures

List of Symbols

α	alpha
β	beta
κ	kappa

List of Abbreviations

7-AAD	7-aminoactinomycin D
AAbs	autoantibodies
AAC	area above curve
ADP	adenosine diphosphate
ANOVA	analysis of variance
ATP	adenosine triphosphate
AUC	area under curve
BCA	bicinchoninic acid
BMI	body mass index
BSA	bovine serum albumin
cAMP	cyclic adenosine monophosphate
CD	control diet
cDNA	complementary DNA
CGM	continuous glucose monitor
CNS	central nervous system
CRE	cyclic adenosine monophosphate response element
DAB	3,3′-diaminobenzidine
DAG	diacyl glycerol
DEG	differentially expressed gene
DIA	data-independent acquisition
DMEM	Dulbecco's modified eagle medium
DNA	deoxyribonucleic acid

DTT	dithiothreitol
ECAR	extracellular acidification rate
EdU	5-ethynyl-2'-deoxyuridine
EGF	epidermal growth factor
ELISA	enzyme-linked immunosorbent assay
EPAC	exchange proteins activated by cAMP
ER	endoplasmic reticulum
ERK1/2	extracellular signal-regulated protein kinase
FACS	fluorescence-activated cell sorting
FBS	fetal bovine serum
FCS	fetal calf serum
FDR	false discovery rate
FFA	free fatty acid
GFP	green fluorescent protein
GO	gene ontology
GPCR	G-protein-coupled receptor
GSEA	gene set enrichment analysis
GSIS	glucose-stimulated insulin secretion
GTT	glucose tolerance test
h	hours
HbA_{1C}	glycated hemoglobin A1C
HBSS	Hank's balanced salt solution
HEK-293	human embryonic kidney 293

HEPES	2-[4-(2-hydroxyethyl)piperazin-1-yl]ethanesulfonic acid
HFD	high-fat diet
hIAPP	human IAPP
HRP	horseradish peroxidase
IBMX	3-isobutyl-1-methylxanthine
IP	intraperitoneal
IP_3	inositol 1,4,5-triphosphate
IPGTT	intraperitoneal glucose tolerance test
ITT	insulin tolerance test
IV	intravenous
IVGTT	intravenous glucose tolerance test
KRB	Krebs-Ringer bicarbonate
LADA	latent autoimmune diabetes in adults
LC-MS/MS	liquid chromatography tandem mass spectrometry
LGLF	low-glucose low-FBS media
mIAPP	mouse IAPP
min	minutes
mRNA	messenger ribonucleic acid
NF-κB	nuclear factor kappa B
OGTT	oral glucose tolerance test
OIS	oncogene-induced senescence
p-eIF2α	phosphorylated eukaryotic translation initiation factor 2 subunit 1
PAM	peptidyl-glycine alpha-amidating monooxygenase

PBS	phosphate-buffered saline
PCSK1 (PC1/3)	proprotein convertase subtilisin/kexin type 1 (prohormone convertase 1/3)
PCSK2 (PC2)	proprotein convertase subtilisin/kexin type 2 (prohormone convertase 2)
PDAC	pancreatic ductal adenocarcinoma
PDI	protein disulfide isomerase
PIP_2	phosphatidylinositol 4,5-bisphosphate
PKA	protein kinase A
POMC	proopiomelanocortin
PP	pancreatic polypeptide
qPCR	quantitative polymerase chain reaction
RAMP	receptor-activity modifying protein
rIAPP	rat IAPP
RIPHAT	rat *Ins2* promoter human IAPP transgenic
RNA	ribonucleic acid
RPMI	Roswell Park Memorial Institute
scRNAseq	single-cell RNA sequencing
SD	standard deviation
SP3	single-pot solid-phase-enhanced sample preparation
sXbp1	spliced X-box binding protein 1
T1D	type 1 diabetes
T2D	type 2 diabetes
TBS	tris-buffered saline
TCGA	The Cancer Genome Atlas

TUNEL	terminal deoxynucleotidyl transferase dUTP nick end labeling
UPR	unfolded protein response
USD	United States Dollar

Acknowledgements

I would not be where I am today without an incredible amount of support from many individuals. Thank you, Elizabeth for your never-ending patience and support, and understanding that home by 6pm typically means home by 9pm. Thank you for encouraging me to step back when needed, and to jump on opportunities that arise. The time away from research with you is what enables me to come back research refreshed every day. A very big hug and thank you to my family and parents for supporting and encouraging me during graduate school and throughout life. I am forever grateful for your love and support that has enabled me to take on challenges in life and enjoy the process.

Thank you, Dr. Verchere for taking the risk of bringing me on as a graduate student despite my minimal experience in a laboratory. From our discussions on life to those on research, I feel as though I have grown so much both as a researcher and as an individual during my PhD studies. Your mentorship has greatly facilitated this growth and it has been both a fun and challenging PhD. Thank you for helping to strike this balance. Thank you as well to all members of the Verchere Laboratory. It has a been an enriching experience both in and out of the lab, and the hard work has been punctuated by many laughs throughout. Thank you, Dr. Jaques Courtade for your mentorship early in my studies when I was new to the lab, and many, many thanks to Dr. Yi-Chun Chen for mentorship, friendship, and heaps of discussion on processing and islet biology over the years. I have learned so much from you and am incredibly grateful to have worked with you. Thank you, Dr. Galina Soukhatcheva, Dr. Derek Dai, and Mitsu Komba for providing endless technical and organizational support. Thank you to my committee members Dr. Angela Devlin, Dr. Francis Lynn, Dr. Janel Kopp, and Dr. David Schaeffer for your contributions over the years and guiding me through new areas of biology and life. Thank you as

well to all the members of the diabetes research community at BCCHR and across Vancouver. It has been a blast to navigate graduate school and learn alongside you, and I cherish the friendships that have developed throughout these studies. Thank you, Meg Hughes for helping create the events and programs that make BCCHR and Vancouver such a fun and exciting location for a PhD in diabetes research. Thank you to the core facilities at BCCHR, especially Dr. Jingsong Wang for your hard work in the imaging core that has enabled much of the microscopy work throughout my PhD. Thank you to the animal care facility staff at BCCHR and MBF for their assistance and dedication in providing excellent care for mice.

Thank you to the members of the Graduate Student Facilitator Team at CTLT, and those I have had the pleasure to teach alongside and grow with as an educator. Thank you, Dr. Scott Covey for encouraging me to pursue graduate studies, and fostering my interest in diabetes research. Thank you to friends in Vancouver, both old and new, who have also helped me to strike a balance throughout this PhD. Whether skiing, biking, climbing, or catching up over a beer in this beautiful place we call home, your friendships have supported me throughout my research endeavours and kept me looking forward to every day here.

Lastly, thank you to the agencies that have provided funding for this research: BC Children's Hospital Research Institute, Canadian Institutes of Health Research, and Canadian Cancer Society. Thank you for the hard work both and your donors do every day to help improve the health of individuals in Canada and worldwide.

Dedication

To my parents, Scott and Lisa.

Thank you for everything.

Chapter 1: Introduction

1.1 Pancreas function

The pancreas is a multipurpose organ with dual exocrine and endocrine functions. It is intricately linked to metabolism from digestion of macronutrients through to regulation of glycemia, and it integrates and releases a multitude of signals to tightly control these processes. Functionally, the pancreas contains two major compartments – the exocrine and endocrine pancreas.

1.1.1 The exocrine pancreas

The exocrine compartment accounts for the vast majority of the pancreas volume and contains two major cell types, acinar and ductal cells. Tightly packed rosettes of acinar cells release digestive enzymes to branching ducts which eventually reach the major pancreatic duct. The pancreatic duct merges with the common bile duct and drains to the duodenum to provide a mixture of secretions essential for the digestion and absorption of macronutrients.

Acinar cells are specialized secretory cells that synthesize and secrete abundant proteins. Lipases, amylases, and proteases are synthesized and stored as inactive zymogens in regulated secretory vesicles (granules) that are released upon stimulation of acinar cells. Macronutrients in the duodenum stimulate the release of cholecystokinin, which acts as an endocrine signal to activate acinar cells and release digestive enzymes, and also acts to stimulate vagal afferent signalling and acute induction of satiety in mice[1].

Ductal epithelial cells create lumens to carry acinar secretions to the duodenum. They have additional roles of water secretion to flush and carry the digestive enzymes, and bicarbonate secretion to prevent premature activation of digestive zymogens and neutralize acidity in the

duodenum from chyme. Secretin, released from the duodenum in response to increased acidity, stimulates ductal cell release of water and bicarbonate.

1.1.2 The endocrine pancreas

The endocrine compartment accounts for approximately 1% of the pancreas mass[2]. It is organized into island-like clusters throughout the exocrine tissue that were first noted in 1869 by Paul Langerhans[3], and were later named the islets of Langerhans, or more commonly, pancreatic islets. The human pancreas contains over 3 million islets[4] distributed throughout the pancreas as innervated and highly perfused mini-organs[5]. Endocrine cells within the islet synthesize their respective hormones as prohormones that are processed and stored in granules in the regulated secretory pathway. Each cell-type contains extensive exocytotic machinery and finely tuned stimulus-secretion coupling to respond to extracellular cues.

Beta cells are the most abundant and account for 55-60% of the human islet[6–8]. In response to rising blood glucose, beta cells secrete insulin which acts on the liver, muscle, and fat to promote glucose uptake and energy storage. Alpha cells are the next most abundant at 30-35% of endocrine cells in the human islet[6,7]. Alpha cells secrete glucagon in response to low blood glucose, which acts on hepatocytes to stimulate glycogenolysis and gluconeogenesis. Delta cells account for approximately 10% of the human islet[6,7], and secrete somatostatin in response to high glucose or islet paracrine factors such as urocortin 3[9]. Islet somatostatin acts largely in a paracrine manner to suppress islet secretions, providing a negative feedback mechanism for neighbouring endocrine cells. Gamma cells constitute less than 5% of islet cells and secrete pancreatic polypeptide (PP) postprandially[10]. PP acts in the hypothalamus to induce satiety[11,12], and on the exocrine pancreas to inhibit ductal and acinar secretions. The final endocrine cell type is the ghrelin-expressing epsilon cell, which peaks during development at up to 30% of the

endocrine population, and rapidly drops around birth to less than 1% in adulthood[13]. Ghrelin is an orexigenic signal released in the fasted state that acts on the hypothalamus[14]. In addition to endocrine cells, islets contain macrophages (other immune cells are rare but present[15]), endothelial cells, pericytes, stellate cells, and nerve fibers that all contribute to islet function and maintenance[16].

Mouse islets largely resemble human islets; however, several architectural differences exist that are worth noting[17]. Mouse islets contain a 75% majority of beta cells, 20% alpha cells, and less than 10% delta cells, making beta cells relatively more abundant in mouse islets[6–8]. In humans, the endocrine populations are dispersed throughout the islet, whereas in mice beta cells dominate the islet core while alpha cells predominantly occupy the mantle[7]. This results in relatively higher beta- to non-beta-cell contacts in human islets. Despite these differences, mice have provided a useful model for studying islet function in health and diabetes.

1.1.3 Beta-cell physiology: proprotein and granule biosynthesis

Beta cells are specialized endocrine cells responsible for the biosynthesis and secretion of insulin into the circulation. They are tuned for insulin biosynthesis, and it is estimated that a beta cell can synthesize 1 million proinsulin molecules per minute[18]. Beta cells achieve rapid proinsulin production by storing a large stable pool of insulin transcripts as polysomes that are transported to the endoplasmic reticulum (ER) and initiate translation in response to glucose[19]. Within 30-90 minutes proinsulin, proIAPP, and proPCSK1 protein levels are increased in islets[20,21], while mature insulin mRNA can take up to 48 hours to increase in response to glucose[22]. Therefore, proinsulin and proIAPP biosynthesis are largely post-transcriptionally regulated in beta cells.

Peptide prohormones destined for secretion in beta cells traffic though the ER, where the signal peptide is cleaved from the prepropeptide, the propeptide begins folding, and glycosylation may occur. Insulin and IAPP are found both in non-glycosylated and glycosylated forms in islets and circulation in humans and mice[23–26]. Propeptides are trafficked from the ER through the Golgi to insulin secretory granules. In the late Golgi and early granule compartments, the proteolytic processing enzymes PCSK1, PCSK2, and CPE become active and trim propeptides to their mature lengths (reviewed more extensively in section 5.1). C-terminal glycine residues are amidated via the enzyme PAM (peptidyl-glycine alpha-amidating monooxygenase). As granules mature, luminal hydrogen and zinc ion concentrations increase, which facilitates processing enzyme activation[27] and insulin crystallization[28]. Finally, mature granules are stored prior to exocytosis with some associating closely to the plasma membrane to form a readily releasable pool upon beta-cell stimulation.

Given the high levels of peptide prohormone biosynthesis in beta cells, some will be degraded to maintain beta-cell proteostasis. Early misfolded proinsulin in the ER can be degraded via ER-associated degradation or ER-couple autophagy[29]. Later in the secretory pathway, aged granules are degraded by crinophagy or macroautophagy resulting in a granule half-life of 3-5 days[30,31]. However, under nutrient depletion beta cells may also degrade newly synthesized granules[32]. These mechanisms ensure proteostasis within a beta cell while demand for insulin fluctuates.

1.1.4 Normal beta-cell physiology: beta-cell stimulation and exocytosis

Human beta cells in the resting state maintain a net negative membrane potential of approximately -70 mV[33]. This potential is maintained in part through an ATP-sensitive potassium channel (K_{ATP}) composed of four Kir6.2 (*KCNJ11*) and four sulfonylurea receptor

(*ABCC8*; SUR1) subunits. The K_{ATP} channel transports K^+ ions to the extracellular space, against the electrical gradient but with the K^+ gradient to maintain a net negative charge inside the beta cell[33]. Glucose is the primary secretagogue for insulin release and is transported into human beta cells by GLUT1 (*SLC2A1*)[34]. After glucose import, glycolysis and oxidative phosphorylation lead to elevated ATP/ADP ratios, closure of the K_{ATP} channel, and depolarization of the membrane. At approximately -60 mV, voltage-gated Ca^{2+} channels on the plasma membrane open and there is a rapid influx of Ca^{2+} to the cytosol[33]. Synaptotagmin on insulin secretory granules bind Ca^{2+} and trigger SNARE activation, fusion of plasma and vesicle membranes, and exocytosis of insulin[35].

The rate-limiting step for insulin secretion is glucose phosphorylation by glucokinase (*GCK*), a special hexokinase with a lower affinity for glucose than the other hexokinase family members which are not expressed in beta cells. Half-maximal GCK activity and glucose-induced insulin secretion is observed around 8 mM glucose in human islets[36], emphasizing the dependence of insulin secretion on GCK activity. In isolated islets and during an IV glucose bolus in vivo, insulin secretion occurs in two phases: a 10-minute first phase consisting of the readily releasable pool of insulin granules and a sustained second phase of both new and aged insulin granules that continues until the stimulus is removed. Secretion dynamics differ *in vivo* and are thought to consist of a single rising phase (or blending of the phases) as nutrients are more slowly absorbed to circulation, and insulin secretion remains highly pulsatile both *in vivo* and *ex vivo*[37]. Metabolism of fatty acids and amino acids can also stimulate insulin secretion from anaplerotic pathways that drive an increase in the ATP/ADP ratio[38,39].

Mouse beta cells largely resemble human beta cells with a few key differences. Mouse GCK has a higher $S_{0.5}$ than human GCK, resulting in a higher threshold for glucose-induced

insulin release from beta cells and higher glycemic set point in rodents[33]. Human IAPP is also highly amyloidogenic and amyloid deposits are observed in human islets, while mouse IAPP does not form amyloid deposits due to sequence differences (reviewed more extensively in section 6.1). *Iapp* mRNA is also relatively enriched in mouse beta cells relative to human beta cells[40]. Mice also have two insulin genes: *Ins2* is the human ortholog and is more abundantly expressed, while *Ins1* is a rodent-specific retrogene that arose approximately 20 million years ago[41]. Lastly, mouse beta cells express predominantly Glut2 (*Slc2a2*) for glucose transport while human beta cells express predominantly GLUT1[34,42]. Both human and mouse beta cells transport glucose into the cytosol extremely rapidly and this process is not rate-limiting for exocytosis under normal conditions[36].

1.1.5 Coordination of the islet

Islets integrate a plethora of signals to modify secretions and maintain metabolic homeostasis. Paracrine signaling from beta cells has an inhibitory effect on alpha cells from insulin and serotonin release, while urocortin 3 released from beta cells simulates somatostatin release from delta cells[16]. Alpha-cell-derived glucagon and glucagon-like peptide 1 (GLP-1) stimulate beta cells and potentiate insulin release[43]. Delta cells mediate a braking mechanism for the islet in which somatostatin inhibits both alpha- and beta-cell exocytosis, resulting in delta cells contributing to the establishment of a physiological glycemic set point[9]. Ghrelin potently inhibits insulin secretion[44], possibly resulting in epsilon-cell-mediated suppression of insulin release during development when ghrelin-expressing cells are abundant in the islet. Beta cells are also connected via gap-junctions, resulting in coordinated electrical activity throughout beta cells in the islet. Recent evidence in mouse islets suggests that delta cells may also be connected to beta cells via gap-junctions, facilitating even more rapid communication than paracrine

interactions among islet cell types[45]. Metabolically distinct hub beta cells with high cell-cell connectivity across the islet also play a role in coordinating islet responses to glucose in mice[46]. Recent recognition of heterogeneity among islet cell types has been facilitated by the development and application of single-cell RNA sequencing (scRNAseq) to human pancreas biology[47]. Research into understanding the extent to which heterogeneity coordinates islet function is ongoing.

Islet and beta-cell activity are also regulated by signals originating from outside the islet. The incretin hormones glucose-dependent insulinotropic polypeptide (GIP) and GLP-1 are released from enteroendocrine cells in response to feeding and potentiate beta cells to increase insulin release[48]. Islet parasympathetic innervation releases acetylcholine which inhibits delta cells and stimulates beta cells to release insulin and lower blood glucose[5,49]. Conversely, islet sympathetic innervations release norepinephrine, stimulating glucagon release and an increase in blood glucose[50]. Other nutrients in addition to glucose can also augment insulin release from beta cells. For example, free fatty acid receptor 1 (*FFAR1*; GPR40) activation by long-chain fatty acids such as palmitate can also potentiate insulin release from beta cells[51].

Beta-cell potentiation and inhibition occurs largely through G protein-coupled receptor (GPCR) signalling. Activation of $G_{\alpha s}$- and $G_{\alpha q}$-coupled receptors potentiates insulin release, while activation of $G_{\alpha i}$-coupled receptors inhibits insulin release[52]. $G_{\alpha s}$ signalling activates adenylyl cyclase causing an increase in cyclic adenosine monophosphate (cAMP), which in turn activates protein kinase A (PKA) and exchange protein activated by cAMP 2 (EPAC2) to further stimulate insulin release from beta cells. $G_{\alpha q}$-coupled receptors activate phospholipase C, which catalyzes hydrolysis of phosphatidylinositol 4,5-bisphosphate (PIP_2) into the secondary messengers diacyl glycerol (DAG) and inositol 1,4,5-trisphosphate (IP_3). IP_3 is released to the

cytosol where it binds to the IP_3R, a ligand-gated calcium channel, on the ER membrane and stimulates further release of calcium ions to the cytosol to increase exocytosis. DAG remains in the membrane and activates protein kinases C and D1, which likely facilitate insulin release via cortical F-actin remodeling and phosphorylation of SNARE complex proteins[53]. $G_{\alpha i}$-coupled signaling inhibits insulin secretion by inhibiting adenylyl cyclase and reducing cAMP levels – a mechanism in direct opposition to $G_{\alpha s}$-signaling.

The human genome is estimated to contain approximately 1,000 GPCRs, with about half corresponding to endogenous ligands[54]. Given the complexity of both GPCR distribution on islet cell types and downstream signaling, much remains to be elucidated on the coordination and regulation of islet endocrine cells. Insights into these interactions and signalling mechanisms have provided new therapeutics for diabetes, such as incretin mimetics, and will likely yield further therapeutics as our understanding of islet physiology progresses.

1.2 Diabetes mellitus

Diabetes mellitus, or more commonly just diabetes, is a metabolic disease defined by persistent hyperglycemia. In Canada, 3.2 million individuals live with diabetes[55]. Worldwide, over 537 million adults (age 20-79) live with diabetes[56] and the prevalence is expected to rise from 9.3% to 10.9% by 2045[57]. It is further estimated that 7.5% of adults have impaired glucose tolerance and 50% of the individuals with diabetes are undiagnosed[57]. The global expenditure on diabetes care is an estimated $760 billion USD annually and has doubled in the last decade[58]. In addition to costs, complications from diabetes include a wide range of comorbidities and result in a significant mental burden for disease management. There are two major types of diabetes, type 1 and type 2 diabetes, that have different pathologies.

1.2.1 Type 2 diabetes

Type 2 diabetes (T2D) accounts for 90% of the diabetes in Canada and is characterized by a relative insufficiency of insulin, often in the context of obesity or insulin resistance. Beta cells are thought to compensate early in insulin resistance with increased beta-cell function and mass, but eventually succumb to the rising demands for insulin. As T2D develops, beta-cell function declines and apoptosis increases resulting in a relative insufficiency of insulin, and the development of T2D[59]. The causes of T2D are thought to be heterogeneous, with a complex interaction between genetic predisposition and the environment. Genome-wide association studies have revealed numerous genetic components to T2D, with many variants residing in non-coding regions for which disease-causing mechanisms are unknown[60]. T2D risk-conferring variants in known genes are dominated by those associated with beta-cell function[61], highlighting the importance of beta-cell failure in T2D development. In the environment, obesity can increase insulin resistance and the risk of T2D[62]. A sedentary lifestyle also increases the risk of T2D[63]. Although diet and lifestyle both contribute, they are not the sole cause of T2D for many, given the genetic components.

Type 2 diabetes is diagnosed in Canada by the presence of one of the following measures: (i) fasting (8 hour minimum) plasma glucose ≥ 7.0 mM; (ii) HbA_{1C} ≥ 6.5% (in adults); (iii) blood glucose ≥ 11.1 mM at 2 hours in a standardized 75g oral glucose tolerance test; or (iv) random glycemia ≥ 11.1 mM at any time of day regardless of meal intervals[64]. Diabetes is confirmed with two measurements in the diabetic range of any of the above tests, with the exception of random glycemia ≥ 11.1 mM which can only be used for one of two confirmation measurements. Prediabetes, a stage in which individuals are at high risk of developing diabetes, is defined by HbA_{1C} of 6.0-6.4%, fasting glycemia of 6.1-6.9 mM, or 7.8-11.0 mM blood

glucose 2 hours after a 75g oral glucose tolerance test. Although typically diagnosed over the age of 25, T2D in youth is also becoming more prevalent and affects 1.54 per 100,000 Canadians under 18 years old[65].

1.2.2 Type 1 diabetes.

Type 1 diabetes (T1D) accounts for 9% of the diabetes in Canada, or about 0.8% of the Canadian population. It is typically diagnosed with similar hyperglycemic criteria to T2D, but is differentiated from T2D with clinical presentation of diabetic ketoacidosis, a young age of onset, and typically the presence of one or more islet autoantibodies[64]. T1D results from autoimmune-mediated destruction and dysfunction of beta cells[66]. Historically it was believed complete beta-cell loss occurred in T1D. However, circulating low levels of proinsulin are detected in over half of individuals with T1D and some residual beta-cell mass is detected at autopsy[67,68]. Insulitis and beta-cell destruction occur in waves in T1D, ultimately resulting in insufficient remaining functional beta cells, hyperglycemia and T1D diagnosis[69]. Several autoantibodies (AAbs) have been identified in T1D targeting key beta-cell proteins. The most common autoantibodies include insulin (IAA), glutamic acid decarboxylase (GADA), protein tyrosine phosphatase (IA2A), and zinc transporter 8 (ZnT8A). Islet AAbs do not guarantee T1D development, but indicate high risk of T1D development especially if multiple AAbs are detected. Children with two AAbs have a 70% chance of developing T1D[70].

The causes of T1D remain elusive. Genome-wide association studies have identified loci and variants conferring increased T1D risk[71], and specific human leukocyte antigen haplotypes increase the risk of T1D[72]. Concordance studies in monozygotic twins have shown there is a heritable component to T1D[73], but the concordance rate of 65% suggests additional environmental triggers are present in T1D pathogenesis. Viral infections and dietary factors have

been proposed[74], but the contributions of these and other undefined triggers remain largely unknown.

1.2.3 Monogenic diabetes, gestational diabetes, and late autoimmune diabetes in adults

Monogenic diabetes and latent autoimmune diabetes in adults (LADA) account for about 1% of people with diabetes. Monogenic diabetes is a unique collection of diabetes pathologies that is defined by a single gene variant in a patient, often in a key beta-cell gene, that results in hyperglycemia. Variants in a subset of genes, including *KCNJ11*, *ABCC8*, and *INS* often result in monogenic neonatal diabetes that occurs before 6 months of age[75]. Variants in other genes such as *GCK*, *HNF1A*, *HNF4A*, and *HNF1B* can lead to diabetes development in adolescence or early adulthood, known as mature-onset diabetes of the young (MODY), which is inherited in an autosomal dominant pattern[75]. Gestational diabetes occurs in over 5% of pregnancies in Ontario[76], and is defined as impaired glucose tolerance first recognized in pregnancy[77], and typically resolves postpartum. However, gestational diabetes confers a large increase in the risk of developing T2D[78]. LADA is a form of diabetes that is similar to T1D, but occurs with heterogenous severity. Individuals with LADA are distinguished from adult-onset T1D by an age over 30 years old, no requirement of exogenous insulin for at least 6 months after diabetes diagnosis, and the presence of at least one islet AAb[79]. The diagnostic criteria and route of clinical care in LADA is an ongoing debate.

1.2.4 Hallmarks of diabetes in human islets

Although T1D and T2D have different etiologies, there are common hallmarks in addition to hyperglycemia. Beta-cell mass ultimately declines as disease progresses in both[59,68]. Additionally, beta-cell function declines during progression, resulting in reduced first-phase insulin secretion during IVGTT prior to diabetes[80,81]. Postprandial suppression of glucagon

release from alpha cells is also lost in T1D and T2D, contributing to postprandial hyperglycemia in both diseases[82,83]. Increased immune cells are found in islets in diabetes, with islet macrophages increased in both T1D and T2D[84,85].

Altered beta-cell prohormone processing is observed in T1D and T2D. Elevated ratios of proinsulin:insulin and proIAPP:IAPP are detected in the circulation in both diseases, suggesting common mechanisms of beta-cell decompensation[86,87]. Islet amyloid is detected in over half of T2D cases[88–90], and recently it has also been found to a lesser extent in T1D[91,92]. It is currently unclear to what extent and when islet amyloid is involved in the pathogenesis of T1D, and the frequency with which it occurs in T1D. Although not a known hallmark of T1D islets, islet amyloid may induce similar beta-cell dysfunction as it does in T2D. Beta-cell ER-stress is also present in T1D and T2D[93,94], possibly due to increased secretory demands on residual beta cells. Loss of beta-cell maturity also occurs in T1D and T2D islets, contributing to the functional decline of beta cells in both diseases[95].

The hallmarks above highlight the similar states in which beta cells and islets exist in T1D and T2D, despite different pathological mechanisms. Investigation into causes or therapeutic corrections of the phenotypes may benefit individuals with T1D and T2D. Given observations of islet stress and dysfunction in transplant studies[96], characterization of these hallmarks is also likely relevant to transplantation of stem-cell derived beta-like cells as a therapy for diabetes.

1.2.5 Diabetes therapies

Early therapeutics in T2D focused on enhancement of insulin secretion (insulin secretagogues) including sulfonylureas and meglitinides that bind to SUR1 causing K_{ATP} channel closure and insulin release. These drugs often only have several years of efficacy before insulin

insufficiency returns[97], and carry increased risk of hypoglycemia and body weight gain due to the decoupling of insulin release from glycemia[98]. New advancements in secretagogues have focused on GLP-1 and GIP single or dual incretin mimetics that enhance insulin secretion in a glucose-dependent manner, reducing hypoglycemic risk. GLP-1 has also been shown to help preserve beta-cell mass and function, and reduces body weight, suggesting beneficial effects beyond its role in beta-cell potentiation[99].

Insulin sensitizing agents are also used in T2D. Metformin is among the most widely used first-line pharmaceutical in T2D and reduces hepatic glucose output. Thiazolidinediones, such as rosiglitazone, are also used to improve insulin resistance via activation of peroxisome proliferator-activated receptors[98]. SGLT2 (sodium-glucose cotransporter 2) inhibitors, called gliflozins, are a recently approved therapeutic that inhibits glucose reuptake in the kidneys, facilitating glucose excursion in the urine. Gliflozins are effective at reducing glycemia without uptake into cells, leading to the additional benefit of weight loss. However, due to the lack of insulin signaling, gliflozins can lead to euglycemic diabetic ketoacidosis in some patients[100]. In addition to pharmaceuticals, lifestyle adjustments as a therapy in T2D are associated with lower HbA_{1C}, reduced body weight, improved quality of life, and reduced health care costs, making lifestyle management a high priority therapeutic option in T2D[101].

Therapies for T1D were slow in the first half-century after the discovery of insulin, but recent advancements are having remarkable impacts. Insulin pumps allow for continuous basal and bolus releases of insulin, facilitating insulin dosing. Continuous glucose monitors (CGMs) also have had a remarkable impact, facilitating glycemic tracking and patient learning of their unique glycemic regulation. CGMs have been shown to improve time in the euglycemic range, and minimize time spent in hyper- and hypo-glycemic ranges[102]. However, pumps and CGMs

also carry a significant mental burden of continuous monitoring and adjustment. Islet transplantation was pioneered in the late 1990's and resulted in independence from exogenous insulin and excellent glycemic control for 7 individuals with T1D[103]. However, transplant recipients must maintain immunosuppressive regimens, and about half of recipients become insulin-dependent after 5 years[104]. Given the limited availability of human islets for transplantation, intensive research efforts have focused on producing beta cells from stem cells. Stem-cell-derived beta-like cells have made immense progress in the last decade and may yield a scalable source of beta cells for transplantation and therapy in T1D. Transplantation of stem-cell-derived therapeutic cells are in early clinical trials[105,106] with further results eagerly anticipated. Despite remarkable therapeutic improvements in the last decades, diabetes management continues to be challenging. Further therapies are ultimately needed to improve islet function and actions in T1D and T2D, and may also benefit the function of transplanted tissue.

1.3 Diabetes, obesity, and cancer

Uncontrolled diabetes results in microvasculature complications that can lead to terminal conditions if left unmanaged. There are numerous conditions associated with diabetes, and this thesis investigates two diabetes-associated complications: increased obesity and risk of cancer.

1.3.1 Diabetes and obesity

The association between T2D and obesity is well established with approximately half of individuals with T2D having a BMI of ≥ 30 in the United States[107]. Excessive adiposity contributes to insulin resistance and participates in the decline of beta-cell dysfunction in diabetes[62]. An acute increase in free fatty acids (FFAs) can increase insulin sensitivity, while acute reductions improve insulin sensitivity and glucose tolerance[108,109]. Although FFAs can potentiate insulin release as described earlier, chronically elevated FFAs, particularly in the

presence of hyperglycemia can drive beta-cell dysfunction and increased basal insulin release[110,111]. The resultant effect is hyperinsulinemia, where insulin signaling in the periphery continues to promote glucose uptake, inhibit lipolysis, and increase body weight gain. Therapy with early-generation insulin secretagogues like sulfonylureas, or exogenous insulin, maintain high levels of insulin signalling and lead to increased body weight gain in T2D. In this context, insulin resistance and secretion continue to rise, creating a detrimental feedback loop that compromises beta-cell function.

It is becoming increasingly apparent that hyperinsulinemia can precede and drive insulin resistance in T2D pathogenesis. This suggests an underlying beta-cell defect, where inappropriate insulin release from beta cells initiates the detrimental cycle of increased secretion and resistance. This has been shown to occur in humans followed longitudinally, where individuals with insulin hypersecretion but undetectable insulin resistance have a higher incidence of T2D or impaired glucose tolerance and increased fat mass after a 3 year follow-up[112]. Additionally, increased insulin levels are observed in obesity prior to the development of insulin resistance[113]. Reducing insulin levels in mice protects against high-fat diet-induced obesity[114], and chronic insulin infusion for 6 weeks in lean rats leads to increased weight gain and impaired glucose tolerance[115]. Deletion of the insulin receptor in adipocytes also leads to reduced obesity and increased longevity in mice[116]. Altogether, the data in rodents and humans suggest that hyperinsulinemia can precede insulin resistance and drive adiposity.

In T1D and T2D, islet-derived hormones circulate at a perturbed ratio. Insulin is administered exogenously, restoring circulating insulin, but other islet hormones are not corrected. Hyperglucagonemia occurs in both T1D and T2D. Glucagon receptors have been identified at low levels in adipocytes, and glucagon stimulates glucose uptake and lipolysis in

isolated human adipocytes, but only at supraphysiological concentrations 5-500-fold higher than found in circulation[117]. Although hyperglucagonemia contributes to increased hepatic glucose output and hyperglycemia in diabetes, it is unlikely to directly affect adipocytes. Glucagon also stimulates energy expenditure[118], further decreasing the likelihood it contributes to adiposity in diabetes. IAPP is also reduced or absent in the circulation of individuals with diabetes and is typically not administered with exogenous insulin. IAPP has been shown to reduce body weight through suppression of appetite and increased energy expenditure, and loss of IAPP in diabetes may contribute to increased adiposity (reviewed in Chapter 4). IAPP replacement therapy has been shown to reduce body weight and improve glycemic control in T1D and T2D[119,120], highlighting the benefits of restoring additional hormones beyond insulin.

1.3.2 Diabetes and cancer

Diabetes is associated with a 1.2-2 fold increased risk in developing cancer, including cancers of the liver, endometrium, pancreas, breast and colon, with the sole exception being reduced risk of prostate cancer in diabetes[121,122]. In addition to increased risk, there is also an increased risk of mortality in cancer patients with diabetes. Although the increased risks are low for many cancers, it suggests that biological and pathological mechanisms may be shared between diabetes and cancer.

Hyperinsulinemia contributes part of the increased risk in T2D. In individuals without diabetes, increased circulating insulin creates a 2-fold increased risk of cancer mortality in both obese and non-obese individuals[123]. Several cancers, including breast and lung, have increased insulin receptor and IGF-1 receptor expression, and insulin can signal through both receptors including a hybrid IGF-1/INSR receptor[124]. Constitutively active RAS-RAF-MEK-ERK or PI3K-AKT signalling pathways are frequently found in cancer, and drive proliferative and anti-

apoptotic signaling in cancer cells[125]. Insulin receptor and IGF-1 receptor signalling both signal through PI3K-AKT and MEK-ERK pathways and may drive further pro-survival and proliferative signalling within cancer cells. Additionally, hyperglycemia in diabetes may provide increased glucose availability for increased insulin-mediated glucose uptake in cancer cells, which are highly glycolytic. High glycolysis rates in tumour cells yields ATP and metabolites for cell growth, and increased lactate that is released to create an immunosuppressive tumour microenvironment. Hyperglycemia may also contribute to cancer cell invasiveness and metastasis[126]. IAPP has also been proposed as a tumour suppressor[127], raising the question of whether IAPP loss increases cancer risk in diabetes. Thus, there is both epidemiological and physiological evidence suggesting that hyperinsulinemia and hyperglycemia contribute to the elevated risk of cancer in diabetes.

An additional risk factor for cancer that is difficult to separate from T2D is obesity. A high BMI is associated with increased risk of developing many cancers, with higher BMIs conferring an even stronger risk resulting in a positive relationship between BMI and cancer risk for several tissues[128]. Reductions in body weight can lower the risk of cancer – intentional weight loss of 20 lbs or more was found to reduce cancer incidence by 11% over a 7-year period in a cohort of over 21,000 women[129]. The adipokines leptin and adiponectin have also been proposed to contribute to tumourigenesis in obesity. Leptin can stimulate cancer cell proliferation and survival, and adiponectin can induce cell cycle arrest and apoptosis. The two adipokines have been proposed to provide balancing effects in the lean state, and the increase in leptin relative to adiponectin in obesity may contribute to increased cancer risk[130]. Chronic adipose inflammation in obesity is also thought to sustain the tumour microenvironment through the production of local and circulating proinflammatory cytokines that promote tumour growth[131]. In summary, obesity

contributes to cancer risk independent of diabetes, but diabetes-associated obesity remains a prevalent mechanism driving cancer risk in diabetes.

1.4 Summary and thesis investigation

Diabetes is a complex metabolic disease involving numerous tissues. Distinct and separate pathologies cause T1D and T2D, but several shared hallmarks are present including hyperglycemia, reduced functional beta-cell mass, errors in prohormone processing, and disproportional islet-derived hormones in the circulation. Improving our understanding of beta-cell dysfunction and failure mechanisms shared in T1D and T2D may provide therapeutic avenues to restore beta-cell function or prevent its decline. Further understanding the complex hormonal balances that become disrupted in diabetes may also lead to better diabetes care, resulting in reduced risk of comorbidities and improved quality of life for those affected by diabetes.

This thesis aims to improve our understanding of the beta-cell dysfunction that occurs early in diabetes pathogenesis. Namely, it investigates the impact of beta-cell prohormone processing errors on beta-cell function and glucose homeostasis. Loss of beta-cell prohormone processing occurs early in diabetes pathogenesis and alters the beta-cell secretome. This thesis further investigates how beta-cell prohormone processing errors influence the aggregation of the beta-cell hormone IAPP, which declines in circulation with insulin as diabetes progresses. Lastly, this thesis investigates the impact of IAPP loss, as observed in diabetes, on body weight, glycemia, and pancreatic cancer. The overall hypothesis of this thesis is that reduced mature IAPP and beta-cell prohormone processing errors can cause beta-cell dysfunction and increase the risk of obesity and hyperglycemia. The overarching goal is to improve our understanding of

the impact beta-cell prohormone processing errors have on beta-cell functional decline, and the impact of IAPP loss that results from beta-cell decline.

Chapter 2: Methods and Materials

2.1 Animals

All animal husbandry and procedures were performed according to the Canadian Council on Animal Care guidelines, and all experiments were approved by the University of British Columbia Animal Care Committee (protocols A14-0222, A16-0100, A19-0127, and A20-0073).

2.1.1 *Iapp*-null mice

Congenic Iapp-null animals were generated by backcrossing $Iapp^{+/-}$ mice[132] in-house to C57BL/6J mice in-house for over 10 generations. Mice were housed at BC Children's Hospital Research Animal Care Facility on a 12-hour light/dark cycle at 22°C. $Iapp^{+/-}$ mice were intercrossed to generate null and wild-type animals from the same breeding pairs. Breeders were fed a 9% fat diet (Teklad 2919), and animals were weaned to a standard chow diet (Teklad 2918; 6% kcal from fat). At 6-8 weeks of age, mice were switched to a high-fat diet (45% kcal from fat; Research Diets D12451) or a matched control diet (10% kcal from fat; Research Diets D12450H).

2.1.2 *Iapp*-null pancreatic cancer mouse model

$Kras^{LSL\text{-}G12D/+}$ mice (B6.129S4-$Kras^{tm4Tyj}$/J)[133] were kindly provided by Dr. Francis Lynn (University of British Columbia). Iapp and Kras are both located on chromosome 6 in mice separated by approximately 3 Mb. $Iapp^{-/-}$ and $Kras^{LSL\text{-}G12D/+}$ mice were bred, and heterozygous animals were backcrossed to C57BL/6J mice. A recombinant $Iapp^{-}$ $Kras^{LSL\text{-}G12D}$/$Iapp^{+}$ $Kras^{+}$ mouse was identified in the F2, which was then bred to $Trp53^{flox/flox}$; $Pft1a^{CreERTM/+}$ mice[134,135] on a mixed CD1-C57BL/6J background (courtesy of Dr. Janel Kopp, University of British Columbia). A separate line of $Iapp^{+}$ $Kras^{LSL\text{-}G12D}$ / $Iapp^{-}$ $Kras^{+}$; $Trp53^{flox/flox}$; $Ptf1a^{CreERTM/+}$ mice

were generated and maintained. Experimental animals were generated through breeding the Iapp^{-} *Kras*$^{LSL\text{-}G12D}$ */ Iapp*$^{+}$ *Kras*$^{+}$*; Trp53*$^{flox/flox}$ animals with the *Iapp*$^{+}$ *Kras*$^{LSL\text{-}G12D}$ */ Iapp*$^{-}$ *Kras*$^{+}$*; Trp53*$^{flox/flox}$*; Ptf1a*$^{CreERTM/+}$ animals so that all experimental genotypes were generated from each breeding pair (Figure 5). Mice were housed at the UBC Modified Barrier Facility.

2.1.3 *Ins1*$^{cre/+}$*; Pcsk1*$^{flox/flox}$ mice (Pcsk1^{betaKO})

Pcsk1$^{tm1a(EUCOMM)Wtsi}$ mice[136] (C57BL/6N) were obtained from Infrafrontier/EMMA and crossed to *FLPo*$^{Tg/0}$ mice[137] (B6.Tg(CAG-flpo)1Afst; CMMT, University of British Columbia) to generate *Pcsk1*$^{flox/+}$ mice, which were the bred to *Ins1*$^{cre/+}$ mice[138] (B6(Cg)-Ins1$^{tm1.1(cre)Thor}$/J; The Jackson Laboratory). *Pcsk1*$^{flox/+}$ female mice were crossed with *Pcsk1*$^{flox/+}$*; Ins1*$^{cre/+}$ males to generate all experimental genotypes. Mice were housed at BC Children's Hospital Research Animal Care Facility on a 12-hour light/dark cycle at 22°C. Breeders were fed a 9% fat diet (Teklad 2919), and animals were weaned to a standard chow diet (Teklad 2918; 6% kcal from fat) at 3 weeks old. Experimental animals were either maintained on standard chow diet or switched to a high-fat diet (45% kcal from fat; Research Diets D12451) beginning at 8-9 weeks old. Mice were additionally backcrossed to mTmG transgenic mice[139] (B6.129(Cg)-Gt(ROSA)26Sor$^{tm4(ACTB\text{-}tdTomato,\text{-}EGFP)Luo}$/J; The Jackson Laboratory) to create Pcsk1^{betaKO} mTmG$^{Tg/0}$ mice.

2.1.4 *Ins1*$^{cre/+}$*; Pcsk2*$^{flox/flox}$ mice (Pcsk2^{betaKO})

Pcsk2^{flox} animals were generated in-house as previously described[140]. Pcsk2^{betaKO} and controls were generated as above for Pcsk1^{betaKO} by crossing to *Ins1*$^{cre/+}$ mice, and housed identically.

2.1.5 *Ins1$^{cre/+}$; Pcsk1$^{flox/flox}$; Pcsk2$^{flox/flox}$* mice (DPC^{betaKO})

Pcsk1^{betaKO} and Pcsk2^{betaKO} mice were crossed, and F1 heterozygous mice interbred to generate *Pcsk1$^{flox/flox}$; Pcsk2$^{flox/flox}$; Ins1$^{cre/+}$* (DPC^{betaKO}) and *Pcsk1$^{flox/flox}$; Pcsk2$^{flox/flox}$; Ins1$^{+/+}$* (DPC^{betaWT}) breeders. DPC^{betaWT} female mice were then bred to DPC^{betaKO} male mice to generate experimental animals. Animals were housed as described above for Pcsk1^{betaKO} mice.

2.1.6 *Ins1$^{cre/+}$; Pcsk1$^{flox/flox}$;* hIAPP$^{Tg/0}$ mice (Pcsk1^{betaKO} hIAPP$^{Tg/0}$)

Pcsk1^{betaKO} mice were crossed to hIAPP$^{Tg/0}$ mice[141,142] (FVB/N-Tg(Ins2-IAPP)RHFSoel/J; The Jackson Laboratory). Mice were then backcrossed to Pcsk1^{betaKO} animals, and F2 *Pcsk1$^{flox/flox}$ Ins1$^{+/+}$;* hIAPP$^{Tg/0}$ female mice were crossed to Pcsk1^{betaKO} male mice to generate F3 experimental animals (87.5% C57BL/6J, 12.5% FVB/N background). Animals were housed as described above for Pcsk1^{betaKO} mice.

2.2 Procedures in mice

2.2.1 Blood glucose and body weight monitoring

Mice were fasted for 4 h in a fresh cage from approximately 10 AM – 2 PM. Following body weight measurement a small drop of blood was collected from the distal tip of the tail by lancing with a 25 G needle. Blood glucose was measured using a OneTouch Ultra Mini glucometer.

2.2.2 Survival analysis

Mice were monitored for random-fed body weight, appearance, and behaviour weekly. At any sign of distress, animals underwent daily monitoring and were euthanized according to a predetermined animal distress scoring chart (Appendix A).

2.2.3 Glucose tolerance tests

Mice were fasted for 6 h in a fresh cage from approximately 8 AM – 2 PM. Mice were administered glucose in a sterile buffered saline solution via intraperitoneal (IP) injection. Glucose doses were adjusted for age, sex, and diet of the animals (0.8-2.0 g/kg body weight). Blood glucose was measured prior to injection (0 min), followed by 15, 30, 60, and 120 min time points as described above.

2.2.4 Insulin tolerance tests

Mice were fasted for 4 h from approximately 10 AM – 2 PM, and administered insulin (0.8-1.6 U/kg body weight; Novo Nordisk) via IP injection. Glucose was measured prior to injection (0 min), and at 15, 30, 60, 90, and 120 min post-injection. Any animal developing behavioural signs of hypoglycemia was administered glucose via IP injection. For experiments in which mice were recovered, the final timepoint included is the next timepoint after recovery, and values were imputed for recovered mice as 1.0 mM.

2.2.5 Blood collection and ELISA

Mice were fasted for 4 h and blood was collected from the medial or lateral saphenous veins into EDTA Microvette® capillaries. Samples were stored on ice during collection, and centrifuged at 2000 x g at 4°C for 5 min. Plasma was stored at -80°C until further analysis. Plasma analytes were analyzed by ELISA (enzyme-linked immunosorbent assay) for: proinsulin (Mercodia, 10-1232-01), insulin for Pcsk1^{betaKO} model (Meso Scale Discovery, K152BZC), insulin for IAPP-null model (Alpco, 80-INSMR-CH10), glucagon (Mercodia, 10-1281-01).

2.2.6 Body composition analysis

Mice were weighed, and body composition (lean and fat percentage) was determined using an EchoMRI-100 (EchoMRI) on conscious restrained mice.

2.2.7 Tamoxifen injections

Tamoxifen (Toronto Research Chemicals) was dissolved in corn oil (20 mg/mL) by sonication, and 0.2 μm filter sterilized. Mice were administered 3 tamoxifen doses (5 mg tamoxifen / 40 g body weight) on alternating days over a 5-day period. Tamoxifen was administered via subcutaneous injection.

2.3 Cell culture

PANC-1 cells were kindly provided by Dr. Wan Lam (University of British Columbia) and maintained in ATCC-formulated DMEM (Gibco 11960044 base medium supplemented with 10% FBS, GlutaMAX, sodium pyruvate, penicillin, and streptomycin). H1299 cells were purchased from ATCC and cultured in ATCC-formulated RPMI-1640 (Gibco 11875093 base medium supplemented with 10% FBS, glucose, HEPES, sodium pyruvate, penicillin, and streptomycin). HEK-CRE-hCALCR-hRAMP3 cells were passaged in DMEM (Gibco 11960044 base medium supplemented with 10% FBS, GlutaMAX, penicillin, and streptomycin).

2.4 Peptides

Davalintide, pramlintide, and rIAPP (rat IAPP) peptides were obtained from MedImmune (Courtesy of Dr. James Trevaskis). Peptides were dissolved in 1,1,1,3,3,3-Hexafluoro-2-propanol (MilliporeSigma) at 1 mg/mL, lyophilized in single-use aliquots (50-200 μg / tube), and stored at -20°C. Lyophilized peptide mass was confirmed by BCA assay (Pierce, Thermo Scientific) with a sample tube from each lot after lyophilization. Lyophilized peptides were reconstituted in assay media for experiments.

2.5 PANC-1 and H1299 proliferation and death

Cell proliferation and death were determined by live-cell imaging (Molecular Devices ImageXpress) with live/dead nuclear stains in humidified and incubated (37°C, 5% CO_2)

conditions. PANC-1 cells were seeded at a density of $4x10^3$ cells/well on a 96-well ViewPlate (PerkinElmer) and adhered overnight. The following day, cells were washed in their forthcoming media, and treated with 0.25-25 µM pramlintide, davalintide, rIAPP, cycloheximide, or gemcitabine in complete growth media or reduced FBS (10% to 0.1% FBS) and glucose media (25 mM to 2.5 mM glucose). Cells were labelled with Hoechst 33342 (0.05 µg/mL) and propidium iodide (0.5 µg/mL) for 1 h prior to imaging. Cells were imaged every 2 h for 48-62 h at 9 non-overlapping sites per well, and a minimum of 3 technical replicate wells were used for n = 1 replicate. Images were analyzed using MetaMorph (Molecular Devices) analysis software. H1299 cells were assayed similarly but with $1x10^3$ cells/well seeding density and 0.2 µg/mL Hoechst 33342.

2.6 Pramlintide activity assay

HEK-293 cells expressing cAMP response element (CRE)-driven luciferase (HEK-CRE cells) were kindly provided by Dr. Timothy Kieffer (University of British Columbia). A plasmid containing human CALCR and RAMP3 sequences under a bidirectional CMV promoter (pBI-hCALCR-hRAMP3) was generated in-house. HEK-CRE cells were transfected with the linearized plasmid using Lipofectamine 3000 (Invitrogen), and a stable HEK-CRE-hCALCR-hRAMP3 cell was isolated and clonally expanded. HEK-CRE-hCALCR-hRAMP3 cells were seeded at 10^4 cells / well. Following overnight adherence, cells were washed with secretion assay buffer and incubated with pramlintide in secretion assay buffer for 5 h. Following treatment, cells were lysed and luciferase expression analyzed using a Bright-Glo luciferase assay (Promega) following manufacturer's protocol.

2.7 Extracellular acidification rate

Extracellular acidification rate (ECAR) was assessed using a Seahorse XFe96 Analyzer following manufacturer's protocols. PANC-1 cells were seeded in a Seahorse XF cell culture plate at a density of $1x10^4$ cells / well in normal growth media and left overnight to adhere. Once adhered cells were treated for 48 h with 0.25 - 25 μM pramlintide, davalintide, or rIAPP in complete growth media or media with reduced FBS (10% to 0.1% FBS) and glucose (25 mM to 2.5 mM glucose). After 48 h, cells were washed and incubated in Seahorse XF base medium (Agilent 102353-100) supplemented with GlutaMAX (2 mM final concentration) for 1 hour in a non-CO_2 incubator at 37°C. ECAR was measured in basal medium with 10 mM glucose (MilliporeSigma, G7021), 1 μM oligomycin (MilliporeSigma, O4876), and 50 mM 2-deoxy-glucose (MilliporeSigma, D8375). H1299 cells were assayed similarly, except for seeding density ($5x10^3$ cells / well) and addition of 2 μM oligomycin was used during the assay. Glycolysis was measured by (maximum ECAR rate during glucose phase) – (last basal ECAR rate measured before glucose injection). Multiple (5-7) technical replicates were tested for each condition.

2.8 Transmission electron microscopy

Islets were submitted to the Electron Microscopy Facility at McMaster University, Faculty of Health Sciences for embedding, sectioning, and imaging. Freshly isolated islets were fixed in 2% glutaraldehyde (v/v) in PBS during overnight shipping. Islets were then post-fixed in 1% osmium tetroxide in 0.1M sodium cacodylate buffer for 1 hour and then dehydrated through a graded ethanol series (50%, 70%, 70%, 95%, 95%, 100%, 100%). Final dehydration was done in two changes of 100% propylene oxide. Samples were infiltrated with and embedded in Spurr's resin and polymerized overnight in a 60°C oven. Thin sections were cut on a UCT

ultramicrotome (Leica) and picked up onto copper grids. Unstained sections were viewed in a JEM 1200 EX TEMSCAN transmission electron microscope (JEOL) operating at an accelerating voltage of 80kV. Images were acquired with an AMT 4-megapixel digital camera (Advanced Microscopy Techniques).

2.9 Islet assays

2.9.1 Islet isolation and culture

Mice were euthanized under surgical plane anesthesia (isoflurane inhalation). Pancreases were perfused with 1070 U/mL collagenase type XI (MilliporeSigma C7657) in 1X HBSS (Gibco 14185-052) via injection through the pancreatic duct. Following dissection pancreases were incubated in collagenase at 37°C for 15 min followed by manual shaking until homogenous (approximately 4-6 min). Digestion was stopped by addition of HBSS containing 1 mM $CaCl_2$ and placing samples on ice. Islets were washed and filtered using a 70 µm strainer and hand-picked under a dissection microscope to fresh RPMI-1640 (Gibco 11875-093) supplemented with 10% FBS, GlutaMAX, penicillin, and streptomycin, and cultured in 37°C, 5% CO_2 incubation conditions.

2.9.2 Islet dispersion

Following isolation, islets were rested overnight and then hand-picked to 1.5 or 15 mL tubes. Islets were washed in PBS and resuspended in Accutase (2-5 µL/islet; Innovative Cell Technologies AT-104). Islets were digested for 15 min at 37°C and dispersed with gentle pipetting up/down 15-20 times using a P1000 tip. Digestion was stopped with addition of 4x volume of islet culture media. Cells were centrifuged at 300-500x g for 4 min at 4°C, and resuspended in culture medium for downstream applications.

2.9.3 Proliferation of dispersed islets

One-hundred dispersed islets were resuspended in 500 µL RPMI-1640 (Gibco 11879-020) with 5 mM glucose, 10% FBS, GlutaMAX, penicillin, and streptomycin. Dispersed islets were split to 250 µL/well of an 8-well chamber slide (Nunc Lab-Tek II). Additional media (250 µL) containing 5 mM or 35 mM glucose was added for final glucose concentrations of 5 mM or 20 mM, and dispersed islets were cultured for 48 h. Media (350 µL) was removed after 48 h and 150 µL fresh media (5 or 20 mM glucose) containing EdU (10 µM final concentration; Toronto Research Chemicals) was added for an additional 24 h (72 h dispersed culture time). Cells were then washed in PBS and fixed twice for 10 min in 4% PFA at room temperature. EdU was detected by click chemistry following manufacturers protocol (Invitrogen C10337). Insulin was detected using guinea pig anti-insulin (1:2 in PBS; Agilent Dako IR002) overnight at 4°C, followed by Alexa-594 goat anti-guinea pig secondary (1:200 in PBS; Invitrogen A-11076) for 1 h at room temperature. Nuclei were detected using Hoechst 33342 (10 µg/mL; Invitrogen) for 1 h in the secondary antibody reaction. Coverslips were mounted with ProLong Gold antifade (Invitrogen P36930) and imaged on a Leica SP5 confocal microscope. Images (30-40 per well) were taken, resulting in over 1000 beta cells analyzed per replicate.

2.9.4 Islet proliferation co-culture (Transwell®)

Following overnight recovery, islets from C57BL/6J male mice were picked to the bottom chamber (30 per well) and islets from DPC^{betaKO} or DPC^{betaWT} mice were picked to the top chamber (100 per well) of a 24-well Transwell® plate with a pore size of 0.4 µm in the polyester membrane. Islets were cultured for 72 h in low (5 mM) or high (20mM) glucose serum-free RPMI-1640 medium (Gibco 11879-020) supplemented with 1% BSA, GlutaMAX, penicillin, and streptomycin. EdU was added at a final concentration of 10 µM for the final 24 h

of the 72 h high/low glucose culture, after which islets were dispersed and resuspended in PBS. Suspended cells were seeded to a 96-well µ-plate (Ibidi), centrifuged at 500x G for 5 min, and immediately fixed twice for 10 min in 4% PFA at room temp. EdU, insulin, and nuclei were detected as described above for dispersed islets but with a TRITC-conjugated secondary antibody (1:100 in PBS; Invitrogen PA1-28594). Plates were imaged on an ImageXpress Micro confocal high-content system (Molecular Devices) and over 2000 beta cells were analyzed per mouse.

2.9.5 Islet ER stress: glucose and thapsigargin treatment

Following overnight recovery, 50 or 100 islets per mouse were cultured in 5, 15, or 25 mM glucose RPMI-1640 (Gibco 11879-020; supplemented with 10% FBS, GlutaMAX, penicillin, and streptomycin) in a 6-well dish. After 72 h, islets were washed in PBS, and islet pellets were stored at -80°C until lysis. For thapsigargin treatment, islets were recovered overnight and then 50 islets per well were transferred to a 6-well dish containing standard islet culture media. Islets were treated with 1 µM thapsigargin or 0.1% DMSO for 6 h, washed once with PBS, and islet pellets stored at -80°C until lysis.

2.9.6 Calcium imaging

Freshly isolated islets were seeded to glass coverslips in 35 x 10 mm dishes (15 islets per dish) and cultured for 3 days in standard islet culture media to allow adhesion. Coverslips and islets were transferred to a 2 mL perifusion chamber and loaded for 30 min with 5 µM Fura-2 AM dye (Invitrogen F1201), followed by perifusion for 30 min in basal buffer to flush excess dye and equilibrate islets. Islets were perifused at 2.5 mL/min in Ringer's solution containing varying glucose concentrations (or tolbutamide or 30 mM KCl as indicated) with 5.5 mM KCl, 2 mM $CaCl_2$, 1 mM $MgCl_2$, 20 mM Na-HEPES, and 149 mM NaCl. Islets were imaged every 10

seconds using a Leica DMI6000 inverted microscope and a 10x objective. Fura-2 was excited at 340 nm and 380 nm and emissions collected with 502 nm and 538 nm filters, respectively. Intracellular calcium concentrations are expressed as a ratio of the 340/380 emission intensities.

2.9.7 Insulin secretion

Islets were rested for 24-48 h following isolation, and perifused on a Perifusion V4 system (Biorep Technologies). Equal numbers and sizes of islets (80-100) were picked to chambers containing Bio-Gel P4 beads (Biorep Technologies, PERI-BEADS-100), and perifused at 100 µL/min in basal KRB buffer for 60 min prior to the start of collection. Islets were perifused in KRB (pH 7.4) containing varying glucose as indicated (or 30 mM KCl) and 133 mM NaCl, 4.7 mM KCl, 1.2 mM KH_2PO_4, 1.2 mM $MgSO_4$, 1.9 mM $CaCl_2$, 5 mM $NaHCO_3$, 10 mM HEPES, and 0.25% BSA. Perifusate was analyzed by ELISA for insulin (Alpco STELLUX chemiluminescence rodent ELISA) or proinsulin (Mercodia rat/mouse proinsulin ELISA) as indicated.

2.10 Tissue collection, histology, immunostaining and imaging

Mice were euthanized under surgical plane anesthesia (isoflurane inhalation) and perfused with 5 mL cold PBS followed by 5 mL cold 4% PFA. Pancreases were dissected and fixed overnight at 4°C in 4% PFA, and stored in 70% ethanol at 4°C. Fixed pancreases were embedded in paraffin, and series of 5 µm sections were collected every 150-200 µm. Sections were rehydrated through series of xylene, 95% ethanol, and 70% ethanol washes, and antigen retrieval was performed using 10 mM sodium citrate (pH 6.0) buffer at approximately 95°C for 20 minutes. Sections were blocked for 1 h at room temperature using 5% horse serum (or Agilent Dako serum-free protein block for MafA immunostaining) and incubated with primary antibodies diluted in PBS overnight at 4°C and secondary antibodies (with 2.5 µg/mL DAPI) for

1 h at room temperature. Slides were mounted with ProLong Gold (Invitrogen) and imaged using 20x or 40x oil immersion objectives on a Leica SP5 II confocal microscope, or a 20x objective on an Olympus BX61 fluorescence microscope.

Beta-cell area analyses were performed using immunohistochemistry on 3-5 sections per mouse separated by approximately 200 μm between sections. Following perfusion and tissue collection, section processing, and antigen retrieval as above, sections were incubated with BLOXALL (Vector Laboratories) for 15 min, blocked with 5% horse serum, and incubated overnight at 4°C with guinea pig anti-insulin (1:4 in PBS; Agilent Dako IR002). Following PBS washes, sections were incubated with HRP-conjugated goat anti-guinea pig (1:200 in PBS; Invitrogen A18769) for 1 hour at room temperature and immunostaining visualized with DAB substrate (Pierce, Thermo Scientific 34002) for 7 minutes. Sections were counterstained with hematoxylin, dehydrated through 50%-100% ethanol series and xylene, and mounted with Permount (Fisher Scientific). Tiled images were acquired with a Panoramic Midi II slide scanner (3D Histech) for sections from 30-week-old animals and with a BX61 (Olympus) microscope for sections from 4.5-week-old animals. All primary and secondary antibodies and dilutions are included in Table 1.

2.11 Western blot

Islets were lysed in NP-40 lysis buffer with a protease inhibitor cocktail containing EDTA (Roche cOmplete ULTRA 5892970001), centrifuged at 14,000x g for 20 min at 4°C and the supernatant collected for western blot. For (pro)IAPP western blots, samples were resolved on a 15% tris-tricine gel. For PCSK1, BiP, and phospho-eIF2α western blots, samples were resolved on a 4-20% tris-glycine gradient gel (Bio-Rad 456-1094). Protein was transferred to a polyvinylidene difluoride membrane (or nitrocellulose membrane for proIAPP) by wet transfer

and the membrane was blocked with Odyssey blocking buffer (diluted 1:2 in PBS; LI-COR 927-40000). Membranes were probed with primary antibodies overnight at 4°C, and secondary antibodies for 1 h at room temperature (for antibodies and dilutions see Table 1). Blots were scanned on an Odyssey 9120 scanner (LI-COR). For analysis of (pro)insulin by western blot, islets were lysed as above, and resolved using a 15% non-reducing urea (6 M) gel. Protein was transferred to a nitrocellulose membrane via wet transfer, and blocked, probed, and visualized as above.

2.12 Proteomics

2.12.1 Islet top-down proteomics

Islet pellets were analyzed at the BCCHR Analytical Core for Metabolomics and Nutrition. Spectra were manually reviewed in MassHunter Profinder (Agilent) and compared to expected masses of the indicated proteins. Peak areas of identified ions were quantified and expressed as a ratio of $Pcsk1^{betaKO}$ / $Pcsk1^{betaWT}$.

2.12.2 Beta-cell bottom-up proteomics

Dispersed islets were filtered using a 40 μm strainer and resuspended in FACS buffer (PBS supplemented with 2% BSA) with 7-AAD. GFP^{+} $Tomato^{-}$ $7\text{-}AAD^{-}$ live beta cells ($Pcsk1^{betaKO}$ mTmG transgenic mice) were sorted on a FACSAria IIu cell sorter (BD Biosciences). Over 70,000 live beta cells per mouse were collected. Following sorting, cells were washed twice with 1 mL cold PBS, centrifuged at 500x g for 3 min at 4°C, and clean cell pellets were snap-frozen in liquid nitrogen and stored at -80°C. Cells were lysed in 50 mM HEPES (pH 8.5) with 3% SDS, digested with benzonase, reduced with dithiothreitol (DTT), and alkylated with chloroacetamide. Proteins were purified by an SP3 protocol with binding to a 1:1 ratio of hydrophilic and hydrophobic magnetic beads (GE SpeedBeads; GE45152105050250 and

GE65152105050250) and washing with 80% ethanol. Purified proteins were digested with trypsin overnight at 37°C. Following trypsinization, peptides were cleaned via C18 stage-tip, and all organics removed by speed vac. Samples were resuspended in 0.1% formic acid in water for LC-MS/MS analysis.

Peptide concentration was determined by NanoDrop (Thermo Fisher Scientific) and 1 µg of peptides per sample were analyzed by 2 h data-independent acquisition (DIA) LC-MS/MS analysis on a Q Exactive HF Orbitrap (Thermo Fisher) coupled to an Easy-nLC 1200 (Thermo Fisher Scientific). Spectra were searched by directDIA (Spectronaut, Biognosys) with a precursor q-value cutoff of 0.001. Identified proteins were filtered for 30% completeness and missing values imputed to allow downstream differential expression analysis. Differential expression was analyzed using Limma with a q-value cutoff of < 0.05.

2.13 EdU labelling and proliferation *in vivo*

Mice were administered 100 µL of EdU (5 mg/mL; Toronto Research Chemicals) daily at 9 AM for 3 consecutive days beginning at 28 days old. On the 4^{th} day (72 h EdU labelling), mice were euthanized, perfused, and pancreases dissected, fixed, and processed as described above (section 2.10). Littermate cre-negative controls were used. A minimum of 3 sections (separated by 200 µm between sections) per animal were analyzed for EdU incorporation using a Click-iT EdU detection kit (Invitrogen C10337) following manufacturers protocols. Insulin and nuclei were detected as written above (section 2.10). Islets in sections were imaged using a 40x oil immersion objective on a Leica SP5 II confocal microscope, with at least 20 islets per mouse imaged and analyzed.

2.14 Quantitative PCR (qPCR)

RNA was isolated from islet pellets using a PureLink RNA Micro kit (Invitrogen 12183-016) with on-column DNA digestion, and quantified using a NanoDrop 2000c (Thermo Fisher Scientific). SuperScript VILO (Invitrogen) was used for cDNA synthesis, and qPCR was performed on a Viia 7 real-time PCR instrument (Thermo Fisher Scientific) using Fast SYBR Green master mix (Applied Biosystems, Thermo Fisher Scientific; 4385612). Differential gene expression was quantified using the $2^{-\Delta\Delta Ct}$ method with *Rplp0* as a housekeeping gene. Primer sequences are listed in Table 2.

2.15 RNA sequencing

Islets were isolated from 14-week-old mice fed a HFD (45% kcal from fat; Research Diets D12451) for 6 weeks. Immediately following isolation and picking by hand, RNA was extracted using a RNeasy Plus Micro Kit (Qiagen 74034) and stored at -80°C. RNA integrity numbers were checked on 2/6 samples using an Agilent 2100 Bioanalyzer and both had values of 10. Sequencing was performed using general methods at the BRC Sequencing Core (University of British Columbia). NEBnext Ultra ii Stranded mRNA (New England Biolabs) was used for library preparation, and sequencing was performed on an Illumina NextSeq 500 with paired end 42bp × 42bp reads. 16-28 million reads per sample were obtained, and alignment and differential expression was performed using STAR and DESeq2 in the RNA Express application (Illumina).

2.16 Bioinformatics

Significant upregulated or downregulated genes or proteins were ranked by q-value and input as separate ordered queries to gProfiler for functional enrichment analysis (FDR < 0.05) of GO biological process and Reactome pathways. Gene set enrichment analysis (GSEA) was performed using a gene list ranked by the sign of the fold change multiplied by $-\log_{10}$ of the p-

value, with gene sets Mouse_GOBP_AllPathways_no_GO_iea_March_01_2021_UniProt or Mouse_GOBP_AllPathways_no_GO_iea_October_01_2021_symbol curated by the Bader Laboratory (University of Toronto). Significantly enriched pathways and processes were visualized as networks using the EnrichmentMap plugin in Cytoscape, and related nodes annotated using the AutoAnnotate plugin.

2.17 Islet amyloid

Pancreas sections from 31-week-old Pcsk1^{betaKO} hIAPP$^{Tg/0}$ and control mice were collected as written above including perfusion, antigen retrieval, and immunostaining for insulin (section 2.10). Following the secondary antibody, sections were stained for 2 min with 0.5% (m/v) thioflavin S (0.2 μm filtered) and washed twice in 70% ethanol followed by twice in water. Sections were mounted using ProLong Gold antifade (Invitrogen). Whole pancreas sections were tiled using a 10x objective on a BX61 fluorescence microscope (Olympus). Thioflavin S fluorescence was visualized using a FITC excitation/emission filter set. Three sections per mouse (separated by 200 μm) were analyzed, and islets (defined as clusters of approximately 10 or more insulin-positive cells) were roughly circled manually in each section and cropped images of circled islets were generated using a custom-built FIJI plugin. Cropped images were then analyzed using ilastik and CellProfiler, and 49-172 islets were analyzed per mouse for amyloid prevalence and severity.

2.18 Image analysis

Images were analyzed using machine learning algorithms for pixel classification in ilastik (amyloid and beta-cell area analyses), and custom-built CellProfiler pipelines and FIJI scripts using an Otsu variable thresholding algorithm. Quantification of images are displayed as area ratios or as cell number ratios as indicated on figures. Images displayed are contrasted identically

between experimental groups, with contrasting, pseudocolouring, scale bars, and montages created using automated custom FIJI scripts.

2.19 Statistical analyses

Data are presented as mean ± SD unless otherwise stated. Data were assumed to be normally distributed and analyzed with parametric tests unless skewed or multi-modal distributions were expected. Data were analyzed by two-tailed Student's t-test with Welch's correction when only two means were compared, or by ANOVA with Holm-Sidak follow-up testing when 3 or more means are compared. Non-parametric testing was performed using Mann-Whitney tests with Holm-Sidak correction for multiple comparisons when more than two experimental groups were compared. Survival curves were compared by log-rank tests and correlations by Spearman correlation. Statistical analyses were performed in Prism 9 (GraphPad) except bioinformatics analyses which were performed in R. P-values are either stated in figures, or listed as *($p < 0.05$), **($p < 0.01$), *** ($p < 0.001$), ****($p < 0.0001$).

Table 1: Antibodies used for western blotting and immunohistochemistry

Antibody	Dilution	Product reference
Primary antibodies		
rabbit anti-Aldh1a3	I: 1:800 in PBS	Novus Biologicals NBP2-15339
rabbit anti-α-amylase	I: 1:250	MilliporeSigma A8273
mouse anti-glucagon	I: 1:200 in PBS	MilliporeSigma G2654
rabbit anti-glucagon	I: 1:150 in PBS	Cell Signaling Technology 2760S
guinea pig anti-insulin	I: 1:2 or 1:4 in PBS	Agilent Dako IR00261-2
rabbit anti-MafA	I: 1:100 in PBS	Bethyl Laboratories IHC00352
rabbit anti-PC2	I: 1:200 in PBS	Thermo Fisher Scientific PA1-058
rabbit anti-IAPP	I: 1:250 in PBS	BMA Biomedicals T-4145
mouse anti-actin	W: 1:2500 in TBS	MP Biomedicals 0869100-CF
rabbit anti-phospho-eIF2α	W: 1:1000 in TBS	Cell Signaling Technology 3398S
rabbit anti-Grp78(BiP)	W: 1:1000 in TBS	Stressgen Biotechnologies SPA-826
mouse anti- amidated IAPP	W: 1:1000 in TBS	MedImmune F025
rabbit anti-insulin	W: 1:2000 in TBS	Cell Signaling Technology 3014S
rabbit anti-PC1/3	I: 1:500 in PBS W: 1:1000 in TBS	Dr. Lakshmi Devi, Icahn School of Medicine at Mount Sinai
mouse anti-β-tubulin	W: 1:1000 in TBS	Cell Signaling Technology 86298S
Secondary antibodies		
Alexa-488 goat anti-guinea pig	I: 1:250 in PBS	Thermo Fisher Scientific A-11073
Alexa-594 goat anti-guinea pig	I: 1:250 in PBS	Thermo Fisher Scientific A-11076
HRP goat anti-guinea pig	I: 1:250 in PBS	Thermo Fisher Scientific A18769
TRITC goat anti-guinea pig	I: 1:250 in PBS	Thermo Fisher Scientific PA1-28594
Alexa-594 goat anti-mouse	I: 1:250 in PBS	Thermo Fisher Scientific A32742
Alexa-488 goat anti-rabbit	I: 1:250 in PBS	Thermo Fisher Scientific A-11008
Alexa-594 goat anti-rabbit	I: 1:250 in PBS	Thermo Fisher Scientific A-11012
Alexa-647 goat anti-rabbit	I: 1:250 in PBS	Thermo Fisher Scientific A32733
IRDye800CW goat anti-rabbit	W: 1:10 000 in PBS	Li-Cor 926-32211
IRDye680RD goat anti-mouse	W: 1:10 000 in PBS	Li-Cor 926-68070

I: immunohistochemistry, W: western blot

Table 2: Primer sequences for qPCR

Primer	**Sequence (5' - 3')**
Asns F	GGTTTCTGGCTGTGTGTTCAGAAGC
Asns R	AGTGTCCAGGAAGGAAGGGCTCC
Atf4 F	ATGGCGCTCTTCACGAAATC
Atf4 R	ACTGGTCGAAGGGGTCATCAA
Atf6 F	GACTCACCCATCCGAGTTGTG
Atf6 R	CTCCCAGTCTTCATCTGGTCC
Ddit3 F	CTGGAAGCCTGGTATGAGGAT
Ddti3 R	CAGGGTCAAGAGTAGTGAAGGT
Erdj4 F	CGCTGTGGAGAAGCTGCGTC
Erdj4 R	GATTTGTCGCTCTGAGGCAGACT
Grp78 F	ACTTGGGGACCACCTATTCCT
Grp78 R	ATCGCCAATCAGACGCTCC
Herpud1 F	AAGTTCTTCGGAACCTTTCTCCC
Herpud1 R	CCCATACGTTGTGTAGCCAGA
MafA F	AGGAGGAGGTCATCCGACTG
MafA R	CTTCTCGCTCTCCAGAATGTG
Pdia4 F	GTGCTACTGGAGTTCTATGCACCA
Pdia4 R	ATCGATCTTCGCTACAGCAATGG
Rplp0 F	AGATTCGGGATATGCTGTTGGC
Rplp0 R	TCGGGTCCTAGACCAGTGTTC
Trib3 F	CACAGGCACAGAGTACACCTG
Trib3 R	CATGCTGGTGGGTAGGCAGC
Txnip F	GAGTACAAGTTCGGCTTCGAG
Txnip R	ACCCAGTAGTCTACGCAACCA
Xbp1 F	AGCAGCAAGTGGTGGATTTG
Xbp1 R	GAGTTTTCTCCCGTAAAAGCTGA
Xbp1s F	GAGTCCGCAGCAGGTG
Xbp1s R	GTGTCAGAGTCCATGGGA

Chapter 3: Islet amyloid polypeptide is not a tumour suppressor

3.1 Introduction

There is a well-established association between diabetes and cancer. T1D and T2D confers an increased risk of most cancers[143,144] and a worsened prognosis upon cancer diagnosis. Among the largest associations with diabetes is pancreatic cancer with an approximate 2-fold increase in relative risk and increased mortality[143]. Pancreatic ductal adenocarcinoma (PDAC) comprises over 90% of pancreatic cancer cases and has had a persistently low 5-year survival rate over preceding decades. Immense efforts have moved the survival rate to approximately 8% in Canada[145]. Unraveling the mechanisms driving the association between diabetes and PDAC may provide insight into the pathogenesis of PDAC or therapeutic approaches that decrease incidence or improve outcomes in PDAC.

Hyperglycemia, hyperinsulinemia, inflammation, and T2D-associated obesity have all been shown to confer increased PDAC risk in individuals with diabetes[146]. Obesity is associated with an increased risk of pancreatic cancer independently of diabetes[147], and increased tumour fibrosis and decreased survival is observed in a mouse model of PDAC fed a high-fat diet[148]. Hyperinsulinemia and hyperproinsulinemia, as markers of insulin resistance, have been associated with a greater increased risk of PDAC than hyperglycemia or beta-cell dysfunction[149]. Reductions in endogenous insulin are protective in a mouse model of PDAC development suggesting that hyperinsulinemia may increase PDAC risk in diabetes[150]. However, individuals with T1D maintain an elevated risk for PDAC[151] and suggest additional mechanisms beyond hyperinsulinemia and obesity contribute to the association between diabetes and PDAC. It is worth noting that the results of studies investigating T1D and PDAC have heterogeneous findings, likely due to the small population of individuals with both T1D and PDAC which

results in smaller cohort sizes and less robust statistical analysis of associations. Although some studies show no significant association between T1D and PDAC, many studies find up to a 2.5-fold increased relative risk of PDAC in T1D, and most find an increase in the relative risk of developing non site-specific cancer in T1D[144]. Local pancreatic inflammation and systemic hyperglycemia in diabetes may also increase the risk of PDAC. Elevated HbA_{1C} glycation is associated with increased PDAC risk, but this may be partially due to the associated elevations in insulin[149]. Hyperglycemia is thought to drive increased proliferation and migration, reduced apoptosis, and epigenetic alterations that increase tumour growth[152]. Proinflammatory signalling is involved in the initiation of pancreatic neoplasia[153,154], while M2-skewed macrophages are more prevalent and drive growth and fibrosis of later stage neoplasia and tumours[155,156]. Therefore, it is clear that hyperglycemia, hyperinsulinemia, and inflammation all contribute to increased PDAC risk in diabetes, but additional mechanisms likely exist.

The liver, which is exposed to elevated levels of islet-secreted factors via the portal vein, is among the tissues with the highest increase of cancer risk in diabetes (~2.2-fold increase in relative risk). Given the exocrine pancreas and the liver are both exposed to elevated concentrations of islet-secreted factors, alterations in the islet secretome in T1D and T2D may identify additional factors beyond insulin that drive the association between diabetes and cancer.

IAPP, and the non-aggregating synthetic analog pramlintide, were recently reported to have potent anti-tumour activity in mouse p53-deficient thymic lymphomas[127,157]. Pramlintide was able to regress thymic lymphomas in *Trp53*$^{-/-}$ mice with only twice weekly injections for 3 weeks. The authors further showed that IAPP induced apoptosis via an IAPP receptor and downstream inhibition of hexokinase II and glycolysis. The putative receptor for IAPP is a heterodimer consisting of the calcitonin receptor (*CALCR*), a class B GPCR, complexed with one

of 3 identified receptor activity modifying protein (RAMP) family members (RAMP1-3)[158]. RAMPs are a single-pass transmembrane protein which alter the ligand specificity of CALCR and increase the affinity of the receptor for IAPP over calcitonin[159]. Two splice variants, 'a' and 'b', exist in human CALCR differing only by the presence of a 16 amino acid insert in an intracellular loop of the $CALCR_b$ variant[160]. In total there are six IAPP receptors generated from two CALCR variants and their interaction with one of three RAMPs. All six receptors signal predominantly through $G_{\alpha s}$-coupled mechanisms, mediating downstream signalling by activation of adenylyl cyclase and elevation of intracellular cAMP levels, but can also signal through other G proteins depending on the RAMP and cell type[161]. Increased intracellular cAMP drives downstream signalling through two predominant mechanisms[162]: (i) activation of protein kinase A (PKA)[163]; and (ii) activation of exchange proteins activated by cAMP (EPAC)[164,165]. cAMP signalling in PDAC has been shown to reduce proliferation in cell lines[166] and accelerate tumour growth in mouse models of PDAC[167], highlighting the complexity and duality of cAMP signalling in PDAC.

Human IAPP (hIAPP) readily aggregates and forms amyloid, while rodent IAPP (rIAPP) does not form amyloid under physiological conditions despite sharing 84% sequence homology. Three proline substitutions at positions 25, 28, and 29 drive the reduced amyloidogenicity in rIAPP and are the basis of the synthetic analog pramlintide (Figure 1A). Both rIAPP and pramlintide are capable of binding and signalling at the human IAPP receptors[158]. Salmon calcitonin is an agonist of IAPP receptors, with slightly weaker affinity than IAPP or pramlintide, and is a potent agonist of non-RAMP complexed human CALCR. Davalintide is an IAPP-mimetic peptide with sequence homology to salmon calcitonin and IAPP that was developed in an attempt to produce an IAPP receptor agonist with prolonged circulating half-

life[168]. Although davalintide was found to have a similar potency and circulating half-life to IAPP, it has enhanced duration of signalling which is attributed to its reduced dissociation rate from IAPP receptors[169]. Importantly the N-terminal region is highly similar in IAPP receptor-stimulating ligands – a region thought to drive signalling after ligand binding to class B GPCRs[170]. Fitting with this signalling mechanism, IAPP receptor competitive antagonists are generated from calcitonin lacking the 7 N-terminal residues[171].

In this chapter I investigate the role of IAPP signalling in PDAC to determine if loss of IAPP confers a fraction of the increased pancreatic cancer risk in diabetes. Building on previous literature in which IAPP stimulates apoptosis, and inhibits proliferation and glycolysis[127], I assess apoptosis, proliferation, and glycolysis in PANC-1 and H1299 cells. PANC-1 was chosen as the pancreatic cell line for two reasons: (ii) detectable expression of *CALCR* and *RAMP3* in a microarray dataset (GSE8332)[172]; and (ii) loss of wild-type p53 expression as PANC-1 cells display both copy loss and $TP53^{R273H}$ expression[173,174]. H1299 is a lung non-small cell carcinoma line that was chosen for further analysis given its p53-null status and previously reported sensitivity to pramlintide and IAPP[127]. To study the role of endogenous IAPP in PDAC development and progression, I also generated an $Iapp^{-/-}$ mouse model of PDAC.

3.2 Results

3.2.1 IAPP does not impact glycolysis, proliferation, or cell death in PANC-1 cells

Time-lapse microscopy allows for high resolution kinetic studies of cell death and proliferation under standard incubation (5% CO_2 and 37°C) conditions. The membrane-permeable nuclear dye Hoechst 33342 labels all nuclei while the membrane-impermeable nuclear dye propidium iodide (PI) labels only the nuclei of dead cells with fragmented membranes. Using this approach, we treated PANC-1 cells with 0.25, 2.5, or 25 μM rIAPP,

pramlintide, or davalintide in complete growth media (25 mM glucose and 10% FBS supplemented DMEM) or low-glucose low-FBS media (LGLF media; 2.5 mM glucose and 0.1% FBS supplemented DMEM). Treatment of PANC-1 cells with 0.25 -25 μM rIAPP, pramlintide, or davalintide did not alter proliferation (Figure 1F) or cell death (Figure 1G) after 50 hours in either complete or LGLF media, while cycloheximide (protein synthesis inhibitor) and gemcitabine (chemotherapeutic nucleoside analog) blocked proliferation and induced cell death. There were also no kinetic differences observed in cell death or proliferation with rIAPP, pramlintide, or davalintide when examining growth and death curves (Figure 1B-E) and when quantifying by area under the curve (Figure 1H, I). These findings demonstrate that IAPP does not induce cell death or inhibit proliferation in PANC-1 cells.

To measure the effect of IAPP on PANC-1 glycolysis, the extracellular acidification rate (ECAR) of PANC-1 cells in response to glucose was measured using a Seahorse XFe96 Analyzer. PANC-1 cells were cultured for 48 h in the presence of 0.25-25 μM pramlintide, or 2.5-25 μM rIAPP or davalintide in complete or LGLF growth media prior to analysis. Glycolysis was measured as the change from basal ECAR to glucose-stimulated ECAR. Treatment of PANC-1 cells for 48 h with pramlintide, rIAPP and davalintide did not alter basal or glucose-stimulated ECAR (Figure 2). This finding demonstrates that IAPP does not alter glycolysis in PANC-1 cells.

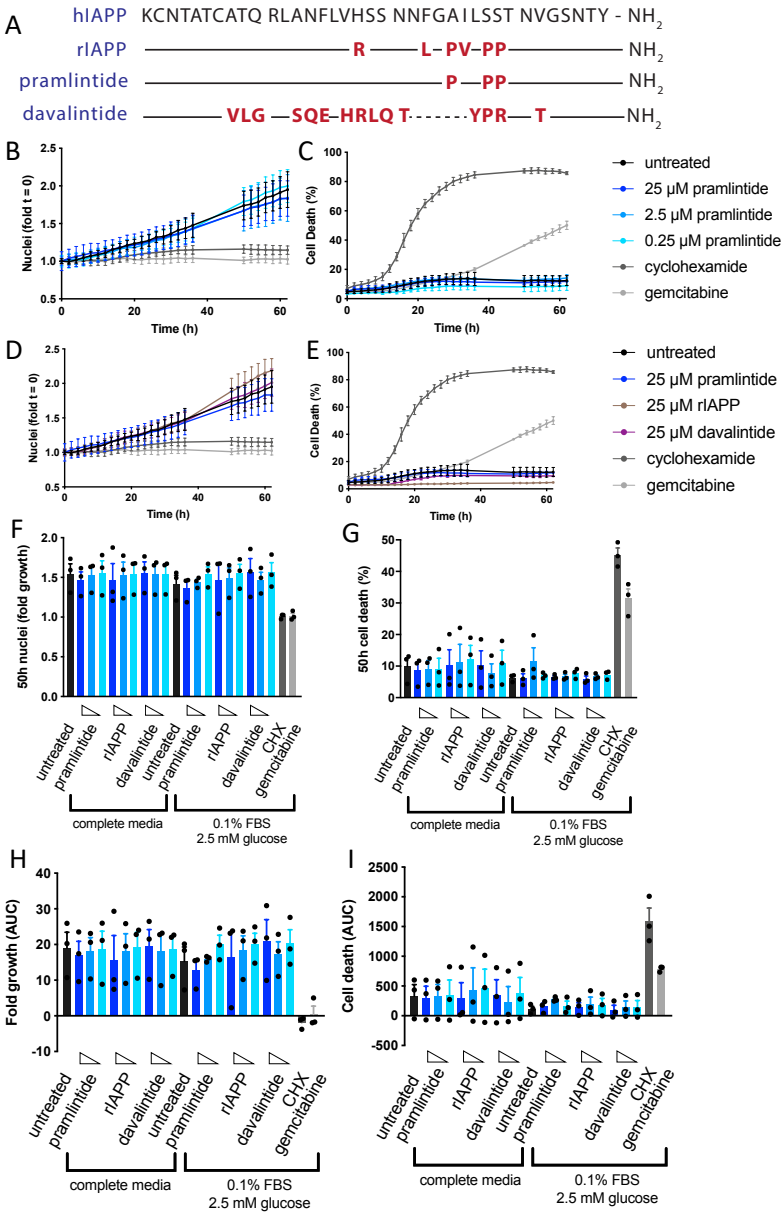

Figure 1: IAPP does not alter cell death or proliferation in the PANC-1 cell line.
(A) Sequence alignments of mature human IAPP (hIAPP), murine IAPP (rIAPP), and the analogs pramlintide and davalintide. All peptides are amidated at the C-terminus. **(B-E)** Representative plots showing proliferation and cell death of PANC-1 cells in complete growth media (25 mM glucose and 10% FBS supplemented) in response to a range of pramlintide concentrations (B,C), or to the highest concentration (25 µM) of each peptide (D,E). Error bars represent SD of technical replicates. **(F,G)** Quantification of 3 independent proliferation and cell death experiments of PANC-1 cells after 50 h incubation with 25 µM (dark blue), 2.5 µM (blue), or 0.25 µM (light blue) rIAPP, pramlintide, or davalintide in either complete growth media or reduced glucose and FBS media. **(H,I)** Alternate quantification of proliferation and cell death by area under the curve (AUC) from 0-50 h. n = 3; error bars represent SD. CHX, cycloheximide (1 mg/mL). Gemcitabine (5 µg/mL).

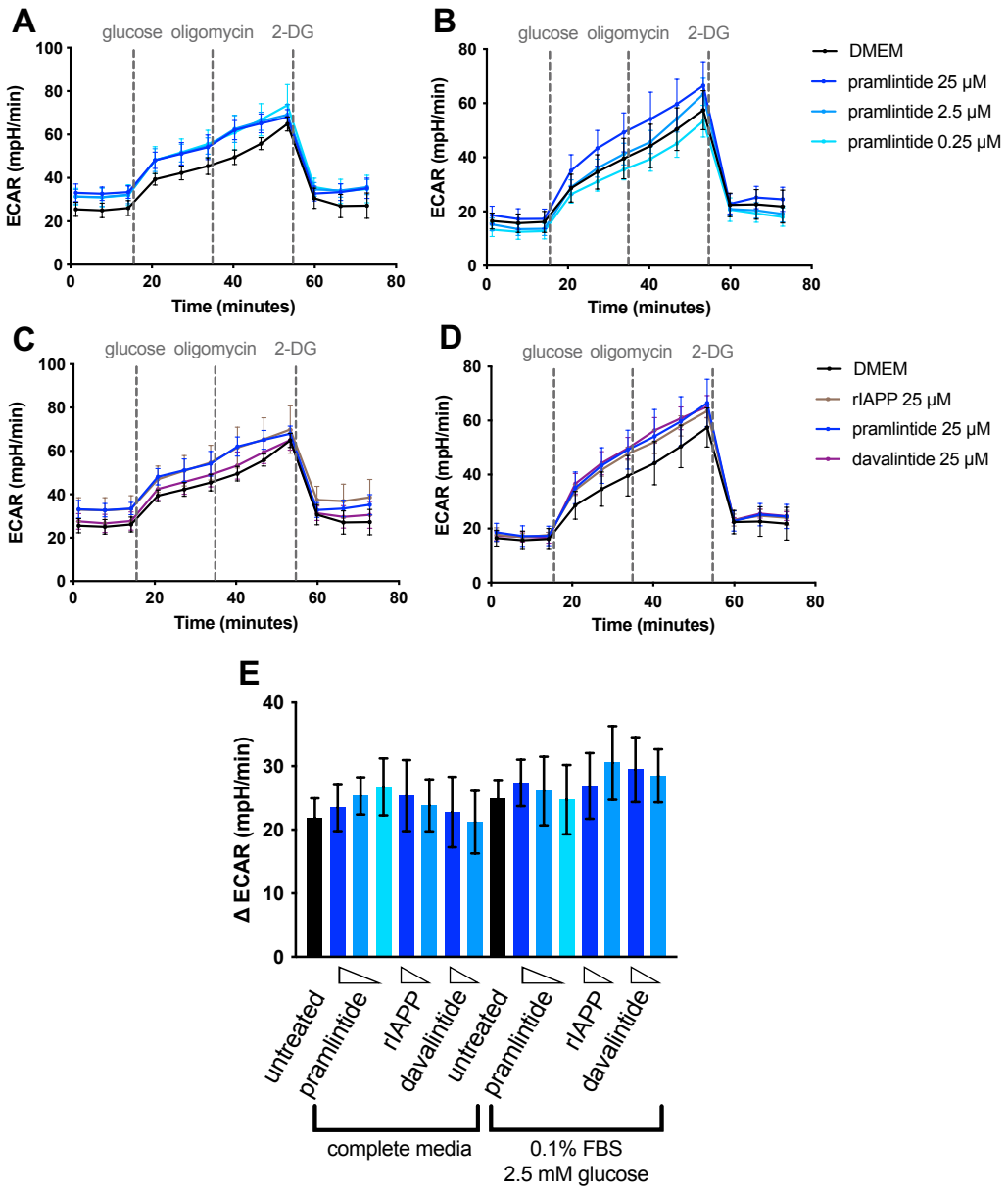

Figure 2: IAPP does not inhibit glycolysis in PANC-1 cells.
(A,B) Representative extracellular acidification rate (ECAR) plots of PANC-1 cells cultured with pramlintide (0.25-25 µM) for 48 h in either complete growth media (A; 25 mM glucose and 10% FBS) or reduced FBS and glucose media (B; 2.5 mM glucose and 0.1% FBS) prior to analysis on a Seahorse XFe96 Analyzer. Error bars represent SD of 5-7 technical replicates. **(C,D)** Representative ECAR plots in PANC-1 cells cultured with pramlintide, rIAPP, or davalintide (25 µM) for 48 h in either complete (C) or reduced glucose and FBS growth media (D) as described in A,B. Error bars represent SD of 5-7 technical replicates. **(E)** Quantification of glycolysis in n = 4 individual experiments with 25 µM (dark blue), 2.5 µM (blue), or 0.25 µM (light blue) pramlintide, rIAPP, or davalintide as indicated. Error bars represent SD.

3.2.2 IAPP does not impact glycolysis, proliferation, or cell death in H1299 cells

PANC-1 cells are not a true TP53-null cell line and contain one R273H mutant allele[174]. Given the lack of IAPP-induced cell death and inhibition of glycolysis and proliferation in PANC-1 cells, I sought to test IAPP actions in a true TP53-null cell line. H1299 cells were chosen due to previously reported sensitivity to IAPP and complete loss of P53 protein[15]. H1299 cells were treated similarly to PANC-1 cells with 0.25 -25 μM pramlintide, rIAPP, or davalintide in complete or LGLF media. After 48 h culture, rIAPP, pramlintide, and davalintide had no impact on H1299 cell number (Figure 3E) or death (Figure 3F) in either complete or LGLF media. Quantifying cell death and proliferation over 48 h by AUC (Figure 3G,H), and inspection of growth and death curves (Figure 3A-D) revealed no kinetic differences of rIAPP, pramlintide, or davalintide on cell death and proliferation. Cycloheximide induced approximately 50% cell death and inhibited H1299 proliferation, while gemcitabine inhibited proliferation with no increase in cell death over 48 h. These results show that time-lapse microscopy effectively detects alterations in cell proliferation and death, and that IAPP analogs do not impact H1299 cell proliferation or death in nutrient-deplete or -replete conditions.

The effects of IAPP signalling on glycolysis were further assessed in H1299 cells. H1299 cells were treated with pramlintide, rIAPP, and davalintide in complete or LGLF media for 48 h prior to analysis on a Seahorse XFe96 Analyzer. Pramlintide, rIAPP, and davalintide had no effect on H1299 glycolysis at any concentration in either media condition (Figure 4), demonstrating that IAPP does not inhibit glycolysis in H1299 cells. Collectively, with the data in PANC-1 cells, these data suggest that IAPP does not induce cell death, or inhibit proliferation or glycolysis in TP53-null or $TP53^{R273H/-}$ cancer cells.

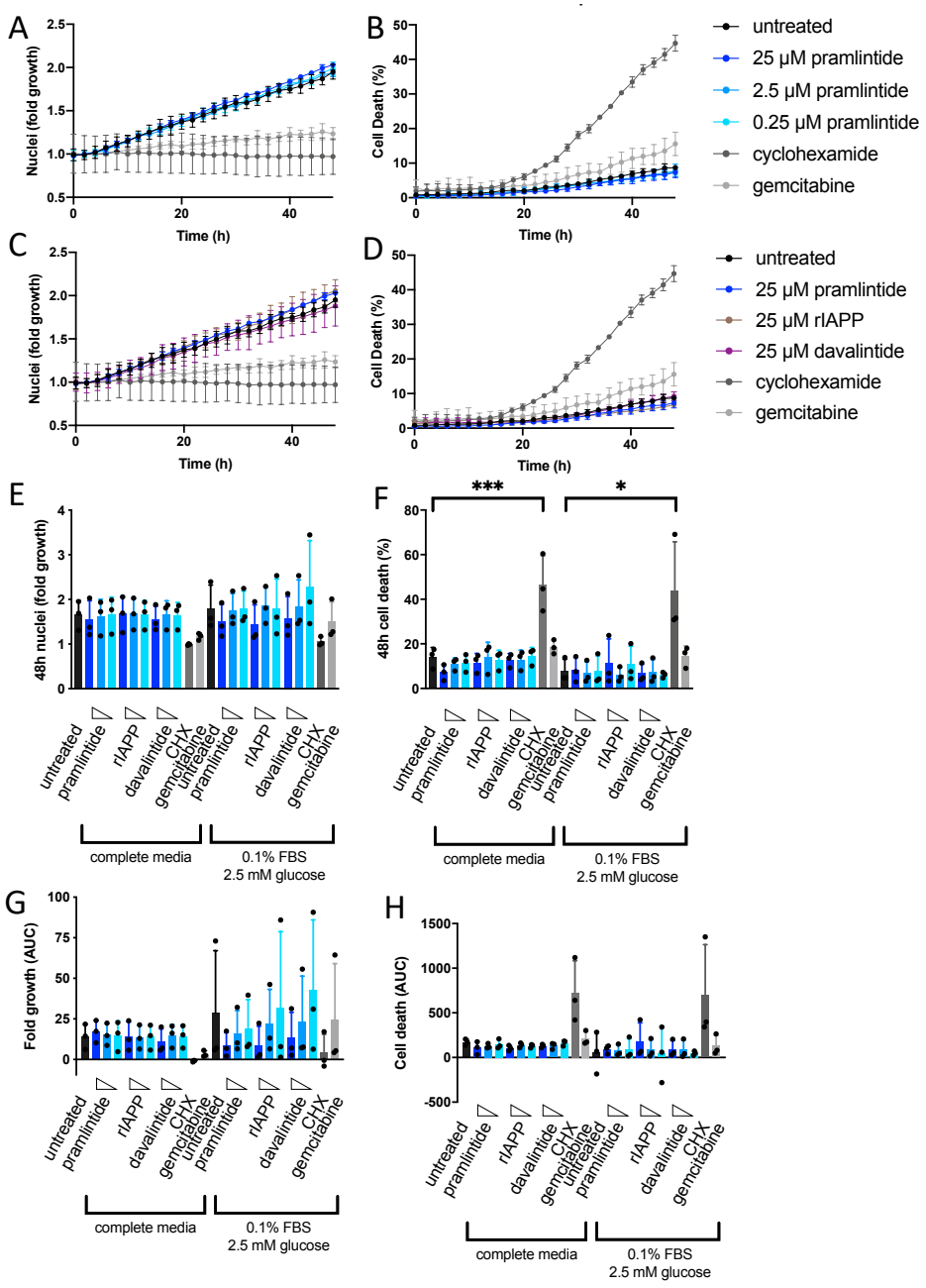

Figure 3: IAPP does not alter cell death or proliferation in the H1299 cell line.
(A-D) Representative plots showing proliferation and cell death of H1299 cells in complete growth media (25 mM glucose and 10% FBS supplemented) in response to a range of pramlintide concentrations (A,B), or to the highest concentration (25 μM) of each peptide (C,D). Error bars represent SD of technical replicates. **(E,F)** Quantification of 3 independent proliferation and cell death experiments of H1299 cells after 48 h incubation with 25 μM (dark blue), 2.5 μM (blue), or 0.25 μM (light blue) rIAPP, pramlintide, or davalintide in either complete growth media or reduced glucose and FBS media. **(G,H)** Alternate quantification of proliferation and cell death by area under the curve (AUC) from 0-48 h. n = 3; error bars represent SD. CHX, cycloheximide (0.5 mg/mL). Gemcitabine (5 μg/mL).

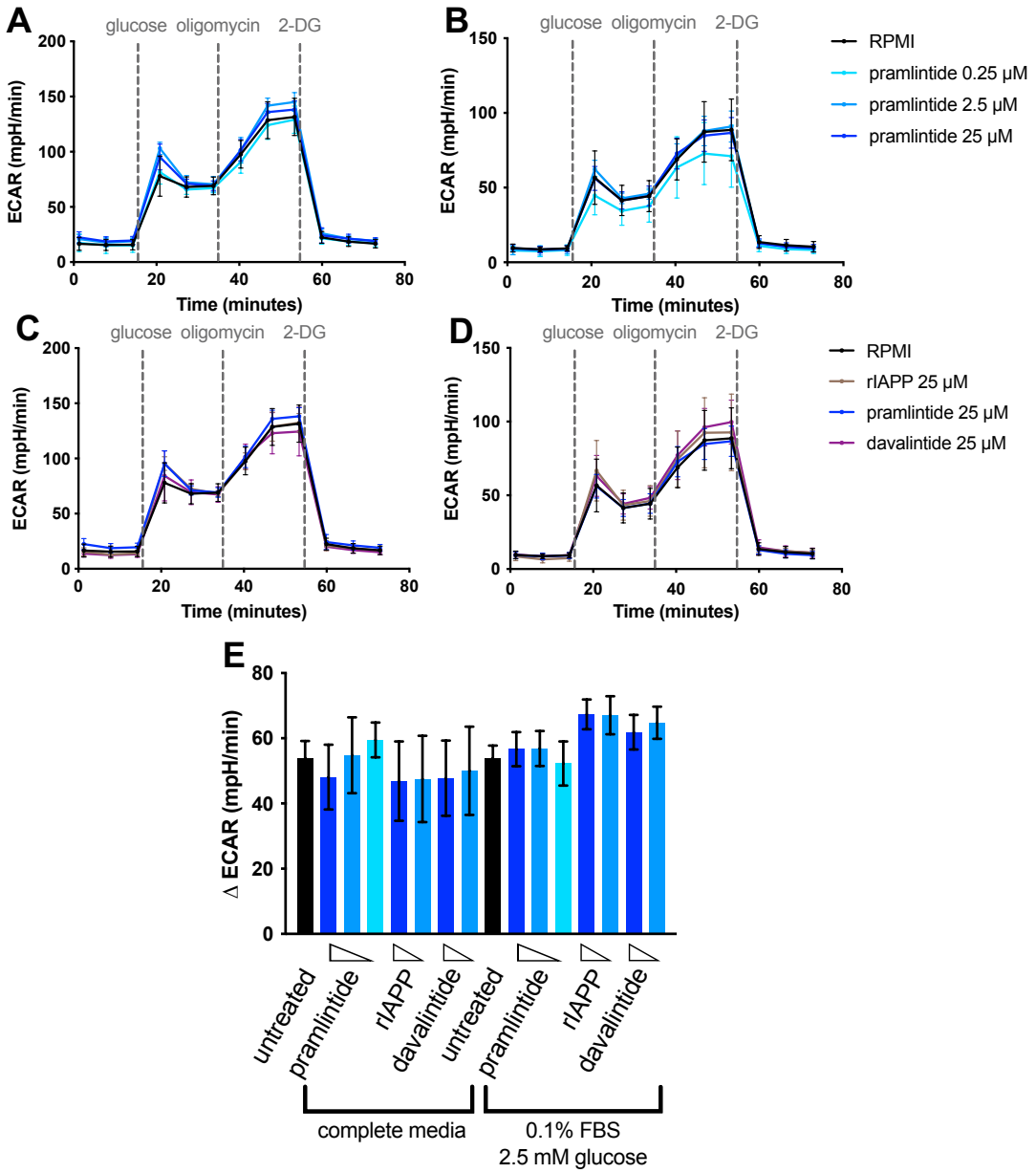

Figure 4: IAPP does not inhibit glycolysis in H1299 cells.
(A,B) Representative extracellular acidification rate (ECAR) plots of H1299 cells cultured with pramlintide (0.25-25 µM) for 48 h in either complete growth media (A; 25 mM glucose and 10% FBS) or reduced FBS and glucose media (B; 2.5 mM glucose and 0.1% FBS) prior to analysis on a Seahorse XFe96 analyzer. Error bars represent SD of 5-7 technical replicates. **(C,D)** Representative ECAR plots in PANC-1 cells cultured with pramlintide, rIAPP, or davalintide (25 µM) for 48 h in either complete (C) or reduced glucose and FBS growth media (D) as described in A,B. Error bars represent SD of 5-8 technical replicates. **(E)** Quantification of glycolysis in n = 4 individual experiments with 25 µM (dark blue), 2.5 µM (blue), or 0.25 µM (light blue) pramlintide, rIAPP, or davalintide as indicated. Error bars represent SD.

3.2.3 Pramlintide is biologically active in an IAPP receptor bioassay

To confirm the biological activity of our peptide preparations, we generated an IAPP receptor activity bioassay (HEK-CRE-hCALCR-hRAMP3 cells; Section 2.6). IAPP receptor activation in the HEK-CRE-hCALCR-hRAMP3 cell line drives adenylyl cyclase activation, increased intracellular cAMP, CREB activation, and luciferase production (Figure 5A). Pramlintide stimulated luciferase production with a sigmoidal dose-response and an EC_{50} of 6.8 nM (Figure 5B), in agreement with reported EC_{50} values of rIAPP at the $CALCR_a$-RAMP3 receptor ranging from approximately 0.1 - 10 nM[158]. To confirm the sensitivity of our live imaging technique to detect cell death, PANC-1 cells were treated with 0.01-100 µg/mL gemcitabine (Figure 5C). PANC-1 cells displayed a concentration-dependent response to gemcitabine-induced cell death. These data collectively suggest that our peptide preparations are biologically active, and our approaches are sufficiently sensitive to detect dynamic differences in cell death.

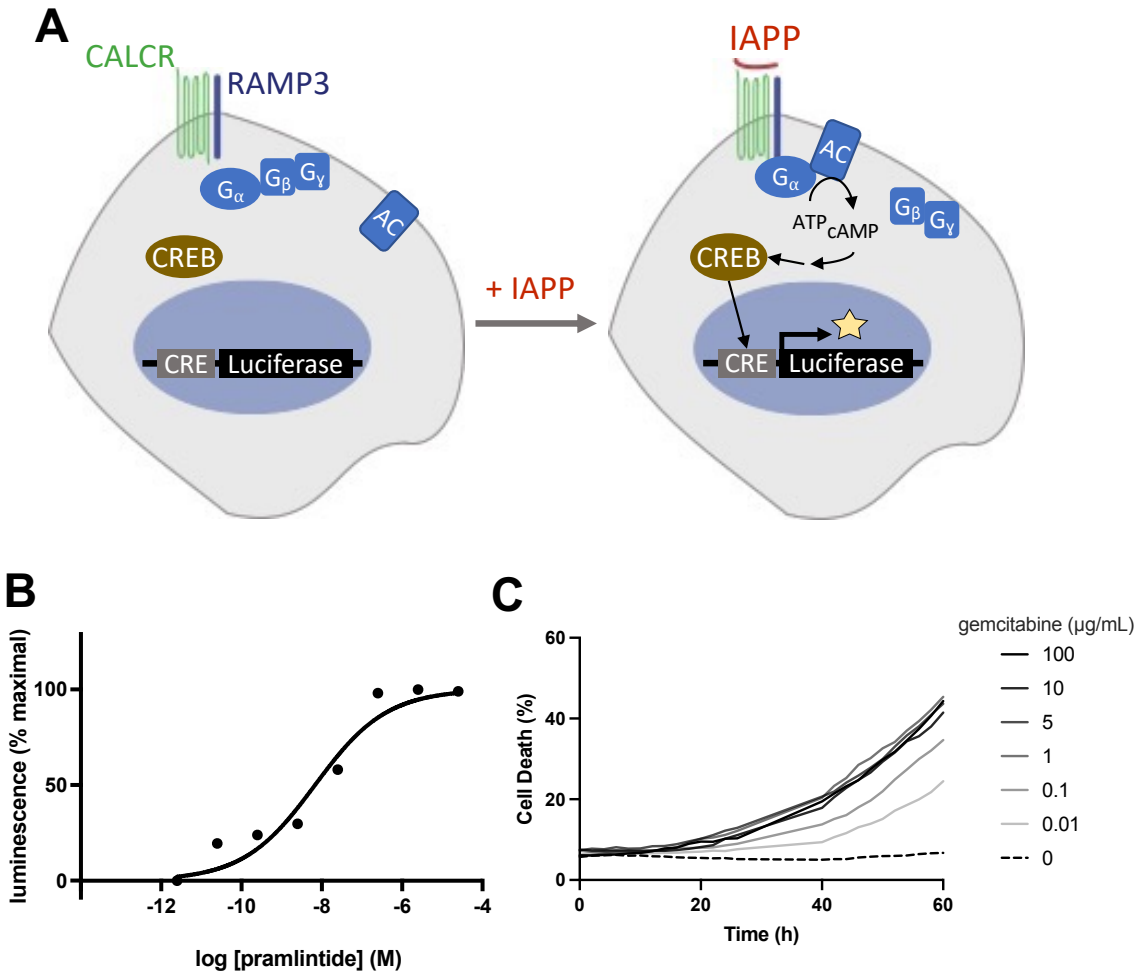

Figure 5: Pramlintide preparations are biologically active and cell death detection is sensitive.

(A) Schematic depicting the IAPP-receptor activity bioreporter assay we developed in which a HEK293 CRE-luciferase cell line was stably transfected with a construct containing human *CALCR* and *RAMP3* under the control of a bi-directional promoter (HEK293-CRE-Bi-CALCR-RAMP3 cells). **(B)** Representative experiment with pramlintide in HEK293-CRE-Bi-CALCR-RAMP3 cells. Pramlintide elicited a sigmoidal concentration-response curve with an EC_{50} of 6.8 nM. Points represent the mean of technical triplicates. **(C)** PANC-1 cells were treated with 0.01-100 µg/mL gemcitabine and a concentration-dependent response in cell death was observed using time-lapse microscopy with Hoechst 33342 and propidium iodide labelling.

3.2.4 IAPP deletion has no effect on survival in a mouse model of PDAC

To investigate the role of IAPP in PDAC development and progression in vivo we developed an IAPP-deficient mouse model of PDAC (*Iapp*$^{-}$ *Kras*$^{LSL\text{-}G12D}$ / *Iapp*$^{-}$ *Kras*$^{+}$; *Trp53*$^{flox/flox}$; *Ptf1a*$^{+/CreERTM}$) and monitored survival. In this model, tamoxifen administration initiates recombination in *Ptf1a*-expressing acinar cells. This results in acinar-cell-specific loss of the tumour suppressor *Trp53* and induction of oncogenic *Kras*^{G12D} by excision of a floxed stop cassette in the *Kras*$^{LSL\text{-}G12D}$ allele. A careful breeding scheme was designed to ensure both *Iapp*-null and wild-type animals were generated from the same breeders (see Methods and Materials section 2.1.2), as *Iapp* and *Kra*s are closely linked by ~3.5 cM on mouse chromosome 6 (Figure 6). Subcutaneous tamoxifen injection at 4-5 weeks of age resulted in the development of fibrotic pancreatic tumours (Figure 6). *Iapp*-null and wild-type mice displayed no difference in survival (Figure 7A), with median survival times of 23.5 weeks in *Iapp*$^{+/+}$ and 26 weeks in *Iapp*$^{-/-}$ mice expressing *Kras*$^{LSL\text{-}G12D/+}$; *Trp53*$^{flox/flox}$; *Ptf1a*$^{CreERTM/+}$. Study endpoint (survival) was determined using a scoring chart for signs of illness in mice that included breathing, hydration, posture, appearance, and body weight (Appendix A). Body weight loss as an endpoint occurred for almost all mice, and macroscopic pancreatic tumours were confirmed by necropsy. Macroscopic tumours were not observed in *Ptf1a*$^{+/+}$ mice. Stratification of mice by sex revealed no sex-specific differences in survival in *Iapp*$^{+/+}$ and *Iapp*$^{-/-}$ mice (Figure 7B). Importantly, no differences in glycemia (Figure 7C) or body weight (Figure 7D) were observed in animals prior to the onset of the first lethal tumour burden at 12 weeks post-tamoxifen. Tumour and pancreas histology show similar tumour morphologies with extensive fibrosis and necrosis regardless of *Iapp* genotype (Figure 7E). These data demonstrate that endogenous IAPP in the pancreas does

not inhibit tumour proliferation, and the lack of IAPP does not accelerate the growth of pancreatic tumours in mice.

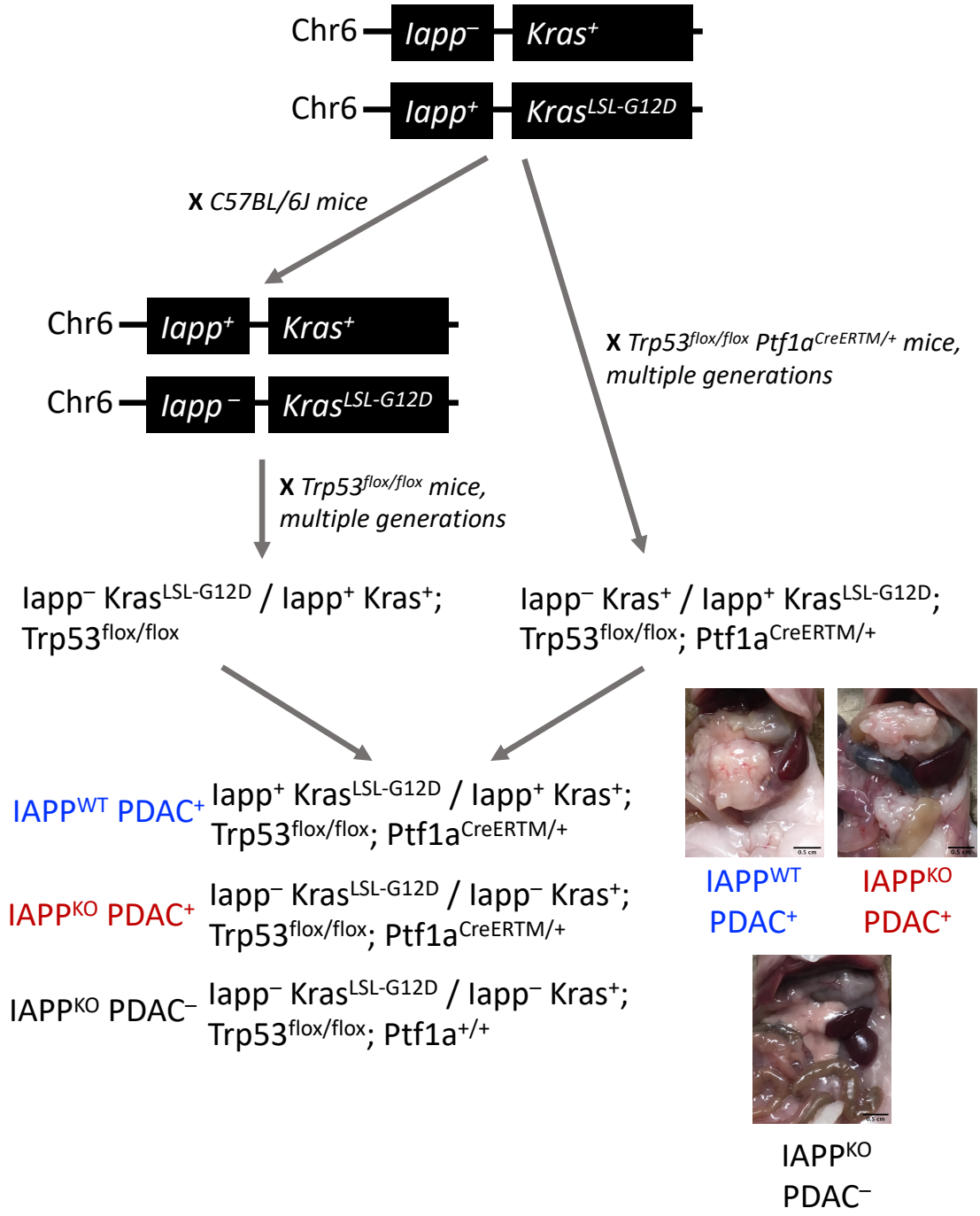

Figure 6: Generation of an IAPP-deficient pancreatic ductal adenocarcinoma model in mice.

Iapp⁻ Kras⁺ / Iapp⁺ Kras$^{LSL-G12D}$ were generated and crossed to C57BL6J mice to generate a recombinant *Iapp⁻ Kras$^{LSL-G12D}$ / Iapp⁺ Kras⁺* mouse. Recombinant and non-recombinant Iapp-Kras mice were then crossed to *Trp53$^{flox/flox}$ Ptf1a$^{CreERTM/+}$* mice for multiple generations and intercrossed to generate an Iapp-deficient mouse model of pancreatic ductal adenocarcinoma (PDAC). After tamoxifen-induced recombination, mice developed lethal PDAC tumours with survival times as indicated in Figure 7.

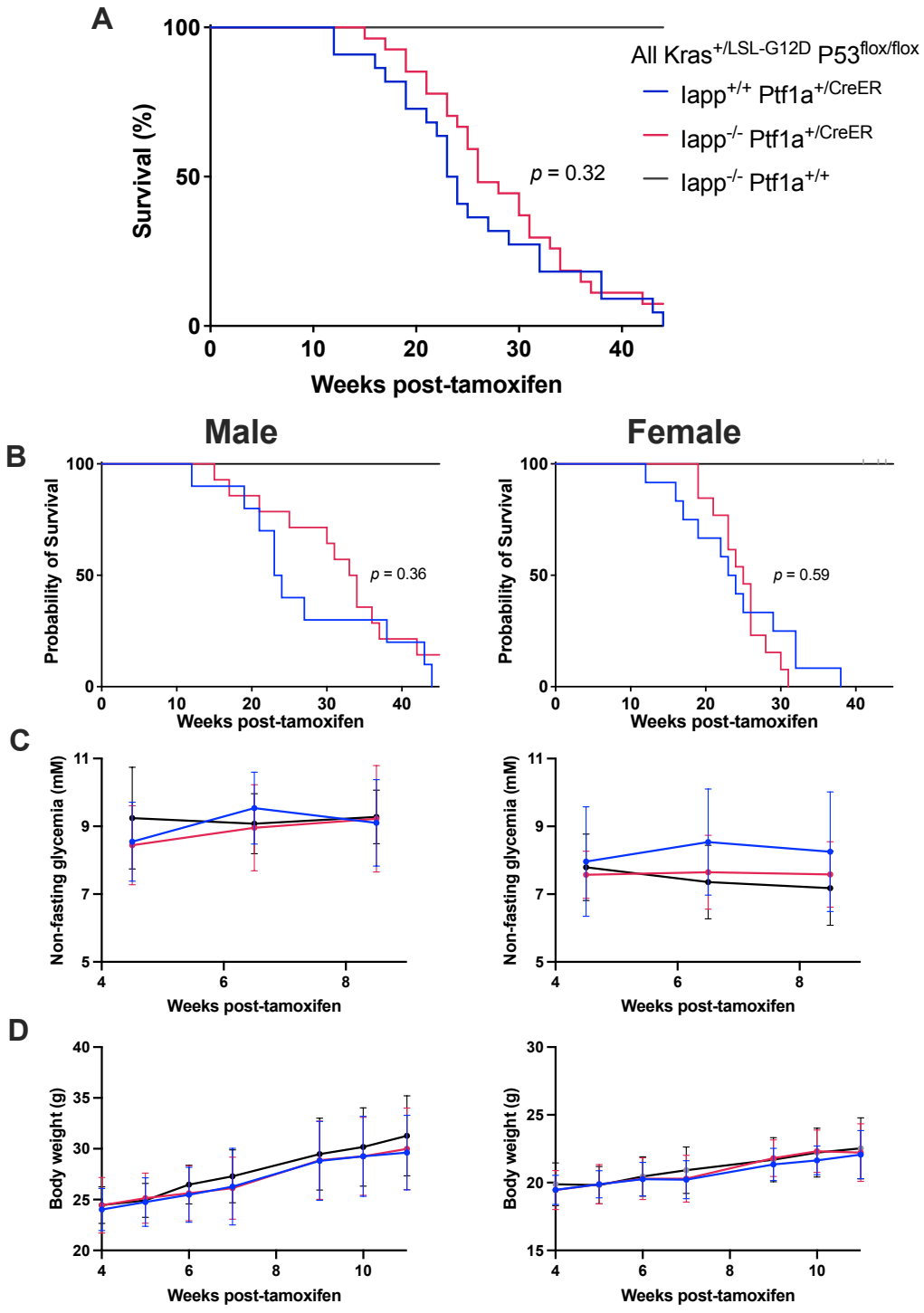

Figure 7: Physiological IAPP levels do not impact survival in a mouse model of pancreatic ductal adenocarcinoma.
(Figure legend on following page)

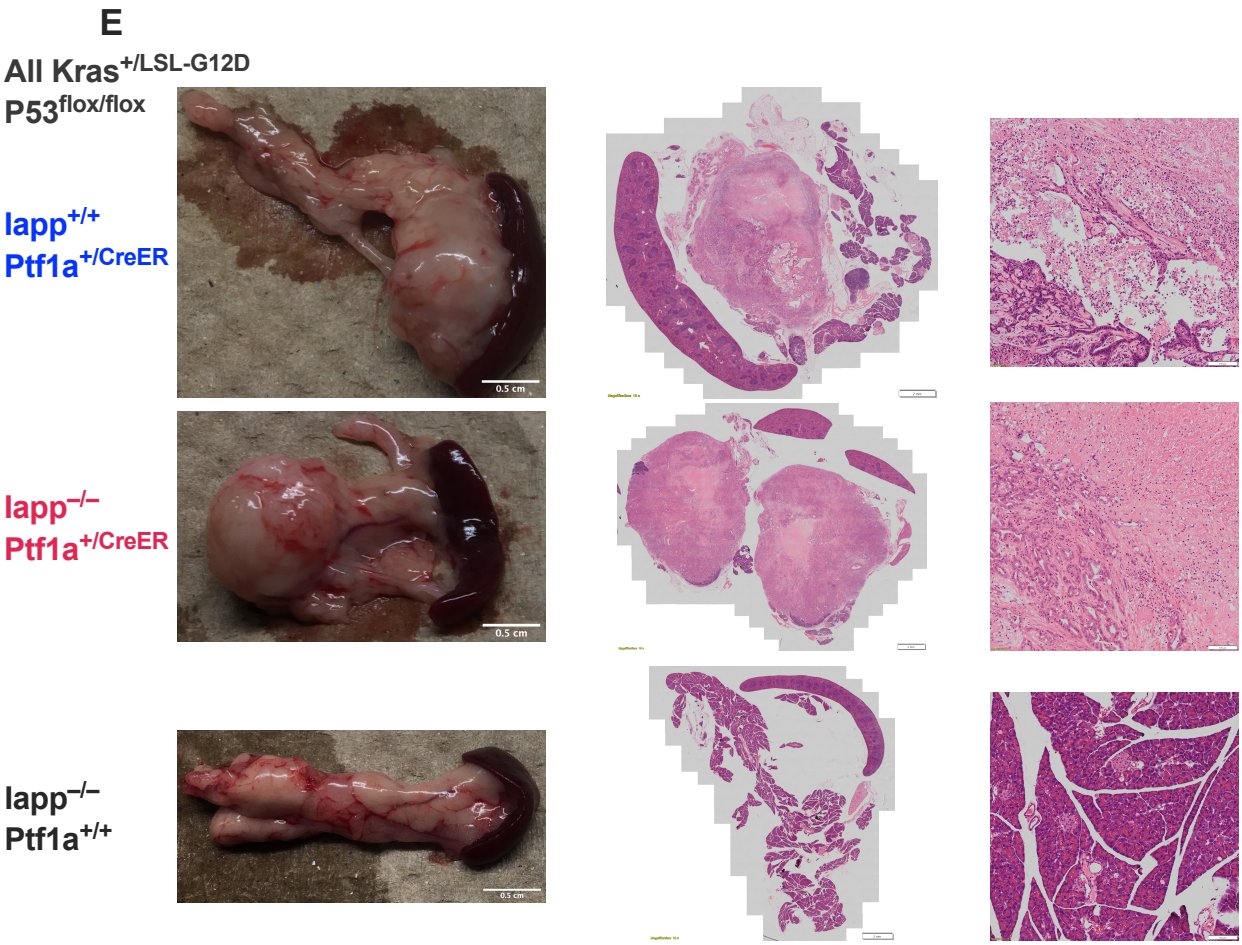

Figure 7 (cont.): Physiological IAPP levels do not impact survival in a mouse model of pancreatic ductal adenocarcinoma. (A) *Iapp*$^{-}$ *Kras*$^{LSL\text{-}G12D}$ */ Iapp*$^{-}$ *Kras*$^{+}$*; Trp53*$^{flox/flox}$*; Ptf1a*$^{+/CreER}$ and *Iapp*$^{+}$ *Kras*$^{LSL\text{-}G12D}$ */ Iapp*$^{+}$ *Kras*$^{+}$*; Trp53*$^{flox/flox}$*; Ptf1a*$^{+/CreER}$ mice develop lethal PDAC tumour burdens with comparable median survival times of 26 and 23.5 weeks post-tamoxifen, respectively (n = 22, 27). Tamoxifen was administered via 3 subcutaneous injections over 5 days beginning at P28-39. **(B)** IAPP-deficiency did not result in sex-specific impacts on PDAC survival. **(C)** Random-fed glycemia and **(D)** body weight were not impacted by IAPP-deficiency in PDAC male or female mice prior to the development of lethal tumour burdens. **(E)** Large pancreatic tumours with fibrosis and necrosis occur in *Kras*$^{+/LSL\text{-}G12D}$*; Trp53*$^{flox/flox}$*; Ptf1a*$^{+/CreER}$ mice with and without IAPP loss.

3.3 Discussion

Our data do not support a role for IAPP as a tumour suppressor in PDAC. For the PANC-1 cell line, IAPP did not inhibit or promote proliferation, apoptosis, or glycolysis. Further, IAPP did not have any effect on the proliferation or death of, or glycolysis in H1299 cells, which have previously reported IAPP sensitivity[127]. The discrepancy between our observations and those reported by Venkatanarayan et al.[127] are challenging to reconcile given they observed rates of apoptosis exceeding 70% in H1299 cells in response to pramlintide. Differences in peptide preparation may cause discrepant findings. However, we generated a bioassay and confirmed the biological activity of our pramlintide preparations. We further confirmed the sensitivity of our time-lapse microscopy approach to detect differing PANC-1 cell death rates in response to varying gemcitabine concentrations. The pramlintide, rIAPP, and davalintide concentrations used in our studies (0.25-25 μM) and by Venkatanarayan et al.[127] (2.5 μM) are approximately 1000-fold above the reported EC_{50} values for IAPP and IAPP-mimetic peptides at the IAPP receptor (0.1-10 nM)[158], and the micromolar concentrations may be sufficiently high to activate other receptors such as the calcitonin receptor-like receptor (CRLR)[175,176]. This may account for the lack of effect in PANC-1 cells if off-target signalling pathways are activated, but it cannot explain the lack of effect we observed in H1299 cells as comparable pramlintide concentrations were used. Rodent IAPP can form small aggregates, but not fibrils, at concentrations of 7.5 μM[177] and 50 μM[178], raising the possibility that Venkatanarayan et al.[127] observed aggregate-induced H1299 cell death in their preparations while our lyophilized peptide preparations have reduced rIAPP aggregation and no cell death.

Culture conditions during peptide treatment may partially explain the disagreement between our findings and those previously reported[127]. HEK-293 cells transfected to stably

overexpress CALCR have a proliferative block in culture medium containing 10% fetal calf serum (FCS) with no evidence of cell death[179]. However, in 0.5% FCS media, the HEK-293 CALCR overexpressing cells exhibit calcitonin-induced cell death[179,180]. If IAPP-induced cell death is dependent on CALCR-driven elevations of cAMP and downstream PKA signalling, the environmental conditions are likely key to IAPP's ability to induce cell death. PKA acts as a kinase for over 200 target peptides[181] – the expression of which, and thus the effects of PKA signalling, may highly depend on a cell's environmental stimuli and the availability of PKA targets in given culture conditions. We tested the effects of IAPP-mimetics in both nutrient-replete, standard growth conditions (10% FBS and 25 mM glucose), and nutrient-deplete (0.1% FBS, 2.5 mM glucose) conditions and observed no effect of IAPP signalling in H1299 and PANC-1 cells. The lack of IAPP-induced effects in both cell lines in either media conditions suggest that any anti-proliferative or pro-apoptotic effects of IAPP-mimetics in cancer may occur only in a very select set of culture conditions, rendering it unlikely to provide a therapeutic benefit.

There are limited studies on IAPP, or IAPP mimetics, in cancer. Venkatanarayan et al.[127,157] have demonstrated in two studies that tumour-produced IAPP (in response to deletion or knockdown of ΔNp63 or ΔNp73) and exogenous pramlintide have strong anti-tumour effects in TP53-null cancers, including regression of TP53-null thymic lymphomas. Pramlintide has also been shown to reduce the viability of two colorectal cancer cell lines, HCT-116 (TP53 wild-type) and HT-29 ($TP53^{R273H}$)[182]. Although HT-29 had a larger reduction in viability in response to pramlintide, HCT-116 also displayed reduced viability in response to pramlintide[182] suggesting IAPP's anti-proliferative effects may not depend on TP53 status. IAPP was also found to act as an anti-proliferative factor in a lentiviral shRNA screen of cells in oncogene-induced senescence

(OIS)[183]. IAPP knockdown increased the proliferation of cells in OIS, which was partially rescued with exogenous IAPP. IAPP had no effect on cells lacking OIS, suggesting IAPP's anti-proliferative actions are restricted to only a subset of cellular states – a finding similar to that of Evdokiou et al.[179] that observed calcitonin-induced cell death only in reduced FCS media.

IAPP was also found among the top 5 most downregulated genes in human PDAC relative to tumour-adjacent tissue[184]. Although this finding may be interpreted as IAPP loss permitting growth of PDAC, it is also an expected observation since IAPP expression is much higher in pancreatic islets than tumour-adjacent tissue, and is normally expressed at very low levels in acinar and ductal cells[185]. Using TCGA data, Li et al.[184] also showed increased survival of PDAC patients with high IAPP expression relative to those with low IAPP expression. Well-differentiated PDAC has been found to display an increased incidence of intratumoural endocrine cells relative to poorly-differentiated PDAC, which may explain the association between IAPP and survival in the TCGA cohort[186]. Further analysis of IAPP and endocrine gene expression is unfortunately confounded by the low tumour content (mean ~ 35%) of PDAC specimens in the TCGA cohort, where IAPP expression and biopsy tumour content are negatively correlated (data not shown). Therefore, the IAPP-high PDAC patient group in the TCGA cohort is also a tumour content-low group for biopsies, which may be reflective of the patient tumour size and prognosis. It does however raise the question of whether high tumour-adjacent IAPP expression may restrict PDAC tumour volume. Our findings in mice and cell lines suggest otherwise though: that IAPP does not influence tumour growth in PDAC.

Although IAPP has not been studied extensively in cancer, signalling by CALCR and the closely related CRLR has been studied extensively with calcitonin and adrenomedullin as ligands that have been found to both inhibit and promote proliferation. Below, I briefly describe some of

the existing evidence for CALCR and CRLR signalling via cAMP as both a pro- and anti-tumour signal.

Overexpression of CALCR decreases cell attachment and increases apoptosis in HEK-293 cells (TP53 wild-type)[180]. Calcitonin was also found to stimulate cAMP production and reduce ERK1/2 phosphorylation in MDA-MB-231 (breast adenocarcinoma cell line; $TP53^{R280K}$) cells[187]. The authors further showed that calcitonin injected subcutaneously to nude mice also reduced the growth of transplanted MDA-MB-231 tumours, while calcitonin had no effect on tumours derived of transplanted MCF-7 cells (breast adenocarcinoma cell line; TP53 wild-type). Ng et al. [188] demonstrated a dual response to calcitonin in T-47D cells (breast carcinoma cell line; $TP53^{L194F}$). Over a short 1-day incubation, calcitonin drove increased DNA synthesis and cell numbers in T-47D cells, but decreased cell numbers over 7-day cultures. Calcitonin was further able to inhibit both insulin- and EGF-induced proliferation in T-47D cells, while IBMX, a phosphodiesterase inhibitor that raises intracellular cAMP levels, had no effect on proliferation. This suggests additional signalling mechanisms beyond $G_{\alpha s}$-coupled CALCR signalling is required for the antiproliferative effects of calcitonin in T-47D cells. Calcitonin has also shown differential responses in cell lines derived from prostate carcinomas and adenocarcinomas – calcitonin reduces proliferation in DU145 ($TP53^{P223L,\ V274F}$) and PC-3 ($TP53^{null}$) cells and increases proliferation in LNCaP cells (TP53 wild-type)[189]. Forskolin, a potent activator of adenylyl cyclase that raises intracellular cAMP levels, reduces PANC-1 ($TP53^{R273H}$) and MiaPaCa ($TP53^{R248W,\ R273H}$) proliferation via cAMP-induced EPAC signalling with no observed contribution by cAMP-induced PKA signalling[166]. Thus, there is a strong body of evidence suggesting CALCR signalling can inhibit proliferation in both TP53 mutant and wild-type cancer

cell lines. There is further evidence that cAMP, a major secondary messenger of CALCR signalling, restricts the proliferation of pancreatic carcinoma cell lines including PANC-1.

Balancing the role of CALCR as an anti-proliferative signalling receptor, there is evidence suggesting CALCR has no role in tumour growth. While calcitonin drove cAMP elevations in K562 cells ($TP53^{null}$) suggesting active CALCR signalling, there was no effect of calcitonin on proliferation[190]. It is worth noting that the authors also investigated IAPP signalling in K562 cells but found no increase in cAMP up to 100 nM IAPP, highlighting the specificity of CALCR for calcitonin in the absence of RAMPs. Ostrovskaya et al.[191] found 2/12 primary glioblastomas were positive for CALCR protein expression, along with 4 cell lines. Of the 4 CALCR-expressing cell lines, SB2b (TP53 wild-type) was the only cell line that exhibited calcitonin-induced and rIAPP-induced cAMP responses. Despite active CALCR signalling, calcitonin did not influence cell number or viability in SB2b cells. Ostrovskaya et al.[191] further show that patients with CALCR-positive and -negative glioblastomas in the TCGA and IVY-GAP cohorts have no differences in outcome. Use of calcitonin in osteoporosis has been associated with increased risk of cancer development in some studies, but a meta-analysis of all available studies suggested no difference in cancer development with the use of exogenous calcitonin[192]. These studies provide evidence suggesting there is no role for CALCR signalling in the proliferation and viability of both TP53-null and wild-type cancers.

There is currently no direct evidence for IAPP as a mitogen. However, CALCR and CRLR signalling have been found to induce proliferation and prevent cell death. Calcitonin has been shown by multiple groups to stimulate the growth of LNCaP cells[189,193]. CALCR knockdown in PC-3M cells (prostate adenocarcinoma; $TP53^{null}$) was shown to drastically reduce tumour volume and increase TUNEL+ apoptotic cells in xenografts, while CALCR

overexpression increased the tumour volume and colony-forming ability of PC-3 cells (prostate adenocarcinoma; $TP53^{null}$)[194]. This suggests that CALCR signalling is tumourigenic, but the findings in PC-3 cells are in stark contrast to Ritchie et al.[189] who show reduced proliferation in response to calcitonin. Similar to the discrepancies between our findings and others on the effects of IAPP in H1299 cells, calcitonin signalling may highly depend on cell environment. CRLR and CALCR share high homology and are both thought to primarily mediate downstream signalling through $G_{\alpha s}$-coupled mechanisms. Additionally, both receptors interact with RAMPs 1-3 and IAPP can bind and signal through the CRLR at supraphysiological concentrations approaching 1 μM[175,176]. An adrenomedullin receptor is formed from CRLR-RAMP2 and CRLR-RAMP3 heterodimers, and adrenomedullin signalling has been widely studied in PDAC. Adrenomedullin expression and secretion have been found in PDAC cell lines, including PANC-1 cells, and adrenomedullin stimulates cell proliferation, invasion, and tumour growth in human PDAC cell lines and xenograft models[195,196]. High tumour adrenomedullin expression is also associated with poor outcome in PDAC[197]. These effects are opposite to those observed with the cAMP-elevating drug forskolin, which reduces proliferation in PANC-1 cells[166]. The divergent findings of both increased and reduced proliferation in PANC-1 cells in response to adrenomedullin-induced and forskolin-induced cAMP elevations highlights the complexity of downstream cAMP signalling in PDAC. The ability of cAMP to act both as a pro- and anti-apoptotic signal is well recognized[198], emphasizing the dependency on tissue environment and cellular milieu. Differences in adrenomedullin and forskolin effects in PANC-1 cells also suggest that additional G-protein-coupled mechanisms beyond $G_{\alpha s}$ signalling may be involved in CALCR and CRLR signalling in PDAC. Thus, our current understanding of CALCR, CRLR,

and cAMP signalling in PDAC remains incomplete, and will likely continue to display variable results in the future depending on the genetic and environmental conditions under investigation.

Although our results in mice suggest no role for endogenous monomeric IAPP in delaying the progression of PDAC, there may still be a role for exogenous IAPP in PDAC. Supraphysiological concentrations of IAPP, achieved through pramlintide, may exert effects that improve outcomes in a subset of PDAC through improved glycemia[199], or incompletely understood effects on the tumour microenvironment. Our results in cell lines suggest no direct effect of IAPP on cancerous cells. However, the lymphoma regression observed by Venkatanarayan et al.[127] in mice is astounding, and we did not investigate the effects of supraphysiological IAPP levels on the tumour microenvironment. We also cannot exclude the potential that endogenous IAPP may influence the early stages of PDAC, such as lesion initiation or progression to PDAC, as our mouse model develops PDAC tumours rapidly following tamoxifen exposure.

Human IAPP differs from rodent IAPP by its propensity to aggregate, forming toxic oligomers and elongated fibrils. Although the data in this chapter does not support a role for monomeric IAPP signalling in PDAC, human IAPP aggregates are a hallmark of islets in T2D[200] and may increase the risk of PDAC. Circulating IAPP levels, and the IAPP:C-peptide ratio, are increased in pancreatitis and pancreatic cancer[201–204], suggesting increased IAPP biosynthesis and secretion from beta cells. IAPP secretion relative to insulin secretion is also increased in rat islets co-cultured with, or exposed to conditioned media from, human pancreatic cancer cell lines PANC-1 and HPAF[205–207]. Elevated IAPP secretion may result in increased islet amyloid and inflammation creating a positive feedback loop.

IAPP aggregates induce a proinflammatory response in islet macrophages[208,209], and may skew the local pancreatic environment toward a state more amenable to neoplasia. Evidence of islet IAPP-induced alterations in the exocrine pancreas have been observed in hIAPP-transgenic rats, which display increased pancreatic ductal and ductal gland proliferation[210]. This was shown to be independent of hyperglycemia by the authors – hyperglycemia and hyperinsulinemia in rats induced by chronic glucose infusion did not induce proliferation of ductal cells. In addition to rodent models expressing human IAPP, macrophage-secreted proinflammatory cytokines have also been shown to promote acinar to ductal metaplasia via NF-κB signalling in mouse acinar cells[153]. It is reasonable to speculate that islet IAPP aggregates in T2D may contribute to a local pro-inflammatory environment that promotes exocrine neoplasia.

Although there is existing evidence in the literature that monomeric IAPP signalling may influence PDAC tumourigenesis, there is also evidence suggesting no role, or even a mitogenic role, for IAPP signalling in PDAC and cancer. Our results in this chapter do not support a role for monomeric IAPP in PDAC cell proliferation, apoptosis, or glycolysis. Our results also show no effect of endogenous IAPP loss on PDAC survival, and suggest that reduced IAPP levels in diabetes do not influence the risk or outcome of PDAC. Further studies characterizing the islet environment in diabetes, and its crosstalk with the exocrine pancreas, may decipher novel mechanisms that explain the strong association between diabetes and PDAC.

Chapter 4: The role of islet amyloid polypeptide in glycemia and adiposity

4.1 Introduction

IAPP was first isolated and identified from amyloid plaques in insulinomas in 1986 by Westermark et al[211]. As the second most abundant transcript in mouse beta cells[212], IAPP has generated much interest as an abundant signalling factor and as an amyloidogenic protein. The amyloidogenic aspects of IAPP biology are well characterized, and the role of islet amyloid in the pathogenesis of T2D is widely recognized[213], but the extent to which islet amyloid contributes to T2D pathogenesis remains unknown. The role of IAPP signalling in metabolism has proven challenging though. A wide range of biological actions have been documented for IAPP, often with disagreements in the literature[214].

IAPP immunoreactivity has been detected in lysates of human pyloric antrum[215], and *Iapp* mRNA (in situ hybridization) and protein (immunohistochemistry) are colocalized in rodent stomachs[216]. Islet beta cells are the most abundant source of IAPP and are responsible for circulating levels of IAPP[201]. IAPP in the islet can also be found in a fraction of somatostatin-expressing delta cells in rodents[217], but minimal IAPP is observed in human delta cells[218]. IAPP is also observed in the CNS (discussed below).

IAPP receptors (CALCR and at least one of three RAMPs) are found in multiple tissues throughout the body. Tissues with the highest expression include the hypothalamus, area postrema, solitary nucleus, kidney, muscle, and placenta[219]. Most expression data are at the mRNA level, which does not guarantee functional expression of the receptor at the cell surface. Robust detection of GPCRs at the protein level can be challenging due to the low abundance of GPCRs, and requirement for a highly specific and rigorously validated antibody. Radioligand binding assays can also provide insight into IAPP receptor expression, but do not provide

information on the resulting biological and physiological actions of receptor signalling in the target cell. The use of exogenous IAPP at physiological concentrations, with and without IAPP receptor-specific inhibitors or genetic modification, provides a robust approach for determining functional IAPP receptor expression while providing insight into the biological actions of IAPP.

The best characterized biological actions of IAPP are in appetite regulation and gastric emptying. Both peripherally and centrally administered IAPP have been shown to induce satiety in rodents[220,221], primarily through reductions in meal size[222]. Subcutaneous administration of IAPP (pramlintide) is also effective at inducing satiety and reducing meal size in humans[223], with accompanying reductions in body weight[224]. Gastric emptying is delayed by IAPP administered centrally or peripherally in rats[225,226], which along with postprandial glucagon suppression[227] is thought to be one of the mechanisms through which exogenous IAPP-mimetics improve postprandial glycemic control in individuals with T1D[228]. Additional metabolic roles for IAPP have been proposed in energy expenditure[229], glucose uptake[230,231], adipocyte function[232], bone resorption[233], vasodilation[234–236], and islet paracrine and autocrine regulation[214,237].

The effects of IAPP on body weight are thoroughly documented in humans and animal models, and are thought to occur primarily through receptors in the CNS[224,238,239]. IAPP induces satiety when administered peripherally or centrally, with more potency during central administration suggesting action in the brain[229]. Lesion of the area postrema abrogates anorexia induced by peripherally administered IAPP[240], and infusion of the IAPP receptor inhibitor AC187 into this region induces hyperphagia in rats[241]. Thus, the area postrema is a target tissue of peripheral IAPP that mediates part of its anorexic actions. The hypothalamus is also involved in IAPP signaling, and IAPP expression is widely detected in the hypothalamus. Neurons in the lateral hypothalamus were shown to contain IAPP immunoreactivity colocalized with a synapse

marker at the border of neurons expressing the leptin receptor (ObRb), and IAPP signalling was shown to stimulate ObRb neurons and potentiate leptin signaling[242]. IAPP-receptor and LepR co-expression has also been found in the area postrema[243], and the synergistic effects of leptin and IAPP are well documented in rodents and humans[224]. IAPP-induced ERK phosphorylation has also been reported in POMC neurons of the arcuate nucleus[244], and *CalcR* deletion in POMC neurons results in increased body weight gain, food intake, and adiposity in male mice, with a mild impairment in glucose tolerance[245]. Female and HFD-fed $CalcR^{\text{POMC-KO}}$ mice did not display any body weight gain, adiposity, or glycemic phenotype, suggesting sex and diet-specific effects of hypothalamic IAPP signalling. Acute peripheral IAPP injections also retained their efficacy in $CalcR^{\text{POMC-KO}}$ mice, suggesting that POMC-expressing neurons are not the target of peripherally-derived postprandial IAPP. In addition to appetite regulation, centrally administered IAPP has been shown to induce sympathetic nervous activity and increase brown fat thermogenesis, body temperature, and energy expenditure; peripherally administered IAPP retains many of the same effects, albeit with weaker induction[229,246]. Cumulatively, these data support a role for IAPP in regulating energy expenditure and intake primarily within the CNS.

IAPP actions have also been documented in the periphery, with roles in islet and adipocyte function, skeletal muscle, and bone resorption. Within the islet, IAPP is reported to suppress insulin, glucagon, and somatostatin secretion in stimulated states[247], but with inconsistent findings, even from within individual laboratories[214]. Often the doses required to see an IAPP-induced effect on islet secretion required supraphysiological IAPP concentrations[248]. Although these concentrations are higher than normal circulating IAPP levels, some are within ranges that may be achievable in a paracrine or autocrine setting within the islet (i.e., low nM levels of IAPP). In support of paracrine actions for IAPP, treatment of isolated rat islets with

IAPP antiserum or a N-terminally truncated IAPP peptide (weak IAPP receptor antagonist) can increase arginine-stimulated insulin, glucagon, and somatostatin secretion[249]. IAPP has been found to increase insulin-stimulated glucose uptake to isolated rat adipocytes[231], and in 3T3-L1 adipocytes IAPP was reported to induce proliferation, differentiation, and fatty-acid uptake[232]. IAPP actions in the liver were initially reported, but IAPP was later shown to not impact hepatocyte metabolism on its own, nor to modify insulin- or glucagon-mediated effects[250]. The initial findings may have been due, in part, to the effects of IAPP aggregates, as human IAPP was often used prior to the widespread appreciation for its amyloidogenicity and cytotoxicity. In skeletal muscle, IAPP at modestly supraphysiological levels (high pM – low nM) inhibits glycogen synthesis and insulin-stimulated glucose uptake[251,252], and stimulates glycogenolysis and lactate efflux[253,254]. Absence of IAPP in mice results in reduced bone mass due to increased resorption, possibly via loss of IAPP-induced osteoclast inhibition[233]. IAPP also has reported actions as a vasodilator, but mice lacking IAPP do not have altered islet blood perfusion[234]. IAPP actions continue to be elucidated in the periphery, with efforts focused on both the supraphysiological (pharmacological) and endogenous activities of IAPP in metabolism.

Rodent genetic models with altered *Iapp* or IAPP receptor expression have provided insight into the paracrine and endocrine activities of IAPP, allowing for modification of endogenous IAPP signalling levels *in situ*. These models allow greater insight into the effects of sustained IAPP loss, as observed in diabetes, rather than acute pharmacological studies. An *Iapp*-null mouse was first generated in 1998 by Gebre-Medhin and colleagues[132]. *Iapp*-null male, but not female, mice were found to have increased body weight, and both male and female mice had increased insulin levels and reduced blood glucose during oral and intravenous glucose tolerance tests (OGTT and IVGTT). These initial studies were performed on F3 descendants of a

129Ola/B6 chimeric mouse. The *Iapp*-null mouse was further backcrossed to the C57BL/6J background, and no effects on body weight have been observed in the C57BL/6J background on chow, high-fat (45% kcal from fat; HFD) or control diets (10% kcal from fat; CD)[233,255–257]. *Iapp*-null mice display reduced leptin sensitivity, improved glucose clearance in OGTT and IVGTT with increased insulin secretion[132], no difference in fasting blood glucose[132,234], and have been reported with both elevated[132] and decreased[258] plasma insulin levels. Glycemia has not been thoroughly investigated in the C57BL/6J inbred mouse strain, however, raising the question whether differences in glycemia may exist similar to the differences in body weight observed between *Iapp*-null 129Ola/B6 hybrid and *Iapp*-null congenic C57BL/6J mice. Further differences in *Iapp*-null mouse islet function are suggested by the observation that *Iapp*-null beta cells are more sensitive to alloxan-induced destruction[258].

Clinical trials with IAPP mimetics have been performed leading to the FDA approval of Symlin (pramlintide) in 2005 for use in T1D and T2D when glycemic control is not met with insulin. In 1-year randomized controlled trials, preprandial subcutaneous injections of pramlintide lowered HbA1c and body weight in individuals with T1D and T2D[119,120]. Meal-time pramlintide has also been shown to reduce postprandial hyperglycemia and glucagon, and increase time spent in a euglycemic range[259,260] in T1D. Until recently, solubility issues restricted pramlintide to a separate injection from insulin, limiting its widespread use. Recent advances in co-formulations of insulin and pramlintide allow for simultaneous dual-hormone therapy, and will hopefully improve usage and glycemic control in T1D and T2D[261]. The improved metabolic health with pramlintide highlights the negative impact of IAPP loss on metabolic health, and emphasizes the importance of circulating IAPP in the postprandial state.

The goal of this chapter is to investigate the impact of endogenous IAPP loss on glycemic control and adiposity. Most of the available data on IAPP actions suggest an insulinostatic effect of IAPP, but are derived from exogenous IAPP mimetics or receptor antagonists at supraphysiological concentrations. In this chapter I use the *Iapp*-null mouse, backcrossed in-house for over 10 generations to C57BL/6J mice, to determine the impact of IAPP loss in the context of elevated obesity (HFD-fed) or a leaner control (CD-fed) state. I further age the mice for up to one year of HFD feeding to determine if glycemic or adiposity phenotypes emerge in aged, diet-induced obese mice.

4.2 Results

4.2.1 IAPP-deficient mice have unaltered glycemia and increased insulin sensitivity

Mice were weaned to a standard chow (6% kcal from fat) diet at 3 weeks-old, and switched to HFD (45% kcal from fat) or a matched CD (10% kcal from fat) at 6-8 weeks-old. *Iapp*-null mice did not display any significant differences in body weight or fasting glycemia after 48 weeks of diet (Figure 8).

To further probe the effects of IAPP loss on glycemia, glucose tolerance was assessed by IPGTT. Intraperitoneal administration was chosen over oral administration to assess beta-cell function independent of gastric emptying rates, as IAPP has been shown to reduce gastric emptying rates[225,226]. Mice lacking IAPP had comparable glucose tolerance to wild-type controls in both sexes and diets (Figure 9). Insulin sensitivity was assessed by insulin tolerance tests after 35 weeks of diet. HFD-fed *Iapp*-null male mice displayed significantly increased insulin sensitivity (Figure 10). This finding suggests endogenous IAPP has an inhibitory role on insulin action, possibly in skeletal muscle as reported by others[253,254]. However, the effect of IAPP on counterregulatory actions to insulin-induced hypoglycemia, such as glucagon secretion[249,262],

may be involved as well. Although no hyperglycemia was observed in the fasted state or during glucose tolerance tests, IAPP-deficient animals displayed a trend toward elevated blood glucose that cannot be explained by differences in insulin sensitivity.

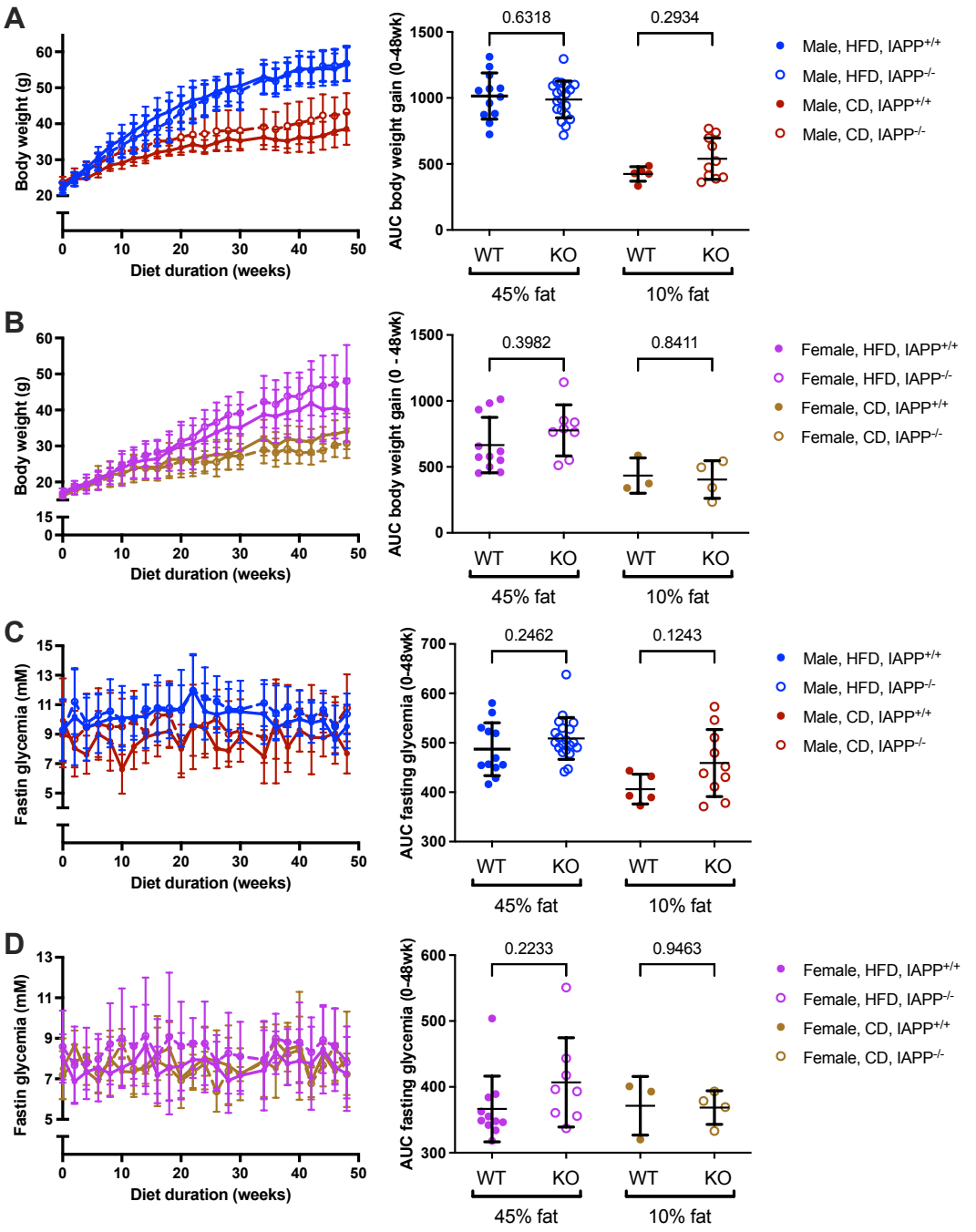

Figure 8: *Iapp* deletion does not significantly impact body weight and glycemia in mice. *Iapp*$^{-/-}$ and *Iapp*$^{+/+}$ C57BL/6J mice were generated from heterozygous breeders and fed a high-fat diet (HFD; 45% kcal from fat) or control diet (CD; 10% kcal from fat) beginning at 6-8 weeks-old. **(A,B)** *Iapp*$^{-/-}$ male and female mice do not have significantly altered body weight. **(C,D)** *Iapp*$^{-/-}$ male and female mice do not have significantly different fasting glycemia in both CD and HFD. No timepoints were significantly different between *Iapp*$^{-/-}$ and *Iapp*$^{+/+}$ mice by repeated measures ANOVA. P-values of AUCs are indicated above the comparisons in the right panels. n = 5-20 male, 3-11 female mice.

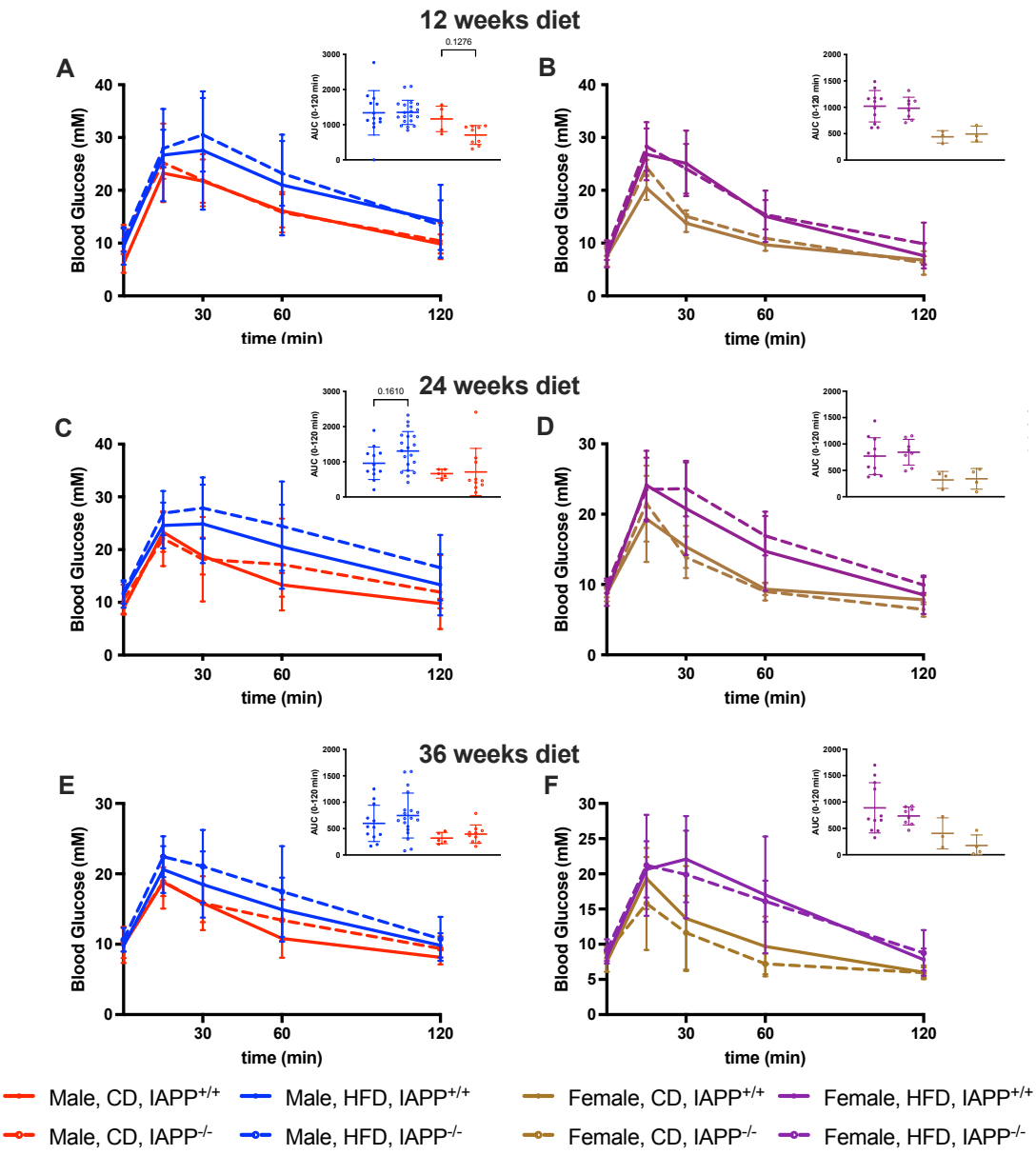

Figure 9: IAPP deficiency does not impact glucose tolerance in mice.
HFD- and CD-fed male and female mice were administered intraperitoneal glucose tolerance tests after 12 **(A,B)**, 24 **(C,D)**, and 36 **(E,F)** weeks of diet. No significant differences were observed between *Iapp*$^{-/-}$ and *Iapp*$^{+/+}$ mice. n = 5-20 male, 3-11 female mice.

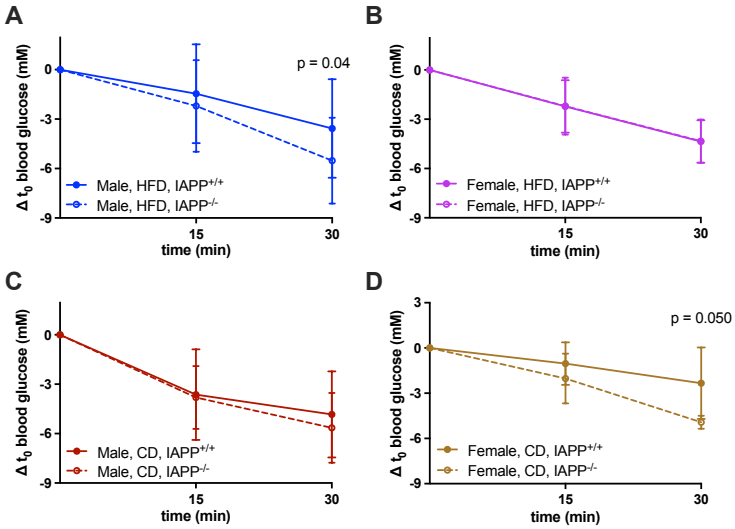

Figure 10: Loss of IAPP causes a mild increase in insulin sensitivity.
(A,B) HFD-fed and **(C,D)** CD-fed male and female mice were administered intraperitoneal insulin tolerance tests after 35 weeks of diet. IAPP loss in HFD-fed males resulted in a modest increase in insulin sensitivity. n = 6-22 male, 3-11 female mice.

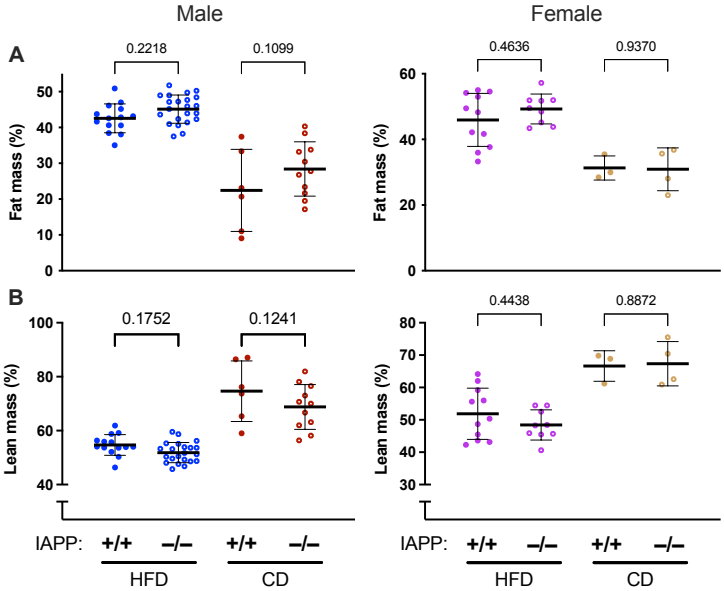

Figure 11: Trend toward increased adiposity in *Iapp*-null male mice.
High-fat diet (HFD) and chow diet (CD) fed *Iapp*$^{-/-}$ and *Iapp*$^{+/+}$ mice were assessed for lean and fat mass after 36 weeks of diet using an Echo MRI body composition scanner. Fat and lean mass are displayed as a percentage of body weight. **(A)** IAPP-deficiency results in a trend toward increased body fat mass composition in male mice, but not female mice. **(B)** IAPP-deficiency caused a trend toward reduced lean body mass composition in HFD- or CD-fed male mice, but not female mice. n = 6-22 male, 3-11 female mice.

4.2.2 IAPP loss does not cause significant adiposity in mice

After 36 weeks of diet (44 weeks-old), body composition was analyzed using an Echo MRI body composition scanner. *Iapp*-null mice displayed no significant differences in body composition (Figure 11).

After 48-54 weeks of diet, animals were euthanized. Tissues were collected and weighed for CD-fed male mice, where the strongest trend in body composition differences was observed, and a fraction of HFD-fed male mice as controls. Increased adiposity was not observed in the inguinal or mesenteric fat pad masses in CD-fed *Iapp*-null mice at study endpoint (Figure 12). Elevated brown fat activity has been observed in response to IAPP in mice[246], and we also measured interscapular brown fat mass and detected no significant difference in CD-fed *Iapp*-null and wild-type mice (Figure 12 D). Liver and pancreas masses were also unchanged in male mice (Figure 12 E, F).

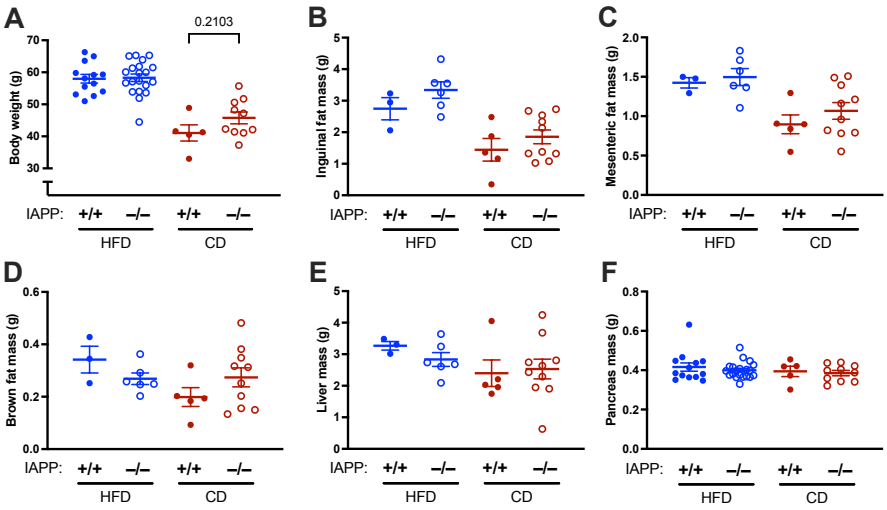

Figure 12: Control diet (CD)-fed *Iapp*$^{-/-}$ male mice do not have significantly increased fat pad mass.
After 48-54 weeks of diet animals were euthanized and tissues were collected and weighed. **(A)** Body weight trended higher in CD-fed *Iapp*$^{-/-}$ male mice. **(B)** Inguinal, **(C)** mesenteric, and **(D)** brown fat masses trended upward in CD-fed *Iapp*$^{-/-}$ male mice but are not significantly increased. **(E)** Liver mass was unaltered in CD-fed *Iapp*$^{-/-}$ male mice. **(F)** *Iapp* deletion had no effect on pancreas mass in HFD- or CD-fed male mice. n = 5,10 CD-fed, 3-20 HFD-fed.

4.2.3 Islet function and mass is unaltered in male mice lacking IAPP

IAPP is the second most abundant insulin granule peptide, and is present at a molar ratio of approximately 1:100 with insulin[263]. To determine if loss of such a major granule constituent altered insulin granule morphology, freshy isolated *Iapp*-null and wild-type islets were analyzed by transmission electron microscopy (TEM). Loss of IAPP resulted in no qualitative differences in insulin granule number (Figure 13 A,B) or morphology (Figure 13 D,C). Both the dense cores and the halos of granules appeared similar in terms of density and size. IAPP loss was confirmed by immunohistochemistry in pancreas sections from *Iapp*-null mice (Figure 13 E). These results confirm that IAPP is not required for granule biogenesis, and mature insulin granules form in the absence of IAPP.

Given the trend of elevated glycemia in the context of increased insulin sensitivity in *Iapp*-null mice, I sought to determine if *Iapp*-null male mice may have reduced beta-cell function. Due to the central actions of IAPP in altering glycemia[245], we characterized glucose-stimulated insulin secretion (GSIS) on isolated islets in a perifusion apparatus *ex vivo*. *Iapp*-null islets did not display any differences in the kinetics (Figure 14 A) or quantity of insulin secreted at basal glucose, or during first and second phase insulin secretion (Figure 14 B-D). The lack of differences in GSIS by perifusion suggest that islet-derived paracrine IAPP does not act to suppress insulin secretion, as others have reported with exogenous IAPP or IAPP signalling blockade[214,249]. With no functional difference in insulin secretion, I next sought to determine if altered beta-cell mass could explain the hyperglycemic trend in CD-fed *Iapp*-null male mice. I detected no difference in beta-cell mass between *Iapp*-null and wild-type male mice (Figure 14 E). Fasting plasma insulin levels are also comparable in *Iapp*-null and wild-type mice (Figure 15 A,B), and further point toward unaltered beta-cell function and mass in *Iapp*-null mice. Fasting

plasma glucagon is also unchanged in *Iapp*-null mice (Figure 15 C,D), indicating that hyperglucagonemia cannot explain the hyperglycemic trend in *Iapp*-null animals.

Cumulatively, these data suggest that beta-cell mass and function is likely not impacted by loss of IAPP in mice. Fasting insulin and glucagon levels are comparable in *Iapp*-null and wild-type mice, and isolated islets display comparable GSIS. Islet function is likely unaltered in mice lacking IAPP. Insulin tolerance tests show enhanced insulin sensitivity in *Iapp*-null mice, despite trends toward adiposity and hyperglycemia, and point to a larger role for IAPP signalling outside of the islet in glycemic regulation. In conclusion, loss of IAPP in mice likely has minimal impact on islet function, but may influence glycemia through mechanisms external to the islet.

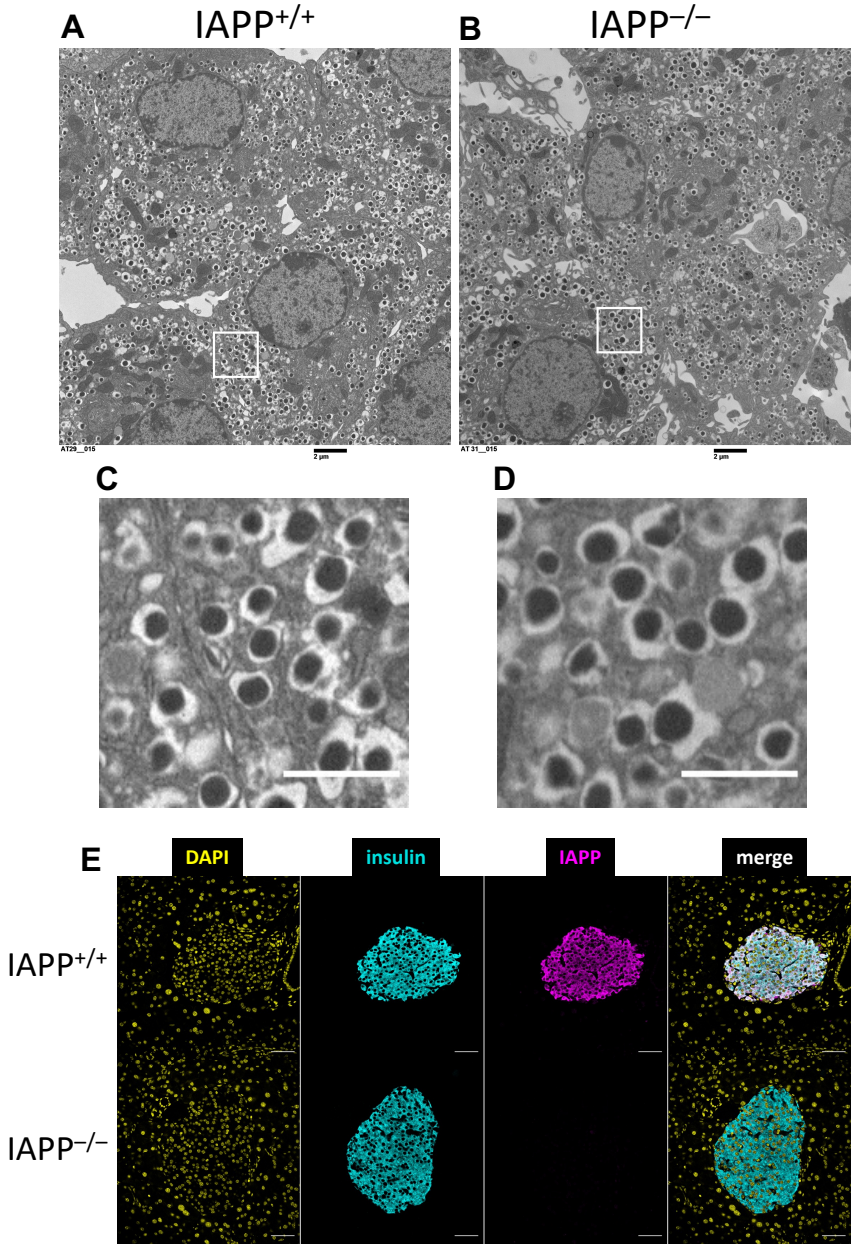

Figure 13: Insulin granule morphology is not altered in *Iapp*$^{-/-}$ mouse beta cells.
Mature, dense-core insulin granules dominate the cytoplasm of beta cells in islets isolated from 16-week-old **(A)** *Iapp*$^{+/+}$ and **(B)** *Iapp*$^{-/-}$ mice. **(C)** An expanded view of the white box in panel A and **(D)** an expanded view of the white box in panel B, highlighting the similarities in *Iapp*$^{+/+}$ and *Iapp*$^{-/-}$ insulin granules. Both genotypes contain granules with similar core densities and halo sizes despite loss of IAPP in the granule. Scale bars in panels C and D represent 0.5 µm. **(E)** Immunohistochemistry confirmation of IAPP loss in pancreas sections from *Iapp*$^{-/-}$ mice. Scale bars represent 50 µm.

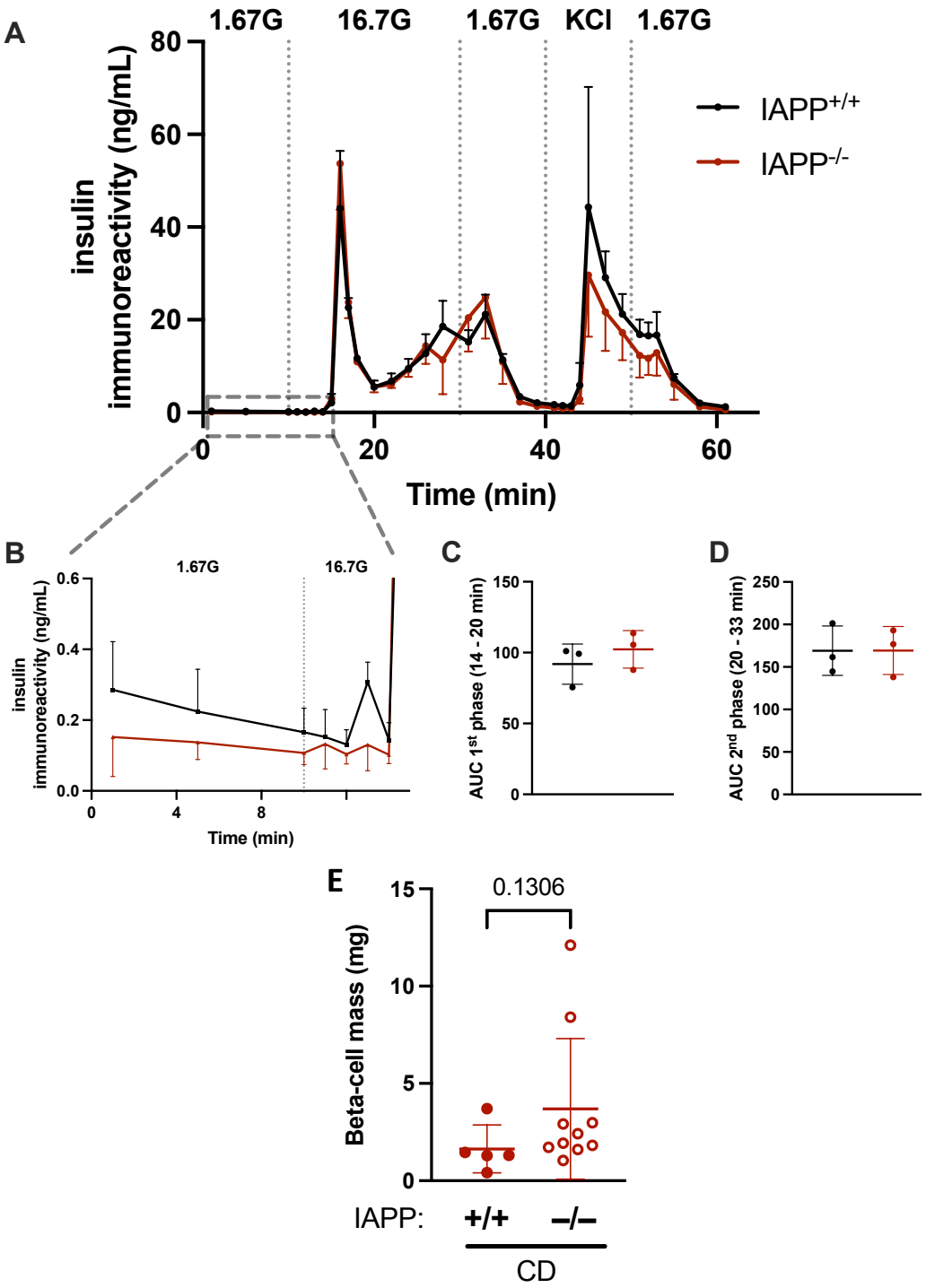

Figure 14: Loss of IAPP does not influence insulin secretion or beta-cell mass.
(A) Islets isolated from 15-18-week-old *Iapp*$^{+/+}$ and *Iapp*$^{-/-}$ mice show no kinetic differences in glucose- or KCl-stimulated insulin secretion. **(B)** Basal secretion rates are comparable in *Iapp*$^{+/+}$ and *Iapp*$^{-/-}$ islets. Area under the curve of **(C)** 1st phase and **(D)** 2nd phase insulin secretion are comparable in *Iapp*$^{+/+}$ and *Iapp*$^{-/-}$ islets. **(E)** IAPP loss did not significantly alter beta-cell mass in CD-fed male mice.

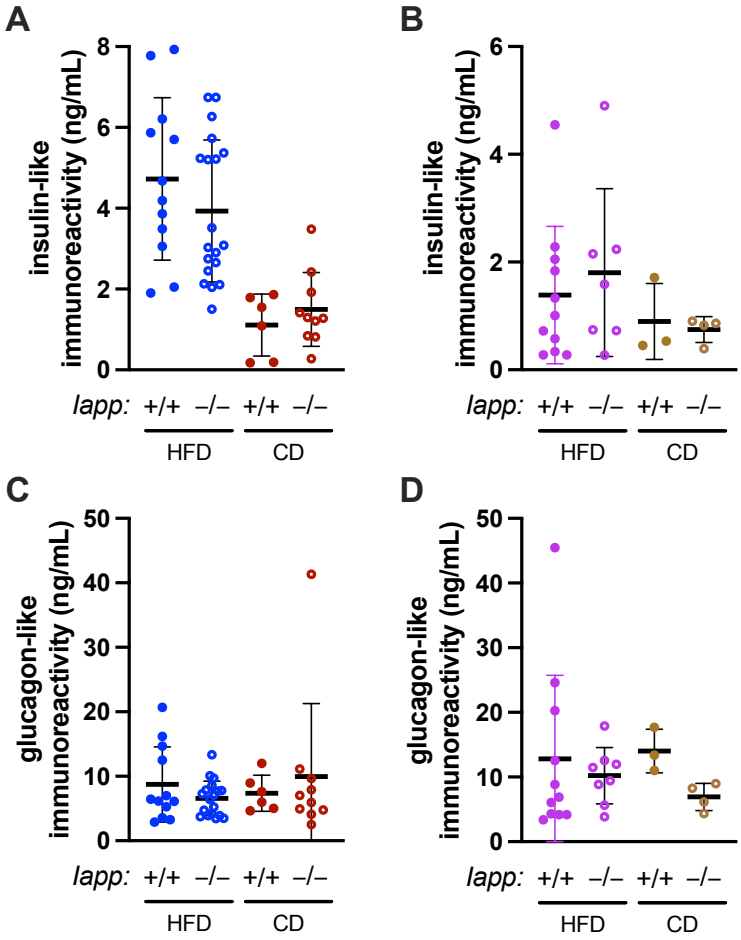

Figure 15: Global IAPP loss does not alter fasting plasma insulin or glucagon. Plasma was collected from 4 h-fasted mice after 48-54 weeks of diet duration. **(A,B)** Plasma insulin and **(C,D)** glucagon are unaltered in male and female *Iapp*$^{-/-}$ mice relative to diet-matched wild-type control mice. n = 6-19 male, 3-11 female mice.

4.3 Discussion

IAPP levels drop alongside those of insulin in individuals with T1D and late-stage T2D, and the effects of IAPP loss remain incompletely understood. To better understand the impacts of IAPP loss in diabetes, I analyzed global *Iapp*-null mice on a congenic C57BL/6J background for changes in adiposity and glycemia, in an obese (HFD-fed) and leaner control state (CD-fed).

Our findings in *Iapp*-null mice partially support a wide body of literature pointing to IAPP as a peptide that negatively regulates weight gain. Initial studies in a hybrid 129Ola/B6 mouse background showed that IAPP deletion resulted in increased body weight in male mice – an expected finding given prior studies found that exogenous IAPP suppressed appetite and increased energy expenditure. However, subsequent studies using congenic C57BL/6J *Iapp*-null mice reported no body weight effect in the absence of IAPP[255,256]. We detect a small, non-significant trend toward elevated body weight and adiposity in *Iapp*-null male mice, straddling the middle-ground of current evidence in the *Iapp*-null mouse.

There is evidence of synergistic interactions between IAPP and leptin signalling in humans and rodents[224], with recent mechanisms pointing to paracrine IAPP actions potentiating LepR-expressing neurons in the hypothalamus[242]. In a state of reduced leptin activity, the loss of IAPP may further reduce leptin's actions and drive further adiposity. To our surprise, and that of others[255], the absence of IAPP does not worsen diet-induced obesity in rodents, a state in which leptin sensitivity is reduced[264,265]. In agreement with our results showing a trend towards increased body weight only in CD-fed *Iapp*-null male mice, deletion of *CalcR* in POMC neurons results in increased body weight gain only in CD-fed male mice that was lost in HFD-fed animals[245]. Leptin-induced STAT3 phosphorylation was found to be comparable in the hypothalami of $CalcR^{\text{POMC-KO}}$ and $CalcR^{\text{POMC-WT}}$ mice, and acute IAPP responses in the area

postrema remained intact in these animals. These findings suggest chronic hypothalamic IAPP actions on anorexia and energy expenditure may be independent of its potentiation of leptin signaling[245].

Hypothalamic IAPP expression increases in HFD-fed male mice and decreases in HFD-fed female mice[242], but it remains unknown whether hypothalamic IAPP production remains intact in T1D and T2D. However, circulating levels of IAPP are lost in T1D and late-stage T2D due to loss of beta-cell function and mass. Chronic IAPP paracrine signalling in the hypothalamus may remain intact in diabetes, and therefore some of IAPP's actions on satiety and energy expenditure may also remain intact. The benefits of replacing acute IAPP signaling postprandially are clear in T1D and T2D though, with improved glycemic control attributable in part to delayed gastric emptying[266,267] and reductions in postprandial hyperglucagonemia[227,268,269]. Sustained use of exogenous IAPP mimetics may also enhance chronic IAPP signalling in the hypothalamus, and help improve adiposity in diabetes.

Most studies on IAPP paracrine actions within the islet have used supraphysiological levels of IAPP in isolated islets or perfused rat pancreases. IAPP-receptor inhibition has provided some insight into endogenous IAPP signalling, and mostly agrees with the findings of synthetic IAPP mimetics; that is, IAPP has a dampening effect on islet endocrine cells and reduces insulin, glucagon, and somatostatin secretion. However, high levels of receptor inhibitors may inhibit off-target receptors, such as the calcitonin-gene-related peptide receptor, questioning whether the observed dampening of islet secretions is truly due to IAPP signalling. True paracrine concentrations of IAPP are also not known, and supraphysiological levels may represent a valid islet paracrine level that signals through "off-target" receptors. The lack of GSIS differences between *Iapp*-null and wild-type islets suggests no paracrine role for endogenous IAPP in the

rodent islet. Paracrine signalling could be reduced in a perifusion paradigm if secreted factors are removed quickly, but likely not entirely lost as differences in paracrine-modulated insulin secretion from Ucn3-null and Sst-null islets are readily detected in perifusion apparatuses[9,270]. The lack of effect in *Iapp*-null islets could be further confirmed in a static GSIS paradigm in which paracrine signalling is enriched. Our model also differs from loss of IAPP in T1D and T2D in that IAPP was deleted globally and constitutively, rather than reduced at juvenile or adult ages with diabetes onset. Although unlikely, I cannot discount any developmental compensatory mechanisms in *Iapp*-null mice that may replace some IAPP actions, such as an increase in islet delta-cell mass or function that would act to suppress insulin and glucagon secretion in the absence of IAPP.

IAPP at 10-100 pM (high circulating levels) has been shown to have a suppressive effect on GSIS in Min6 cells and dispersed mouse islets, and a dual-effect on beta-cell proliferation[237]. At 5.5 mM glucose, 100 pM IAPP enhanced proliferation and Erk1/2 phosphorylation in dispersed mouse beta cells, while at 25 mM glucose 100 pM IAPP reduced Erk1/2 phosphorylation and beta-cell proliferation[237]. Our findings in mice, however, do not support a role for IAPP in the maintenance of beta-cell mass, similar to earlier observations in *Iapp*-null mice showing comparable beta-cell mass to wild-type controls[258]. Our model is not specific to beta-cell loss of IAPP though, and disruption of hypothalamic IAPP may influence beta-cell mass, as hypothalamic lesions have been shown to regulate beta-cell mass in rodents[271].

Iapp-null mice were originally reported to have elevated insulin secretion and improved glucose tolerance[132]. However, in additional studies using mice of a similar genetic background (F3 descendants of a chimeric 129Ola/B6 mouse)[132,258], or an unknown background[233], there were no differences in circulating insulin between *Iapp*-null and wild-type mice. Our results

corroborate the latter findings, and further expand the available data to include no circulating insulin differences in female and HFD-fed *Iapp*-null mice. We also detected no differences in circulating fasting glucagon levels in *Iapp*-null mice, in contrast with the reported actions of IAPP on suppression of glucagon secretion[249]. However, we did not measure glucagon levels in a postprandial state when *Iapp*-induced suppression of glucagon secretion has been observed, and hypoglycemia-induced glucagon secretion is not influenced by IAPP[269]. This suggests that IAPP does not inhibit glucagon secretion in fasting conditions, but rather that IAPP may inhibit glucagon secretion specifically during conditions of elevated glycemia.

We observed increased insulin sensitivity in *Iapp*-null mice, which largely agrees with proposed roles for IAPP as an inhibitor of skeletal muscle glucose uptake and glycogen synthesis, and stimulator of glycogen catabolism and lactate production[254,272]. Loss of IAPP in the null mice may result in increased insulin signalling and glucose uptake in skeletal muscle. IAPP has been found to not significantly alter basal or insulin-induced glucose uptake in hepatocytes[250]. Despite improvements in insulin sensitivity, *Iapp*-null mice do not have improved glucose tolerance. Our data show comparable plasma insulin levels and *ex vivo* islet GSIS in *Iapp*-null and wild-type mice. With no difference in insulin secretion and improved insulin action, *Iapp*-null mice may have reduced suppression of hepatic gluconeogenesis during elevated glycemia. This mechanism would agree with the reductions in postprandial hyperglucagonemia and glycemia observed in T1D and T2D individuals treated with pramlintide[227,268]. Given the overall improvement of glycemia with preprandial pramlintide injections, the negative impact of IAPP on skeletal muscle glucose uptake is likely outweighed by the positive impact of reduced gluconeogenesis and delayed gastric emptying. There may also be distinct mechanisms governing chronic and acute IAPP signalling in skeletal muscle, as acute

IAPP (or mimetic) infusion in humans does not significantly impact glucose disposal or insulin sensitivity[230,273]. Alterations in glucose disposal and insulin sensitivity after long-term use of pramlintide have yet to be investigated, and will be challenging to dissociate from improvements in glycemic control with reduced meal-time insulin.

Overall, our data in mice suggest that IAPP loss leads to a modest increase in insulin sensitivity, but not a significant change in body weight, adiposity, or glycemia. Genetic differences between the hybrid 129Ola/B6 and congenic C57BL/6J strains are likely to influence metabolic phenotypes of IAPP loss. We did not observe any insulin secretion or granule differences in *Iapp*-null islets *ex vivo*, or any differences in beta-cell mass. Our data suggest that loss of IAPP likely has minimal impact on beta-cell function and mass. Further work in human islets will be required to determine if the beta-cell-specific loss of IAPP in diabetes has detrimental effects on human islets. Conditional knockout-ready *Iapp* mice are also now available ($Iapp^{tm1a}$)[136], and will become useful tools for dissecting what are likely independent roles of circulating and paracrine IAPP in energy homeostasis and islet function.

Chapter 5: Glycemia and beta-cell function in mice with beta-cell specific deletion of *Pcsk1* and *Pcsk2*

5.1 Introduction

Type 1 (T1D) and type 2 diabetes (T2D) are characterized by a loss of beta-cell mass and function as the diseases progress, resulting in a reduction of beta-cell hormones including insulin and IAPP. In addition to reduced levels of these hormones, the processing efficiency of beta-cell hormones declines during diabetes pathogenesis, and results in increased levels of prohormones relative to mature hormones[86,87,274]. Peptide hormones are synthesized as larger precursor propeptides and modified by proteolytic and other post-translational modifications to yield mature, biologically active peptides. These mature peptides can act locally in the islet as paracrine factors, or they can enter the bloodstream and travel to target tissues as endocrine hormones. In the islet, four major proteolytic processing enzymes are enriched in the regulated secretory pathway: PCSK1, PCSK2, CPE, and PAM[275]. The prohormone convertases PCSK1 and PCSK2 are the most abundant of the nine-member PCSK (proprotein convertase subtilisin/kexin) protease family in islets, and are the two endoproteases responsible for cleaving propeptides internally at paired basic residues in insulin granules. CPE (carboxypeptidase E) is an exopeptidase that trims paired basic residues at the C-terminus of peptides, and PAM (peptidylglycine alpha-amidating monooxygenase) also acts at the C-terminus to trim glycine residues and C-terminally amidate peptides. PCSK1, PCSK2, CPE, and PAM are all enriched in the secretory granule[276] and provide the majority of proteolytic processing activity in islet endocrine cells including the beta cell.

Insulin granules are generated via trafficking of proinsulin to the regulated secretory pathway in beta cells with over 99% efficiency[277]. Signal peptide cleavage from preproinsulin occurs during translation and translocation to the ER to generate proinsulin[278]. Initial folding, disulfide bond formation, and dimerization of proinsulin occurs prior to ER exit. During maturation in the Golgi proinsulin, processing intermediates, or mature insulin form hexamers around two Zn^{2+} ions[28], with the exact timing and species still unclear. As hexamers form they begin to exit the Golgi in immature secretory granules that continue to acidify and increase granule zinc concentrations[279,280]. The ER has the highest free Ca^{2+} ion concentration along the secretory pathway; granules are very high in calcium but it remains sequestered by abundant Ca^{2+}-binding proteins within the granule[281]. The low pH and high calcium provide optimum conditions for PCSK activity (discussed below). The increasing Zn^{2+} and lowering pH drives further processing and crystallization of insulin to generate a mature insulin secretory granule – a dense secretory granule core of mostly insulin, a peripheral halo containing other granule peptides (including IAPP), and enrichment of membrane proteins for exocytosis signalling[282]. Upon maturation, insulin secretory granules may traffic to the readily releasable pool at the plasma membrane where pre-docked granules can readily fuse with the plasma membrane for a rapid secretory response[283].

The exact processing sequence and location within the secretory pathway of human beta-cell prohormones remains incompletely understood. Insulin was first discovered to be derived from the longer proinsulin peptide in 1967 by Steiner and colleagues[284]. Proinsulin contains 3 peptide chains: B-chain, C-peptide, and A-chain (from N- to C-terminus). After signal peptide removal, proinsulin begins folding in the ER with assistance from abundant chaperones[285]. Three intramolecular disulfide bonds (CysB7-CysA7, CysB19-CysA20, and CysA6- CysA11) are

critical to proper proinsulin folding and form rapidly during translation[286]. PCSK1 is thought to cleave first at the B-chain / C-peptide junction to generate split-32,33-proinsulin, which is rapidly trimmed by CPE to des-31,32-proinsulin (Figure 16A). PCSK2 is then thought to cleave at the C-peptide / A-chain junction to liberate mature insulin and an extended C-peptide. Following CPE-mediated trimming of the paired basic residues, C-peptide is produced in a 1:1 ratio with mature insulin. Alternatively, PCSK2 may act first to generate split-65,66 proinsulin, and following CPE-mediated trimming the des-64,65 proinsulin intermediate. However, PCSK1 is thought to act first in human beta cells for several reasons: (i) des-64,65 proinsulin peptides are not detectable in human islets[287,288] or circulation[274]; (ii) PCSK1 is likely more abundant than PCSK2 in human beta cells[289–292]; and (iii) the pH optimum of PCSK2 is lower than that of PCSK1 (PCSK1 and PCSK2 reviewed extensively in 2012 by Hoshino and Lindberg[27]).

ProIAPP processing in the insulin secretory granule follows a trajectory similar to proinsulin (Figure 16B). The signal peptide is cleaved during translation and translocation to the ER to generate the 67-residue human proIAPP peptide. An intramolecular Cys^{13}-Cys^{18} (residue numbering of proIAPP) disulfide bond is formed in the ER. Sorting of proIAPP to the regulated secretory pathway is also highly efficient in adult beta cells, but is less efficient than proinsulin in immature (neonatal) islets where abundant proIAPP also sorts to the constitutive pathway[293]. In the late Golgi and early secretory granule compartment, proIAPP is cleaved near the C-terminus by PCSK1 to generate $proIAPP_{1\text{-}51}$[294,295]. Trimming by CPE at the C-terminus yields $proIAPP_{1\text{-}49}$[296], and a C-terminal glycine residue that is further trimmed and amidated by PAM resulting in a C-terminally amidated $proIAPP_{1\text{-}48N}$[297]. PCSK2 removes the N-terminal propeptide of proIAPP by cleaving C-terminally to Arg^{11}, resulting in mature, amidated IAPP ($IAPP_{1\text{-}37N}$)[298,299]. Alternatively, PCSK2-mediated cleavage can occur prior to amidation, generating a

non-amidated proIAPP$_{1-38}$ processing intermediate. It is not currently clear yet whether amidation occurs prior to PCSK2 activity. PCSK2 activity in rodent islets is also essential for processing of proIAPP to mature IAPP. Mice lacking PCSK2 do not generate mature IAPP because PCSK1 has minimal activity at the N-terminal cleavage site, while mice lacking PCSK1 can produce mature IAPP[295,299].

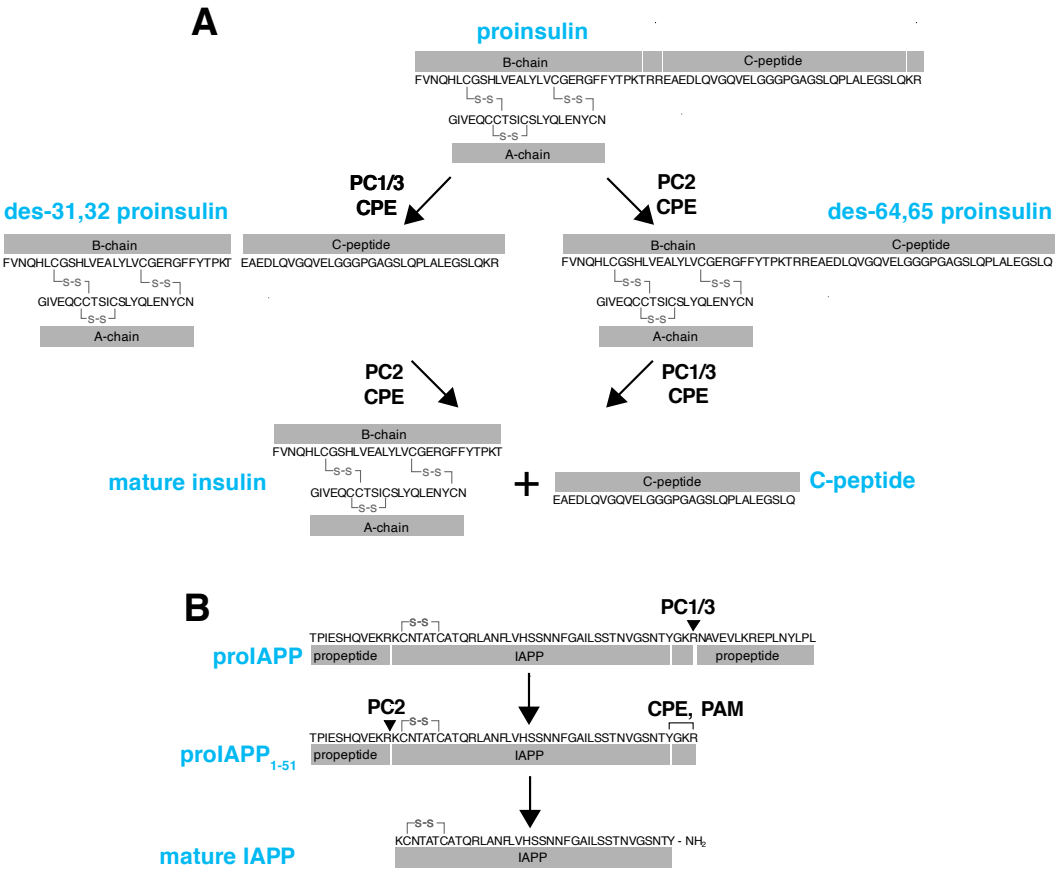

Figure 16: Proinsulin and proIAPP proteolytic processing.
(A) Proinsulin is initially cleaved by PC1/3 (PCSK1) at the B-chain / C-peptide junction, followed by carboxypeptidase E (CPE)-mediated removal of the pair of basic residues remaining on the C-terminus of the B-chain. PC2 (PCSK2) then cleaves at the A-chain / C-peptide junction to produce mature insulin. CPE trims the pair of basic residues remaining on the extended C-peptide, and yields mature C-peptide in a 1:1 ratio with mature insulin. **(B)** ProIAPP is processed similarly with PC1/3 initiating the processing at the C-terminus, to produce a proIAPP$_{1-51}$ intermediate that is further trimmed by CPE and amidated by peptidyl-glycine alpha-amidating monooxygenase (PAM) at the C-terminus to yield an amidated proIAPP$_{1-48N}$ intermediate. PC2 then cleaves the N-terminal propeptide resulting in mature IAPP$_{1-37N}$. PC2 may also act prior to CPE and PAM to generate additional processing intermediates.

The regulation and activity of PCSK1 and PCSK2 correlate well with the regulated secretory pathway and luminal environment of insulin secretory granules. PCSK1 and PCSK2 are highly similar and contain four functional domains: pro-, catalytic-, P-, and C-terminal domains[27]. The prodomains are autocatalytically cleaved, but remain bound and function as a chaperone and inhibitor to prevent premature activity of PCSK1 and 2[300,301]. The catalytic domain is highly similar in both with a catalytic triad of Asp, His, and Ser residues, and an oxyanion hole that stabilises the initial reaction intermediate. The P-domain functions to regulate enzyme activity through conformational changes induced by calcium binding and pH changes, and is involved in trafficking to the secretory pathway. The C-terminal domain is involved in membrane interactions that assist in trafficking PCSK1 and PCSK2 to secretory granules.

PCSK1 and PCSK2 both exist as a zymogen until they reach their pH optimum in the presence of sufficient calcium. PCSK1 exists as a low-activity isoform with the full C-terminal domain that has a broad pH optimum of 5-6.5. Autocatalytic cleavage at two locations in the C-terminal tail results in 2 isoforms of PCSK1 with higher activity but a narrower pH optimum of 5-5.5 and elevated Ca^{2+} requirements[302]. PCSK2 displays even lower pH requirements than PCSK1 for prodomain cleavage and optimal activity[303,304]. Thus, the conditions within maturing granules favour activation of PCSK1 prior to activation of PCSK2. The preferential activity of PCSK1 at the proinsulin B-C junction[305] and the proIAPP C-terminal cleavage site[295], and the intermediates observed, also provide evidence for PCSK1 activity occurring prior to PCSK2. PCSK2 also has a substrate preference for des-31,32 proinsulin over intact proinsulin[306]. Taken together, these provide reasonable evidence that PCSK1 acts prior to PCSK2 in the insulin secretory granule.

The events leading to reduced PCSK1 and PCSK2 activity in beta cells during T1D and T2D pathogenesis are incompletely understood. Reduced processing activity in beta cells has been documented to an extent in each pathology though, and the current evidence provides conflicting clues as to possible causes. In T1D, low amounts of residual beta cells can be found in the pancreas, and more than half of individuals with over 50-year disease duration have detectable plasma C-peptide[307]. In a separate T1D cohort, proinsulin was still detectable in 90% of individuals with undetectable C-peptide, and the circulating proinsulin:C-peptide (PI:C) ratio was elevated in T1D[67]. ProIAPP$_{1\text{-}48N}$:IAPP is also elevated in T1D, indicating that the processing defect is not unique to proinsulin within the beta cells[86]. Islet autoantibody-positive (AAb+) individuals also have elevated PI:C that increase further leading up to T1D diagnosis[308], and PI:I area by immunostaining is elevated in AAb+ and T1D pancreas sections[309]. Rodriguez-Calvo et al. also found in the same study that beta-cell mass is unaltered in AAb+ individuals[309]. This suggests that impaired processing of proinsulin to insulin occurs early in T1D pathogenesis, prior to the decline in beta-cell mass and onset of hyperglycemia. Studies in human pancreas extracts and laser-capture micro-dissected islets have shown reduced PCSK1 protein and transcript levels in T1D, and inflammatory cytokines can reduce *PCSK1* transcript levels in human islets[310,311]. PCSK2 protein and mRNA were found unaltered in T1D islets and pancreas extracts, respectively, but PCSK2 transcript and protein abundance have been shown to decline in human islets with cytokine treatment[310–312]. T1D remission is also associated with a lower circulating PI:C ratio[313]. The evidence in T1D points to islet inflammation as a potential mechanism for reduced processing activity in beta cells, possibly through reductions in PCSK1 levels. Islet transplant recipients also have elevated circulating PI:C and proIAPP$_{1\text{-}48N}$:IAPP ratios [86,314], further pointing to inflammation as a potential mechanism driving altered beta-cell prohormone

processing. Recipients of islet auto-transplants also have elevated PI:C ratios[314] suggesting additional mechanisms beyond adaptive islet inflammation can drive impaired beta-cell prohormone processing.

Individuals with T2D or impaired glucose tolerance also have an increase in circulating PI:C[315–317]. Early during the compensatory stage of pre-T2D while beta-cell mass is expanding there may also be an improvement in beta-cell prohormone processing, as the PI:I ratio is negatively correlated with BMI in individuals with normal glucose tolerance[317]. In rodent islets with high blood perfusion there is increased PCSK1 protein but not RNA[318], indicating that beta cells (or at least rodent beta cells) have the capacity to increase processing with demand. Alternatively, the increased PCSK1 abundance may be due to increased glucose-induced translation of *Pcsk1* in highly perfused islets[20]. Regardless of potential early improvements in function, individuals with impaired glucose tolerance have elevated circulating PI:C, suggesting that the decline in processing efficiency occurs early in T2D pathogenesis. The PI:C ratio is highest in the fasted state due to the longer circulating half-life of proinsulin over C-peptide or insulin[319,320], but elevated PI:C is still observed during beta-cell stimulation[274]. The stimulated secretion of increased PI:C suggests the defect lies with the beta cell rather than altered clearance of proinsulin and C-peptide. High-performance liquid chromatography studies have shown that intact proinsulin and the des-31,32 proinsulin processing intermediate are responsible for the elevated PI in T2D plasma, while des-64,65 or split-65,66 proinsulin is not detected in circulation[274]. This suggests a possible defect in PCSK2 activity in human beta cells, as *Pcsk2* deletion in mice generates an increase in the des-31,32 intermediate[321]. This is fitting with the proIAPP processing impairment found in T1D, but does not correlate with the normal PCSK2 and reduced PCSK1 expression in T1D islets[310,311], and suggests that PCSK1 and 2 expression

may correlate poorly with their activity in human beta cells. Circulating proIAPP was also found elevated in T2D[87], but it is currently unclear whether this is intact proIAPP or a processing intermediate. It is still not clear whether there is a defect in the activity of PCSK1, PCSK2, or both in human beta cells in T2D. It is also worth noting that much of the work delineating proinsulin and proIAPP processing pathways has been in rodent islets, and recent evidence suggests very low expression of PCSK2 in human beta cells[289], challenging the canonical model of proinsulin processing.

Observations and studies in humans over the last two decades have helped elucidate some of the roles of *PCSK1* and *PCSK2* in glycemic regulation. The first human with null activity of PCSK1 was identified in adulthood in the late 1990s, and presented with obesity, normal fasting glycemia, reactive hypoglycemia, elevated 2 h glycemia in an OGTT, undetectable circulating mature insulin, and elevated proinsulin, split-65,66 proinsulin, and des-64,65 proinsulin[322]. Since then, more individuals with homozygous or compound heterozygous null mutations have been identified[323]. Individuals with *PCSK1* mutations have a challenging and dynamic clinical presentation. Following normal gestational terms and birth weights, malabsorptive diarrhea and severe failure to thrive requires parenteral nutrition and careful monitoring beginning in the first weeks of life despite mostly normal intestinal biopsies[323]. Of the 13 individuals identified in the largest cohort to date[323], 6 died during the neonate-childhood period due to complications arising from chronic diarrhea and central venous line sepsis. The dependency on parenteral feeding diminishes over time, and most are able to survive with enteral feeding by 18 months of age with diarrhea improving with ageing into adulthood. Diabetes insipidus occurred in 8/13 individuals with an average age of diagnosis at 18 months old, and was managed with vasopressin therapy (desmopressin). Further complications exist with varying penetrance on hypothyroidism, growth

hormone deficiency, hypoadrenalism, and hypogonadism, highlighting the importance of *PCSK1* throughout much of the endocrine system.

Prader-Willi syndrome, resulting from the loss of a paternal chromosome 15 segment, also results in reduced *PCSK1* expression which has been attributed to loss of paternal *SNORD116*[324]. Prader-Willi is a spectrum disorder with a high range of symptoms, but the obesity, hyperphagia, impaired glucose tolerance, and elevated PI:I[324,325] is similar to that of individuals lacking functional PCSK1. Single nucleotide polymorphisms (SNPs) have also been identified in *PCSK1* and are associated with obesity, increased insulin sensitivity, elevated fasting proinsulin, and strangely improved 2h OGTT glycemia and lowered fasting glycemia (Table 3). The latter two may be due to the increased circulating half-life of proinsulin that is thought to cause reactive hypoglycemia in patients carrying *PCSK1* mutations, as proinsulin retains about 10% of insulin's activity at insulin receptors[326,327]. The two most common non-synonymous *PCSK1* SNPs rs6232 (N221D; catalytic domain, <5% allele frequency) and linked rs6234/rs6235 (Q665E/S690T; C-terminal tail domain, 24% allele frequency) are not associated with increased diabetes risk though, despite being associated with increased plasma proinsulin (Table 3). Although *PCSK1* SNPs are not associated with T2D, islet *PCSK1* expression is negatively correlated with HbA1c levels[328] indicating loss of PCSK1 may occur with progression of hyperglycemia. PCSK1 activity outside of the islet may also influence the risk of diabetes given the essential role of PCSK1 in processing the gut-derived incretins GLP-1 and GIP[329,330]. The current evidence suggests reduced PCSK1 activity, from polymorphisms or other genetic conditions, alters glycemic control in humans but does not cause frank diabetes as a MODY (maturity-onset diabetes of the young) gene.

The available data on *PCSK2* variation in humans is much more limited than *PCSK1*. No individuals with complete *PCSK2* deficiency have been identified. In an era where exome sequencing is widely performed, this suggests functional *PCSK2* expression is required for viability in humans. A simple tandem repeat variant in intron 2 of *PCSK2* was found enriched in a Japanese T2D cohort, but was not associated with altered fasting PI:C, glucose, BMI, or HbA1c[331]. Other non-coding polymorphisms in *PCSK2* have been associated with elevated OGTT AUC, and increased, decreased, and unaltered T2D risk (Table 3). One extremely rare non-synonymous *PCSK2* variant was identified in an Old-Order Amish population (R430W) and was twice as prevalent in the T2D population[332]. $PCSK2^{R430W}$ was further found to have no difference in enzyme activity or trafficking, but did display a broadened pH optimum suggesting a conformational change[332]. Additional missense mutations have been found for *PCSK2*, but at such a rare frequency that associating the polymorphism with a phenotype is challenging. This includes several missense variant SNPs in *PCSK2* that are present in the T2D Knowledge Portal but are extremely rare and not associated with T2D or elevated fasting proinsulin [333]. However, rs1383425066 (*PCSK2* missense variant) and several splice region variants in *PCSK2* are associated with elevated BMI[333]. The effect of *PCSK2* polymorphisms on beta-cell function and glycemia are also difficult to interpret, as PCSK2 is required for the processing of proglucagon to glucagon[334].

Table 3: Human polymorphisms in *PCSK1* and *PCSK2*

Processing Enzyme	Identified variants	Clinical phenotype	References
PCSK1	Various homozygous null	Malabsorptive diarrhoea, obesity, elevated proinsulin, high 2 h OGTT glucose and 65,66 split proinsulin, 5 h postmeal hypoglycaemia, diabetes insipidus	[322,323,335–337]
	rs6232	Obesity, higher insulin sensitivity, improved 2 h OGTT glucose	[338–341]
	rs6234/rs6235	Obesity, elevated fasting proinsulin, lowered fasting glucose	[338–341]
PCSK2	rs2021785	T2D and/or nephropathy risk	[342]
	rs200711626	Trend toward increased prevalence in T2D (not significant—very rare SNP enriched through founder effect)	[332]
	rs2208203	Altered insulin secretion and fasting glucagon levels	[343]
	rs2269023	Elevated fasting glycaemia, and AUC glucose and insulin	[344]
	rs2284912	Decreased fasting glycaemia	[344]
	rs6044695	Decreased fasting glycaemia	[344]
	Simple tandem repeats in intron 2	>20 repeats associated with T2D	[331]

OGTT: oral glucose tolerance test, T2D: type 2 diabetes, SNP: single nucleotide polymorphism, AUC: area under the curve

Mouse models have aided our understanding of *PCSK1* and *PCSK2* in beta-cell function and glycemia. The first *Pcsk1*-null mouse was generated via deletion of promoter elements and the first exon, and resulted in pre- and perinatal lethality, with only 7/21 *Pcsk1*-null mice born surviving to 7 days-old[305,345]. Similar to humans, the mice had diarrhea, normal gastrointestinal histology, and elevated proinsulin levels, but did not develop obesity and had 40% reduced body weight to controls at 6 weeks of age. The knock-out mice display comparable glucose tolerance to wild-type mice, while heterozygotes have mildly impaired glucose tolerance. Proinsulin processing is impaired in knock-out and heterozygous mice, with proinsulin accounting for approximately 90% and 12% of total insulin, respectively, while wild-type littermates have approximately 5% proinsulin[305]. A $Pcsk1^{N222D}$ point mutant mouse model was later generated and better mirrors human PCSK1 deficiency, with elevated body weight and hyperphagia, islet hypertrophy, increased proinsulin and impaired glucose tolerance, but no development of diabetes[346]. A follow-up study found no change in beta-cell proliferation or death despite islet hypertrophy in $Pcsk1^{N222D}$ mouse islets[347]. An additional $Pcsk1^{V96L}$ mouse has also been isolated from an obesity mutagenesis screen that alters the splice acceptor site of the first codon in *Pcsk1* exon 3, leading to the production of a truncated (but not frameshift-mutant) PCSK1 product[348]. $Pcsk1^{V96L/V96L}$ mice display a phenotype similar to $Pcsk1^{N222D/N222D}$ mice with increased proinsulin, hyperphagia, obesity, and transient diarrhea[348]. Isolated islets from these mice have provided excellent tools for characterizing proinsulin and proIAPP processing in PCSK1-deficient beta cells. However, the simultaneous hyperphagia, obesity, and altered endocrine processing outside of beta cells make it difficult to attribute loss of PCSK1 in beta cells to any functional changes in islets or glycemia.

In the late 1990s, the Steiner laboratory generated the first *Pcsk2*-null mouse by insertion of a neomycin cassette into exon 3. These mice appeared normal at birth, but displayed mildly reduced growth rates, hypoglycemia, and lower glycemia during glucose tolerance tests[349]. Lowered glycemia in the *Pcsk2*-null mice is attributed to the lack of mature glucagon from alpha cells, and *Pcsk2*-null islets contain highly expanded delta- and alpha-cell fractions[349]. These mice also lacked normal processing of prosomatostain (proSst) to Sst_{1-14}, and instead produced primarily Sst_{1-28} and intact proSst[349]. Glucagon replacement with mini-pumps or AAV6-RGP-PCSK2 viral infection restores glycemia and normal islet architecture in *Pcsk2*-null mice, which points to glucagon deficiency as the primary glycemic defect in these animals[140,334]. Proinsulin processing is also impaired in *Pcsk2*-null mice, with proinsulin accounting for approximately 35% of total insulin in the pancreas and 60% of total insulin in the circulation, while wild-type littermates have approximately 6% and 15% proinsulin in the pancreas and in the circulation, respectively[349]. Increased intact proinsulin and des-31,32 proinsulin were found elevated in the *Pcsk2*-null mice, and the conversion rate of proinsulin to mature insulin was slowed in the absence of PCSK2[321]. In comparison to the proinsulin processing blockade in *Pcsk1*-null mice, it was suggested that PCSK2 plays a lesser role than PCSK1 in proinsulin processing, but is still important to enhance the speed and efficiency of proinsulin conversion[321]. Cell-specific deletion of *Pcsk2* was achieved in the last decade with the generation of a $Pcsk2^{flox/flox}$ mouse[140]. Deletion of *Pcsk2* in delta and beta cells by *Pdx1*-CreER and tamoxifen resulted in no difference in glycemia or glucose tolerance in mice, but a complete blockade in islet proIAPP processing when crossed to the RIP-Cre mouse[140]. This finding provides further evidence that in mice, beta-cell *Pcsk2* is dispensable for maintaining euglycemia, but it is still important for proper beta-cell prohormone processing.

Although the effects of beta-cell PCSK1 and PCSK2 activity on glycemia are challenging to interpret in human genetics studies and mouse models with global genetic modifications, they have assisted in partially deciphering the regulation of *PCSK1* and *PCSK2* gene activity. The paternal inactivation of *Snord116* in Prader-Willi syndrome is thought to reduce *Pcsk1* and *Pcsk2* expression via reduction of the transcription factor *Nhlh2*[324]. Further work has shown NHLH2 can heterodimerize with STAT3 and bind to the *Pcsk1* promoter[350]. PAX6 has also been shown to bind the *Pcsk1* promoter, and reductions in PAX6 have been suggested to reduce PCSK1 levels and increase circulating proinsulin[351,352]. PAX6 binding and regulation of the *Pcsk1* promoter was not found in an inducible model of *Pax6* deletion in beta cells (*MIP-CreER*$^{Tg/0}$*; Pax6*$^{flox/flox}$), despite significant islet and beta-cell changes, questioning *Pax6* as a regulator of *Pcsk1* expression[353]. A key beta-cell maturity transcription factor, *MafA*, has also been shown to positively regulate *Pcsk1* expression[354]. The *Pcsk2* promoter is bound and positively regulated by NHLH2, C-MAF, and NEUROD1[355,356]. Glycosylation of PCSK1 and PCSK2 is also required for protein exit from the ER to the Golgi[357,358]. Therefore, alterations in the above transcription factors, or glycosylation, may impair PCSK1 and PCSK2 activity in beta cells.

The aim of this chapter is to elucidate the role of beta-cell *Pcsk1* and *Pcsk2* in beta-cell function and glycemic control. There is strong evidence for declining PCSK1 and PCSK2 activity in beta cells in diabetes. Currently, it remains unknown whether reduced PCSK1 and PCSK2 activity in beta cells drives further beta-cell dysfunction and dysglycemia, or if reduced PCSK1 and PCSK2 activity in beta are merely bystander biomarkers of failing beta cells. To investigate the roles of *Pcsk1* and *Pcsk2* in beta-cell function, I used an *Ins1*^{cre} mouse crossed to *Pcsk1*$^{flox/flox}$ and *Pcsk2*$^{flox/flox}$ mice to drive deletion of *Pcsk1* and/or *Pcsk2* in mouse beta cells.

5.2 Results

5.2.1 Proinsulin and proIAPP processing errors in mice lacking *Pcsk1* or *Pcsk2* in beta cells

Pcsk1^{tm1a} and *FLPo*^{Tg} mice were crossed to generate conditional *Pcsk1*^{flox} mice. *Pcsk2*^{flox} mice were previously generated in our laboratory[140]. *Pcsk1*^{flox} and *Pcsk2*^{flox} animals were bred to *Ins1*$^{cre(Thor)}$ mice to generate mice lacking *Pcsk1* or *Pcsk2* only in beta cells. For *in vivo* studies, *Pcsk1*$^{flox/+}$ *Ins1*$^{cre/+}$ males were crossed with *Pcsk1*$^{flox/+}$ *Ins1*$^{+/+}$ females to avoid potential maternal diabetes or fetal programming during gestation and nursing. *Pcsk2*^{flox} animals were bred using the same strategy.

I confirmed the absence of PC1/3 (PCSK1) protein in *Pcsk1*$^{flox/flox}$ *Ins1*$^{cre/+}$ (Pcsk1^{betaKO}) mouse beta cells, and the absence of PC2 (PCSK2) protein in *Pcsk2*$^{flox/flox}$ *Ins1*$^{cre/+}$ (Pcsk2^{betaKO}) mouse beta cells, by immunohistochemistry of mouse pancreas sections (Figure 17 A,B). Deletion of the floxed *Pcsk1* and *Pcsk2* alleles by *Ins1*^{cre} was qualitatively robust. Beta-cell *Pcsk1* deletion resulted in minimal residual PC1/3 immunoreactivity in islets, a result confirmed by western blot of Pcsk1^{betaKO} islet lysates in which minimal PC1/3 protein was detectable (Figure 17C). *Pcsk1*$^{flox/+}$ *Ins1*$^{cre/+}$ (Pcsk1^{betaHET}) islet lysates also show reduced PC1/3 protein relative to *Pcsk1*$^{+/+}$ *Ins1*$^{cre/+}$ (Pcsk1^{betaWT}) control islets, suggesting that loss of one *Pcsk1* allele may lead to haploinsufficiency (Figure 17C). *Pcsk2* deletion was specific to beta cells, and non-beta islet cells retained PC2 immunoreactivity (Figure 17B). These results confirm that *Ins1*$^{cre(Thor)}$ induces robust and near-complete recombination specific to mouse beta cells within the islet, as reported by Thorens et al.[138]

As expected, Pcsk1^{betaKO} mice displayed fasting hyperproinsulinemia, with plasma proinsulin levels 150-200 fold higher than Pcsk1^{betaWT} mice in both males and females (Figure 18

A,B). Plasma proinsulin was consistently elevated from 10-24 weeks old (Figure 18 C,D). Pcsk1^{betaHET} animals trended toward hyperproinsulinemia, suggesting haploinsufficiency of Pcsk1 (Figure 18A-D). Plasma insulin immunoreactivity was also elevated in Pcsk1^{betaKO} male and female mice (Figure 18 E,F), likely due to cross-reactivity of proinsulin forms in the insulin ELISA and increased secretion of des-64,65 proinsulin in Pcsk1^{betaKO} mice. Given the magnitude of the increase and that the cross-reactivity is unlikely to exceed 100%, these data suggest elevated total (pro)insulin in the circulation of Pcsk1^{betaKO} mice.

Beta-cell proinsulin and proIAPP processing in Pcsk1^{betaKO} and Pcsk2^{betaKO} islets revealed differing substrate preferences for the two prohormone convertases. Using a non-reducing urea gel, islet lysates from Pcsk1^{betaKO} mice showed reduced mature insulin and elevated proinsulin (Figure 19A). Pcsk1^{betaKO} islets also appear to show an increase in the des-64,65 intermediate, but it is difficult to discern from intact proinsulin (see Figure 19A). Qualitative top-down proteomics of Pcsk1^{betaKO} islet lysates revealed an increased abundance of peaks corresponding to the masses of proinsulin, des-64,65 proinsulin, and split proinsulins, and reduced des-31,32 proinsulin and mature insulin (Figure 19C). However, standard peptides were not analyzed and the quantification in Figure 19C is therefore qualitative. Pcsk2^{betaKO} islets showed a slight elevation in proinsulin by western blot, but contained comparable mature insulin to Pcsk2^{betaWT} islets (Figure 19A). Pcsk1^{betaHET} islets had impairments in proinsulin processing comparable to Pcsk2^{betaKO} islets with ample mature insulin but elevated proinsulin, suggesting haploinsufficiency of *Pcsk1* in mouse beta cells. ProIAPP followed a markedly different processing pattern compared to proinsulin in Pcsk1^{betaKO} and Pcsk2^{betaKO} islets: islets from animals lacking beta-cell Pcsk1 contained ample mature IAPP, while animals lacking beta-cell *Pcsk2* contained minimal mature IAPP and elevated proIAPP$_{1\text{-}48N}$ (Figure 19B). These data

indicate that *Pcsk1* plays a much larger role in proinsulin processing but is not required for proIAPP processing, while *Pcsk2* plays a larger role in proIAPP processing but is not required for proinsulin processing, in keeping with previous studies in mice with whole-body *Pcsk1* or *Pcsk2* deficiency[305,321].

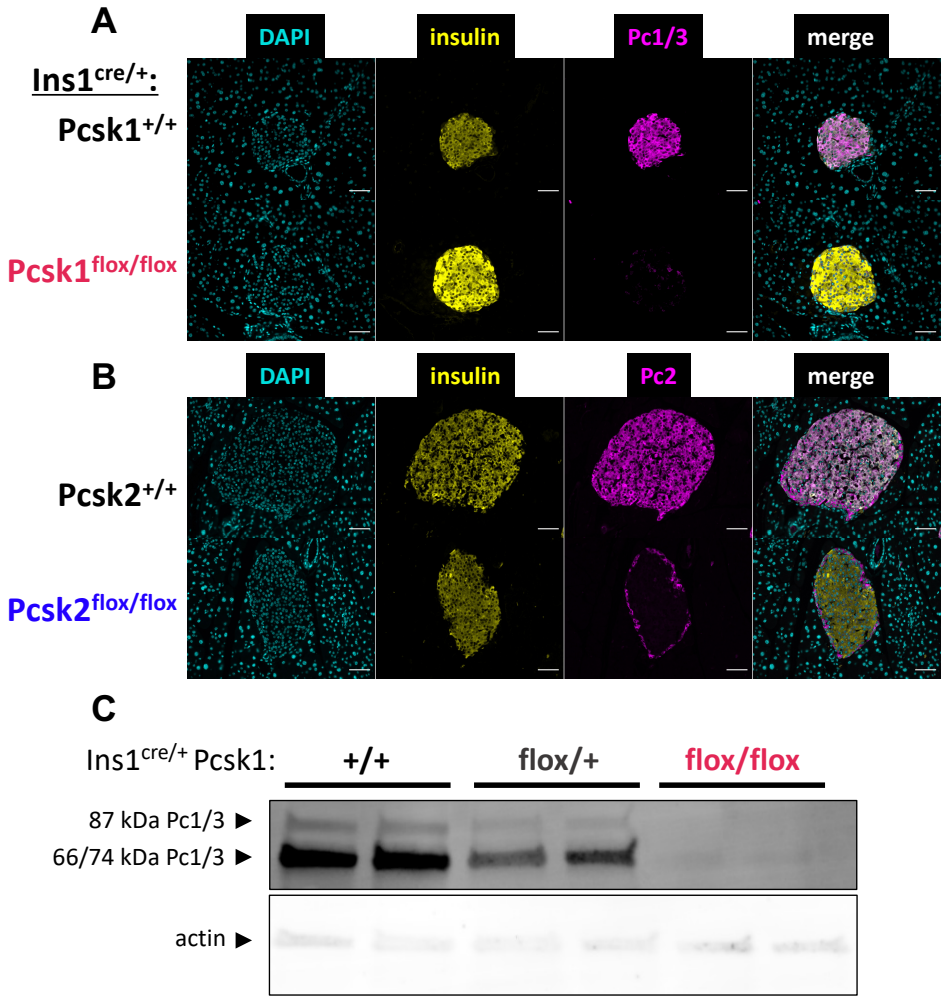

Figure 17: Robust deletion of *Pcsk1* and *Pcsk2* in beta cells by *Ins1*-cre-recombinase. **(A)** Deletion of *Pcsk1* in beta cells of $Pcsk1^{flox/flox}$; $Ins1^{cre/+}$ mice was demonstrated by immunohistochemistry. **(B)** Deletion of *Pcsk2* in beta cells of $Pcsk2^{flox/flox}$; $Ins1^{cre/+}$ mice was demonstrated by immunohistochemistry. Note the mantle of non-beta cells in the islet that retain PCSK2 immunoreactivity in $Pcsk2^{flox/flox}$; $Ins1^{cre/+}$ mice. **(C)** Deletion of *Pcsk1* was further confirmed by western blot of islet lysates. Islets from $Pcsk1^{flox/flox}$; $Ins1^{cre/+}$ mice show minimal PCSK1 protein suggesting nearly complete deletion of *Pcsk1*, while heterozygotes display reduced islet PCSK1 protein relative to $Pcsk1^{+/+}$; $Ins1^{cre/+}$ mouse islets. Scale bars represent 50 μm.

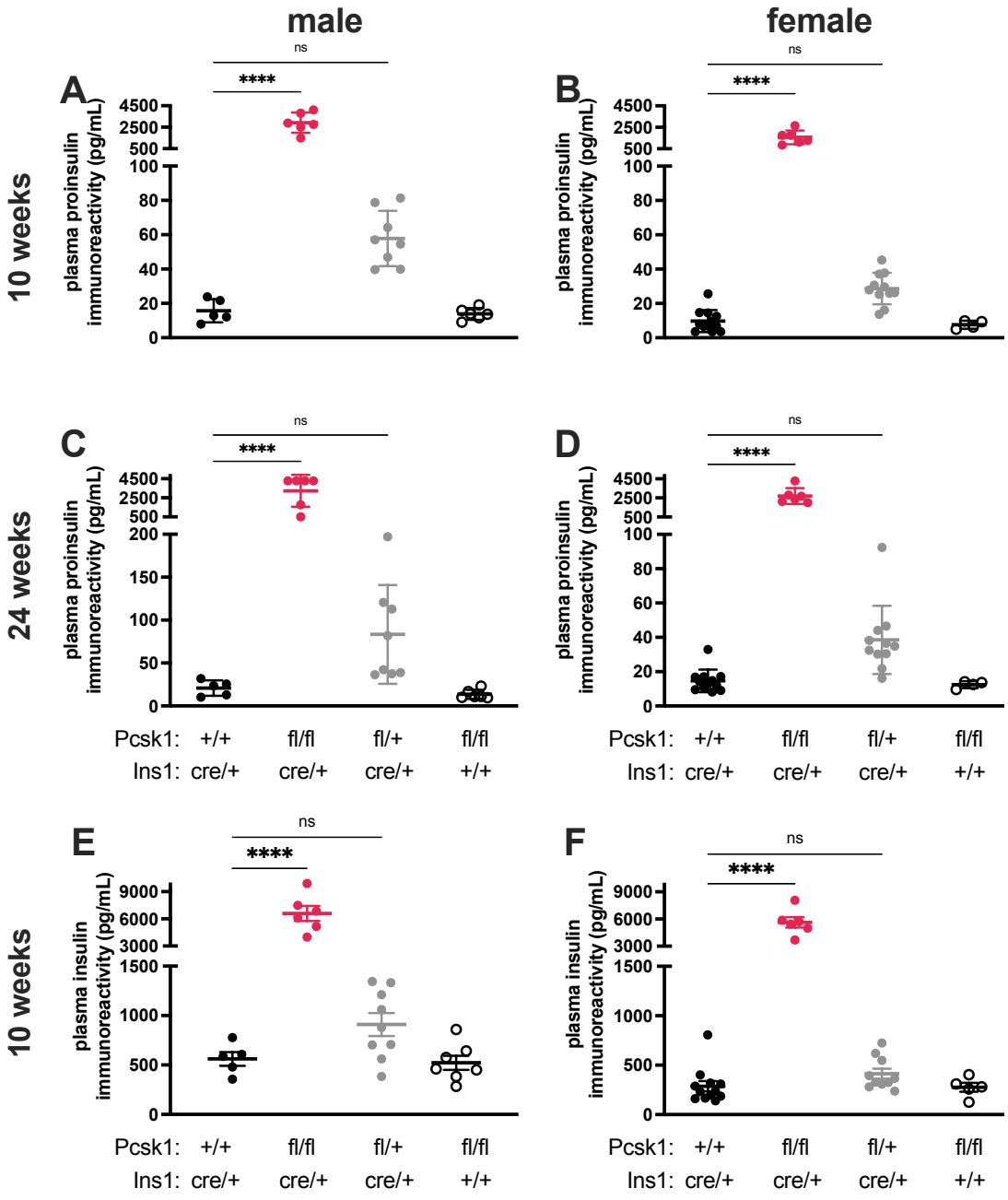

Figure 18: Elevated circulating immunoreactive proinsulin and insulin in *Pcsk1*$^{flox/flox}$ *Ins1*$^{cre/+}$ mice.

(A,B) Fasting plasma proinsulin was measured by ELISA at 10 weeks of age in male and female mice, and again at **(C,D)** 24 weeks of age. Plasma proinsulin was consistently over 150-fold higher in male and female Pcsk1^{betaKO} mice relative to Pcsk1^{betaWT} mice at both ages. (E,F) Fasting plasma insulin was measured by ELISA at 10 weeks of age in male and female mice. Note that the insulin ELISA cross-reactivity with the des-31,32 proinsulin intermediate or other proinsulin processing intermediates is not known. **** $p < 0.0001$, ns = not significant. n = 4-12 female, 5-9 male mice.

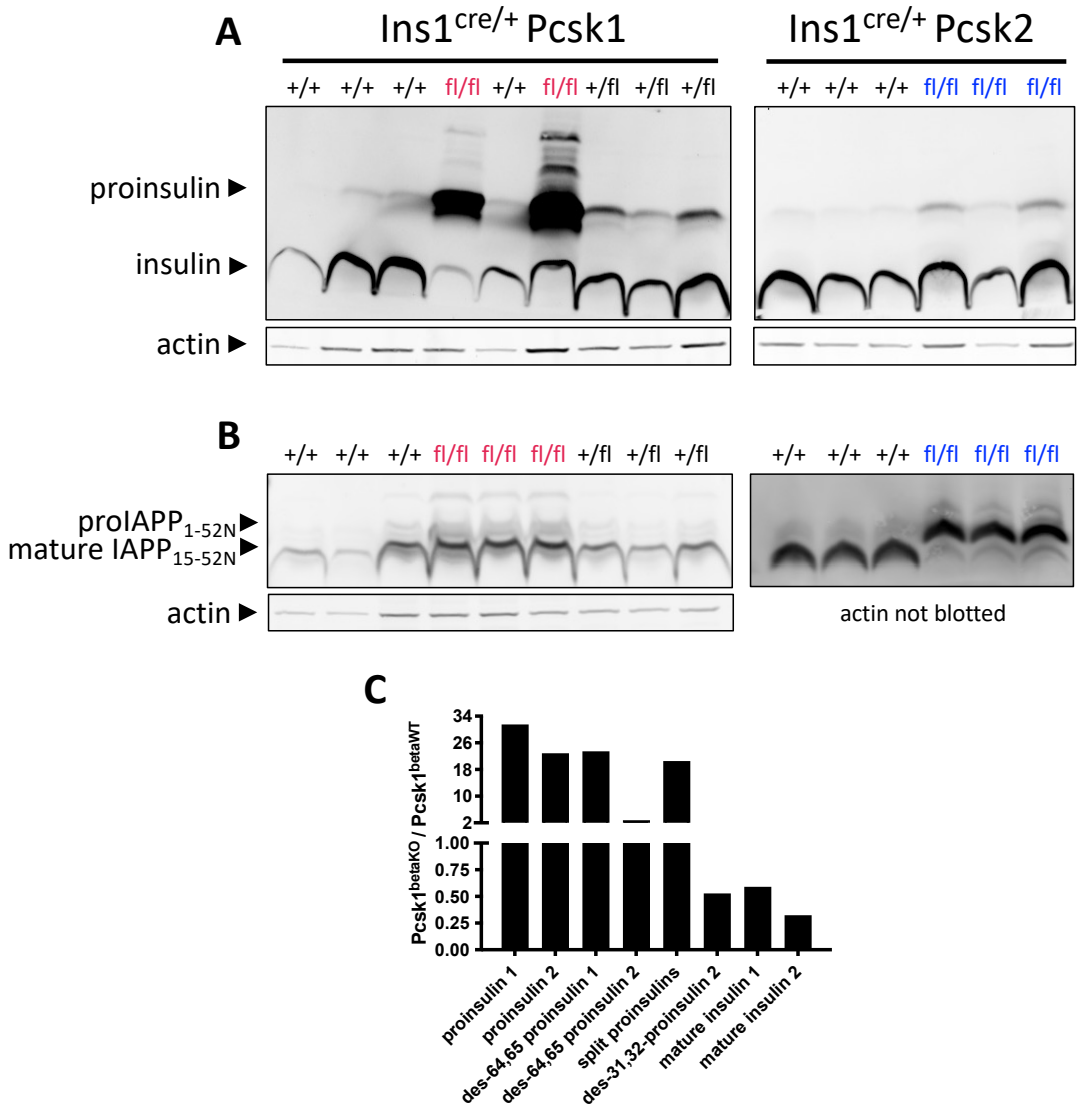

Figure 19: *Pcsk1* and *Pcsk2* requirements differ for proinsulin and proIAPP processing in mice.

(A) Islet lysates were resolved on a non-reducing urea gel and blotted with an antibody that detects insulin, proinsulin, and processing intermediates. Elevated proinsulin is detected in *Pcsk1*- and *Pcsk2*-null islets, with a larger defect in islets lacking *Pcsk1*. Pcsk1^{betaHET} islets display impairments in proinsulin processing comparable to or worse than *Pcsk2*-null islets, and all islets contain detectable mature insulin. **(B)** Islet lysates were resolved on a reducing tris-tricine gel and probed with an antibody targeting the amidated C-terminus of (pro)IAPP. *Pcsk1*-null islets contain ample mature IAPP, while *Pcsk2*-null islets have minimal mature IAPP and elevated proIAPP$_{1\text{-}52N}$. **(C)** Pcsk1^{betaKO} and Pcsk1^{betaWT} mouse islet lysates (n = 1) were analyzed by top-down mass spectrometry. Peaks were manually annotated for mouse proinsulin, insulin, and processing intermediates, and quantified as a ratio of Pcsk1^{betaKO} / Pcsk1^{betaWT}. Standard peptides were not included rendering the ratio qualitative.

5.2.2 Deletion of Pcsk1, but not Pcsk2, increases diabetes susceptibility in mice

Female mice lacking *Pcsk1* or *Pcsk2* did not display any differences in fasting glycemia or body weight (Figure 20 A-D) from 5-30 weeks old. Male mice lacking *Pcsk1* or *Pcsk2* did not display any differences in body weight over the same period (Figure 20 E,F). Juvenile (i.e., 5-15 weeks old) Pcsk1^{betaKO} male mice were euglycemic, but developed fasting hyperglycemia in adulthood beginning at 18-20 weeks old (Figure 20G). Pcsk2^{betaKO} male mice did not display sustained fasting hyperglycemia (Figure 20H). Glucose tolerance tests showed similar patterns to fasting glycemia measurements. Female mice lacking beta-cell *Pcsk1* or *Pcsk2* had no impairment in glucose tolerance at 12 or 26 weeks old (Figure 21 A-D). Male mice lacking beta-cell *Pcsk1* or *Pcsk2* also had no differences in glucose tolerance at 12 weeks old, but by 26-weeks-of-age Pcsk1^{betaKO} male mice developed impaired glucose tolerance while Pcsk2^{betaKO} male mice retained normal glucose tolerance (Figure 21 E-H). Given the reduced islet mature insulin and normal glucose tolerance in young Pcsk1^{betaKO} mice, we also investigated insulin sensitivity in Pcsk1^{betaKO} mice with insulin tolerance tests. Pcsk1^{betaKO} mice had similar insulin-stimulated reductions in fasting glycemia compared to Pcsk1^{betaWT} mice with the exception of 28-week-old female Pcsk1^{betaKO} mice, which displayed a larger reduction in blood glucose 60 minutes post-insulin injection (Figure 22A-D). However, there was no significant difference in the area above the curves between PCSK1-deficient and control mice at any age and either sex, suggesting that beta-cell PCSK1 deficiency does not drastically alter insulin sensitivity.

Given the remarkable ability of Pcsk1^{betaKO} mice to largely maintain euglycemia despite major impairments in proinsulin processing, I next sought to characterize the ability of beta-cell *Pcsk1*- and *Pcsk2*-deficent mice to adapt to beta-cell stress. Mice were fed a high-fat diet (HFD; 45% kcal from fat) beginning at 8-9 weeks old and monitored for changes in glycemia and body

weight. No differences were observed in the fasting glycemia or body weight of Pcsk1^{betaKO} and Pcsk2^{betaKO} female mice, and no female mice developed diabetes (Figure 23 A-F). Of the 10 HFD-fed Pcsk1^{betaKO} male mice, 4 developed diabetes (sustained fasting glycemia > 15.9 mM) beginning after 14 weeks of diet (Figure 24A). In contrast, only 1/10 Pcsk2^{betaKO} and 1/16 Pcsk2^{betaHET} male mice developed diabetes (Figure 24B). Several Pcsk1^{betaKO} mice that did not develop diabetes experienced transient fasting hyperglycemia (Figure 24C). The remaining 9/10 Pcsk2^{betaKO} and 15/16 Pcsk2^{betaHET} male mice had comparable glycemia to Pcsk2^{betaWT} mice over the 30 weeks of HFD (Figure 20D). Body weight was unaltered in HFD-fed male mice lacking beta-cell *Pcsk1* and *Pcsk2* in comparison to HFD-fed control mice (Figure 24 E,F). Glucose tolerance tests revealed comparable handling of a glucose bolus in Pcsk1^{betaKO} and Pcsk2^{betaKO} male and female mice after 4 weeks of HFD and after 14 (Pcsk1^{betaKO}) or 20 (Pcsk2^{betaKO}) weeks of HFD (Figure 25 A-H). Interestingly, after 14 weeks of HFD and shortly preceding the development of diabetes, Pcsk1^{betaKO} mice did not display significantly impaired glucose tolerance; the shape of the curve was similar to that of Pcsk1^{betaWT} indicating comparable glucose clearance, but glycemia tended to be higher at each time point (Figure 25G).

Analysis of insulin secretory granules revealed a complete lack of dense-core granules in Pcsk1^{betaKO} beta cells, while beta cells from Pcsk2^{betaKO} mice had comparable insulin granules to Pcsk2^{betaWT} controls (Figure 26A). Pcsk1^{betaKO} granules resemble immature insulin granules with a pale lumen and no halo, while Pcsk2^{betaKO} beta cells contain a blend of mature and immature insulin granules comparable to control animals (Figure 26B).

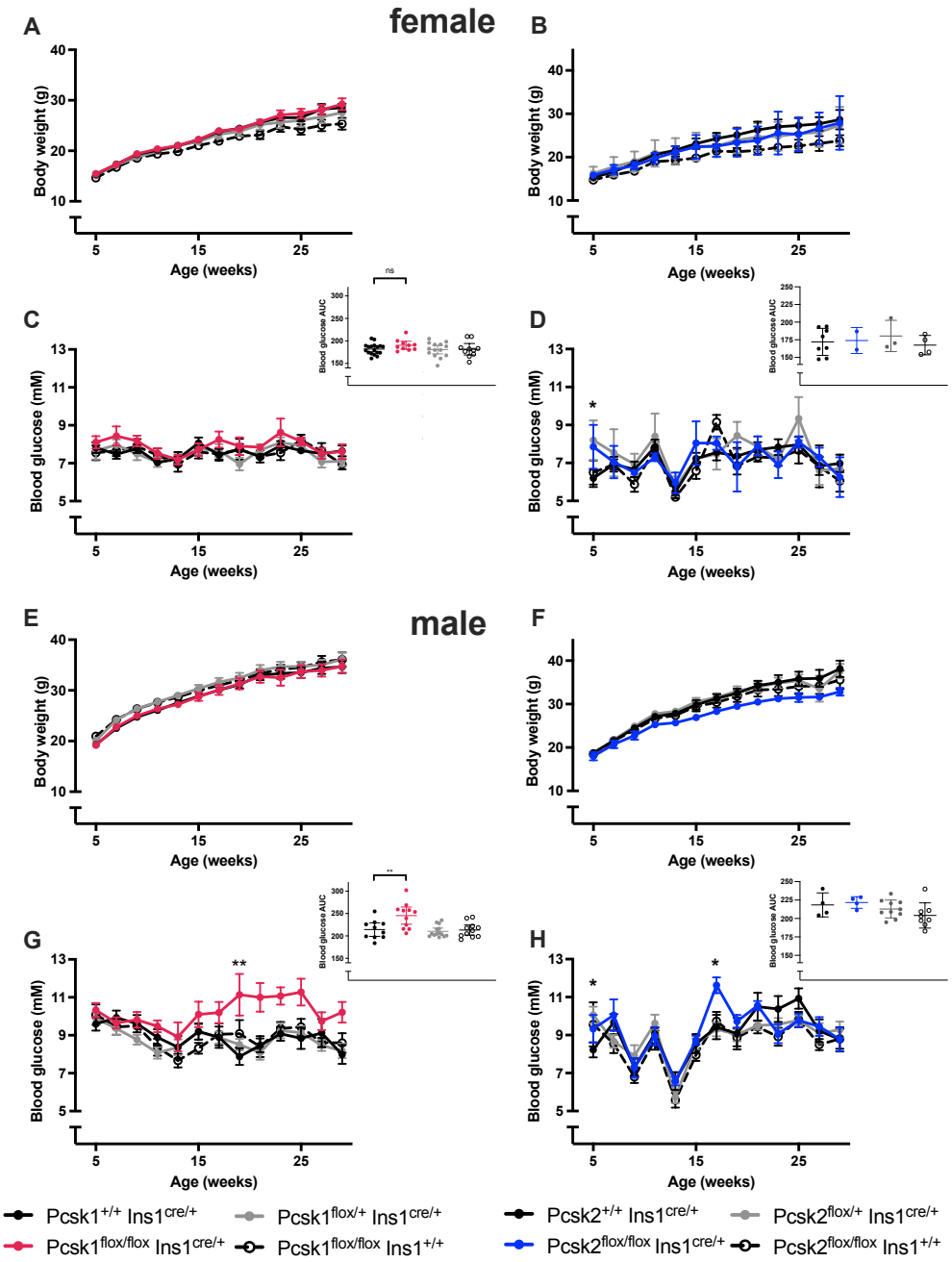

Figure 20: Pcsk1^{betaKO}, but not Pcsk2^{betaKO} mice develop sex-specific fasting hyperglycemia with age.

(A-D) Pcsk1- and Pcsk2-betaKO or heterozygous female mice do not develop any differences in fasting body weight or glycemia between 5-29 weeks of age. **(E,F)** Male Pcsk1- and Pcsk2-betaKO or heterozygous mice do not have differences in body weight gain from 5-29 weeks of age**. (G)** Juvenile Pcsk1^{betaKO} male mice have normal fasting glycemia but develop fasting hyperglycemia with age. **(H)** Pcsk2^{betaKO} male mice do not display consistent fasting hyperglycemia. n = 9-18 Pcsk1^{betaKO}, 2-10 Pcsk2^{betaKO} mice.

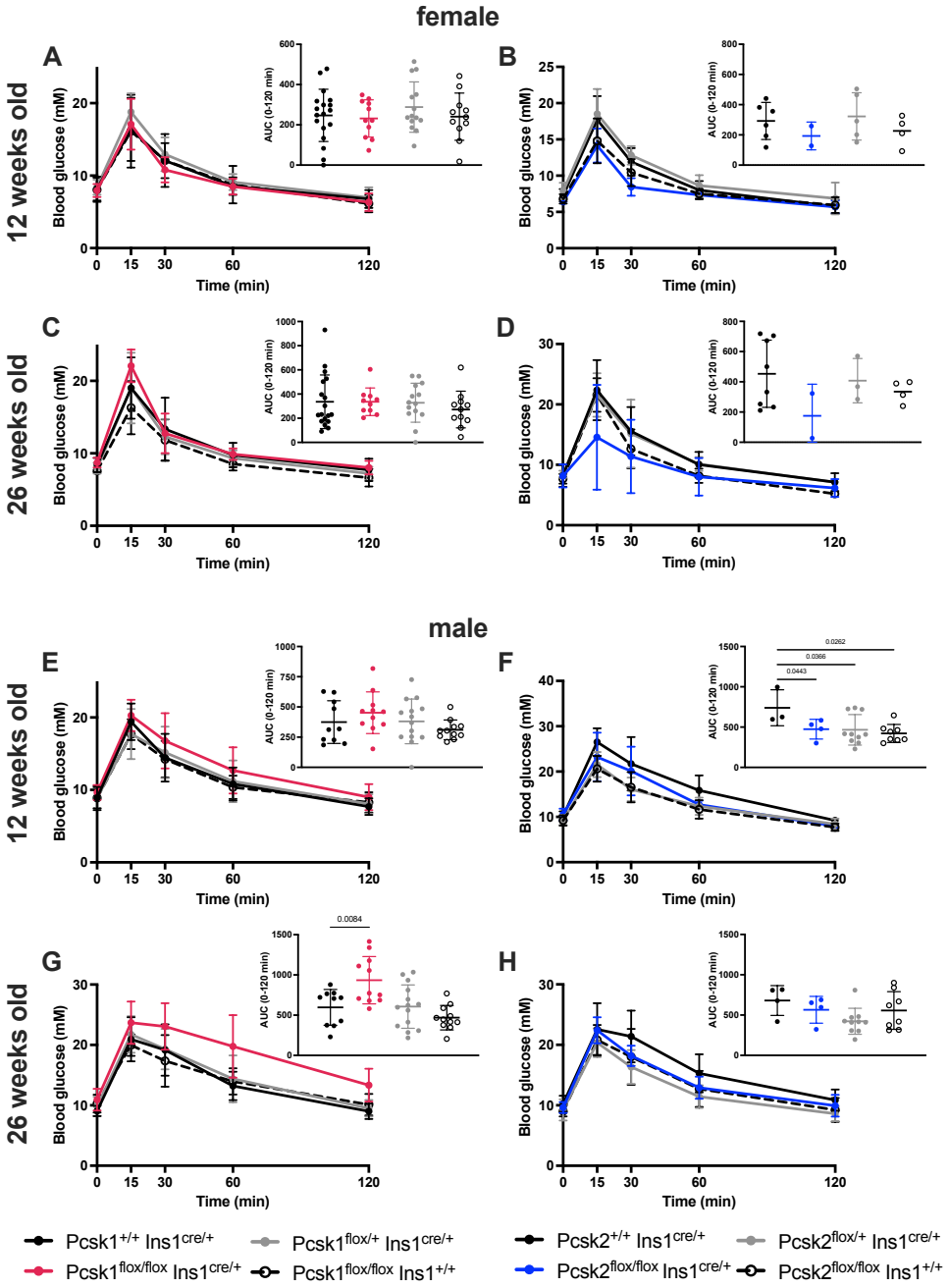

Figure 21: Pcsk1^{betaKO}, but not Pcsk2^{betaKO} mice develop sex-specific impaired glucose tolerance with age.

Mice were administered intraperitoneal glucose tolerance tests after a 6 hour fast at the ages indicated above. **(A-D)** Female Pcsk1^{betaKO} and Pcsk2^{betaKO} mice do not display impaired glucose tolerance at 12 or 26 weeks of age. **(E,F)** Male Pcsk1^{betaKO} and Pcsk2^{betaKO} mice do not display impaired glucose tolerance at 12 weeks of age. **(G)** At 26 weeks of age Pcsk1^{betaKO} male mice display impaired glucose tolerance, while **(H)** Pcsk2^{betaKO} male mice have normal glucose tolerance. AUC (area under curve) is calculated from the y-intercept as baseline. n = 9-18 Pcsk1^{betaKO}, 2-10 Pcsk2^{betaKO} mice.

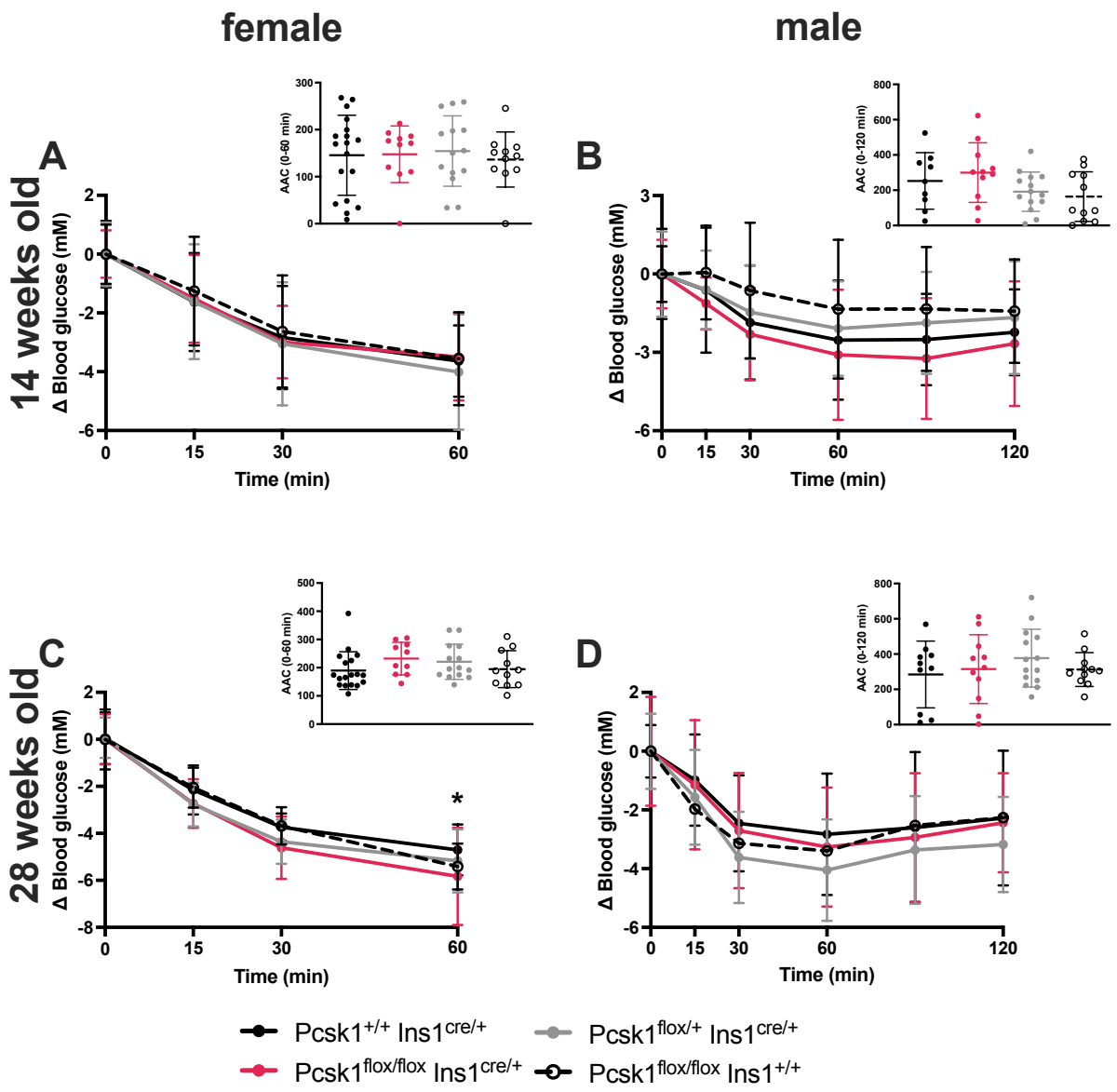

Figure 22: Beta-cell Pcsk1 deficiency does not markedly alter insulin sensitivity. Mice were administered intraperitoneal insulin tolerance tests after a 4 hour fast at the ages indicated above. **(A,B)** Male and female Pcsk1^{betaKO} mice at 14 weeks of age display no difference in insulin-induced decreases in glycemia. **(C)** Female Pcsk1^{betaKO} mice display mildly increased insulin sensitivity at 28 weeks old relative to Pcsk1^{betaWT} mice, with a greater insulin-induced reduction in blood glucose 60 minutes post-injection. **(D)** Pcsk1^{betaKO} male mice at 28 weeks of age have comparable insulin tolerance to Pcsk1^{betaWT} male mice. n = 11-18 female, 9-11 male mice.

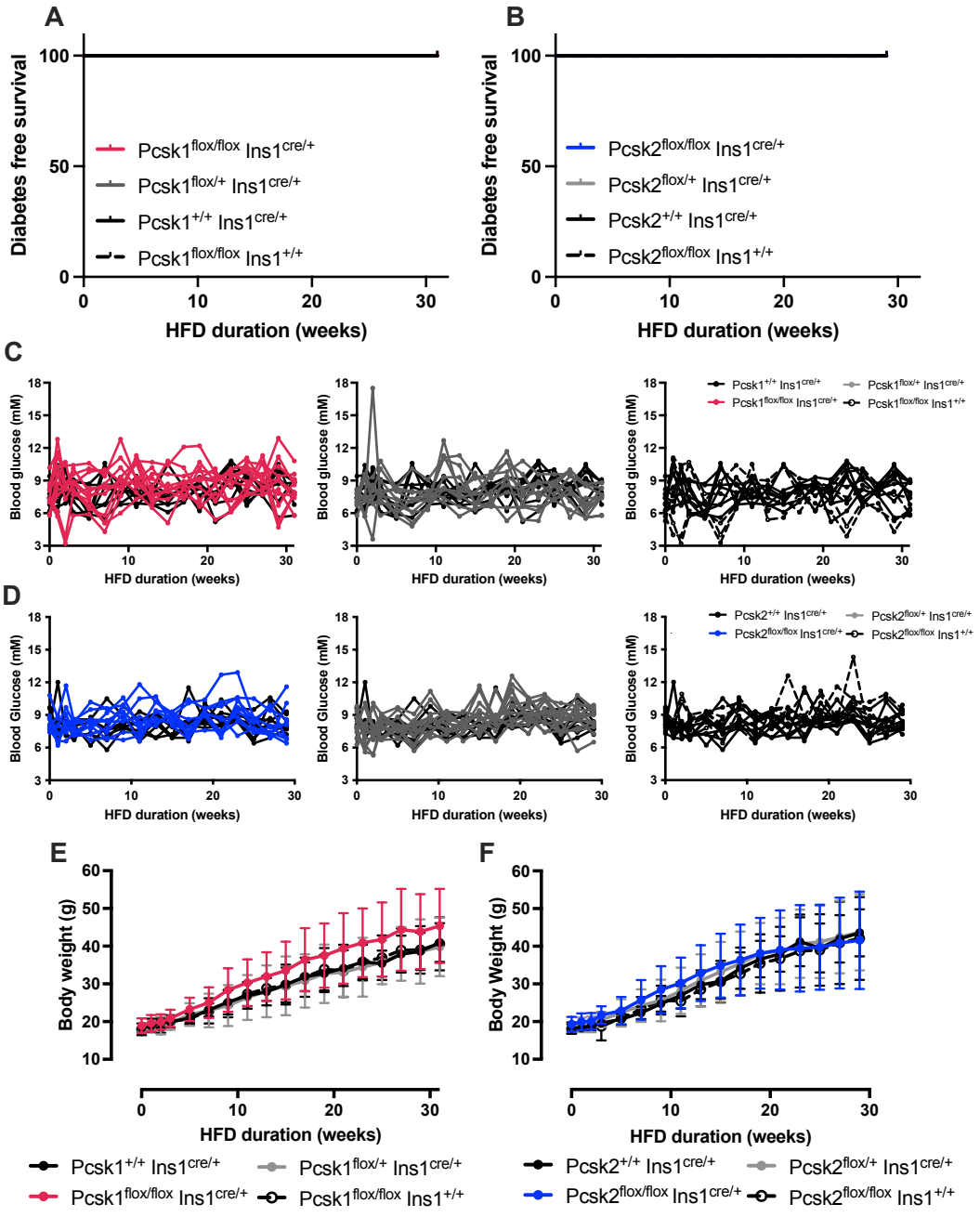

Figure 23: High-fat diet does not induce diabetes in beta-cell *Pcsk1*- or *Pcsk2*-deficient female mice.

Mice were switched from standard chow diet to a high-fat diet (HFD) at 8-9 weeks of age. **(A,B)** No female mice developed diabetes (sustained fasting glycemia > 15.9 mM) after 30 weeks of diet duration in either model. **(C,D)** Pcsk1^{betaKO} and Pcsk2^{betaKO} female mice have comparable fasting glycemia to control mice. Individual mice are plotted with control animals to better visualize any spontaneous or variable changes in glycemia. **(E,F)** Pcsk1^{betaKO} and Pcsk2^{betaKO} mice do not display altered body weight gain relative to control mice. n = 5-13.

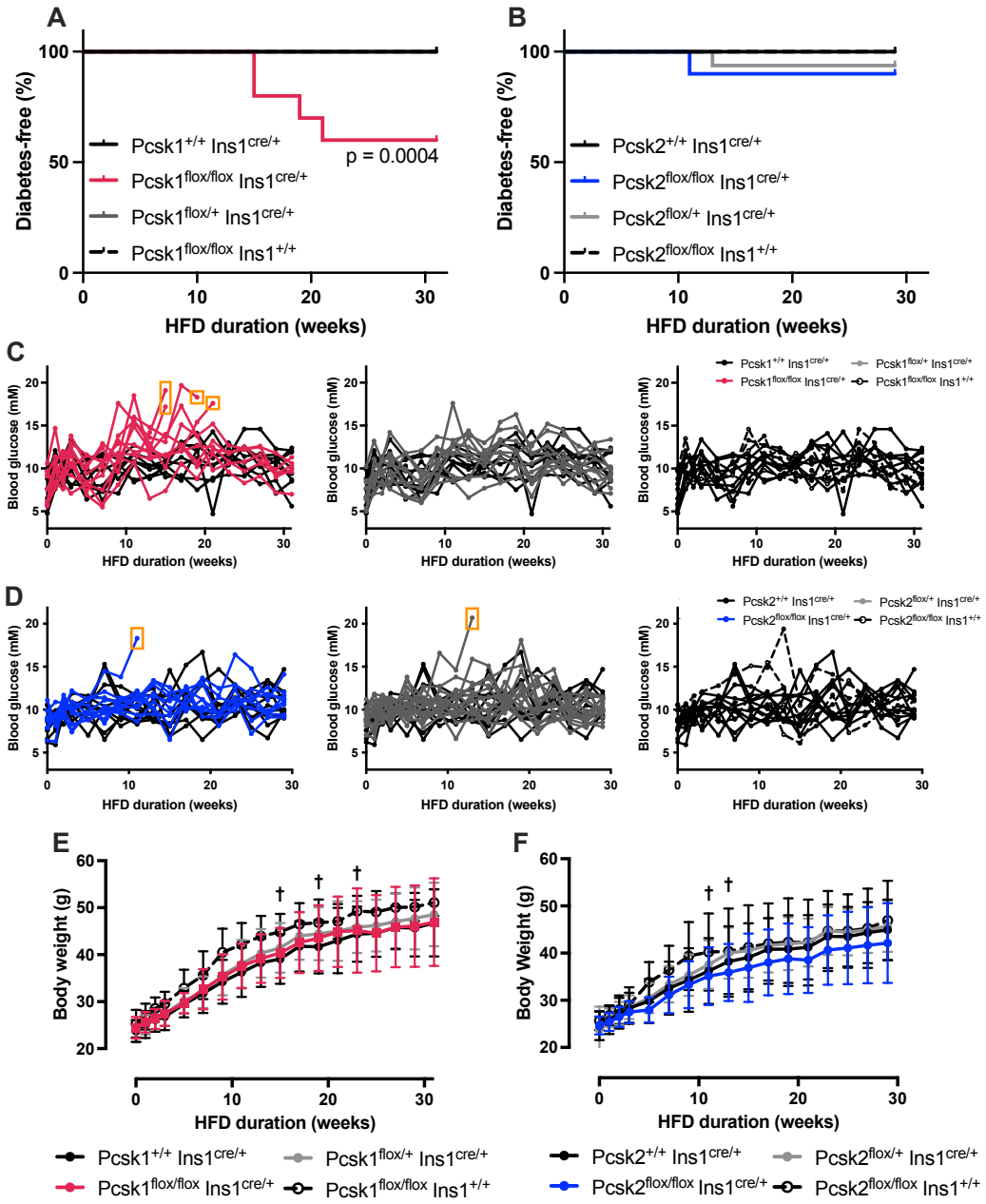

Figure 24: High-fat diet induces diabetes in Pcsk1^{betaKO}, but not Pcsk2^{betaKO} male mice. Mice were switched from standard chow diet to a high-fat diet (HFD) at 8-9 weeks of age. **(A,B)** HFD-feeding induces diabetes (sustained fasting glycemia > 15.9 mM) in 4/10 Pcsk1^{betaKO} male mice, while 1/10 Pcsk2^{betaKO} and 1/16 Pcsk2^{betaHET} male mice developed diabetes by 30 weeks of diet duration. **(C)** Pcsk1^{betaKO} male mice develop variable hyperglycemia and diabetes beginning at 15 weeks of age, while **(D)** the majority of Pcsk2^{betaKO} male mice maintain glycemia comparable to control mice. Individual mice are plotted with control animals to better visualize any spontaneous or variable changes in glycemia. Orange boxes represent animals euthanized due to sustained hyperglycemia. **(E,F)** Pcsk1^{betaKO} and Pcsk2^{betaKO} mice do not display altered body weight gain relative to control mice. † marks weeks in which hyperglycemic mice were euthanized. n = 4-16.

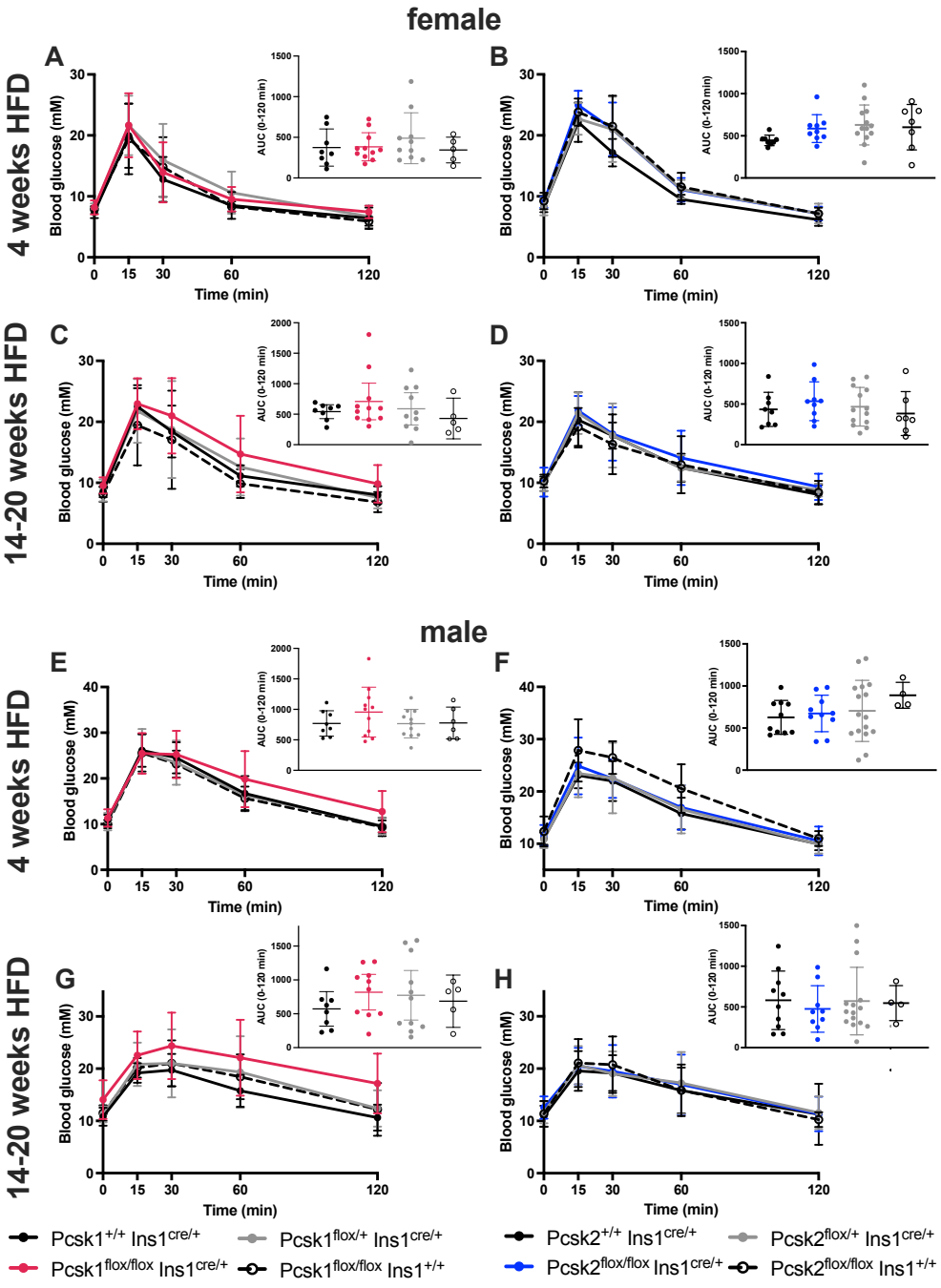

Figure 25: *Pcsk1* or *Pcsk2* deficiency in beta cells does not further worsen high-fat diet-induced impairments in glucose tolerance.
Mice were administered intraperitoneal glucose tolerance tests after a 6 hour fast. **(A,B,E,F)** *Pcsk1* or *Pcsk2* deletion in beta cells does not impact glucose tolerance after 4 weeks of high-fat diet (HFD) in female or male mice. **(C,G)** *Pcsk1* deletion does not significantly worsen glucose tolerance after 14 weeks of HFD, although male Pcsk1^{betaKO} mice display a trend toward elevated 2 h glycemia (p = 0.08). **(D,H)** *Pcsk2* deletion in beta cells does not impair glucose tolerance in female and male mice after 20 weeks of HFD. n = 5-13 female, 4-16 male mice.

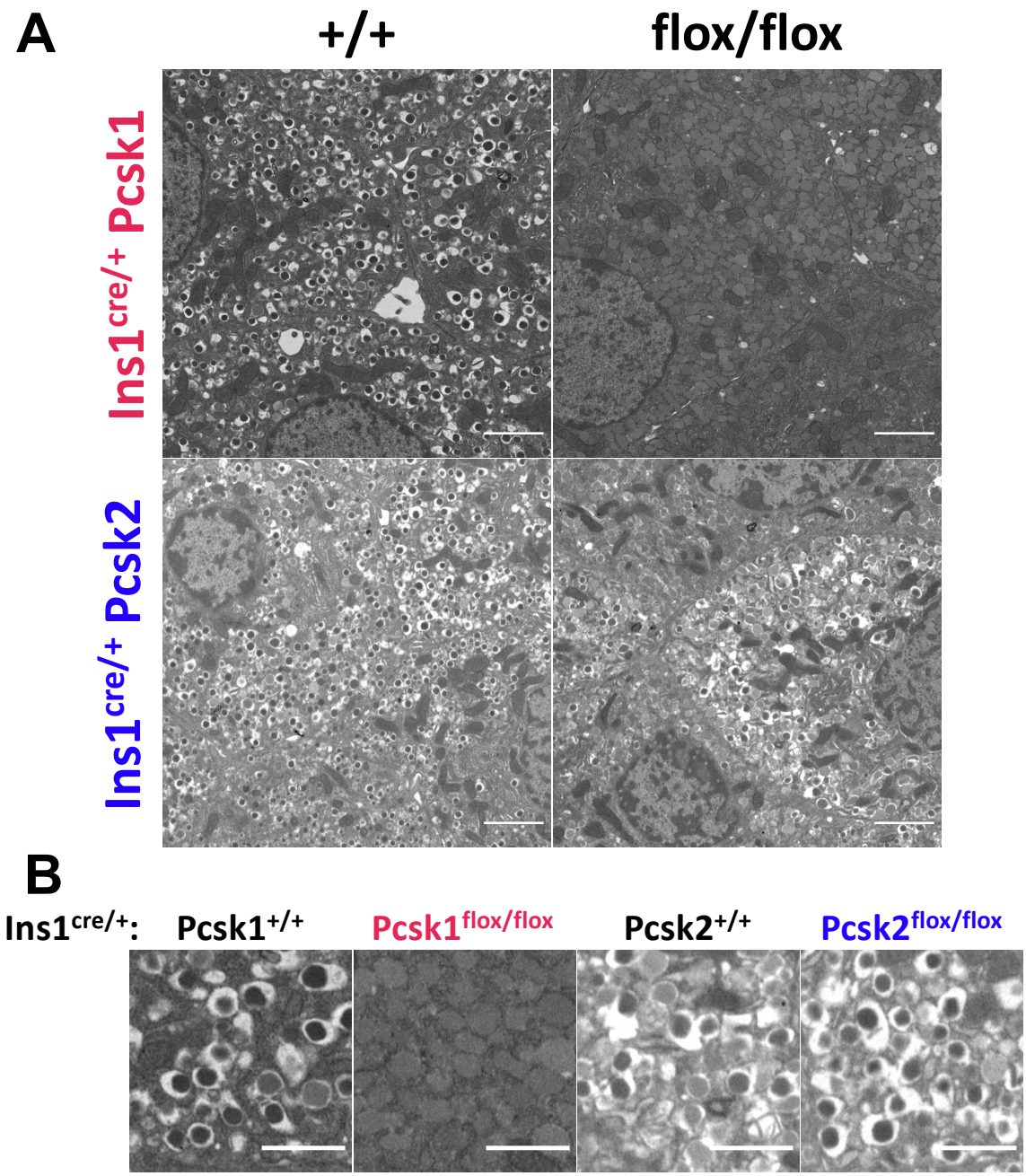

Figure 26: Deficiency of *Pcsk1*, but not *Pcsk2*, causes immature-like insulin secretory granules in beta cells.
Freshly isolated islets from 7-week-old mice were fixed and imaged by transmission electron microscopy. Pcsk1^{betaKO} insulin secretory granules are pale and diffuse, lacking a dense core and translucent halo, while Pcsk2^{betaKO} insulin secretory granules closely resemble control granules. Scale bars represent 2 µm in (A) and 1 µm in (B). Images are representative of 10-15 images per mouse. Islets from 2 mice per genotype were imaged.

5.2.3 Deletion of both Pcsk1 and Pcsk2 blocks proinsulin processing and causes hyperglycemia in mice

Pcsk1^{betaKO} mice still produced mature insulin, suggesting Pcsk2 can process proinsulin to mature insulin in mice. I next generated beta-cell specific double prohormone convertase *Pcsk1-Pcsk2* knockout mice (DPC^{betaKO}: *Pcsk1$^{flox/flox}$; Pcsk2$^{flox/flox}$; Ins1$^{cre/+}$*) to further characterize the contributions of Pcsk2 and beta-cell prohormone processing on glycemic regulation. DPC^{betaKO} and control DPC^{betaWT} (*Pcsk1$^{flox/flox}$; Pcsk2$^{flox/flox}$; Ins1$^{+/+}$*) mice had comparable body weight in both male and female mice (Figure 27 A,B). Female DPC^{betaKO} mice developed moderate fasting hyperglycemia early in adulthood, while male DPC^{betaKO} mice developed more marked fasting hyperglycemia present at all ages measured (5-31 weeks old) (Figure 25 C,D). Inspecting the fasting measurements of mice individually revealed that DPC^{betaKO} male mice, but not female DPC^{betaKO} mice, had highly fluctuating week-to-week glycemia with hyperglycemic excursions over 20 mM that returned to lower levels within a week (Figure 27 E,F). In keeping with the fasting hyperglycemia we observed significantly impaired glucose tolerance as early as 10-weeks-of-age in male and female DPC^{betaKO} with a more pronounced phenotype in male mice (Figure 27 G,H).

Isolation of DPC^{betaKO} islets yielded pale islets (Figure 28A) and typically we observed more isolated islets from each pancreas in comparison to age-matched DPC^{betaWT} control mice (Figure 28 C,D). DPC^{betaKO} islets contained no mature insulin and only intact proinsulin when analyzed with a non-reducing western blot (Figure 28B). These data show that complete lack of beta-cell PCSK1 and PCSK2 activity results in negligible proinsulin processing, and hyperglycemia and impaired glucose intolerance in both male and female mice, with a larger

impact on the glycemic regulation of male mice. The glycemic, body weight, and proinsulin and proIAPP processing phenotypes of Pcsk1^{betaKO}, Pcsk2^{betaKO}, and DPC^{betaKO} mice are summarized in Table 4.

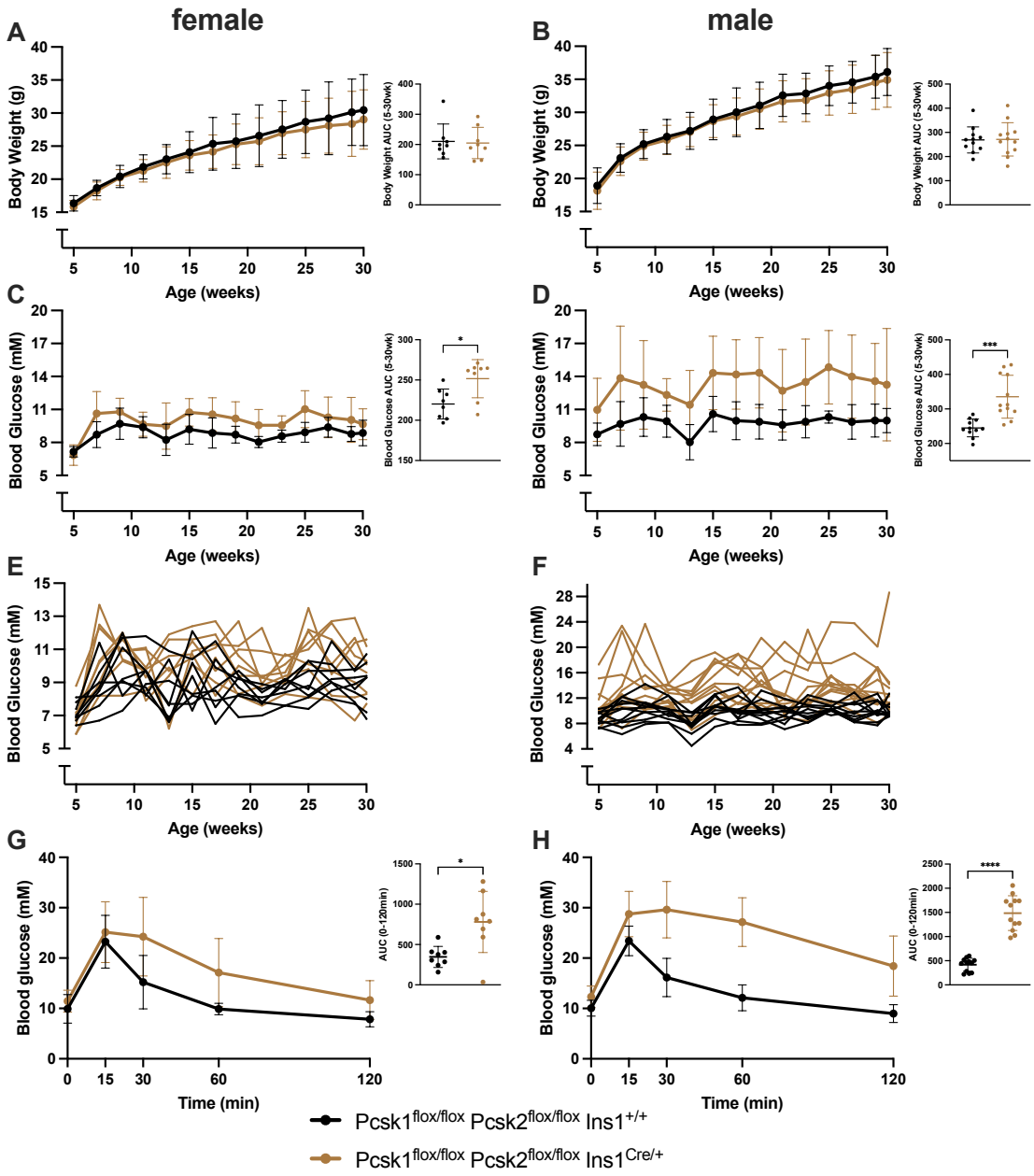

Figure 27: Mice lacking both *Pcsk1* and *Pcsk2* in beta cells develop hyperglycemia. **(A,B)** *Ins1*$^{cre/+}$*; Pcsk1*$^{flox/flox}$*; Pcsk2*$^{flox/flox}$ (DPC^{betaKO}) female and male mice show no differences in body weight relative to *Ins1*$^{+/+}$*; Pcsk1*$^{flox/flox}$*; Pcsk2*$^{flox/flox}$ (DPC^{betaWT}) control mice from 5-31 weeks of age. **(C,D)** Both female and male DPC^{betaKO} mice develop fasting hyperglycemia. **(E,F)** Plotting individual replicate mice shows the large fasting glycemia swings in individual DPC^{betaKO} mice, with some male mice differing by > 10 mM between measurements**. (G,H)** Intraperitoneal glucose tolerance tests at 10 weeks of age show female and male DPC^{betaKO} mice have significantly impaired glucose tolerance in early adulthood. n = 8-12 mice.

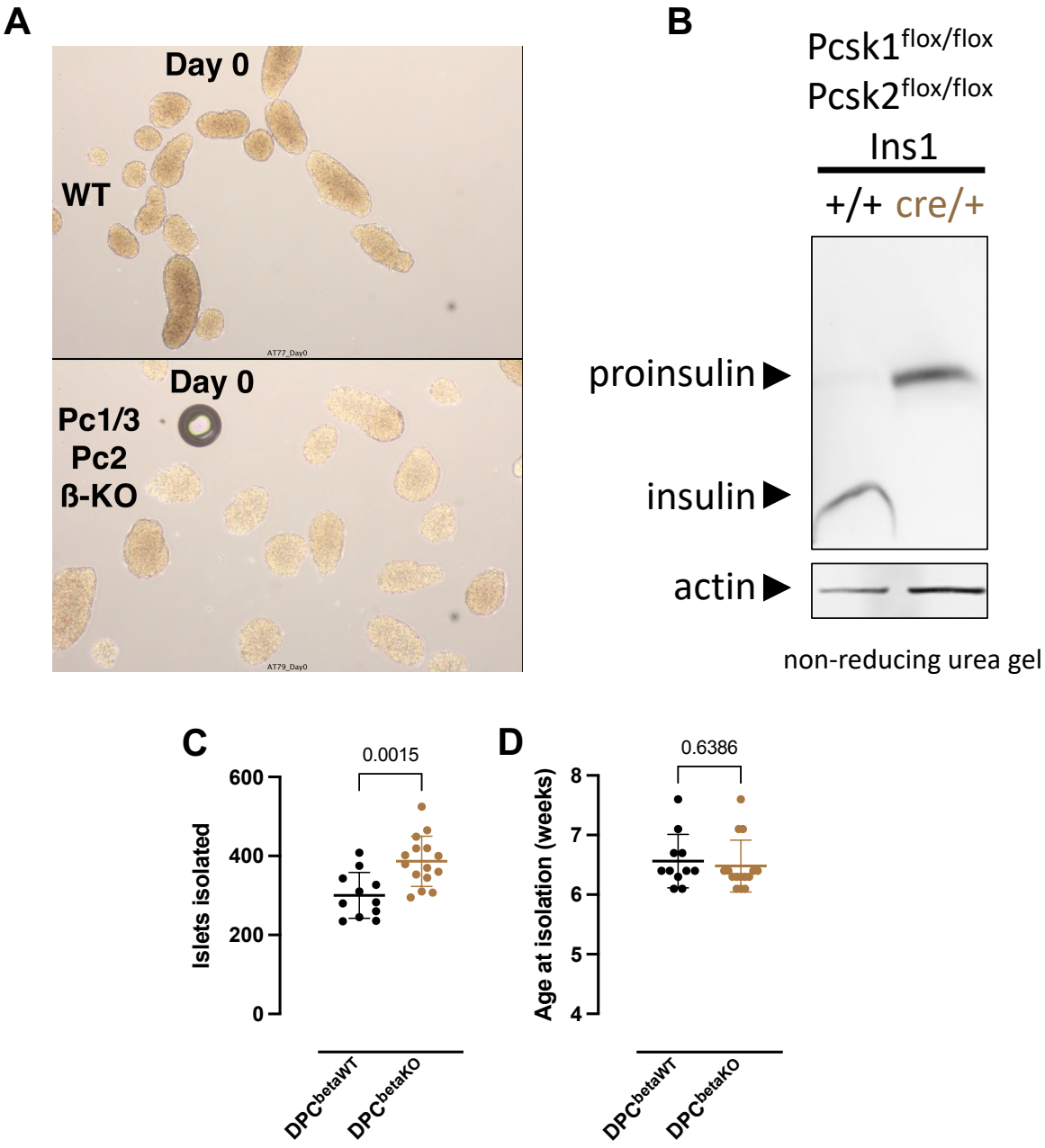

Figure 28: DPC^{betaKO} islets are pale and lack mature insulin.
(A) Freshly isolated DPC^{betaKO} islets are pale in colour upon isolation. **(B)** Lysates from freshly isolated islets were analyzed by a non-reducing urea gel and western blot with a pan-(pro)insulin antibody. DPC^{betaKO} islets contained no detectable mature insulin by western blot. **(C)** DPC^{betaKO} mice yield an increased number of isolated islets. **(D)** Age of mice for islets isolated in (C). In (D) bar represents median, and comparison was performed using Mann-Whitney test.

Table 4: Summary of mouse beta-cell PCSK deficiency phenotypes

Model	Mature insulin	Mature IAPP	Body weight	Fasting glycemia	Glucose tolerance
Pcsk1^{betaKO} CD	reduced	–	–	hyperglycemia (with age in males)	impaired (with age in males)
Pcsk1^{betaKO} HFD	NA	NA	–	hyperglycemia (in males)	impaired (in males)
Pcsk2^{betaKO} CD	–	reduced	–	–	–
Pcsk2^{betaKO} HFD	NA	NA	–	–	–
DPC^{betaKO}	not detected	NA	–	hyperglycemia	impaired

– normal
NA, not assessed

5.2.4 Impaired beta-cell prohormone processing increases beta-cell mass while reducing beta-cell proliferative capacity

To better characterize the adaptive mechanisms of islets in response to deficient beta-cell processing activity, we quantified beta-cell mass and insulin / glucagon ratios in Pcsk1^{betaKO} and DPC^{betaKO} mice. Pancreas sections from 30-week-old DPC^{betaKO} male mice displayed abundant islets, and a marked number of large islets that lacked proportional glucagon immunoreactivity (Figure 29A). Pcsk1^{betaKO} displayed a similar but more modest phenotype, with trends toward a 50% increase in beta-cell area and a reduced alpha/beta cell ratio (Figure 29 B,C). Pancreas mass was found unaltered in a subset of Pcsk1^{betaKO} mice (Figure 29D), suggesting beta-cell area measurements are representative of beta-cell mass in Pcsk1^{betaKO} mice. DPC^{betaKO} male mice displayed a larger increase in beta-cell area than Pcsk1^{betaKO} mice, with a doubling of insulin^{+}/pancreas area (Figure 29E). DPC^{betaKO} islets also contained a reduced ratio of

glucagon^{+}/insulin^{+} area (Figure 29F), while the area of glucagon^{+} immunoreactivity per islet trended downward in DPC^{betaKO} mice (Figure 29G). These data suggest that beta-cell mass is expanded in response to deficient beta-cell prohormone processing activity, but that alpha cell mass is unchanged, resulting in an altered islet architecture with abundant beta cells compared to non-beta cells.

Hyperglycemia can drive beta-cell proliferation[359], so I next sought to analyze beta-cell proliferation and mass at an early age prior to the onset of hyperglycemia in Pcsk1^{betaKO} and DPC^{betaKO} mice. Even by 4.5 weeks of age, Pcsk1^{betaKO} male mice already tended to have increased beta-cell area / pancreas area (Figure 30A), although this was not significant; however, there was no difference in beta-cell proliferation (EdU incorporation) at 4.5 weeks of age (Figure 30B). At 4.5 weeks of age, DPC^{betaKO} male mice had an over two-fold increase in beta-cell mass, yet a similar lack of difference in beta-cell proliferation (Figure 30 D,E). Male Pcsk1^{betaKO} mice had comparable random-fed glycemia to control animals from 4-4.5 weeks old, while DPC^{betaKO} mice were hyperglycemic at this age (Figure 30 C,F).

With hyperglycemia present in young (4 weeks old) DPC^{betaKO} mice, I next assessed the proliferation of processing-deficient beta cells *ex vivo* in dispersed islets under controlled glucose concentrations. Male DPC^{betaKO} beta cells had significantly reduced glucose-stimulated proliferation (Figure 31B). Female DPC^{betaKO} islets (Figure 31A) and male Pcsk1^{betaKO} islets (Figure 31C) also trended toward reduced glucose-stimulated proliferation, but additional replicates are required for statistical analysis. Of note, DPC^{betaKO} islets from male mice are isolated from an environment in which random-fed glycemia is significantly elevated at 6 weeks old (Figure 31E). To determine if the reduced proliferation of DPC^{betaKO} beta cells is via a secreted or cell intrinsic mechanism, I co-cultured DPC^{betaKO} and DPC^{betaWT} islets with

C57BL/6J acceptor islets in a cell-contact-free Transwell® system (Figure 32A). Glucose-stimulated proliferation of C57BL/6J beta cells was similar whether cultured with DPC^{betaKO} or DPC^{betaWT} islets, whereas DPC^{betaKO} donor islets had markedly reduced glucose-stimulated proliferation (Figure 32B). These data suggest that processing-deficient beta cells have reduced proliferation via a cell intrinsic mechanism, rather than from a secreted factor.

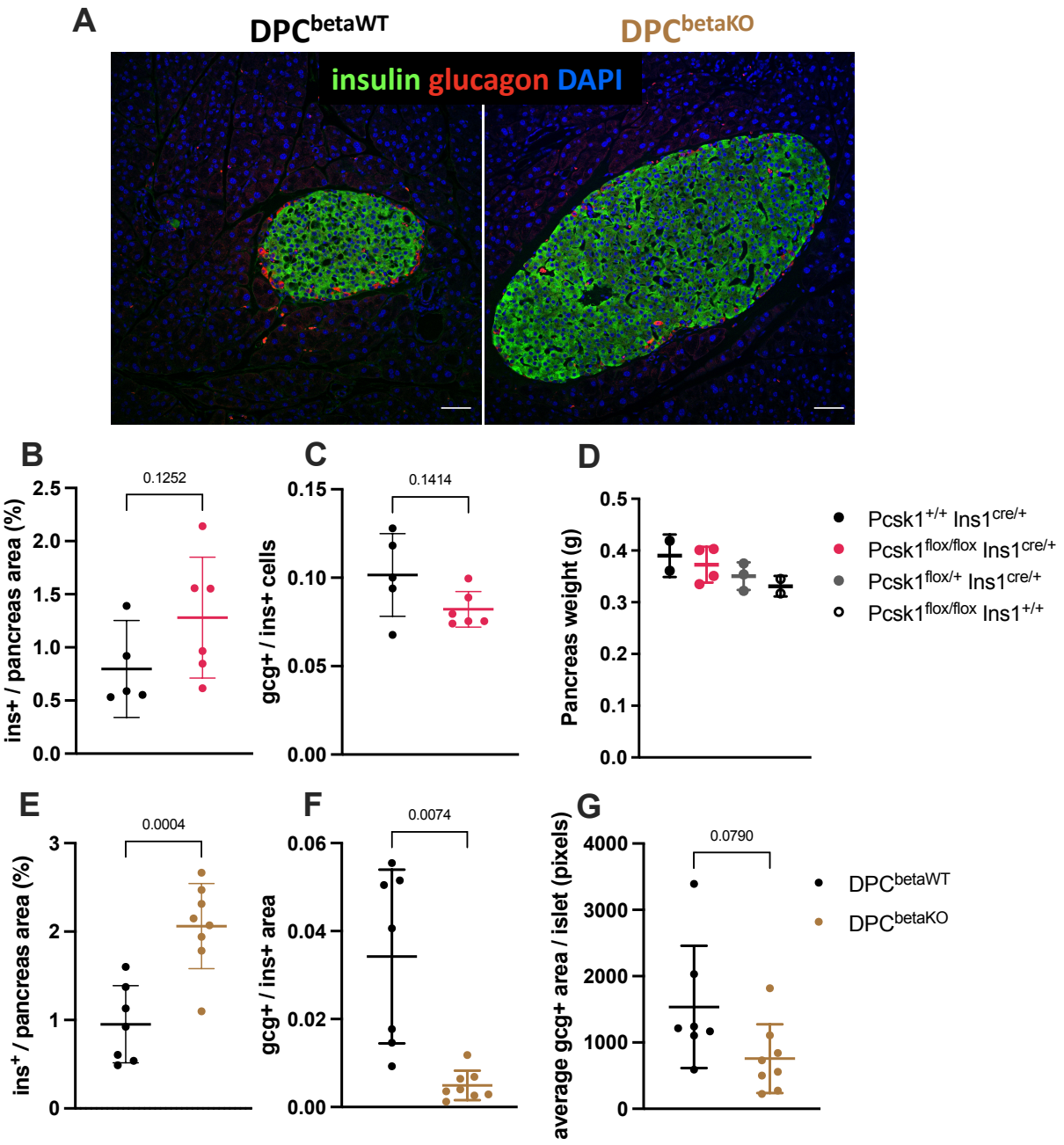

Figure 29: Pcsk1^{betaKO} and DPC^{betaKO} mice have increased beta-cell mass.
Pancreas sections from 30-week-old male mice were analyzed by immunohistochemistry. **(A)** DPC^{betaKO} pancreas sections contained hyperplastic islets with minimal glucagon immunoreactivity. **(B)** Pcsk1^{betaKO} mice trended toward an approximate 50% increase in insulin^{+} pancreatic area. (C) The ratio of glucagon^{+} to insulin^{+} cells was not significantly altered in Pcsk1^{betaKO} islets. (D) Pancreas mass was unaltered in Pcsk1^{betaKO} mice. (E) DPC^{betaKO} mice had two-fold higher insulin^{+} pancreas area than DPC^{betaWT} control. (F) DPC^{betaKO} islets have reduced glucagon^{+} area relative to insulin^{+} area. (G) Glucagon^{+} area per islet trended downward in DPC^{betaKO} islets. Scale bars represent 50 µm.

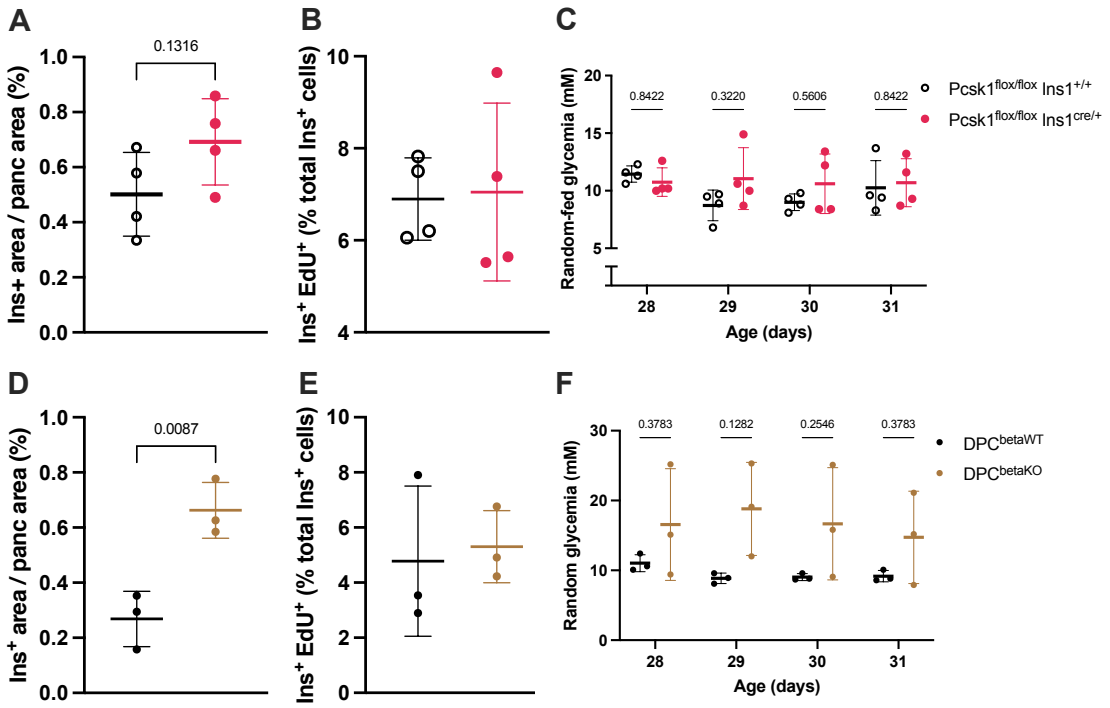

Figure 30: Beta-cell mass is increased by 4.5 weeks of age in Pcsk1^{betaKO} and DPC^{betaKO} male mice.

Male mice were injected daily with EdU for 3 days from 28-30 days-old and pancreases collected at 31 days-old for sectioning and analysis by immunohistochemistry. (A) Pcsk1^{betaKO} mice trended toward a 50% increase in insulin^{+} pancreas area. (B) Beta-cell proliferation was unaltered in Pcsk1^{betaKO} mice. (C) Pcsk1^{betaKO} mice did not have significantly elevated random-fed glycemia when measured daily prior to EdU injections. (D) DPC^{betaKO} mice had over a two-fold increase in insulin^{+} pancreas area. (E) Beta-cell proliferation was unaltered in DPC^{betaKO} mice. (F) DPC^{betaKO} mice trended toward random-fed hyperglycemia from 28-31 days old with a large range of blood glucose values.

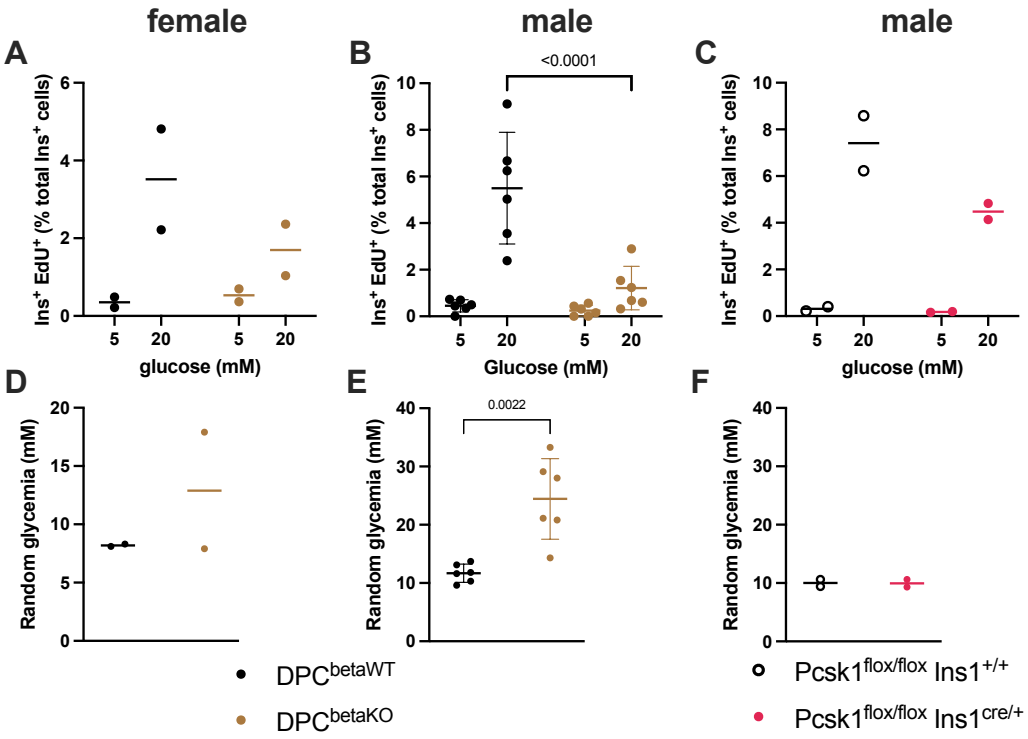

Figure 31: *Pcsk1*- and double *Pcsk1-Pcsk2*-deficient beta cells have reduced proliferative capacity in response to glucose.
Islets were isolated from 6-8 week-old mice, dispersed, and cultured for 72 h in 5 or 20 mM growth medium with 10% FBS. Dispersed islets were labelled with EdU for the final 20 hours. **(A)** Female DPC^{betaKO} mouse islets trended toward reduced proliferation at 20 mM glucose relative to DPC^{betaWT} islets in the same conditions. **(B)** DPC^{betaKO} male islets had significantly reduced glucose-induced beta-cell proliferation. **(C)** $Pcsk1^{betaKO}$ male islets trended toward reduced glucose-stimulated proliferation. **(D-F)** Random-fed glycemia measurements from mice in (A-C) the day of islet isolations. DPC^{betaKO} male mice had significant hyperglycemia, while DPC^{betaKO} female mice trended toward hyperglycemia. $Pcsk1^{betaKO}$ male mice were euglycemic.

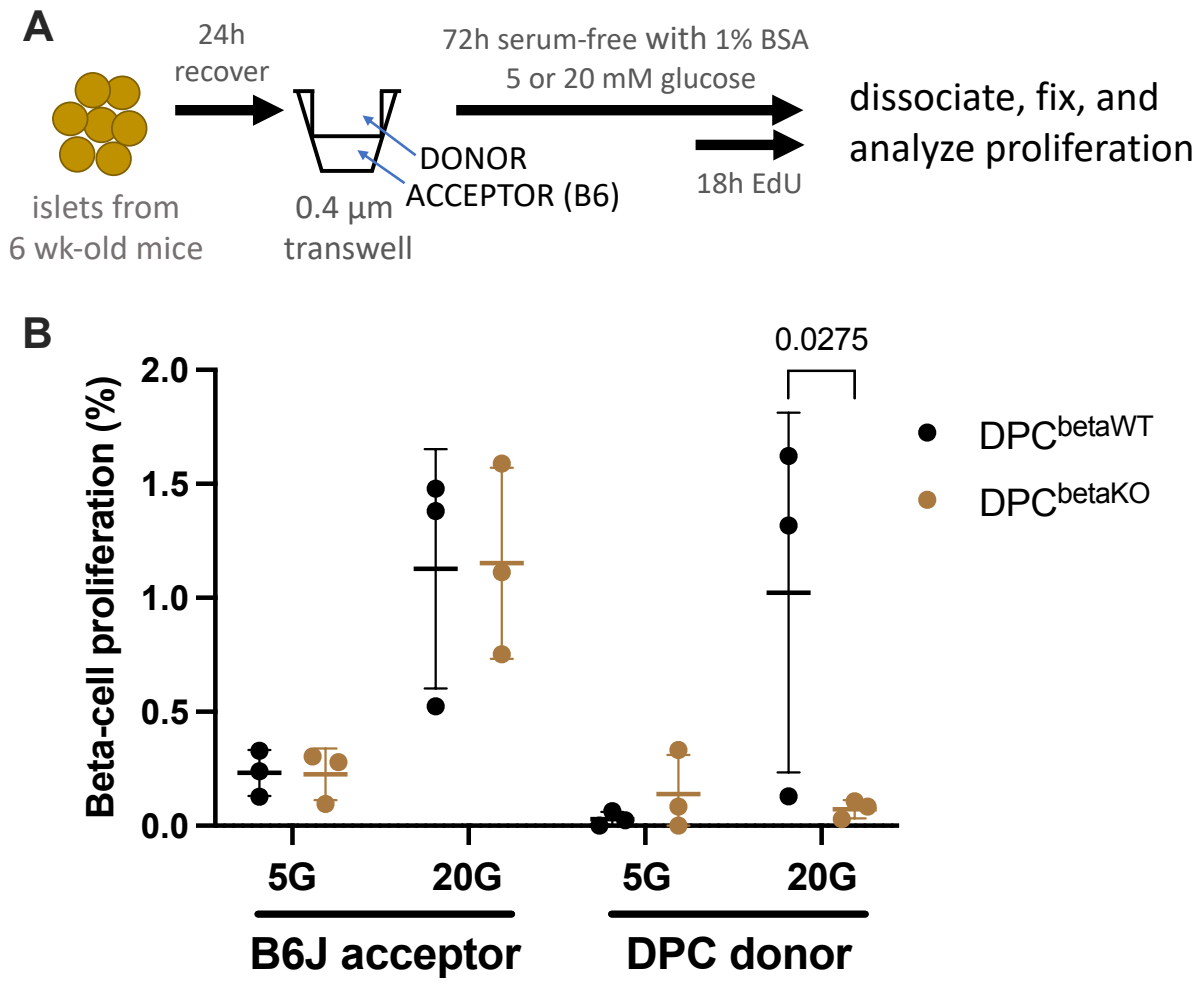

Figure 32: DPC^{betaKO} islets likely do not secrete an anti-proliferative factor.
(A) Schematic outlining experimental protocol. Islets were isolated from 6-7 week-old male DPC^{betaKO}, DPCbetaWT, and C57BL/6J (B6J) mice. Following overnight recovery, 30 B6J acceptor islets were cultured under 100 DPC^{betaKO} or DPC^{betaWT} islets for 72 hours in serum-free media containing 1% BSA and 5 or 20 mM glucose. EdU was added for the final 18 hours. After 72 hours, islets were collected, dissociated, centrifuged onto a 96-well imaging plate, and fixed. EdU labelling and insulin immunohistochemistry was analyzed by microscopy. **(B)** B6J acceptor beta cells displayed equivalent glucose-stimulated proliferation when cultured with DPC^{betaWT} or DPC^{betaKO} islets. DPC^{betaWT} beta cells proliferate in response to 20 mM glucose, while DPC^{betaKO} beta cells display negligible glucose-stimulated proliferation.

5.2.5 The islet transcriptome in beta-cell Pcsk1 deficiency

To better characterize the islet adaptations in Pcsk1^{betaKO} mice prior to diabetes development, we performed RNA sequencing of islets isolated from male Pcsk1^{betaKO} and Pcsk1^{betaWT} mice after 6 weeks of HFD, at which time random-fed glycemia was comparable in the Pcsk1^{betaKO} and Pcsk1^{betaWT} control mice from which islets were isolated (11.3 vs 12.2 mM; p = 0.60). We identified 131 upregulated and 117 downregulated differentially expressed genes (DEGs) (Figure 33A). The significantly upregulated genes included abundant markers of exocrine tissue. Of the significant DEGs, 11 of the 15 with the largest fold increase in Pcsk1^{betaKO} islets were exocrine (10) or ductal (1) markers such as *Zg16*, *Cela1*, and *Amy2b* (Figure 33B). In pancreas sections, there was no alpha-amylase immunoreactivity in Pcsk1^{betaKO} islets, suggesting that the exocrine markers were derived from contaminant exocrine tissue that was consistently higher in Pcsk1^{betaKO} islets (Figure 33D). As expected, *Pcsk1* was the most downregulated DEG, with Pcsk1^{betaWT} islets containing 16-fold higher *Pcsk1* expression than Pcsk1^{betaKO} islets (Figure 33C).

Functional enrichment analysis revealed mostly downregulated pathways in Pcsk1^{betaKO} mice (Figure 34A). Gene Ontology (biological processes) and Reactome pathways were analyzed for over-representation in significant DEGs, and EnrichmentMap was used to generate a network of over-represented processes and pathways ($q < 0.01$) with high similarity. Actin and cytoskeleton regulatory processes were enriched in Pcsk1^{betaKO} islets, driven in part by significant reductions in the actin binding proteins filamin (*Flna*), villin 1 (*Vil1*), vinculin (*Vcl*) and alpha-actinin (*Actn4*), and by reduced actin (*Actg1*) expression. Other downregulated processes of note are those involved in cell-junction and sterol biosynthesis. One cluster of upregulated processes associated with digestion was found, and was driven by the increased

expression of exocrine markers in Pcsk1^{betaKO} islets (Figure 34A). Gene set enrichment analysis (GSEA) was also performed, as GSEA uses a ranked differential expression list of all identified genes, rather than only significant DEGs. This allows for detection of pathways or processes in which many of the members trend in a common positive or negative direction, including those in which few or no genes are significantly differentially expressed. GSEA revealed only significantly downregulated processes ($q < 0.05$) in Pcsk1^{betaKO} islets, with the majority involving cholesterol biosynthesis processes (Figure 34B). This finding suggests that cholesterol biosynthesis may be altered in Pcsk1^{betaKO} islets.

Motif analysis flanking transcriptional start sites of significant DEGs by iRegulon revealed FOX (forkhead box) family transcription factor motifs present in the upregulated DEGs, including Foxo and Foxa family motifs (Table 5). SRF (serum response factor) motifs were found enriched in the significantly downregulated DEGs, with many target genes associated with actin and cytoskeletal processes (Table 5). These data suggest that increased Foxo and reduced Srf signaling may be driving functional adaptations in Pcsk1^{betaKO} islets.

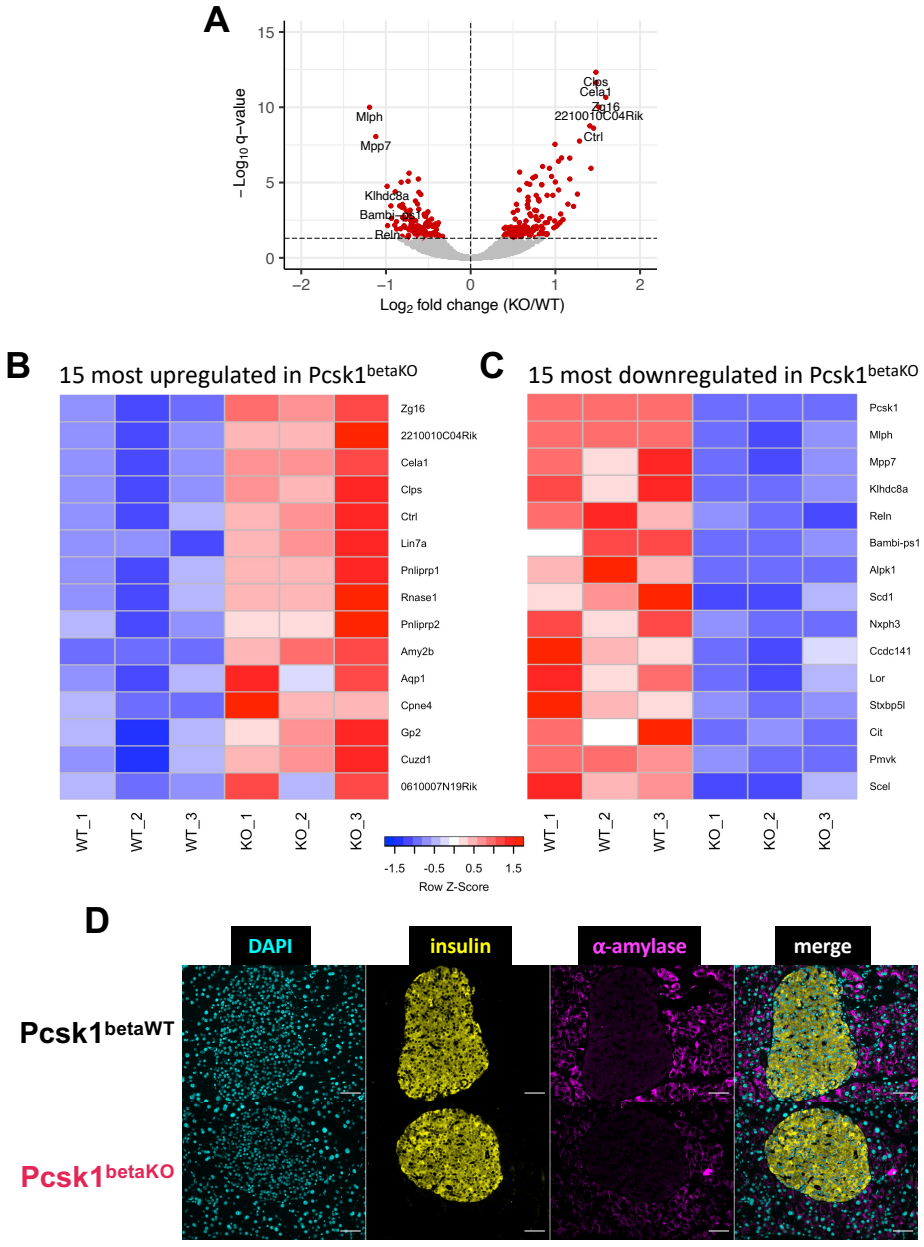

Figure 33: RNA sequencing of islets from high-fat diet-fed Pcsk1^{betaKO} mice.
RNA sequencing was performed on freshly isolated islets from Pcsk1^{betaKO} and Pcsk1^{betaWT} control mice fed a high-fat diet (HFD) for 6 weeks. **(A)** Gene expression of 131 and 117 genes were found upregulated and downregulated, respectively, by differential expression analysis of Pcsk1^{betaKO} (KO) and Pcsk1^{betaWT} (WT) islets. **(B)** Heat map displaying individual replicate expression of the 15 most upregulated genes shows higher expression of exocrine genes in all Pcsk1^{betaKO} islets. **(C)** Heat map displaying individual replicate expression of the 15 most downregulated genes in Pcsk1^{betaKO} islets. **(D)** Alpha-amylase immunoreactivity was not observed in Pcsk1^{betaKO} pancreas sections. Scale bar represents 50 µm. *Pcsk1* (Log_2 fold change -4.1, $q < 3.02 \times 10^{-171}$) was omitted from (A) for clarity.

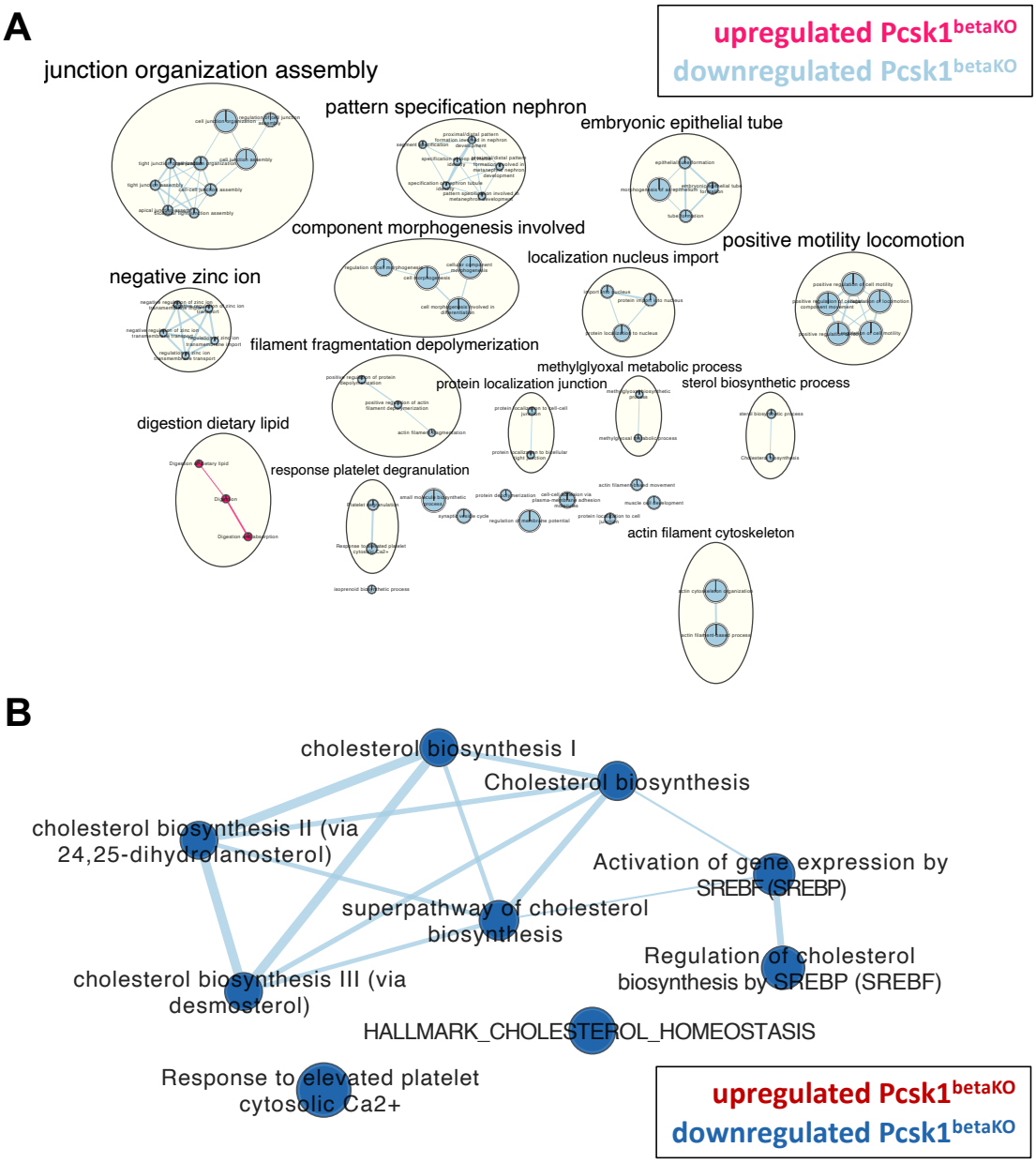

Figure 34: Pcsk1^{betaKO} islet functional and gene set enrichment analysis.
(A) Functional enrichment analysis (FDR < 0.05) of GO biological process and Reactome pathways in Pcsk1^{betaKO} islets. **(B)** Gene set enrichment analysis highlights altered cholesterol metabolism in Pcsk1^{betaKO} islets. Networks in (A,B) were visualized using EnrichmentMap. Edge thickness reflects increased similarity coefficient and node size reflects number of genes in pathway.

Table 5: iRegulon motif analysis of significant DEGs in Pcsk1^{betaKO} islets

	Rank	Motif id	AUC	NES	Cluster Code	Transcription factor
Pcsk1-betaKO Upregulated Motifs	1	taipale-RRGWACANNNTGTWCYY-AR-DBD	0.077	5.282	M1	Ar,Pgr,Nr3c1,Nr3c2
	2	taipale-RRGWACANNNTGTWCYY-AR-full	0.068	4.451	M1	Ar,Pgr,Nr3c1,Nr3c2
	3	taipale-RRGNACANNNTGTNCYY-Ar-DBD	0.067	4.344	M1	Ar,Nr3c1,Pgr,Nr3c2
	4	taipale-WGTAAAYAN-FOXB1-full	0.067	4.312	M2	Foxb1,Foxa2,Foxl1,Foxa1,Foxk1,Foxc2,Foxd3,Foxd2,Hltf
	5	flyfactorsurvey-foxo_SANGER_10_FBgn0038197	0.067	4.297	M2	Foxo3,Foxo4,Foxo1,Foxo6
	6	transfac_public-M00476	0.066	4.224	M2	Foxo4,Foxo1,Foxo3,Foxf2,Foxj3,Foxk1,Foxa2,Foxl1,Foxj1,3110039M20Rik,Foxo6
	7	transfac_pro-M00802	0.065	4.113	M3	Pou1f1
	8	homer-M00063	0.064	4.031	M2	Foxp1,Foxj3,Foxa2,Foxj1,Foxo3,Foxf2,Foxo1,Foxk1,Hltf,Foxo6
	9	iDMMPMM-SLP1	0.063	3.988	M2	Foxg1,3110039M20Rik,Foxk1,Foxl1
	10	swissregulon-FOXO1-3-4.p2	0.063	3.915	M2	Foxo3,Foxo1,Foxo4,Foxk1,Foxj3,Foxl1,Foxa2,Foxj1,Foxf2,Foxd1,Foxc2,Hltf,3110039M20Rik,Foxp1,Nr3c1,Pgr,Foxo6,Foxd2
Pcsk1-betaKO Downregulated Motifs	1	transfac_public-M00215	0.114	7.359	M1	Srf
	2	transfac_pro-M00810	0.112	7.238	M1	Srf
	3	transfac_pro-M00922	0.099	6.116	M1	Srf
	4	transfac_pro-M01007	0.098	6.071	M1	Srf
	5	homer-M00183	0.098	6.061	M1	Srf
	6	taipale-MCCATATAWGGN-SRF-DBD	0.098	6.026	M1	Srf
	7	factorbook-SRF	0.097	5.946	M1	Srf
	8	transfac_pro-M01304	0.092	5.555	M1	Srf
	9	transfac_public-M00186	0.089	5.309	M1	Srf
	10	taipale-NNMCCATATAWGGKNN-SRF-full	0.089	5.258	M1	Srf

5.2.6 Beta cells deficient in prohormone convertase activity do not have elevated ER stress

Given the apparent increase in insulin biosynthesis in Pcsk1^{betaKO} islets, it was somewhat surprising to not observe increased markers of ER-stress by RNA sequencing. To further probe the ER-stress response of prohormone convertase-deficient beta cells, I analyzed the expression of unfolded protein response (UPR) pathways in DPC^{betaKO} islets cultured for 72 hours in 5, 15, and 25 mM glucose. To our surprise, the UPR appeared unaltered at the transcript level in

DPC^{betaKO} mice relative to control DPC^{betaWT} islets in each glucose concentration (Figure 35A). Txnip, a highly glucose-responsive gene, trended toward higher glucose-stimulated expression in DPC^{betaKO} islets. This is in agreement with the significantly higher (1.8-fold) *Txnip* expression that was observed Pcsk1^{betaKO} islets (Figure 37A). We further determined protein levels of the ER-chaperone BiP (GRP78) and phosphorylated eIF2α (p-eIF2α). BiP protein expression in DPC^{betaKO} islets was comparable or lower than control islets at all glucose concentrations (Figure 35B), suggesting no increase in unfolded proteins in the ER of DPC^{betaKO} islets. Levels of p-eIF2α, a signal for translation attenuation, followed an expected pattern in DPC^{betaWT} islets with increased levels at high glucose (Figure 35C). DPC^{betaKO} islets, however, did not increase p-eIF2α at 25 mM glucose (Figure 35C). This finding suggests that there is minimal unfolded protein in the ER of DPC^{betaKO} islets, or that the UPR pathways have reduced functionality.

To further probe UPR activation I treated DPC^{betaKO} islets with thapsigargin, a SERCA (sarco/endoplasmic reticulum Ca^{2+} ATPase) inhibitor that causes dysregulation of ER calcium homeostasis and ER-stress. DPC^{betaKO} and DPC^{betaWT} islets had comparable expression of the canonical UPR mediators *Atf4*, *Atf6*, and spliced *Xbp1*, as well as their respective transcriptional targets *Asns*, *Pdia4*, and *Erdj4* (Figure 36). Further UPR markers *Trib3*, *Herpud1*, and *Grp78* were unaltered in DPC^{betaKO} mice. *Ddit3* (CHOP) was not elevated in DPC^{betaKO} mice suggesting no increase in ER-stress associated apoptosis. Collectively, the data suggest that DPC^{betaKO} islets do not have elevated ER-stress *ex vivo* and have functional UPR activation.

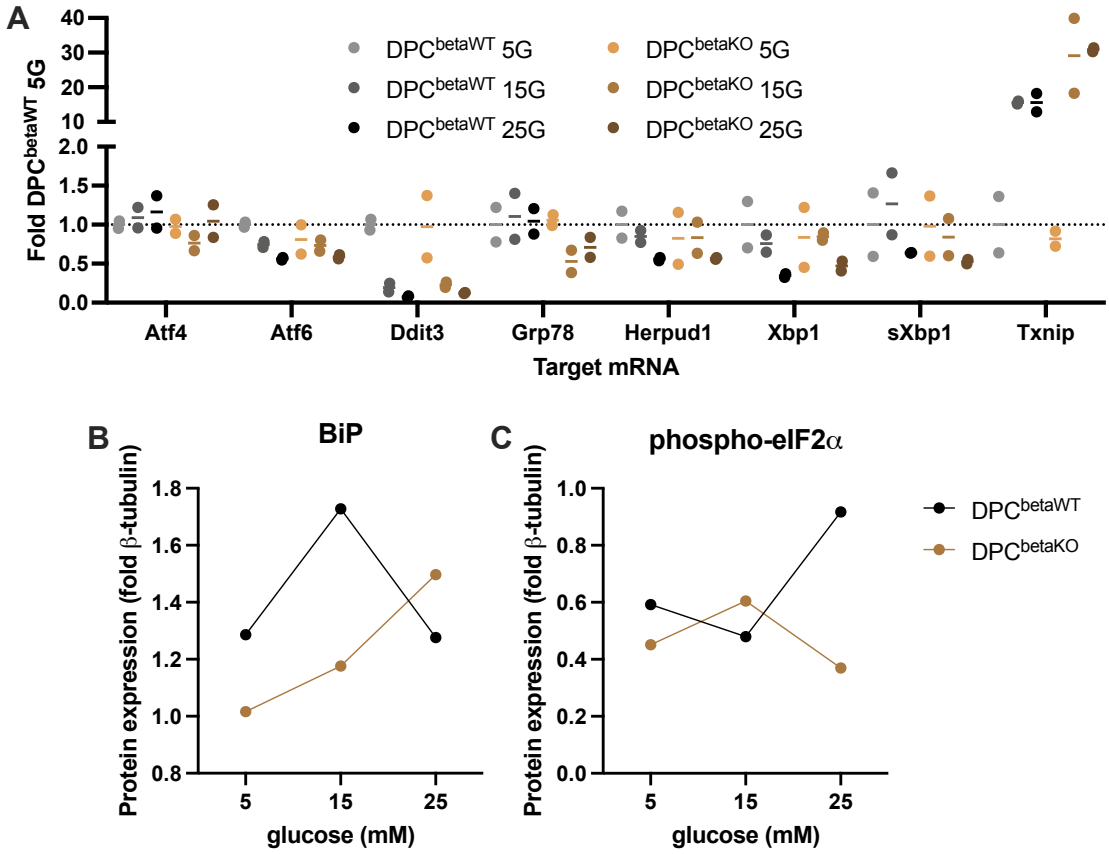

Figure 35: Islets from DPC^{betaKO} mice have similar levels of ER stress markers to DPC^{betaWT} islets.

Islets from 14-week-old male mice were recovered overnight and treated for 72 hours in media with 5, 15, or 25 mM glucose. **(A)** DPC^{betaKO} mice do not display elevated levels of ER-stress-associated transcripts when cultured at low (5 mM), slightly elevated (15 mM), or high (25 mM) glucose with the exception of a trend toward larger glucose-induced *Txnip* expression. **(B)** BiP (GRP78) protein levels rise and fall in DPC^{betaWT} islets in response to increasing glucose, while DPC^{betaKO} islets continue to increase BiP expression with rising glucose. **(C)** High glucose induces eIF2α phosphorylation in DPC^{betaWT} islets, but not in DPC^{betaKO} islets. Results in (B,C) are representative of duplicate experiments.

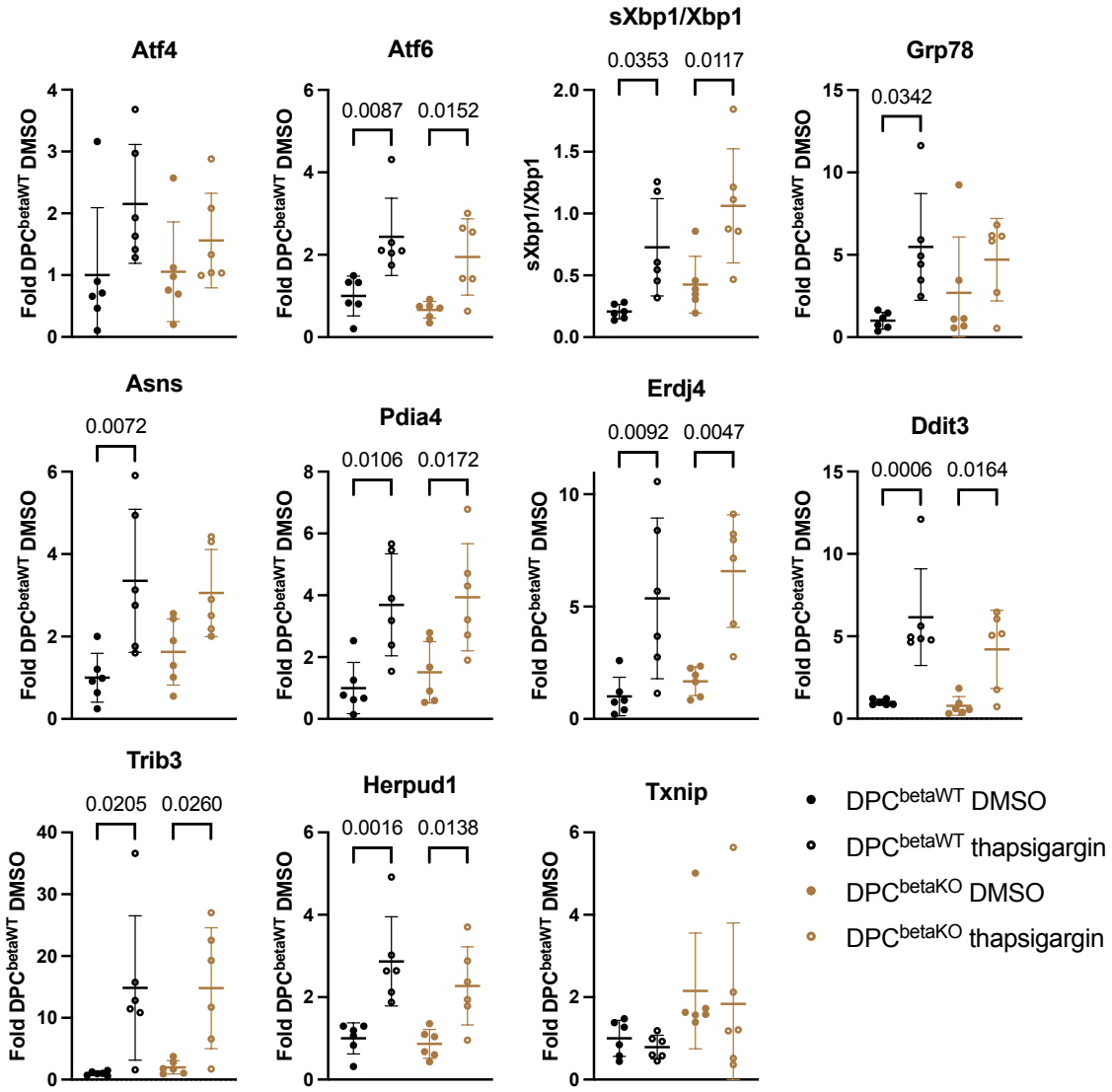

Figure 36: DPC^{betaKO} islets have unaltered basal and thapsigargin-induced unfolded protein responses.

Islets were isolated from 6-week-old mice, recovered overnight, and treated with 1 μM thapsigargin (Tg) for 6 hours. DPC^{betaKO} islets have comparable levels of the canonical unfolded protein response (UPR) effectors *Atf4*, *Atf6*, and spliced *Xbp1*, and their target genes *Asns*, *Pdia4*, and *Erdj4*, respectively. Other markers associated with ER stress (*Trib3*, *Herpud1*, *Grp78*, *Txnip*, and *Ddit3*) are also unaltered in DPC^{betaKO} islets.

5.2.7 Impairments in beta-cell prohormone processing drive an immature beta-cell phenotype and increased glucose responsiveness

Analysis of the Pcsk1^{betaKO} islet RNA-seq data in Figure 33 using Cuffdiff revealed DEGs flagged as outliers in DEseq2. Using Cuffdiff we observed significantly increased expression of *Aldh1a3*, a marker of failing or dedifferentiating beta cells[360] (Figure 37A). In agreement with reduced beta-cell maturity, there was also a significant decrease in *Mafa* and *Foxo1* expression in Pcsk1^{betaKO} islets (Figure 37A). Immunostained pancreas sections from 4.5-week-old DPC^{betaKO} male mice showed abundant ALDH1A3 immunoreactivity in beta cells (Figure 37D). Quantification of ALDH1A3^{HI} beta cells trended toward an increase from 0.3% of beta cells in DPC^{betaWT} to 12% of beta cells in DPC^{betaKO} male mice (Figure 37B). Pcsk1^{betaKO} male mice did not display increased beta-cell ALDH1A3 immunoreactivity at 4.5 weeks old (Figure 37C).

There tended to be fewer beta cells containing high MAFA immunoreactivity in 4.5-week-old DPC^{betaKO} male mice (Figure 38A). Analysis of beta-cell nuclear MAFA intensity showed a trend toward reduced nuclear MAFA levels in DPC^{betaKO} male mice (Figure 38B). The cumulative distribution of nuclear MAFA intensity in beta cells also showed a leftward shift toward lower MAFA intensities in DPC^{betaKO} male mice. Control (DMSO-treated) DPC^{betaKO} islets (from Figure 36) also had significantly reduced *Mafa* expression relative to control DPC^{betaWT} islets (Figure 38D). The reduced expression of *Mafa*, a key beta-cell maturity marker and transcription factor, and the increased expression *Aldh1a3*, a dedifferentiation and dysfunction marker, suggest that DPC^{betaKO} beta cells may have reduced maturity and function.

Using the ratiometric intracellular Ca^{2+} dye Fura-2, I next investigated the glucose-responsiveness of Pcsk1^{betaKO} and DPC^{betaKO} islets by ramping the glucose concentration in islet

perifusion experiments. Ca^{2+} influx provides the signal for insulin secretory granule exocytosis in beta cells. Barring differences in beta-cell Ca^{2+} sensing or signalling, Ca^{2+} influx provides a reasonable marker for beta-cell stimulation and exocytosis activity. $Pcsk1^{betaKO}$ and DPC^{betaKO} islets display accelerated glucose-induced calcium influx at 6 mM glucose, and reduced Ca^{2+} oscillation amplitudes at higher glucose concentrations (Figure 39 A,B). At 15 mM glucose, $Pcsk1^{betaKO}$ and DPC^{betaKO} islets lacked oscillations in intracellular Ca^{2+} and maintained high intracellular Ca^{2+} concentrations. When stepped abruptly from 1.67 to 16.7 mM glucose, DPC^{betaKO} islets also displayed accelerated Ca^{2+} influx (Figure 39C). DPC^{betaKO} islets did not show altered Ca^{2+}-influx kinetics in response to a depolarizing KCl stimulus (Figure 39C). To test whether the accelerated phenotype was due to alterations upstream or downstream of K_{ATP}-channel closure, I exposed islets to increasing concentrations of the K_{ATP}-channel inhibitor tolbutamide in 3 mM glucose. DPC^{betaKO} and DPC^{betaWT} islets had comparable responses to tolbutamide, suggesting comparable resting membrane potentials and electrical activity (Figure 39D) and that any differences in glucose-stimulated Ca^{2+}-influx lie upstream of the K_{ATP} channel in glucose metabolism or beta-cell potentiation.

Insulin secretion is challenging to assess in $Pcsk1^{betaKO}$ and DPC^{betaKO}, as ELISAs do not discriminate between some proinsulin processing intermediates and mature insulin. Mature insulin ELISAs also do not extensively cross-react with intact proinsulin, necessitating the use of different ELISAs for DPC^{betaKO} and DPC^{betaWT} islets. Thus, strict quantitative comparisons are not appropriate between processing-deficient and control islets, but kinetic differences can still be observed in a perifusion experimental design. $Pcsk1^{betaKO}$ islets did not display altered glucose- or KCl-stimulated (pro)insulin secretion differences in comparison to control mice (Figure 40A). First- and second-phase insulin secretion content was, qualitatively, not

diminished in Pcsk1^{betaKO} islets (Figure 40 B,C). Basal insulin release was also not likely increased in Pcsk1^{betaKO} islets (Figure 40D). DPC^{betaKO} islets had increased proinsulin secretion at 9 mM glucose compared to the insulin secretion of DPC^{betaWT} islets (Figure 40E). Separate proinsulin and insulin ELISAs were used to analyze the perifusates of DPC^{betaKO} and DPC^{betaWT} islets, making direct quantity comparisons challenging; however, the ratio of AUCs for 9 mM glucose (20-30 min) / 6 mM glucose (10-20 min) can be used as an approximate measure of fold-increase in secretion. Relative to 6 mM glucose, DPC^{betaKO} islets had a 36-fold increase in proinsulin secretion at 9 mM glucose while DPC^{betaWT} islet displayed a 1.6-fold increase in insulin secretion (Figure 40F). These data suggest that DPC^{betaKO} islets have a reduced glucose threshold for (pro)insulin secretion.

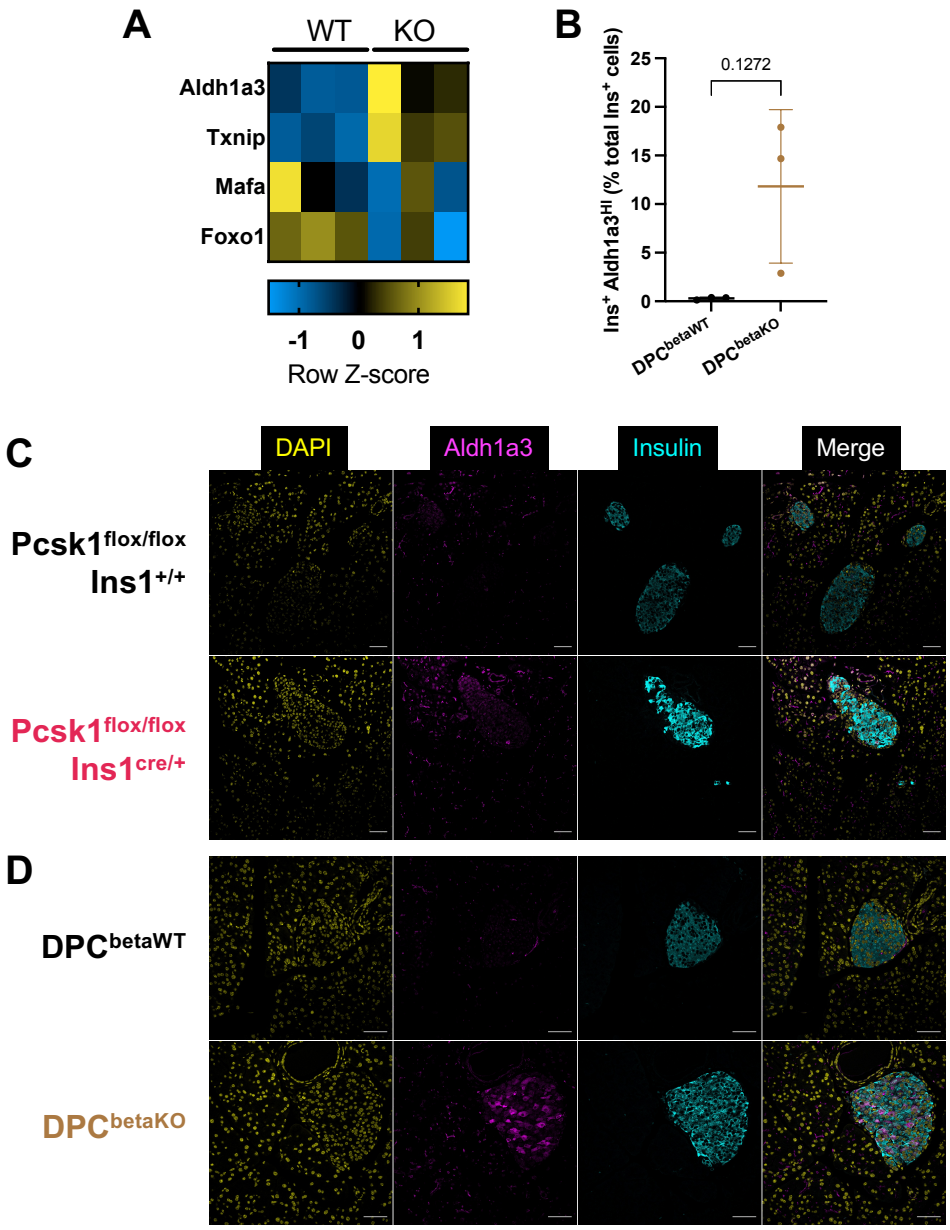

Figure 37: Beta cells from Pcsk1^{betaKO} and DPC^{betaKO} mice have increased expression of Aldh1a3, a marker of beta-cell dysfunction.
(A) Analysis of high-fat diet-fed Pcsk1^{betaKO} mouse islet RNA seq (from Fig. 33) using Cuffdiff revealed an expression signature of failing beta cells, with significantly elevated *Aldh1a3* and decreased *Mafa* and *Foxo1* expression. *Aldh1a3* and *Mafa* were detected as outliers in DEseq2 due to variable expression and low number of replicates in Pcsk1^{betaKO} islets. **(B)** Aldh1a3^{HI} beta cells are more abundant in 4-week-old male DPC^{betaKO} pancreas sections. **(C)** Aldh1a3 expression is not increased by 4 weeks of age in the beta cells of Pcsk1^{betaKO} mice. **(D)** Example images from quantification in (B). In all islets, including those of comparable size, DPC^{betaKO} mice have increased beta-cell expression of Aldh1a3. Scale bars represent 50 µm. n = 3 mice.

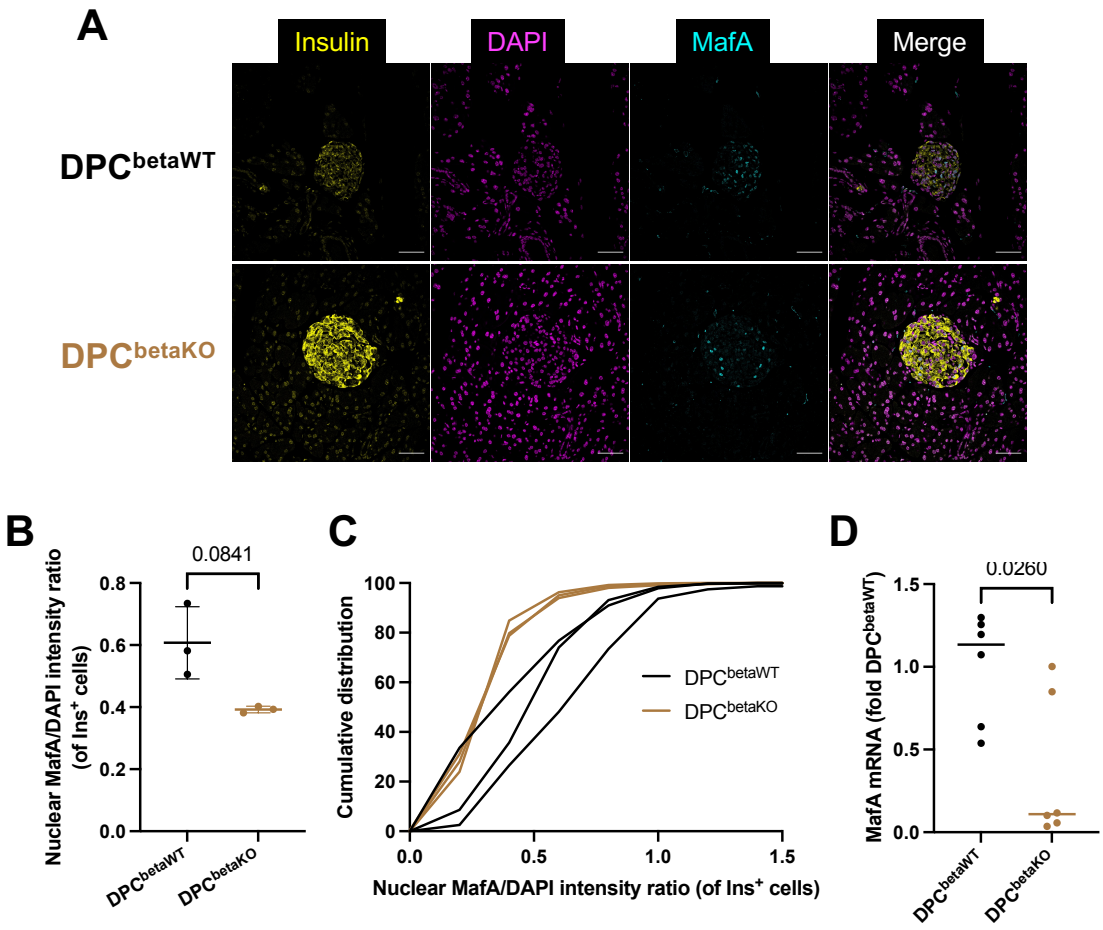

Figure 38: DPC^{betaKO} mice have reduced nuclear MafA immunoreactivity.
Pancreas sections were analyzed from 4-week-old male mice**. (A)** DPC^{betaKO} mice had fewer beta cells with high nuclear MafA intensity than littermate DPC^{betaWT} control mice. **(B)** Quantification of mean nuclear MafA intensity, normalized to DAPI intensity, of DPC^{betaKO} beta cells. **(C)** Cumulative distribution of nuclear MafA intensity in beta cells reveals DPC^{betaKO} beta cells are left-shifted toward a lower nuclear MafA intensity. Scale bars represent 50 µm. n = 3 mice. **(D)** *Mafa* transcript is reduced in DPC^{betaKO} islets (RNA from DMSO controls in Figure 36). Line represents median, and p-value displayed is from a Mann-Whitney test.

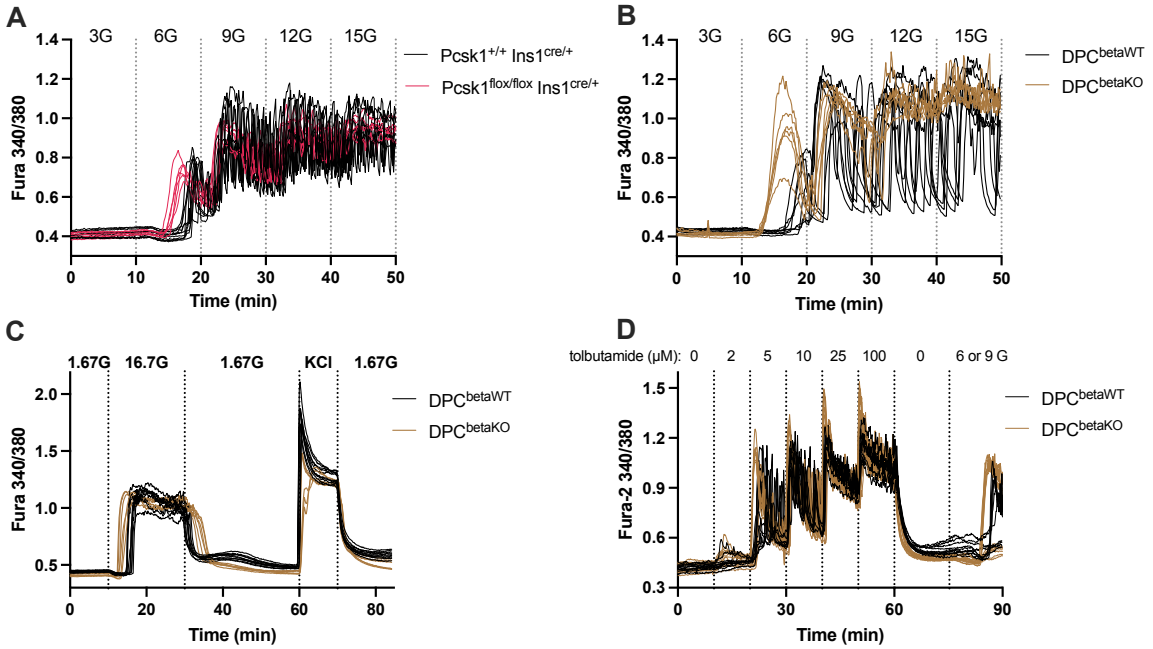

Figure 39: Pcsk1^{betaKO} and DPC^{betaKO} mice have accelerated glucose-induced calcium influx.

Intracellular calcium levels of 3-day rested islets were recorded using Fura-2 dye on a perifusion apparatus. **(A,B)** Pcsk1^{betaKO} and DPC^{betaKO} male islets have accelerated calcium influx in response to 6 mM glucose, and reduced amplitude of calcium oscillations at higher glucose while ramping glucose concentrations from 3 mM to 15 mM. **(C)** Male DPC^{betaKO} islets have accelerated glucose-induced calcium influx stepping from 1.67 mM to 16.7 mM glucose, and a slight delay in returning to baseline intracellular calcium upon returning to basal 1.67 mM glucose. Response times to 30 mM KCl were comparable in DPC^{betaKO} and DPC^{betaWT} islets. **(D)** DPC^{betaKO} and DPC^{betaWT} islets have comparable calcium influx responses to ramping concentrations of the K_{ATP}-channel inhibitor tolbutamide. Islets were perifused with 6 mM glucose (non-responders) or 9 mM glucose (responders) after tolbutamide ramps. In each graph calcium data from individual islets are plotted from 3-10 islets / mouse, 2 mice / genotype.

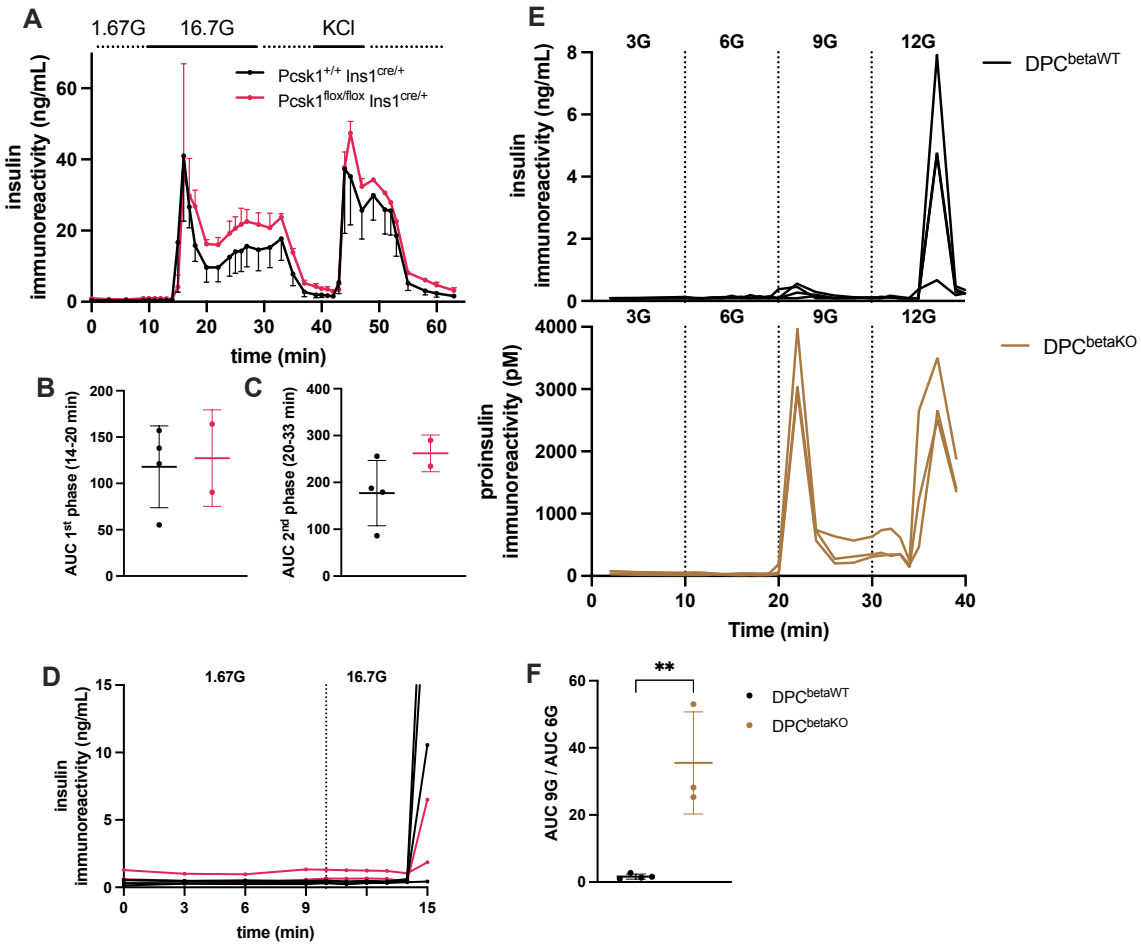

Figure 40: Deletion of prohormone convertases lowers the glucose threshold for insulin secretion.

(A) Pcsk1^{betaKO} islets from male mice displayed comparable glucose-stimulated insulin secretion kinetics when stepped from 1.67 to 16.7 mM glucose, and in response to KCl. **(B,C)** First and second phase insulin secretion AUCs are similar for islets from Pcsk1^{betaKO} and Pcsk1^{betaWT} mice. **(D)** Basal insulin secretion at 1.67 mM glucose is comparable in Pcsk1^{betaKO} mice. Quantities should be interpreted qualitatively due to Pcsk1^{betaKO} mice secreting abundant proinsulin and proinsulin processing intermediates that have unknown cross-reactivity with the insulin ELISA. **(E)** DPC^{betaKO} islets from male mice have a larger secretory response to 9 mM glucose than DPC^{betaWT} islets. **(F)** Quantification of (E). The ratio of 9 mM glucose AUC / 6 mM glucose AUC is elevated in DPC^{betaKO} islets. 'G' represents "mM glucose" in panels A, D, and E.

5.2.8 Proteomic characterization of beta cells lacking Pcsk1

To further characterize Pcsk1-deficient beta cells, I generated a *Pcsk1*$^{flox/flox}$*; Ins1*$^{cre/+}$*; mTmG*$^{Tg/0}$ (Pcsk1^{betaKO}) mouse line with *Pcsk1*$^{+/+}$*; Ins1*$^{cre/+}$*; mTmG*$^{Tg/0}$ (Pcsk1^{betaWT}) controls. This allowed for enrichment of recombined GFP^{+} beta cells by fluorescence-activated cell sorting and removed contaminating exocrine tissue. Sorted beta cells were analyzed by label-free shotgun proteomics. Pcsk1^{betaKO} beta cells contained 37 upregulated and 27 downregulated proteins relative to Pcsk1^{betaWT} beta cells, and PCSK1 was found to be the most downregulated protein confirming deletion of Pcsk1 in beta cells (Figure 41A). Among the most upregulated proteins were INS2, confirming the elevated islet (pro)insulin levels observed by western blot, and ALDH1A3, further suggesting an abundant population of dysfunctional beta cells (Figure 41B). NNT (nicotinamide nucleotide transhydrogenase) was among the most downregulated proteins (Figure 41 A,C). A pair of *Nnt* mutations exist in C57BL/6J that result in minimal translation of a truncated NNT product. *Nnt* and *Pcsk1* are both located on chromosome 13 in mice and separated by approximately 27 cM. The *Pcsk1*^{flox} allele was generated on a C57BL/6N genetic background that contains functional *Nnt* and were interbred with *Ins1*^{cre} mice (C57BL/6J background) for several generations. Therefore, the reduction in NNT is likely due to a linked *Nnt*^{B6J} allele cosegregating with *Pcsk1*^{flox}, and the *Nnt*^{B6N} allele with *Pcsk1*$^{+}$, in the majority of these mice (Figure 41 B,C).

Functional enrichment analysis was performed on significantly upregulated and downregulated proteins. Upregulated proteins in Pcsk1^{betaKO} were enriched in processes associated with anterograde transport, translation, and insulin receptor signalling, while downregulated proteins were enriched in sphingolipid metabolism (Figure 42A). The enrichment

pathways associated with insulin or insulin receptor signalling were driven in part by the large upregulation of INS2. Similarly, the downregulated pathway “Peptide hormone biosynthesis” was driven in part by the large reduction in PCSK1. Gene set enrichment analysis, which includes all quantified proteins in the analysis, also highlighted enrichment of anterograde and retrograde transport processes in $Pcsk1^{betaKO}$ beta cells (Figure 42B). Surprisingly, given the increased glucose responsiveness of $Pcsk1^{betaKO}$ and DPC^{betaKO} islets (Figures 39,40), proteins associated with oxidative phosphorylation were significantly (FDR < 0.05) downregulated in $Pcsk1^{betaKO}$ beta cells (Figure 42B).

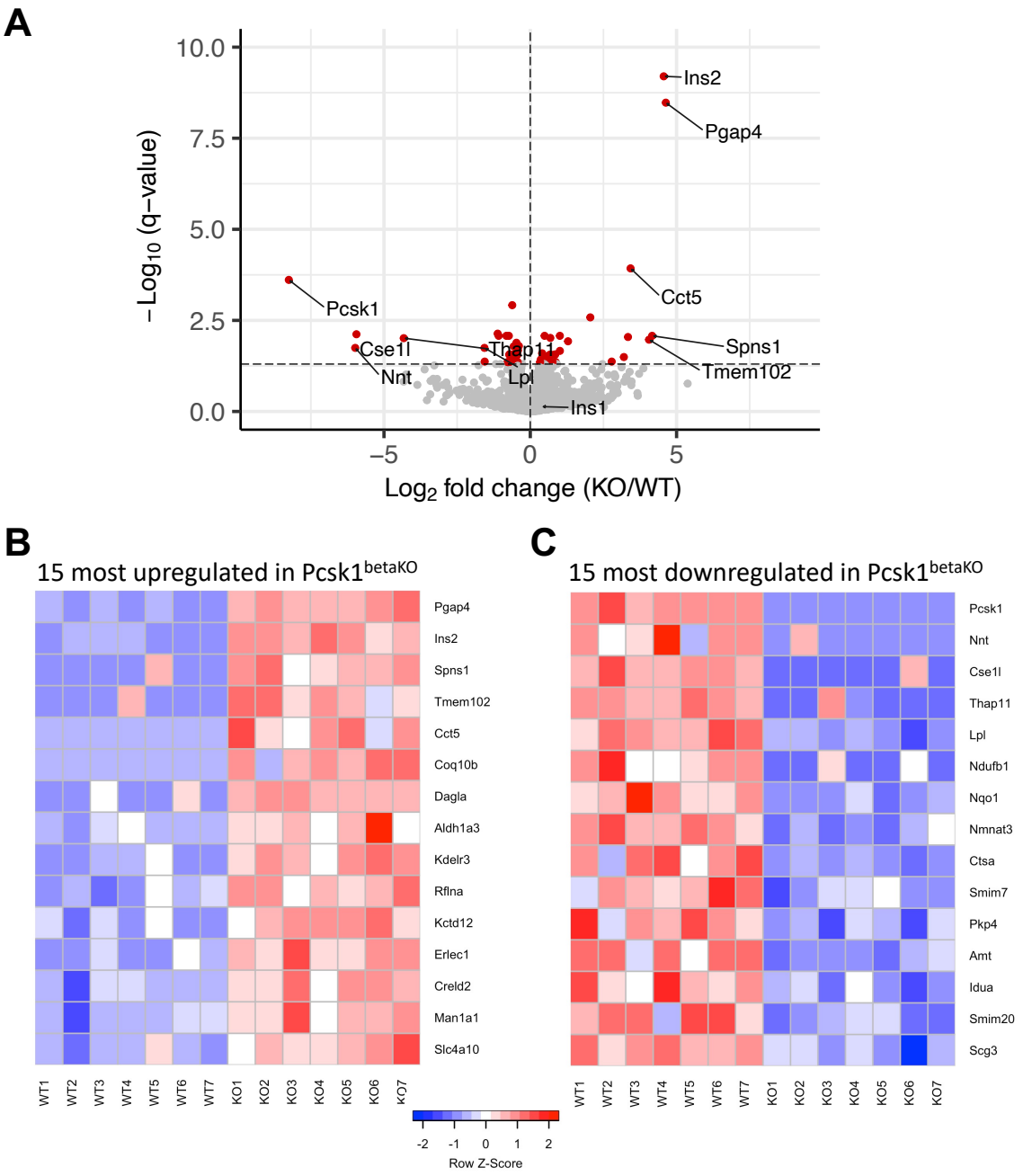

Figure 41: Proteomics of sorted beta cells from Pcsk1^{betaKO} mice.
Freshly isolated islets from 13-week-old *Ins1$^{cre/+}$; Pcsk1$^{flox/flox}$; mTmG$^{Tg/0}$* (KO) and *Ins1$^{cre/+}$; Pcsk1$^{+/+}$; mTmG$^{Tg/0}$* (WT) male mice were dispersed, FACS sorted for GFP^{+} beta cells, and analyzed by label-free shotgun proteomics. **(A)** Of the 4,766 proteins quantified in Pcsk1^{betaKO} beta cells, 64 proteins were differentially expressed at an FDR < 0.05. **(B,C)** Heat maps displaying individual replicate expressions of the 15 most upregulated and downregulated proteins by Pcsk1^{betaKO} beta cells.

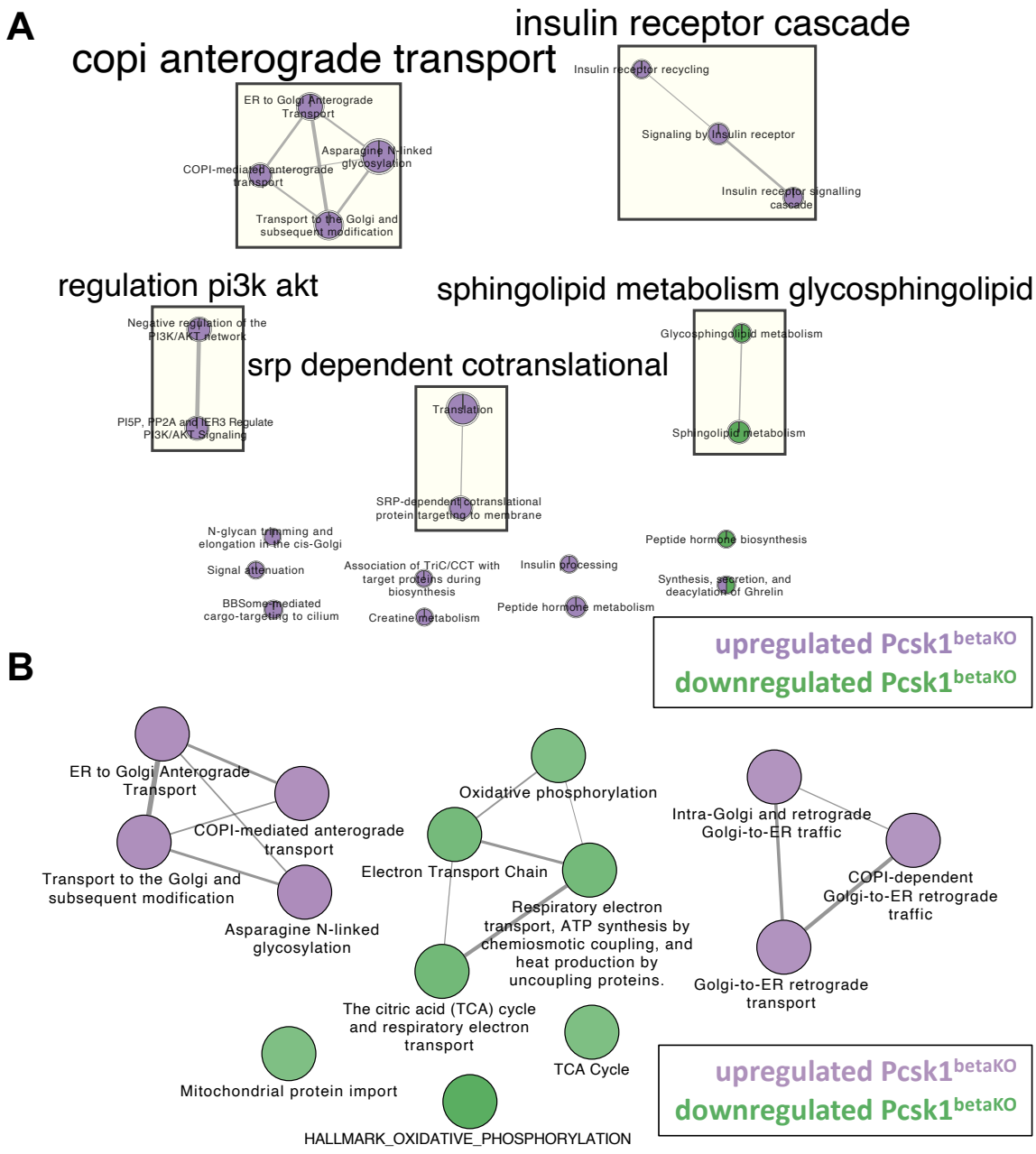

Figure 42: Functional enrichment analysis of *Pcsk1*-deficient beta-cell proteome.
(A) Functional enrichment analysis (FDR < 0.05) of GO biological process and Reactome pathways in Pcsk1^{betaKO} beta cells. Translation and trafficking pathways are enriched in *Pcsk1*-deficient beta cells. (**B)** Gene set enrichment analysis reveals similar trafficking pathways enriched in *Pcsk1*-deficient beta cells, while oxidative phosphorylation gene signatures are reduced in *Pcsk1*-deficient beta cells. Networks in (A,B) were visualized using EnrichmentMap. Edge thickness reflects increased similarity coefficient and node size reflects number of genes in pathway.

5.3 Discussion

The results in this chapter highlight the importance of beta-cell prohormone processing for proper beta-cell function and glucose homeostasis. Our data support a larger role for PCSK1 in the processing of proinsulin and maintenance of euglycemia. This is largely in agreement with evidence in human beta cells where reduced *PCSK2* expression is found relative to neighbouring alpha cells[289–292]. However, *Pcsk2* is still involved in the proper function of mouse beta cells. Our data show *Pcsk2* is required for processing of proIAPP in mice. Moreover, *Pcsk2* deletion did modestly elevate proinsulin levels in islet lysates, suggesting that *Pcsk2* does play a role in mouse proinsulin processing, either directly or indirectly within the beta cell. These findings in proinsulin and proIAPP processing are similar to those previously observed in global *Pcsk1*- and *Pcsk2*-null mice[295,299,305,321], and further suggest that *Pcsk2* can partially compensate for *Pcsk1* absence as the DPC^{betaKO} mice lack detectable mature insulin.

Reduced islet and pancreatic PCSK1 expression, but not PCSK2 expression, has been observed in T1D[310,311]. Functional redundancy via PCSK2 activity may help partially preserve beta-cell function during diabetogenic stress. However, the elevated processing intermediates detected in the circulation of individuals with T1D and T2D (proIAPP$_{1\text{-}48N}$ and des-31,32 proinsulin) suggest reduced beta-cell PCSK2 activity in diabetes[86,274]. Other islet endocrine cells contain abundant PCSK2, and if beta cells express low amounts of *PCSK2*, it may present a challenge to detect reduced *PCSK2* expression in beta cells specifically. Further, PCSK2 activity is also modified post-transcriptionally – glycosylation and proper folding of PCSK2 is required for trafficking to granules[358] and the altered beta-cell ER and Golgi[361] environments in T1D and T2D may impair trafficking of PCSK2 to insulin secretory granules. Interestingly, Pcsk2^{betaKO} islets had similar proinsulin processing impairments to haploinsufficient Pcsk1^{betaHET} islets.

Although Pcsk1^{betaHET} and Pcsk2^{betaKO} mice were normoglycemic, diabetes susceptibility may be increased and HFD was an insufficient beta-cell stressor to unmask a glycemic phenotype.

The overall glycemic phenotypes in our beta-cell processing models mirror our observations in proinsulin processing. It is remarkable that female and young male Pcsk1^{betaKO} mice have normal fasting blood glucose and glucose tolerance given the degree of proinsulin processing impairment. With ageing or HFD-induced insulin resistance[362], we observed hyperglycemia and impaired glucose tolerance in Pcsk1^{betaKO} male mice. As only 4/10 HFD-fed and no chow-fed Pcsk1^{betaKO} male animals developed uncontrolled hyperglycemia, we conclude that loss of *Pcsk1* in beta cells increases the risk of diabetes but alone is insufficient to cause diabetes. We also did not observe reactive hypoglycemia in Pcsk1^{betaKO} animals monitored up to 4 hours post-glucose injection (data not shown), suggesting non-beta-cell mechanisms may be involved in the reactive hypoglycemia observed in humans with PCSK1 mutations[322]. Although a crude measure of insulin sensitivity, insulin tolerance tests showed minimal insulin sensitivity differences in Pcsk1^{betaKO} mice. Female Pcsk1^{betaKO} mice had slightly higher insulin sensitivity than female controls, which may partially explain their ability to remain normoglycemic. However, male mice did not have altered insulin sensitivity. Fasting plasma insulin immunoreactivity was approximately 10-fold higher in Pcsk1^{betaKO} mice, and likely represents a mixture of mature insulin and des-64,65 proinsulin. Given that proinsulin retains approximately 5-10% of insulin's activity at insulin receptors[326,327], there is likely comparable insulin receptor signaling in Pcsk1^{betaKO} mice due to hyper(pro)insulinemia. This also likely explains the comparable body weights observed in all processing-deficient models.

The more severe proinsulin processing and hyperglycemic phenotypes of DPC^{betaKO} mice highlight that loss of *Pcsk2* further worsens *Pcsk1* deficiency. Although female DPC^{betaKO} mice

were hyperglycemic, they have a remarkably minor phenotype given their complete lack of mature insulin. Male mice displayed more pronounced and highly variable hyperglycemia suggesting DPC^{betaKO} mice may have slow proinsulin secretion and/or proinsulin's actions on the insulin receptor are slower than insulin. Our perifusion data in isolated islets show robust secretion of (pro)insulin in DPC^{betaKO} and Pcsk1^{betaKO} islets which points toward the delay being due to proinsulin's reduced activity at the insulin receptor. The highly variable glycemia and sluggish proinsulin actions (relative to insulin) point toward extended periods of hyperglycemia that likely do not return to normal fasting values within a 4 hour fast in DPC^{betaKO} male mice. This may also explain why fasting glycemia is not lower in DPC^{betaKO} mice despite the lowered glucose threshold for beta-cell secretion – they may never reach glycemic values sufficiently low for insulin secretion to be inhibited. Thus, there is likely a sustained increased secretory demand on DPC^{betaKO} beta cells to which female mice respond better[363]. The observed increase in (pro)insulin content by western blot and mass spectrometry in Pcsk1^{betaKO} islets support an increase in secretory demand and proinsulin biosynthesis in processing-deficient beta cells.

Beta-cell mass was increased as expected in processing-deficient islets. Although area measurements are used to represent mass, we observed no significant differences in pancreas mass for the fraction of Pcsk1^{betaKO} mice tested, indicating area is likely representative of mass. Pcsk1^{betaKO} and DPC^{betaKO} male mice displayed similarly increased beta-cell mass at 4 and 30 weeks old, with no differences in proliferation rates at 4-4.5 weeks old. This suggests an early increase in beta-cell mass, either from an expansion of beta-cell progenitors or a rapid expansion of beta cells postnatally, that is then sustained as mice age. In contrast to the evidence *in vivo*, DPC^{betaKO} beta cells had reduced proliferation in response to glucose *ex vivo*, likely due to a cell-intrinsic mechanism, as co-cultured wild-type islets were not affected. A reduction in beta-cell

proliferation was also noted in *Pcsk1*$^{+/N222D}$ and *Pcsk1*$^{N222D/N222D}$ mouse beta cells, along with elevated UPR and proteasomal gene sets, but no increase in apoptotic beta cells[347]. Cell death was not determined for DPC^{betaKO} islets but is unlikely to account for the reduced proliferation. *Ddit3* expression was not increased in DPC^{betaKO} islets cultured in similar conditions, and neither were most ER-stress markers. We also did not observe ER distension, a hallmark of ER-stress, in TEM images of Pcsk1^{betaKO} beta cells. However, some markers of ER-stress and cell death were observed. *Txnip* expression, which can drive beta-cell apoptosis[364], tended to increase in high-glucose-cultured DPC^{betaKO} islets and was upregulated in freshly isolated Pcsk1^{betaKO} islets. In our proteomics analysis, Pcsk1^{betaKO} beta cells had increased abundance of PDIA4 (protein disulfide isomerase) and DNAJB11 (Hsp40 member B11; a BiP cofactor) suggesting some degree of ER stress. Increased abundance of SPNS1 and TMEM102 were also identified which have been associated with necrotic-like and apoptotic death mechanisms, respectively[365,366]. Less canonical death mechanisms may be involved and contributing to the reduced proliferation observed ex vivo. Increased beta-cell death is unlikely to be observed in vivo, however, given the increased mass and normal proliferation rates of beta cells in Pcsk1^{betaKO} and DPC^{betaKO} mice.

Exocrine gene expression presented a challenge for interpreting upregulated gene expression in Pcsk1^{betaKO} islets. Most of the highly upregulated genes were exocrine-specific, including many digestive enzymes. *Amy2b* was found upregulated in Pcsk1^{betaKO} islets, but no islet amylase protein expression was observed by immunostaining in Pcsk1^{betaKO} pancreas sections. This suggests that the increased exocrine gene expression is from contaminating peri-islet exocrine tissue rather than exocrine gene expression in islet cells. Functional enrichment analysis revealed reduced expression of genes associated with actin cytoskeleton and cell-cell junctions processes in Pcsk1^{betaKO} islets. Altered cytoskeleton and cell adhesion (cell-cell or cell-

extracellular matrix adhesions) may impact islet isolation and provide an explanation for the consistent increase in exocrine cell contamination in Pcsk1^{betaKO} islets. Beta-cell cortical filamentous-actin (F-actin) remodeling and focal adhesion dynamics are also critical to proper glucose-stimulated insulin secretion[367]. Vinculin, filamin, and alpha-actinin are all F-actin binding proteins localized to focal adhesions, and are involved in crosslinking F-actin filaments and associating F-actin with integrins[368–370]. The reduced expression of vinculin, filamin, and alpha-actinin in Pcsk1^{betaKO} islets suggests destabilized or reduced focal adhesions in beta cells, and potentially a reduced capacity for exocytosis. However, a defect in second phase insulin secretion, in which F-actin remodelling is critical for the sustained recruitment of new insulin granules to the plasma membrane[370], was not observed in Pcsk1^{betaKO} islets. Upon considering the reduced affinity of insulin ELISAs for the proinsulin products in Pcsk1^{betaKO} beta cells, there is likely enhanced exocytosis in Pcsk1^{betaKO} beta cells. As a key step in insulin exocytosis, and with differential expression of associated genes in Pcsk1^{betaKO} islets detected by RNA sequencing, regulation of the F-actin cytoskeleton and focal adhesion dynamics in Pcsk1^{betaKO} beta cells should be confirmed and further explored. This may provide novel cytoskeletal adaptive mechanisms employed by beta cells in response to deficient prohormone processing.

Additional downregulated genes include those involved in cholesterol biosynthesis pathways. Cholesterol homeostasis is key in secretory granule biogenesis and is thought to assist in forming negative membrane curvature in the inner leaflet of the vesicle membrane. Depletion of cholesterol inhibits formation of secretory vesicles[371] while accumulation of cholesterol in beta cells impairs insulin exocytosis[372]. As increased granule biogenesis and exocytosis are suspected in Pcsk1^{betaKO} beta cells, the reduced expression of genes involved in cholesterol biosynthesis is surprising. Cholesterol production is regulated via the activation of SREBP

transcription factors in response to low cholesterol, and biosynthesis may be low due to elevated cholesterol in Pcsk1^{betaKO} islets. Measurement of islet cholesterol content would provide further insight into the reduced expression of genes involved in cholesterol biosynthesis.

Generating a Pcsk1^{betaKO} mouse with the additional Cre-recombinase reporter transgene mTmG allowed for FACS enrichment of recombined Pcsk1^{betaKO} beta cells and improved detection of upregulated genes. Increased abundance of INS2 protein, which is more abundant than INS1 in mouse beta cells, along with increased proteins associated with trafficking pathways further suggests increased secretory granule biogenesis in Pcsk1^{betaKO} beta cells. The increase in INS2 is unlikely to be accounted for by impaired secretion given we observed no loss of insulin secretion in perifused isolated islets. Thus, translation or degradation of (pro)insulin must be altered in Pcsk1^{betaKO} mice. Further investigation into proinsulin translation by pulse-chase, as well as autophagic and proteasomal flux, could uncover the cause of elevated (pro)insulin in Pcsk1^{betaKO} beta cells, and may provide insight into adaptive mechanisms used by beta cells with impaired processing.

The dedifferentiated phenotype of DPC^{betaKO} and Pcsk1^{betaKO} islets presents a possible mechanism through which processing impairment may negatively impact beta-cell function and mass. Dedifferentiation of beta cells has been observed in T2D[373–375] and may lead to insulin-positive islet cells with reduced functionality. The evidence in this chapter points to an immature phenotype of DPC^{betaKO} and Pcsk1^{betaKO} beta cells; it is not known if these processing-deficient beta cells dedifferentiate or fail to fully mature. The normoglycemia observed in 5-week-old female DPC^{betaKO} and young Pcsk1^{betaKO} mice suggest appropriate beta-cell differentiation occurs during islet development. Elevated ALDH1A3 is detected in dedifferentiated and failing mouse and human T2D beta cells[360,373], but is not abundantly expressed in the developing mouse

pancreas as shown in recent single-cell RNA sequencing studies[376]. The early normoglycemia along with *Aldh1a3* expression suggest that dedifferentiation rather than reduced maturation occurs in processing-deficient islets. Further analyses in embryonic and perinatal pancreases will be required to determine if *Pcsk1* loss from insulin^{+} cells influences islet development.

Pcsk1^{betaKO} and DPC^{betaKO} islets also display reduced *Mafa* expression, a key transcription factor for beta-cell identity and function[377,378]. Reduced *Foxo1* expression was also observed, which has been shown to drive beta-cell dedifferentiation and dysfunction[379]. However, no reductions in other key beta-cell identify genes were observed, including *Pdx1*, *Nkx6.1*, *Nkx2.2*, *Neurod1*, *Pax6*, *Foxa2*, *Ucn3*, *Isl1*, or *Gck*[375]. There was also no increase in the immaturity markers *Neurog3*, *Mafb*, *Fev*, *Ghrl*, or *Npy*, and no increased expression of disallowed genes such as *Ldha*, *Cat*, or hexokinases I, II, or III [375]. The lowered glucose threshold for beta-cell excitability and insulin secretion in Pcsk1^{betaKO} and DPC^{betaKO} islets is similar to neonatal islets[380], in support of an immature beta-cell phenotype.

Proliferating beta cells are also associated with an immature beta-cell phenotype[381]. Despite increases in beta-cell mass, we observed no difference in beta-cell proliferation in vivo at 4.5 weeks of age and reduced maturity in Pcsk1^{betaKO} and DPC^{betaKO} beta cells. We did not assess beta-cell proliferation at 13-14 weeks old when transcriptomics and proteomics was performed, but proliferation is unlikely to be changed at this age as the beta-cell mass increase occurs prior to 4.5 weeks old and does not further increase by 30 weeks old. Foxo family members and MAFA were not detected in our proteomics analysis, but MAFA nuclear intensity trended downward in 4.5-week-old DPC^{betaKO} beta cells. The mechanism for reduced *Mafa* expression is unclear, but may involve the observed reduction in *Foxo1* expression which positively regulates *Mafa*[382]. In sum, the evidence in processing-deficient beta cells suggests an

immature-like beta-cell phenotype that includes a reduced glucose threshold for excitability, increased *Aldh1a3* expression, and reduced *Mafa* expression.

The accelerated glucose-induced calcium influx and lowered glucose threshold for (pro)insulin exocytosis in processing-deficient islets was a consistently observed phenotype. The lack of kinetic differences and comparable amplitudes in response to 30 mM KCl and the K_{ATP} channel inhibitor tolbutamide suggest that the acceleration lies upstream of K_{ATP} channel closure in the glucose-sensing pathway of beta cells. K_{ATP} channel closure occurs in response to elevated ATP/ADP ratios in beta cells, and glucose uptake and metabolism is a major driver of increasing the cytosolic ATP/ADP ratio[36]. Glucose uptake is unlikely to accelerate beta-cell excitation to the extent observed in processing-deficient islets, as glucose uptake is not rate-limiting in beta-cell glucose-sensing[36] and intracellular glucose reaches 90% of extracellular glucose concentrations within 60 seconds in dispersed rat islets[383]. Accelerated glucose metabolism is also unlikely in processing-deficient beta cells, as we detected reduced abundance of proteins involved in oxidative phosphorylation in the $Pcsk1^{betaKO}$ beta-cell proteome. However, these measures are a static snapshot of a dynamic process. ATP synthesis rates in response to glucose should be measured in processing-deficient islets given the conflicting evidence between our beta-cell proteomics and activation data.

Altered paracrine actions may also partially explain the lower glucose setpoint for DPC^{betaKO} Ca^{2+}-influx and insulin secretion. Beta cells dominate the islet in DPC^{betaKO} islets, resulting in a reduced ratio of alpha/beta cells. Although delta cells were not assessed, the ratio of delta/beta cells is also likely to be decreased in DPC^{betaKO} islets given the expansion of beta cells, and somatostatin secreted by delta cells can hyperpolarize beta cells[384]. Somatostatin can further reduce exocytosis in depolarized beta cells[384,385], suggesting somatostatin reduces insulin

secretion by mechanisms beyond only beta-cell hyperpolarization. Reduced somatostatin signaling, via a reduction in the delta/beta cell ratio, could partially be driving the elevated insulin secretion at lower glucose thresholds in DPC^{betaKO} islets. We did not, however, observe differences in islet Sst expression in our RNA sequencing data of Pcsk1^{betaKO} islets, and the accelerated glucose-induced insulin secretion in DPC^{betaKO} mice remains largely unexplained. Future experiments to determine the ATP synthesis rate and resting membrane potential may provide further evidence as to the origin of the increased glucose sensing and lowered exocytosis threshold.

Collectively, our data in processing-deficient mice suggest that loss of beta-cell prohormone processing increases diabetes susceptibility, but alone may be insufficient to cause diabetes. Our data suggest that beta-cell *Pcsk1* has a larger role than *Pcsk2* in proinsulin processing and glycemic regulation, but that *Pcsk2* is still required in mouse beta cells for processing of other secretory granule propeptides, specifically proIAPP. The normal body weight in these models also suggest that beta-cell processing errors do not drive diabetes-associated obesity. Female mice are more resistant to beta-cell processing error-induced hyperglycemia, which may provide islet or peripheral adaptive mechanisms that could benefit humans with T1D or T2D. Beta-cell mass is increased in our processing-deficient models, suggesting a deficit in beta-cell mass and/or function early in life that is compensated for via beta-cell expansion. We did not observe insulin secretion deficits in processing-deficient islets, but an immature phenotype of excitability at lower glucose concentrations, expression of a beta-cell dysfunction marker *Aldh1a3*, and reduced expression of a key beta-cell transcription factor *Mafa*. Proteomics analysis revealed increased insulin content and upregulated trafficking processes in Pcsk1^{betaKO} islets, including many proteins with currently undefined roles in beta cells that may provide

beneficial compensatory mechanisms to preserve beta-cell function under high protein biosynthesis stress. Further work in processing-deficient beta cells will be required to understand the mechanisms leading to reduced proliferative capacity despite increased mass, and reduced maturity concurrent with increased (pro)insulin secretion. These mechanisms may provide avenues to restore or preserve beta cells under secretory stress.

Chapter 6: *Pcsk1* deficiency in beta cells increases islet amyloid deposition in human IAPP-transgenic mice

6.1 Introduction

Islet amyloid deposition is among the most observable histopathological changes in T2D islets. IAPP was discovered to be the major constituent of pancreatic amyloid plaques in 1986[211,386], after initially being described over a century ago from autopsies of individuals with diabetes[387,388]. The largest cohort of pancreases analyzed to date are from T2D (n=235) and non-diabetic (n=533) donors in China, where islet amyloid was found in 40% of T2D pancreases and only 3% of non-diabetic pancreases[88]. In T2D patients, amyloid severity was significantly associated with BMI and HbA_{1C} but not fasting glycemia or diabetes duration[88]. Although amyloid severity (islet amyloid area) and prevalence (frequency of islets with amyloid) are highly heterogenous in T2D, extensive islet amyloid is associated with reduced beta-cell mass and worsening hyperglycemia[389].

The association between T1D and amyloid is less clear and understudied relative to T2D. It was previously assumed there was minimal amyloid in T1D given the reduction in beta cells, and therefore IAPP secretion, during pathogenesis. Recently in 2017, Westermark et al.[91] reported islet amyloid in 2/6 recent onset (3-9 weeks) T1D pancreas tail biopsies from the DiViD study. In 2019 Beery et al.[92] reported islet amyloid in three T1D cases (0-2 years from diagnosis) in the nPOD biobank with no amyloid in non-diabetic matched controls, and Kahn et al.[390] reported islet amyloid in a T1D case with a similar deposition pattern to T2D amyloid. These studies reported similar extents of amyloidosis at far less than T2D, with approximately 0-10% prevalence and 0-40% severity in each, and the total amount of amyloid at less than 0.05% of

pancreatic area. Interestingly, islets containing amyloid were found to be scattered throughout the pancreas in some cases, while confined to particular lobules in others, suggesting potential differences in mechanisms of amyloidogenesis. The age ranges studied varied from 16-35 years-old, and it remains unknown if islet amyloid is present during the pathogenesis of T1D in younger individuals. The growth of recent T1D biobanks has improved access and facilitated these observations. More robust quantifications of amyloid in T1D will be sure to follow, as amyloid can drive islet inflammation[391–393] and may be contributing to T1D pathogenesis in a subset of individuals.

IAPP monomers largely adapt a random coil formation with minimal secondary structure. In amyloid plaques, IAPP adopts a highly structured beta-sheet confirmation that gives rise to amyloid fibrils. Although the mechanisms causing transition from random coil to fibril remain unclear, kinetic and structural analyses of IAPP fibrillogenesis have provided insight[213]. IAPP first forms oligomers in an energetically unfavourable process that involves exposure of hydrophobic residues and sufficient time. During oligomerization, IAPP has been found to adopt alpha-helical secondary structures, and interactions of monomers and oligomers with biological membranes may stabilize the exposed hydrophobic residues[394]. Once oligomers are formed, fibrils extend rapidly until a steady state fibril length is reached. This results in a sigmoidal-shaped amyloid formation curve relative to time with three distinct phases: (i) a prolonged “lag phase” leading to the formation of oligomers; (ii) a rapid fibril “elongation” phase in which fibrils grow exponentially; and (iii) a “plateau” phase in which there is no net increase in fibrils or fibril lengths.

Oligomers are thought to drive the majority of cytotoxicity, and cause membrane damage during fibril elongation[395]. Preformed mature IAPP fibrils induce minimal cell death and

membrane alterations on beta cells, whereas freshly dissolved hIAPP that transitions through lag and elongation phases causes large reductions in cell viability[396,397]. Beta cells may also be more prone to IAPP-aggregate-induced cell death than other cell types – hIAPP induces more cell death in INS-1 cells than GH3 (pituitary) cells[298] and TEM images of human islets show that IAPP fibrils create membrane invaginations on beta cells but do not disrupt neighbouring non-beta endocrine cell membranes[213]. Treatment of freshly dissolved IAPP, but not preformed IAPP fibrils, increases the conductance of planar lipid bilayers and suggests membrane disruption[397]. This was also found in the MIN6 beta-cell line, where exogenous hIAPP increased intracellular Ca^{2+} and apoptosis following fibril formation, which was partially rescued by siRNA-mediated knockdown of the mechanosensitive Trpv4 cation channel[398].

Although mature fibrils are the robustly detectable form of IAPP aggregates in the islets of individuals with T2D, they have been found to be a relatively inert conformation of IAPP aggregates[396]. A significant challenge in diabetes and other amyloid pathologies is detection of the cytotoxic and short-lived oligomers. Conformational antibodies have detected putative IAPP oligomers and continue to improve, but detection remains challenging in biological samples due to questionable cross-reactivity and challenging tissue preparation and staining techniques[399]. Nonetheless, amyloid fibrils *in situ* originate from oligomers and can be readily detected histologically as they remain in tissues. This results in challenging interpretations of amyloid burden, where an increased abundance of mature fibrils can mark either ongoing oligomerization and cell death, or prior oligomer-induced cell death with residual fibrils. This has also created a challenge to model and characterize the conditions under which amyloid forms *in vivo*, as investigators are unable to unequivocally determine if oligomerization is occurring. However,

retrospective analyses can still be informative in deciphering the conditions which may have driven oligomer and amyloid formation.

Much of our knowledge on the formation and effects of amyloid has come from tissue culture of human islets or animal models. Several animal models exist to study islet amyloid in vivo. The amino acid sequence of IAPP is highly conserved between humans and non-human primates[400], who also develop spontaneous islet amyloid. Serial longitudinal sampling in the pancreatic tails of *Macaca nigra* animals as they transitioned from non-diabetic to borderline-diabetic and diabetic revealed increasing islet amyloid in each animal as glucose clearance and insulin secretion declined and glycemia increased[401]. Transplantation of human islets to mice can also provide another model for amyloid formation[402], and amyloid is associated with islet graft failure[96]. This has also been observed clinically in transplanted islets, performed as a therapy for T1D, where human cadaveric donor islets are infused into the hepatic portal vein. Recovery of transplanted islets or histology in the liver grafts upon autopsy have revealed amyloid in transplanted islets ranging from 5-40% prevalence[403,404]. The increased prevalence is likely due to acceleration of amyloid formation due to transplant-associated islet stress. Transplantation of macro-encapsulated human stem-cell derived beta-like cells into mice also resulted in the development of amyloid[404].

Rodents do not develop islet amyloid, which is due primarily to three proline residue substitutions from hIAPP (A25, S28, and S29 in hIAPP). Several early mouse models expressing transgenic hIAPP failed to develop islet amyloid using the following promoters and mouse backgrounds: (i) rat *Ins2* promoter, C57BL/6J[405]; (ii) rat *Ins2* promoter, C57BL/6 x DBA2 hybrid[406]; (iii) rat *Ins1* promoter, FVB/N[407]; (iv) human *INS* promoter, C57BL/6J[408]. This was despite confirmed expression by northern blots, HPLC, IHC, and approximately 5-fold elevated

plasma IAPP immunoreactivity. However, intragranular fibrils were observed by TEM in two of the models[408,409]. In 1996, islet amyloid and hyperglycemia were eventually observed in approximately 80% of aged male mice hemizygous for a rat *Ins2*-hIAPP transgene (hIAPP$^{Tg/0}$) on a C57BL/6 x DBA2 hybrid background when fed a higher fat diet[410], and in younger male mice homozygous for a rat *Ins2*-hIAPP transgene on a FVB/N background strain[142].

Homozygous RIPHAT (Rat *Ins2* Promoter Human IAPP Transgenic) males developed diabetes with loss of circulating insulin and uncontrollable fasting hyperglycemia beginning around 8 weeks of age. A fraction of RIPHAT males did not survive past 16 weeks old, while only 20% of female mice developed mild hyperglycemia by 30 weeks old[142]. Similarly, only 1/9 female hIAPP$^{Tg/0}$ mice developed islet amyloid[410]. Islet secretory stress in mice with experimentally induced insulin resistance drove hyperglycemia and islet amyloid in hemizygous RIPHAT mice[141]. In another beta-cell stress model, male mice with heterozygous RIPHAT and agouti viable yellow expression (RIPHAT$^{Tg/0}$; A^{vy}/A) developed amyloid and more severe hyperglycemia than animals with only agouti viable yellow or RIPHAT expression[411]. Insulin resistance and hyperinsulinemia due to leptin deficiency (*Lep$^{ob/ob}$*) was also able to induce amyloid and further hyperglycemia in an hIAPP$^{Tg/0}$ model that previously lacked extracellular amyloid deposition[405,412]. High-fat diet also induces insulin resistance in mice [362], and increasing fat content beyond the 9% fat diet used by Verchere et al.[410] further increased islet amyloid and reduced insulin secretion in hIAPP$^{Tg/0}$ male mice[413]. Improving insulin sensitivity and reducing beta-cell secretory stress with metformin or rosiglitazone in hIAPP$^{Tg/0}$ mice also reduces islet amyloid[414]. More recently, two strains of hIAPP knock-in mice were created with wild-type hIAPP and hIAPP^{S20G} sequences[415]. Although hIAPP knock-in male mice on chow or HFD developed mildly impaired glucose tolerance, no amyloid was detected after 15 months of high

fat diet. The hIAPP knock-in mice have endogenous levels of IAPP rather than the 2-5 fold increase observed in hIAPP$^{Tg/0}$ mice[142,407]. Cumulatively, the evidence in hIAPP mouse models suggest that amyloid and hyperglycemia form slowly under increased secretory stress conditions similar to T2D, proving this a useful model for studying amyloid formation.

Mouse hIAPP$^{Tg/0}$ islets, human islets, and cell lines have proven useful for characterizing conditions that lead to islet amyloid formation and dissecting mechanisms of amyloid-induced beta-cell dysfunction. Human and hIAPP$^{Tg/0}$ mouse islets cultured *ex vivo* naturally develop amyloid that can be reduced with amyloid inhibitors or via siRNA targeting *IAPP,* which reduce death and improve GSIS after 10 days in culture[416,417]. This parallels observations in mice where hIAPP$^{Tg/Tg}$ mice develop more amyloid relative to hemizygous animals[142], and suggests that the abundance of hIAPP contributes to its amyloidogenicity and ability to induce dysfunction. Beta cells in hIAPP$^{Tg/0}$, but not control mice overexpressing rIAPP, have also been shown to have increased markers of UPR activation and apoptosis along with a buildup of polyubiquinated proteins, suggesting unresolved ER-stress and deficient proteasomal activity[418]. However, ER stress may be a brief and transient phenotype, as UPR activation has also been shown to not occur in hIAPP$^{Tg/0}$ mice during the development of amyloid[419]. Despite minimal ER stress, protein disulfide isomerase (PDI) has been shown to interact with IAPP in human islets, and overexpression of PDI reduces beta-cell death and improves beta-cell function in hIAPP$^{Tg/0}$ islets despite no change in amyloid severity[420]. Thus, it remains unclear to what extent ER stress may be involved in amyloid formation in human islets, but the abundance of hIAPP is closely associated with amyloid formation.

IAPP aggregates activate islet macrophages via TLR2-MyD88 signalling and NLRP3 inflammasome activation that results in the secretion of abundant interleukin 1 beta (IL-1

beta)[391–393,421]. Proinflammatory cytokines including IL-1 beta are elevated in T2D islets and can drive beta-cell dysfunction and amyloid formation in vitro[422]. This creates a detrimental positive feedback loop in which IAPP aggregation increases local IL-1 beta release, driving further IAPP aggregation. Interestingly, depletion of islet macrophages improves glucose tolerance and reduces islet inflammation despite increasing islet amyloid in hIAPP$^{Tg/0}$ mice[393], likely due to loss of amyloid phagocytosis by macrophages[423]. Macrophage depletion also results in reduced IL1-beta production, beta-cell death, and improves islet GSIS and glucose tolerance in hIAPP$^{Tg/0}$ mice[393]. Impaired glucose tolerance and elevated plasma proinsulin:insulin ratios are also observed in hIAPP$^{Tg/0}$ mice, and are improved with subcutaneous delivery of an IL-1 receptor antagonist[424]. Therefore, islet inflammation mediated by macrophages is a major mechanism for IAPP aggregate-induced beta-cell dysfunction.

Additional metabolic perturbations associated with T2D have been shown to alter islet amyloid formation. Culturing hIAPP$^{Tg/0}$ islets in the presence of excess free fatty acids (FFAs) initiates amyloid formation[425]. Excessive beta-cell cholesterol accumulation from either cholesterol loading in cultured islets or via deletion of the cholesterol transporter *Abcc8* in hIAPP$^{Tg/0}$ mice leads to increased islet amyloid deposition[426]. Both FFAs and cholesterol may increase amyloidogenesis through alterations in beta-cell membrane composition, which could facilitate IAPP-membrane interactions and increase IAPP oligomerization[427]. Changes in the cell surface and extracellular matrix (ECM) may also facilitate amyloid deposition. Heparan sulfate proteoglycans (HSPGs) are abundant at the beta-cell surface and in the islet ECM, and are incorporated into amyloid deposits with IAPP fibrils[428]. HPSGs have been shown to bind IAPP and facilitate fibrillogenesis in cell-free assays[429,430], and heparinase reduces amyloid formation and apoptosis in cultured human islets[431]. In particular, heparin sulfate side chains on a perlecan

core have been shown to interact with IAPP, and expression of mutant perlecan lacking heparan sulfate side chains in $hIAPP^{Tg/0}$ mice reduces islet amyloid formation[432].

Reduced proIAPP processing activity also occurs T1D and T2D and is associated with similar timing in the pathologies as amyloid deposition and functional beta-cell decline. This has, in part, led to the hypothesis that reduced proIAPP processing may increase islet amyloid deposition. Another implication for proIAPP in fibrillogenesis is immunoreactivity toward the N- and C-terminal propeptides of IAPP in $hIAPP^{Tg/0}$ and human islets, both in amyloid deposits by immunofluorescence microscopy and in IAPP fibrils by immunogold labelling and TEM imaging[433–435]. In cell-free assays, proIAPP and processing intermediates have been consistently found to display longer lag times and slower aggregation kinetics, particularly intact proIAPP[436–439]. Oxidation and amidation of proIAPP also increase amyloidogenicity, and the aggregation kinetics of (pro)IAPP peptides were found to be: fastest $IAPP_{mature}$ > $proIAPP_{1-48}$ > $proIAPP_{12-51}$ > $proIAPP_{12-67}$ > $proIAPP_{1-67}$ (proIAPP residue numbering in subscript), where full-length $proIAPP_{1-67}$ had very low fibril-forming potential[437]. Despite slow aggregation kinetics, $proIAPP_{1-48}$ and proIAPP have been shown to insert into membranes and induce vesicle leakage in cell-free assays[438]. ProIAPP peptides have also been shown to inhibit (i.e., increase lag time) the aggregation of mature IAPP[438]. A truncated peptide spanning N-terminal proIAPP and part of mature IAPP ($proIAPP_{1-30}$) interacts with heparin and heparin sulfate, and weakly with chondroitin sulfate[430]. Fibril nucleation and rapid $proIAPP_{1-48}$ fibrillization has also been demonstrated in the presence of heparin sulfate and chondroitin sulfate, but this also occurred for mature IAPP suggesting it is not specific to the N-terminal propeptide of IAPP[429].

Although cell-free assays have greatly aided our understanding of IAPP aggregation, the kinetics of oligomerization and fibril formation are highly dependent on the environment. This is

highlighted by aggregation in the presence of lipid vesicles, where increased anionic lipid content can significantly accelerate fibril formation[440]. Given the highly complex and dynamic composition of biological membranes, studying amyloid formation in biological systems is critical to understanding the conditions leading to amyloid formation. Further, altered aggregation kinetics can be challenging to understand, as a prolonged lag phase could represent increased time in which cytotoxic oligomers are present. Biological systems allow for measurement of cellular outcomes during the lag phase, with the caveat that we cannot easily confirm the presence of oligomers. Consideration of both cell-free data and biological data provides a better understanding of amyloidogenesis.

Most evidence of proIAPP processing errors and aggregation point toward a defect in PCSK2 activity. Studies of preproIAPP expression in cell lines with both PCSK1 and PCSK2 (Beta-TC6), only PCSK2 (GH3), only PCSK1 (AtT-20), and neither PCSK1 nor PCSK2 (GH4C1) found that cells lacking PCSK2 have increased proIAPP abundance and intracellular amyloid[441]. In contrast, PCSK1-deficient cells developed no amyloid. Additionally, co-transfection of GH3 cells with *Pcsk2* and human *IAPP* improves viability relative to human *IAPP* transfection alone[298]. Islets from *Pcsk2*-null hIAPP$^{Tg/0}$ mice also displayed elevated amyloid and apoptosis in culture over 10 days relative to *Pcsk2* wild-type hIAPP$^{Tg/0}$ animals[298]. Further, *Pcsk2*-null hIAPP$^{Tg/0}$ islets displayed early graft failure relative to hIAPP$^{Tg/0}$ or *Pcsk2*-null grafts in mouse islet transplants[442]. Cumulatively, there is significant evidence implicating PCSK2-mediated proIAPP processing errors in amyloid formation in mouse and cell models.

PCSK1-mediated processing errors have been less characterized in human IAPP aggregation. Although *Pcsk1* loss has a lesser impact on proIAPP processing (Chapter 5, Figure 19B), and intact proIAPP has reduced amyloidogenicity in cell-free systems, it is reasonable to

speculate that *Pcsk1* deficiency in beta cells may alter amyloid formation. Insulin has been shown to inhibit IAPP aggregation in cell-free assays, while proinsulin inhibits to a much lesser extent[443,444], and we and others have shown significant impairments in proinsulin processing (Figures 18, 19) and altered insulin secretory granule morphology in mice lacking beta-cell *Pcsk1* (Figure 26). In the previous chapter, proteomics and RNA sequencing data in Pcsk1^{betaKO} beta cells and islets suggest altered trafficking and cholesterol biosynthesis which may also indirectly affect IAPP aggregation as mentioned above.

The aim of this chapter is to characterize the impact of beta-cell *Pcsk1* deficiency on IAPP aggregation. Recent evidence suggests that PCSK1 is the predominant PCSK in human beta cells[289]. PCSK1, but not PCSK2, has also been found reduced in islets and pancreas extracts of individuals with T1D[310,311]. Given these recent studies, we hypothesize that PCSK1 deficiency may drive increased islet amyloid formation. To investigate the effect of PCSK1-deficiency on human IAPP aggregation and islet function, we crossed Pcsk1^{betaKO} mice with hIAPP$^{Tg/0}$ mice and analyzed glycemic regulation and islet amyloid deposition.

6.2 Results

6.2.1 Loss of *Pcsk1* in beta cells does not increase glycemia in hIAPP$^{Tg/0}$ mice

Mouse IAPP does not form amyloid under physiological conditions. To study the effect of beta-cell PCSK1 deficiency on IAPP aggregation, we generated a mouse model with beta-cell-specific *Pcsk1* deletion and human IAPP expression. Human proIAPP transgenic mice (hIAPP$^{Tg/0}$) (FVB/N background) were bred with *Ins1$^{cre/+}$ Pcsk1$^{flox/flox}$* mice (B6J/N hybrid background), and backcrossed to *Pcsk1$^{flox/flox}$* animals. All mice studied were F3 descendants (87.5% B6J/N; 12.5% FVB/N). No significant body weight differences were detected up to 31 weeks old in any genotype (Figure 43 A,B). In hIAPP$^{Tg/0}$ males, Pcsk1^{betaKO} mice trended toward

reduced body weight (Figure 43A). Pcsk1^{betaKO} male mice also showed trends toward elevated fasting glycemia relative to Pcsk1^{betaWT} controls, with the effect of *Pcsk1* deletion similar in both hIAPP$^{Tg/0}$ and hIAPP$^{0/0}$ mice (Figure 43C), suggesting that the effect of beta-cell *Pcsk1* loss on fasting glycemia is comparable regardless of hIAPP expression. Interestingly, one Pcsk1^{betaKO} hIAPP$^{Tg/0}$ male mouse developed uncontrolled fasting hyperglycemia at 25 weeks old. However, the remaining 10 mice of the same genotype did not. Female Pcsk1^{betaKO} mice were not hyperglycemic relative to Pcsk1^{betaWT} controls (Figure 43D). In both sexes expression of hIAPP resulted in elevated fasting glycemia regardless of beta-cell *Pcsk1* status.

Glucose tolerance was similarly unaltered in mice lacking beta-cell *Pcsk1* (Figure 44). There was a transient trend toward hyperglycemia at 12 weeks old in hIAPP$^{Tg/0}$ male mice lacking beta-cell *Pcsk1*, but this diminished with age (Figure 44A-C). In both sexes there was a comparable effect of hIAPP expression in both Pcsk1^{betaKO} and Pcsk1^{betaWT} mice, with significant hIAPP-induced impairments in glucose tolerance by 28 weeks old. In summary, *Pcsk1* deletion in beta cells has minimal impact on fasting glycemia or glucose tolerance in male and female mice on a mixed B6JN/FVBN background, while hIAPP expression increases fasting glycemia and impairs glucose tolerance in both sexes. Further, beta-cell *Pcsk1* loss and hIAPP expression have no significant effect on body weight.

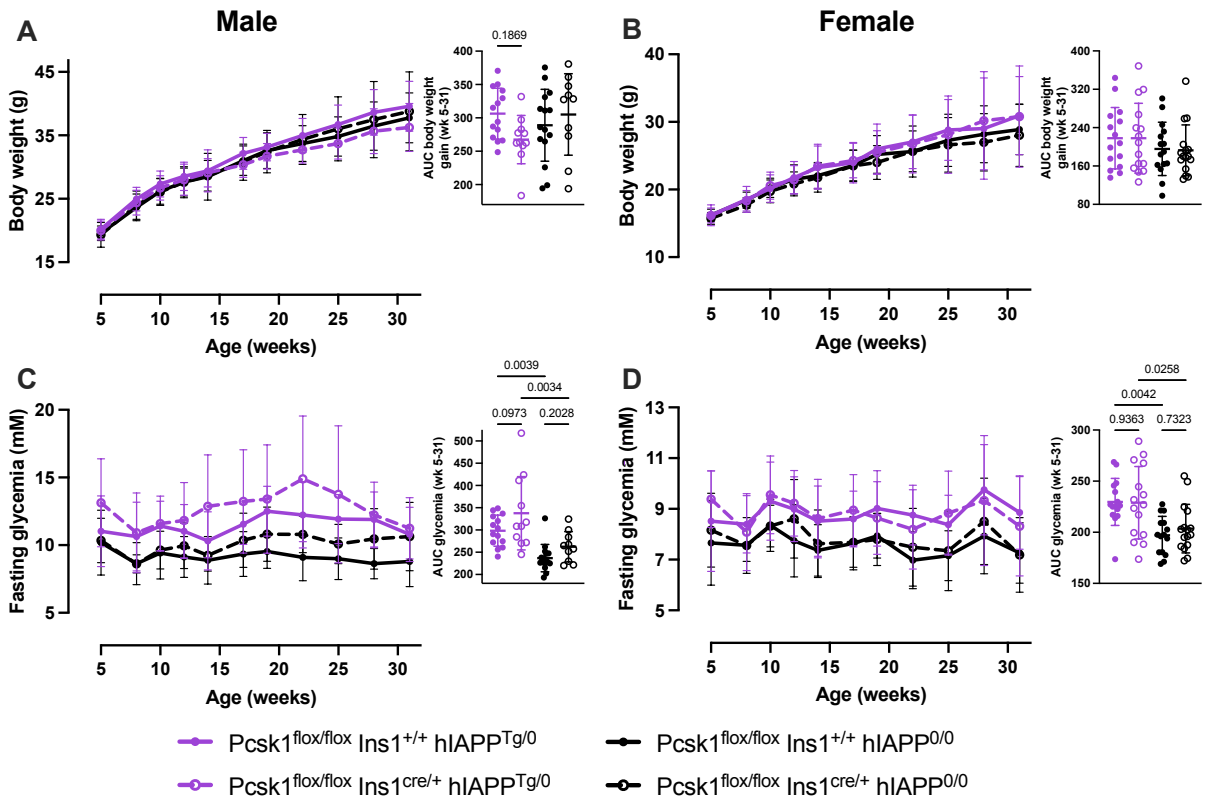

Figure 43: Beta-cell *Pcsk1* deficiency does not significantly impact body weight or glycemia in human proIAPP transgenic mice.

Body weight and blood glucose were measured after a 4 or 6 h fast from 5-31 weeks old. **(A,B)** Male and female mice displayed no significant differences in body weight. AUCs are calculated as weight gain above starting body weight. **(C)** Loss of beta-cell Pcsk1 expression in male mice causes similar trends toward elevated fasting glycemia in both $hIAPP^{Tg/0}$ and $hIAPP^{0/0}$ mice. **(D)** Loss of beta-cell *Pcsk1* expression in female mice does not impact fasting glycemia. $hIAPP^{Tg}$ expression significantly increases fasting glycemia in $Pcsk1^{betaWT}$ and $Pcsk1^{betaKO}$ mice in both sexes. AUCs are calculated as total area under curve as a single measure of lifetime glycemia. n = 10-15 male, 15-16 female mice.

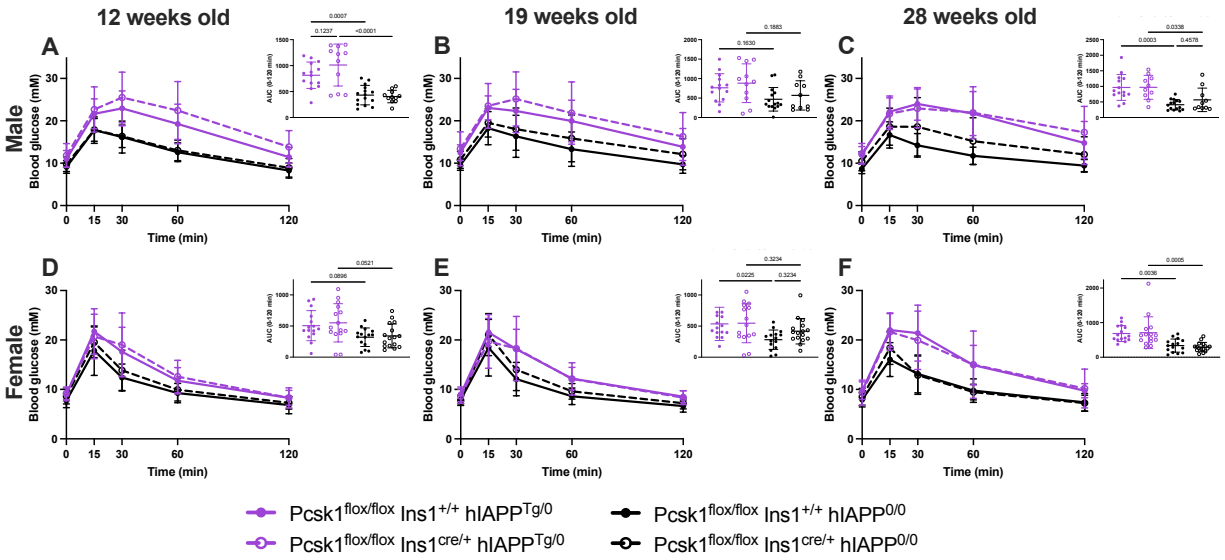

Figure 44: Loss of beta-cell *Pcsk1* does not worsen hIAPP-induced impairments in glucose tolerance.
Mice were fasted for 6 h prior to intraperitoneal glucose tolerance tests (GTT) at the ages indicated. Glucose dose varied by age and sex. **(A-C)** Male Pcsk1^{betaKO} hIAPP$^{Tg/0}$ mice do not have impaired glucose tolerance relative to Pcsk1^{betaWT} hIAPP$^{Tg/0}$ controls. **(D-F)** Female Pcsk1^{betaKO} mice have normal glucose tolerance relative to Pcsk1^{betaWT} controls in both hIAPP$^{Tg/0}$ and hIAPP$^{0/0}$ mice. hIAPP$^{Tg/0}$ mice display impaired glucose tolerance relative to hIAPP$^{0/0}$ controls in both sexes, regardless of beta-cell *Pcsk1* genotype. n = 10-15 male, 15-16 female mice.

6.2.2 Islet amyloid is increased in hIAPP$^{Tg/0}$ mice lacking beta-cell PCSK1 activity

Pancreases were collected from mice at the study endpoint (31 weeks old, apart from one hyperglycemic Pcsk1^{betaKO} hIAPP$^{Tg/0}$ male mouse at 25 weeks old) and analyzed for amyloid. Loss of *Pcsk1* in beta cells increased amyloid prevalence (% amyloid^{+} islets) and severity (amyloid area as a percentage of insulin^{+} area) in hIAPP$^{Tg/0}$ male animals. Although prevalence was over 20% in Pcsk1^{betaWT} hIAPP$^{Tg/0}$ animals, median severity was extremely low at less than 1% – significantly lower than the 8% median severity observed in Pcsk1^{betaKO} hIAPP$^{Tg/0}$ mice (Figure 45 A-C). Amyloid deposits were often found at the interface of beta cells and structures resembling capillaries (Figure 45A), although this was not confirmed with an endothelial cell

stain. Increased islet amyloid deposition in Pcsk1^{betaKO} hIAPP$^{Tg/0}$ mice was particularly evident in larger islets (Figure 45D). Analysis of islet sizes showed that Pcsk1^{betaKO} hIAPP$^{Tg/0}$ islets were not significantly larger than Pcsk1^{betaWT} hIAPP$^{Tg/0}$ islets (Figure 45E), indicating that altered islet size is not responsible for increased amyloid in Pcsk1^{betaKO} hIAPP$^{Tg/0}$ mice. Despite minimal amyloid severity in Pcsk1^{betaWT} hIAPP$^{Tg/0}$ mice, there was a weak non-significant positive correlation of amyloid severity with fasting glycemia, whereas a stronger correlation was observed in Pcsk1^{betaKO} hIAPP$^{Tg/0}$ mice (Figure 45F). Islet amyloid severity and prevalence were well correlated for both genotypes, but increased amyloid severity is observed at a lower prevalence in Pcsk1^{betaKO} hIAPP$^{Tg/0}$ mice, suggesting that amyloid deposits expand more rapidly once seeded in Pcsk1^{betaKO} hIAPP$^{Tg/0}$ mice (Figure 45G).

Female hIAPP$^{Tg/0}$ mice developed very little amyloid as described by others (Figure 46A, top panels). However, beta-cell Pcsk1 deficiency was sufficient to drive an increase in islet amyloid prevalence and severity even in female mice (Figure 46 B,C), and islets with substantial amyloid were more frequent in Pcsk1^{betaKO} hIAPP$^{Tg/0}$ female mice than in Pcsk1^{betaWT} hIAPP$^{Tg/0}$ female mice (Figure 46A, bottom panels). Similar to male mice, increased amyloid severity was more pronounced in larger islets (Figure 46D), while islet sizes were comparable in both genotypes (Figure 46E). Islet amyloid severity was only correlated with fasting glycemia in Pcsk1^{betaKO} hIAPP$^{Tg/0}$ mice (Figure 46F), and both genotypes displayed strong and similar correlations between islet amyloid severity and prevalence (Figure 46G). Although the islet amyloid severity and prevalence is low in hIAPP$^{Tg/0}$ female mice, the lack of amyloid detected in hIAPP$^{0/0}$ mice suggests this is unlikely to be an experimental artefact (Figure 46 B,C). In summary, male and female mice lacking Pcsk1 activity in beta cells display increased islet

amyloid, both in the number of islets affected with amyloid and in the total abundance of amyloid.

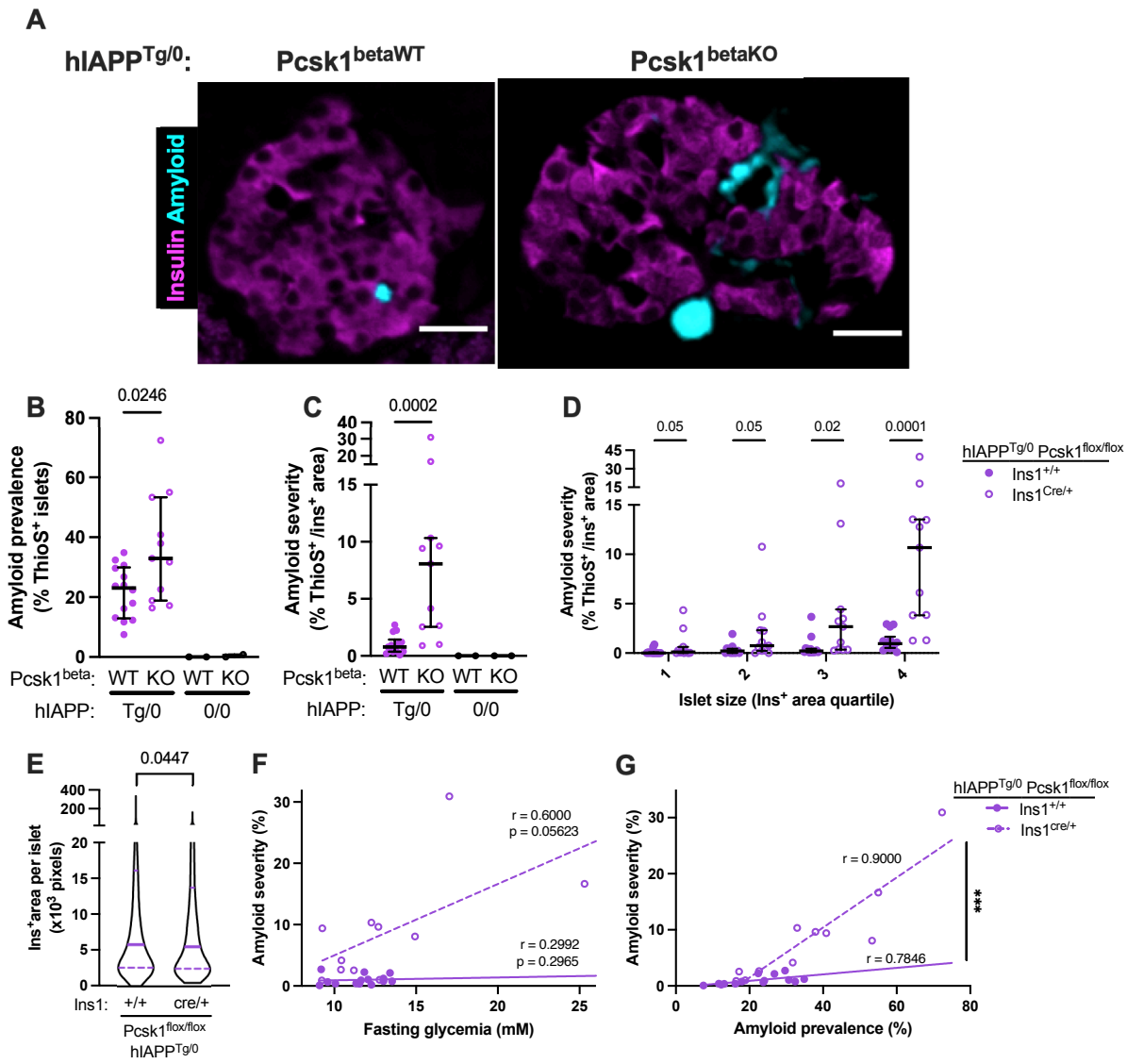

Figure 45: Male hIAPP$^{Tg/0}$ mice lacking beta-cell *Pcsk1* have increased islet amyloid. Mice were euthanized at 31 weeks of age (25 weeks old for one Pcsk1^{betaKO} hIAPP$^{Tg/0}$ mouse) and pancreas sections analyzed for amyloid by Thioflavin S and insulin by immunohistochemistry. **(A)** Images representative of median amyloid severity are shown for each genotype. **(B,C)** Deletion of *Pcsk1* in beta cells increases islet amyloid prevalence and severity in hIAPP$^{Tg/0}$ mice. **(D)** Islets were binned in quartiles by insulin^{+} area, and amyloid severity was calculated for each animal using islets in each quartile. Loss of beta-cell *Pcsk1* induces greater amyloid deposition in larger islets. **(E)** Violin plots of islet insulin^{+} areas analyzed. Pcsk1^{betaKO} hIAPP$^{Tg/0}$ islet size is slightly reduced compared to Pcsk1^{betaWT} hIAPP$^{Tg/0}$ islet size. **(F)** Amyloid severity approached a significant correlation with fasting glycemia in hIAPP$^{Tg/0}$ mice lacking *Pcsk1* in beta cells but not in mice with beta-cell PCSK1 activity. **(G)** Amyloid severity and prevalence were correlated in both genotypes, but Pcsk1^{betaKO} hIAPP$^{Tg/0}$ mice had a significantly steeper slope. Mann-Whitney tests were performed due to non-parametric data. Data is presented as median ± IQR. Scale bars represent 50 µm.

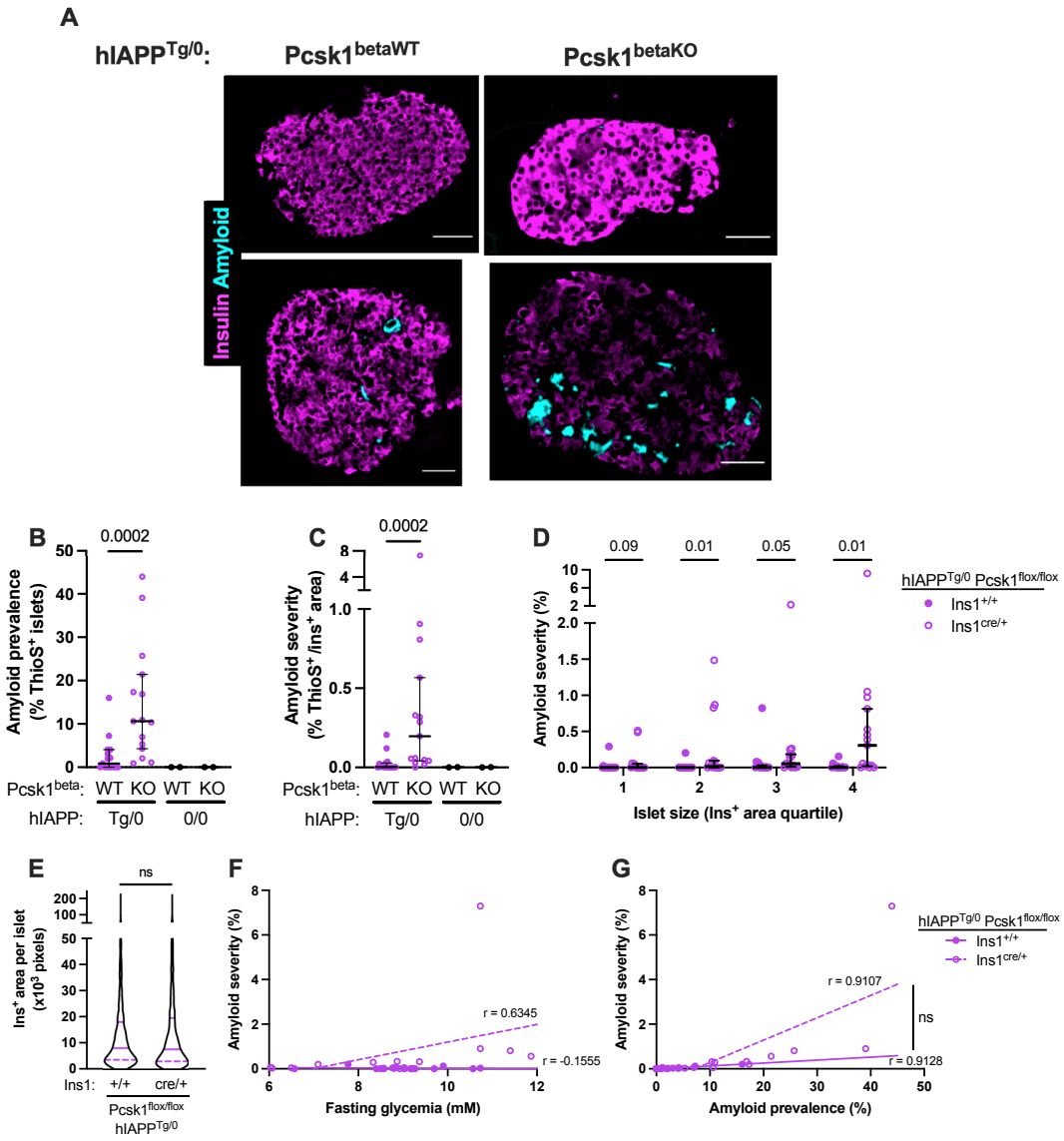

Figure 46: Beta-cell *Pcsk1* loss increases islet amyloid deposition in female hIAPP$^{Tg/0}$ mice. Mice were euthanized at 31 weeks of age and pancreas sections analyzed for amyloid by Thioflavin S and insulin by immunohistochemistry. **(A)** Islets in hIAPP$^{Tg/0}$ female mice displayed less amyloid than males (top panels; representative of median severities), but islets with abundant amyloid were more prevalent and had higher amyloid severity in Pcsk1^{betaKO} females relative to Pcsk1^{betaWT} females (bottom panels). **(B,C)** Amyloid prevalence and severity are increased in hIAPP$^{Tg/0}$ mice lacking *Pcsk1* in beta cells. **(D)** Islets were binned by quartiles of insulin$^+$ area. Increased amyloid severity is most evident in larger islets. **(E)** Violin plots of insulin$^+$ areas for analyzed islets. Islets were comparable sizes in both genotypes. **(F)** Amyloid severity was moderately correlated with fasting glycemia in hIAPP$^{Tg/0}$ mice lacking beta-cell *Pcsk1*, but not in those with beta-cell *Pcsk1* activity. **(G)** Amyloid severity and prevalence were strongly correlated in both genotypes and the regression slopes were not significantly different. Mann-Whitney tests were performed due to non-parametric data. Data is presented as median ± IQR. Scale bars represent 50 µm.

6.3 Discussion

Our data in hIAPP$^{Tg/0}$ mice suggest that reduced beta-cell PCSK1 activity increases islet amyloid. The increased amyloid deposition is independent of significant hyperglycemia as female Pcsk1^{betaKO} and Pcsk1^{betaWT} mice had comparable fasting glycemia, although Pcsk1^{betaKO} males displayed a trend toward hyperglycemia. Although the increase in islet amyloid associated with *Pcsk1* deficiency did not result in significant hyperglycemia, islet amyloid severity was positively correlated with fasting glycemia in Pcsk1^{betaKO} hIAPP$^{Tg/0}$ mice, suggesting that with further ageing Pcsk1^{betaKO} hIAPP$^{Tg/0}$ male mice may develop significant hyperglycemia. The development of islet amyloid is a slow process in humans that likely takes decades to develop, and from studies in monkeys it is thought extensive amyloid deposition is required prior to the onset of diabetes[401]. With further aging, Pcsk1^{betaKO} hIAPP$^{Tg/0}$ mice may have developed amyloid-induced hyperglycemia. Although they were not measured, assessment of beta-cell apoptosis rates and inflammation may provide insight as to whether beta-cell death and functional decline are occurring in Pcsk1^{betaKO} hIAPP$^{Tg/0}$ mice.

Islet amyloid prevalence and severity were strongly correlated in male and female hIAPP$^{Tg/0}$ animals regardless of Pcsk1 expression. However, male Pcsk1^{betaKO} mice displayed increased severity at lower prevalence. This is in contrast to what others have observed in hIAPP$^{Tg/0}$ mice, and what we observed in Pcsk1^{betaWT} hIAPP$^{Tg/0}$ mice, where amyloid develops at low severity across the majority of islets before increasing exponentially once prevalence reaches approximately 80%[445]. This finding suggests that the rate of amyloid growth occurs more rapidly in *Pcsk1*-deficient beta cells once fibrils are seeded. Pcsk1^{betaKO} beta cells may also have increased exocytosis to compensate for the reduced potency of proinsulin. Insulin immunoreactivity is increased in the plasma of Pcsk1^{betaKO} mice (Figure 18E), and Pcsk1^{betaKO}

islets have accelerated glucose-induced calcium influx (Figure 39A) and possibly increased insulin secretion (Figure 40). This may result in increased release of (pro)IAPP in Pcsk1^{betaKO} mice, facilitating rapid amyloid growth once protofibrils are seeded.

In addition to accelerated amyloid deposition, the increase in amyloid prevalence and severity in Pcsk1^{betaKO} hIAPP$^{Tg/0}$ female mice suggests beta-cell Pcsk1 loss is sufficient to create an amyloidogenic milieu, as Pcsk1^{betaWT} hIAPP$^{Tg/0}$ controls contained almost no amyloid similar to previous observations in hIAPP$^{Tg/0}$ female mice[410]. Impaired proIAPP processing in the absence of *Pcsk1* is unlikely to account for the increase in amyloid for several reasons. First, human proIAPP expression in the PCSK2^{+} Pcsk1^{LOW} rat GH3 cell line resulted in no amyloid or proIAPP processing errors using antisera directed toward the N- and C-terminal processing sites, while expression in the PCSK2^{LOW} PCSK1^{+} mouse AtT-20 cell line resulted in detectable amyloid and proIAPP processing errors[441]. Second, mouse proIAPP processing is very mildly impaired in *Pcsk1*-null mouse islets[295], and we observe abundant mature mouse IAPP in Pcsk1^{betaKO} islets from C57BL/6JN mice (Figure 19B). Third, cell-free assays have shown proIAPP peptides delay IAPP aggregation and fibril formation, both in the presence and absence of membranes[436–439]. It is important to recognize that cell line studies omit any islet extracellular matrix-specific effects, and cell-free assays are unable to replicate the complexity of biological membranes – both of which have been shown to modify (pro)IAPP fibrillogenesis; however, these cell-free studies do suggest that impaired processing of proIAPP delays fibril formation rather than accelerating it.

Altered processing of other contents of insulin secretory granules may influence amyloid formation in Pcsk1^{betaKO} mice. Insulin has been shown to interact with hIAPP to inhibit fibrillogenesis, whereas proinsulin has greatly reduced binding to hIAPP and reduced inhibition

of IAPP aggregation[443,444]. Although these interactions have again been studied in cell-free systems, some included lipid membranes with high Zn^{2+} and Ca^{2+} concentrations to mimic the granule environment, and show reduced but relevant insulin-mediated inhibition of IAPP fibrillogenesis[444]. Given the extensive proinsulin processing defects in Pcsk1^{betaKO} mice, reduced inhibition of IAPP aggregation by the loss of mature insulin may contribute to amyloidogenesis in Pcsk1^{betaKO} hIAPP$^{Tg/0}$ mice. Zinc and calcium ions have also been shown to accelerate amyloid formation in cell-free assays[443]. As (pro)insulin crystallization is reduced in Pcsk1^{betaKO} granules (Figure 26), there may be less sequestration and increased availability of granular zinc to further promote nucleation of IAPP fibrils. Lastly, INS2 protein abundance was increased in Pcsk1^{betaKO} beta cells (Figure 41). Although mIAPP expression was not altered, the hIAPP transgene contains the rat *Ins2* promoter and 5'-UTR[141]. This may lead to increased translation and abundance of the hIAPP transgene in Pcsk1^{betaKO} mice relative to Pcsk1^{betaWT} mice. Cholesterol is also critical in secretory granule biogenesis[371], and reduced expression of genes associated with cholesterol biosynthesis were observed in Pcsk1^{betaKO} islets (Figure 28B). As excessive beta-cell cholesterol has been shown to increase amyloid deposition[426], changes in cholesterol biosynthesis in Pcsk1^{betaKO} beta cells could further influence hIAPP aggregation. Altogether, altered proIAPP processing is unlikely to be driving the increase in amyloid in mice with *Pcsk1*-deficient beta cells. Rather, changes in the secretory granule environment, proIAPP abundance, and secretory rates may drive increased islet amyloid.

It is also interesting to speculate that proteostasis may be altered in Pcsk1^{betaKO} hIAPP$^{Tg/0}$ islets. Immunogold labelling in hIAPP$^{Tg/0}$ islets has shown increased lysosomal IAPP in beta cells[405], and increased autophagy has been observed in hIAPP$^{Tg/0}$ and hIAPP-knockin mouse beta cells[446–448]. In hIAPP$^{Tg/0}$ mice, stimulation of autophagy has been reported to reduce hIAPP

oligomer abundance and beta-cell death, and improve glucose tolerance. In contrast, disruption of autophagy further worsens hIAPP-induced cell death, oligomer abundance, and glucose tolerance in hIAPP-expressing mice[449,450]. In Pcsk1^{betaKO} mice we did not observe increased expression of genes or abundance of proteins associated with autophagy. However, given the abundant (pro)insulin content of Pcsk1^{betaKO} islets, autophagic granule degradation (crinophagy) may be reduced relative to proinsulin and proIAPP translation leading to increased IAPP aggregation. Although impaired autophagy does not lead to amyloid in hIAPP$^{Tg/0}$ mice, an increased abundance of IAPP oligomers indicates an environment conducive to fibrillogenesis.

In summary, we observed increased amyloid hIAPP$^{Tg/0}$ mice lacking beta-cell Pcsk1 activity. In male mice this resulted in accelerated amyloid deposition and a trend toward hyperglycemia. In female hIAPP$^{Tg/0}$ mice, beta-cell *Pcsk1* loss was sufficient to initiate amyloid deposition with no differences in fasting glycemia. It is unlikely that altered proIAPP processing is responsible for the increased islet amyloid, but rather alterations in beta-cell prohormone biosynthesis and the secretory granule environment that drive increased amyloid deposition.

Chapter 7: Conclusions

This thesis builds on a large body of literature in beta-cell prohormone processing and IAPP biology. The beta-cell-specific deletion of *Pcsk1* and *Pcsk2* supports earlier observations on proinsulin and proIAPP processing from the islets of whole-body *Pcsk1*- and *Pcsk2*-knockout mice[295,299,305,321]. Namely, that *Pcsk1* is the predominant prohormone convertase involved in proinsulin processing, while *Pcsk2* is the predominant prohormone convertase involved in proIAPP processing. The lack of mature insulin in mice with deletion of both *Pcsk1* and *Pcsk2* also shows that no other endoproteases act on proinsulin in mice. Previous models of whole-body *Pcsk1* and *Pcsk2* deletion generated complex endocrine phenotypes that were challenging to interpret due to expression of *Pcsk1* and *Pcsk2* in multiple endocrine tissues. With cre-lox recombination, the tools were available to investigate the impact of altered PCSK expression specifically in beta cells, and better model and investigate the loss of beta-cell processing activity in diabetes.

It was surprising to us that loss of *Pcsk2* in beta cells did not result in impaired glucose tolerance or fasting hyperglycemia. It was previously believed that *Pcsk2*, at least in mice, played an important role in beta-cell function with respect to glycemic control. Although *Pcsk2* is still required for proIAPP processing, and therefore normal beta-cell function, the data in this thesis suggest it may not play a role in diabetes pathogenesis. This is in agreement with recent evidence highlighting *PCSK1* as the primary prohormone endoprotease in human beta cells, and *PCSK1* deficiencies in dysfunctional human islets. In contrast to loss of *Pcsk2*, loss of *Pcsk1* in beta cells increased the risk of developing diabetes and hyperglycemia. Deletion of both *Pcsk1* and *Pcsk2* in beta cells did result in hyperglycemia, but to a variable extent. Given the entire lack

of endoprotease activity in insulin secretory granules in these mice, we were somewhat surprised these mice were viable, and further surprised that some animals were even euglycemic.

The initial results in young Pcsk1^{betaKO} mice were surprising as well. Early in life Pcsk1^{betaKO} mice had normal glucose tolerance and fasting glycemia despite the large impairment in proinsulin processing. With ageing or HFD, male Pcsk1^{betaKO} mice do become hyperglycemic, but the female mice remain normoglycemic. Further, complete deletion of *PCSK1* is not observed in islets of people with T1D or T2D. Rather, there is a modest reduction in PCSK1 levels and processing efficiency, likely more aligned with the Pcsk1^{betaHET} mice. Given the lack of glycemic phenotype in Pcsk1^{betaHET} mice, it could be concluded that the moderate reductions in PCSK1 in human islets may not be a significant driving factor of dysglycemia in diabetes. However, progression to diabetes is typically a slow process in humans in which there is repetitive or chronic islet stress. The development of hyperglycemia in male Pcsk1^{betaKO} mice with ageing or HFD suggests that beta-cell Pcsk1 deficiency increases the risk of diabetes. Therefore, PCSK1 loss is likely insufficient to causally drive diabetes, but is one of many insults that may contribute to beta-cell dysfunction and diabetes in an additive context. Further studies using a DPC^{betaHET} mouse with an inducible beta-cell-specific cre-recombinase may yield a more pathologically relevant model with acute, partial reductions in PCSK1 and PCSK2 levels, and will further our understanding beta-cell processing deficiencies in diabetes pathogenesis.

Probing beta-cell function and islet alterations in PC-deficient mice yielded further pathological changes beyond glycemia, similar to islets in diabetes. The increased amyloid deposition in Pcsk1^{betaKO} hIAPP$^{Tg/0}$ mice highlights the detrimental role beta-cell *Pcsk1* loss may have in human islets in which IAPP is amyloidogenic. The reduced maturity and proliferative capacity of DPC^{betaKO} islets may also have implications for beta-cell regenerative therapy, as

correcting processing deficiencies may lead to more effective beta-cell regeneration and function. The increased release of (pro)insulin at lower glucose concentrations in DPC^{betaKO} islets also suggests a pathogenic (immature) beta-cell. If processing errors can drive increased insulin exocytosis at lower glucose levels, they may be a mechanism through which early hyperinsulinemia occurs prior to the onset of insulin resistance. Altogether, the data in PC-deficient mice suggest that processing errors in beta cells contribute more to beta-cell dysfunction than just altered processing. This is a new observation for *Pcsk1* in beta-cell function, and the mechanisms through which *Pcsk1* loss alter beta-cell function remain undefined.

Pcsk1^{betaKO} and DPC^{betaKO} mice are a new model in the field of diabetes and islet biology for modelling the early stages of lean T2D. These PC-deficient models likely have beta cells under significant biosynthesis and secretory stress due to the reduced potency of proinsulin signaling, yet they are not obese and have only mild hyperglycemia (especially Pcsk1^{betaKO} mice). Most models of beta-cell secretory stress are accompanied by obesity, such as the agouti viable yellow mice or *Lepr$^{db/db}$* mouse models, or have mutant proinsulin that results in proinsulin misfolding, hypoinsulinemia, and hyperglycemia[451]. Models of reduced peripheral insulin signaling, such as the liver-specific insulin receptor knockout mice, have drastic hyperinsulinemia but also hyperglycemia[452]. Given the reduced but still present potency of (pro)insulin released from Pcsk1^{betaKO} and DPC^{betaKO} beta cells, these are likely unique models to further explore early beta-cell secretory stress in a lean and normoglycemic environment.

Given the large secretory demand placed on PC-deficient beta cells, we were also surprised at the lack of unfolded protein response in DPC^{betaKO} islets. This highlights the remarkable adaptability and capacity of beta cells to synthesize and secrete (pro)insulin. As

PCSK1 and PCSK2 become active in the late Golgi[27], loss of these PCs is unlikely to directly cause ER stress, and the data in this thesis support no indirect ER stress from reduced PC activity. This thesis provides evidence that PC-mediated processing errors do not activate canonical UPR mechanisms in murine beta cells.

Future directions in beta-cell processing errors should focus on human islets. More pathologically relevant reductions in *PCSK1* expression will be informative in determining the role these errors have in beta-cell dysfunction and diabetes pathogenesis. The unaltered *in vivo* beta-cell proliferation and increased beta-cell mass in the PC-deficient mice is also striking. Given that we observed this phenotype at an early pre-pubescent age, there may be developmental implications for PCSK1 loss during embryogenesis or early childhood. We also did not thoroughly characterize cell death in these models, but suspect it is not increased as the beta-cell mass increase is maintained throughout life and no defined apoptotic signatures were observed by RNAseq or proteomics. The proteomics dataset may also provide a reference for beta-cell granule biogenesis and trafficking. These processes remain less understood in beta cells due to the challenging nature of trafficking experiments. It may contain insight into novel mechanisms through which beta cells adapt to increased proinsulin biosynthesis, mechanisms which may be therapeutically relevant to improve beta-cell secretory stress in diabetes. Lastly, the sex differences in PC-deficient mice are also remarkable and suggest that female beta cells are more resilient to PC-mediated processing errors. This implies that when interpreting processing errors as biomarkers of beta-cell function, such as proinsulin:insulin or proIAPP:IAPP ratios, we must consider that these ratios may represent different levels of beta-cell dysfunction depending on the sex.

Once diabetes develops, prohormone processing errors and reduced beta-cell mass and function lead to reduced secretion of mature beta-cell hormones. Reductions in insulin are the most characterized, due to its critical role in metabolism and survival. IAPP is another beta-cell hormone that is lost alongside insulin in diabetes, and the impacts of IAPP loss remain incompletely understood. In this thesis we generated a C57BL/6J congenic *Iapp*-null mouse strain, rather than the hybrid strains used early in the characterization of *Iapp*-null mice, and also studied *Iapp*-null mice in the context of HFD-induced obesity. We found that loss of IAPP resulted in no significant change in fasting glycemia, glucose tolerance, body weight, or adiposity, including in the setting of HFD-induced obesity. IAPP loss did slightly improve insulin sensitivity in HFD-fed male mice, raising the possibility that IAPP loss may be beneficial in diabetes. This is in opposition, however, to the clear benefit IAPP-replacement therapy has in individuals with T1D and T2D[119,120]. We have also shown that IAPP loss does not alter insulin secretion kinetics or quantity in isolated islets, and that circulating insulin and glucagon levels are comparable in $Iapp^{-/-}$ and $Iapp^{+/+}$ mice. This is in disagreement with previous publications reporting insulinostatic actions of supraphysiological concentrations of IAPP, or IAPP receptor inhibitors, and suggests that IAPP does not exert a paracrine effect on insulin secretion ex vivo.

One of the many increased risks associated with diabetes is the development of cancer. Given the previous reports of IAPP and its potent anti-tumour activity, we investigated the actions of IAPP in cancer as an additional complication arising from beta-cell hormone loss in diabetes. Our results in PANC-1 cells consistently showed no effect of non-aggregating human IAPP mimetics on cell proliferation, death, or glycolysis. We were also unable to reproduce the findings of others in H1299 cells[127], where we also observed no effect of IAPP. In a genetic mouse model of pancreatic ductal adenocarcinoma, IAPP loss also had no effect on survival.

Collectively, our data do not support a role for IAPP in the association of diabetes and cancer. However, there may be indirect effects in humans. Given that exogenous pramlintide improves postprandial hyperglycemia and reduces body weight, IAPP replacement may result in better cancer outcomes due to improved glycemic control and adiposity. Longitudinal monitoring for cancer development in patients using pramlintide may provide better insight into whether IAPP replacement therapy reduces the risk of cancer development in diabetes.

This thesis highlights the roles of PCSK1- and PCSK2-mediated processing errors in driving beta-cell dysfunction and diabetes. Although they contribute less than we had initially expected, the results in mice indicate reduced beta-cell function and increased diabetes risk upon the loss of PCSK1 in beta cells. The loss of mature IAPP signalling due to beta-cell processing errors and reduced beta-cell mass and function are unlikely to contribute to the pathogenesis of diabetes or diabetes-associated cancer. However, increased IAPP aggregation due to beta-cell PCSK1 loss may result in increased amyloid-induced beta-cell dysfunction prior to the development of hyperglycemia. Collectively, the data in this thesis suggest there may be therapeutic benefits to preventing the loss of, or restoring, beta-cell prohormone processing activity in diabetes.

References

1. Donovan, M. J., Paulino, G. & Raybould, H. E. CCK(1) receptor is essential for normal meal patterning in mice fed high fat diet. *Physiol. Behav.* **92,** 969–974 (2007).
2. Rahier, J., Guiot, Y., Goebbels, R. M., Sempoux, C. & Henquin, J. C. Pancreatic β-cell mass in European subjects with type 2 diabetes. *Diabetes Obes. Metab.* **10,** 32–42 (2008).
3. Langerhans, Paul. Beiträge zur mikroskopischen Anatomie der Bauchspeicheldrüse: Inaugural-Dissertaton. (1869). at <https://insulin.library.utoronto.ca/islandora/object/insulin%3AT10076>
4. Ionescu-Tirgoviste, C., Gagniuc, P. A., Gubceac, E., Mardare, L., Popescu, I., Dima, S. & Militaru, M. A 3D map of the islet routes throughout the healthy human pancreas. *Sci. Rep.* **5,** 14634 (2015).
5. Tang, S.-C., Baeyens, L., Shen, C.-N., Peng, S.-J., Chien, H.-J., Scheel, D. W., Chamberlain, C. E. & German, M. S. Human pancreatic neuro-insular network in health and fatty infiltration. *Diabetologia* **61,** 168–181 (2018).
6. Brissova, M., Fowler, M. J., Nicholson, W. E., Chu, A., Hirshberg, B., Harlan, D. M. & Powers, A. C. Assessment of Human Pancreatic Islet Architecture and Composition by Laser Scanning Confocal Microscopy. *J. Histochem. Cytochem.* **53,** 1087–1097 (2005).
7. Cabrera, O., Berman, D. M., Kenyon, N. S., Ricordi, C., Berggren, P.-O. & Caicedo, A. The unique cytoarchitecture of human pancreatic islets has implications for islet cell function. *Proc. Natl. Acad. Sci.* **103,** 2334–2339 (2006).
8. Kim, A., Miller, K., Jo, J., Kilimnik, G., Wojcik, P. & Hara, M. Islet architecture. *Islets* **1,** 129–136 (2009).

9. van der Meulen, T., Donaldson, C. J., Cáceres, E., Hunter, A. E., Cowing–Zitron, C., Pound, L. D., Adams, M. W., Zembrzycki, A., Grove, K. L. & Huising, M. O. Urocortin3 mediates somatostatin-dependent negative feedback control of insulin secretion. *Nat. Med.* **21,** 769–776 (2015).
10. Adrian, T. E., Bloom, S. R., Bryant, M. G., Polak, J. M., Heitz, P. H. & Barnes, A. J. Distribution and release of human pancreatic polypeptide. *Gut* **17,** 940–944 (1976).
11. Lin, S., Shi, Y.-C., Yulyaningsih, E., Aljanova, A., Zhang, L., Macia, L., Nguyen, A. D., Lin, E.-J. D., During, M. J., Herzog, H. & Sainsbury, A. Critical role of arcuate Y4 receptors and the melanocortin system in pancreatic polypeptide-induced reduction in food intake in mice. *PloS One* **4,** e8488 (2009).
12. Batterham, R. L., Le Roux, C. W., Cohen, M. A., Park, A. J., Ellis, S. M., Patterson, M., Frost, G. S., Ghatei, M. A. & Bloom, S. R. Pancreatic polypeptide reduces appetite and food intake in humans. *J. Clin. Endocrinol. Metab.* **88,** 3989–3992 (2003).
13. Andralojc, K. M., Mercalli, A., Nowak, K. W., Albarello, L., Calcagno, R., Luzi, L., Bonifacio, E., Doglioni, C. & Piemonti, L. Ghrelin-producing epsilon cells in the developing and adult human pancreas. *Diabetologia* **52,** 486–493 (2009).
14. Yanagi, S., Sato, T., Kangawa, K. & Nakazato, M. The Homeostatic Force of Ghrelin. *Cell Metab.* **27,** 786–804 (2018).
15. Denroche, H. C., Miard, S., Sallé-Lefort, S., Picard, F. & Verchere, C. B. T cells accumulate in non-diabetic islets during ageing. *Immun. Ageing* **18,** 8 (2021).
16. Noguchi, G. M. & Huising, M. O. Integrating the inputs that shape pancreatic islet hormone release. *Nat. Metab.* **1,** 1189–1201 (2019).

17. Hart, N. J. & Powers, A. C. Use of human islets to understand islet biology and diabetes: progress, challenges and suggestions. *Diabetologia* **62,** 212–222 (2019).

18. Steiner, D. F., Park, S.-Y., Støy, J., Philipson, L. H. & Bell, G. I. A brief perspective on insulin production. *Diabetes Obes. Metab.* **11,** 189–196 (2009).

19. Moss, N. D. & Sussel, L. mRNA Processing: An Emerging Frontier in the Regulation of Pancreatic β Cell Function. *Front. Genet.* **11,** 983 (2020).

20. Alarcon, C., Verchere, C. B. & Rhodes, C. J. Translational Control of Glucose-Induced Islet Amyloid Polypeptide Production in Pancreatic Islets. *Endocrinology* **153,** 2082–2087 (2012).

21. Itoh, N. & Okamoto, H. Translational control of proinsulin synthesis by glucose. *Nature* **283,** 100–102 (1980).

22. Evans-Molina, C., Garmey, J. C., Ketchum, R., Brayman, K. L., Deng, S. & Mirmira, R. G. Glucose Regulation of Insulin Gene Transcription and Pre-mRNA Processing in Human Islets. *Diabetes* **56,** 827–835 (2007).

23. Hunter, S. J., Boyd, A. C., O'Harte, F. P. M., McKillop, A. M., Wiggam, M. I., Mooney, M. H., McCluskey, J. T., Lindsay, J. R., Ennis, C. N., Gamble, R., Sheridan, B., Barnett, C. R., McNulty, H., Bell, P. M. & Flatt, P. R. Demonstration of Glycated Insulin in Human Diabetic Plasma and Decreased Biological Activity Assessed by Euglycemic-Hyperinsulinemic Clamp Technique in Humans. *Diabetes* **52,** 492–498 (2003).

24. Yu, Q., Canales, A., Glover, M. S., Das, R., Shi, X., Liu, Y., Keller, M. P., Attie, A. D. & Li, L. Targeted Mass Spectrometry Approach Enabled Discovery of O-Glycosylated Insulin and Related Signaling Peptides in Mouse and Human Pancreatic Islets. *Anal. Chem.* **89,** 9184–9191 (2017).

25. Abdel-Wahab, Y. H., O'Harte, F. P., Ratcliff, H., McClenaghan, N. H., Barnett, C. R. & Flatt, P. R. Glycation of insulin in the islets of Langerhans of normal and diabetic animals. *Diabetes* **45,** 1489–1496 (1996).

26. Mäkimattila, S., Fineman, M. S. & Yki-Järvinen, H. Deficiency of total and nonglycosylated amylin in plasma characterizes subjects with impaired glucose tolerance and type 2 diabetes. *J. Clin. Endocrinol. Metab.* **85,** 2822–2827 (2000).

27. Hoshino, A. & Lindberg, I. Peptide Biosynthesis: Prohormone Convertases 1/3 and 2. *Colloq. Ser. Neuropept.* **1,** 1–112 (2012).

28. Smith, G. D., Pangborn, W. A. & Blessing, R. H. The structure of T6 human insulin at 1.0 Å resolution. *Acta Crystallogr. D Biol. Crystallogr.* **59,** 474–482 (2003).

29. Cunningham, C. N., Williams, J. M., Knupp, J., Arunagiri, A., Arvan, P. & Tsai, B. Cells Deploy a Two-Pronged Strategy to Rectify Misfolded Proinsulin Aggregates. *Mol. Cell* **75,** 442-456.e4 (2019).

30. Pearson, G. L., Gingerich, M. A., Walker, E. M., Biden, T. J. & Soleimanpour, S. A. A Selective Look at Autophagy in Pancreatic β-Cells. *Diabetes* **70,** 1229–1241 (2021).

31. Marsh, B. J., Soden, C., Alarcón, C., Wicksteed, B. L., Yaekura, K., Costin, A. J., Morgan, G. P. & Rhodes, C. J. Regulated autophagy controls hormone content in secretory-deficient pancreatic endocrine beta-cells. *Mol. Endocrinol.* **21,** 2255–2269 (2007).

32. Goginashvili, A., Zhang, Z., Erbs, E., Spiegelhalter, C., Kessler, P., Mihlan, M., Pasquier, A., Krupina, K., Schieber, N., Cinque, L., Morvan, J., Sumara, I., Schwab, Y., Settembre, C. & Ricci, R. Insulin secretory granules control autophagy in pancreatic β cells. *Science* **347,** 878–882 (2015).

33. Rorsman, P. & Ashcroft, F. M. Pancreatic β-Cell Electrical Activity and Insulin Secretion: Of Mice and Men. *Physiol. Rev.* **98,** 117–214 (2018).

34. Coppieters, K. T., Wiberg, A., Amirian, N., Kay, T. W. & von Herrath, M. G. Persistent glucose transporter expression on pancreatic beta cells from longstanding type 1 diabetic individuals. *Diabetes Metab. Res. Rev.* **27,** 746–754 (2011).

35. Huang, C., Walker, E. M., Dadi, P. K., Hu, R., Xu, Y., Zhang, W., Sanavia, T., Mun, J., Liu, J., Nair, G. G., Tan, H. Y. A., Wang, S., Magnuson, M. A., Stoeckert, C. J., Hebrok, M., Gannon, M., Han, W., Stein, R., Jacobson, D. A. & Gu, G. Synaptotagmin 4 Regulates Pancreatic β Cell Maturation by Modulating the Ca2+ Sensitivity of Insulin Secretion Vesicles. *Dev. Cell* **45,** 347-361.e5 (2018).

36. Matschinsky, F. M. & Wilson, D. F. The Central Role of Glucokinase in Glucose Homeostasis: A Perspective 50 Years After Demonstrating the Presence of the Enzyme in Islets of Langerhans. *Front. Physiol.* **10,** 148 (2019).

37. Pørksen, N., Grøfte, T., Greisen, J., Mengel, A., Juhl, C., Veldhuis, J. D., Schmitz, O., Rössle, M. & Vilstrup, H. Human insulin release processes measured by intraportal sampling. *Am. J. Physiol.-Endocrinol. Metab.* **282,** E695–E702 (2002).

38. Farfari, S., Schulz, V., Corkey, B. & Prentki, M. Glucose-regulated anaplerosis and cataplerosis in pancreatic beta-cells: possible implication of a pyruvate/citrate shuttle in insulin secretion. *Diabetes* **49,** 718–726 (2000).

39. Henquin, J.-C., Dufrane, D. & Nenquin, M. Nutrient Control of Insulin Secretion in Isolated Normal Human Islets. *Diabetes* **55,** 3470–3477 (2006).

40. Benner, C., van der Meulen, T., Cacéres, E., Tigyi, K., Donaldson, C. J. & Huising, M. O. The transcriptional landscape of mouse beta cells compared to human beta cells reveals

notable species differences in long non-coding RNA and protein-coding gene expression. *BMC Genomics* **15,** 620 (2014).

41. Shiao, M.-S., Liao, B.-Y., Long, M. & Yu, H.-T. Adaptive Evolution of the Insulin Two-Gene System in Mouse. *Genetics* **178,** 1683–1691 (2008).
42. McCulloch, L. J., van de Bunt, M., Braun, M., Frayn, K. N., Clark, A. & Gloyn, A. L. GLUT2 (SLC2A2) is not the principal glucose transporter in human pancreatic beta cells: implications for understanding genetic association signals at this locus. *Mol. Genet. Metab.* **104,** 648–653 (2011).
43. Capozzi, M. E., Svendsen, B., Encisco, S. E., Lewandowski, S. L., Martin, M. D., Lin, H., Jaffe, J. L., Coch, R. W., Haldeman, J. M., MacDonald, P. E., Merrins, M. J., D'Alessio, D. A. & Campbell, J. E. β Cell tone is defined by proglucagon peptides through cAMP signaling. *JCI Insight* **4,** 126742 (2019).
44. Dezaki, K., Sone, H., Koizumi, M., Nakata, M., Kakei, M., Nagai, H., Hosoda, H., Kangawa, K. & Yada, T. Blockade of Pancreatic Islet–Derived Ghrelin Enhances Insulin Secretion to Prevent High-Fat Diet–Induced Glucose Intolerance. *Diabetes* **55,** 3486–3493 (2006).
45. Briant, L. J. B., Reinbothe, T. M., Spiliotis, I., Miranda, C., Rodriguez, B. & Rorsman, P. δ-cells and β-cells are electrically coupled and regulate α-cell activity via somatostatin. *J. Physiol.* **596,** 197–215 (2018).
46. Johnston, N. R., Mitchell, R. K., Haythorne, E., Pessoa, M. P., Semplici, F., Ferrer, J., Piemonti, L., Marchetti, P., Bugliani, M., Bosco, D., Berishvili, E., Duncanson, P., Watkinson, M., Broichhagen, J., Trauner, D., Rutter, G. A. & Hodson, D. J. Beta Cell Hubs Dictate Pancreatic Islet Responses to Glucose. *Cell Metab.* **24,** 389–401 (2016).

47. Segerstolpe, Å., Palasantza, A., Eliasson, P., Andersson, E.-M., Andréasson, A.-C., Sun, X., Picelli, S., Sabirsh, A., Clausen, M., Bjursell, M. K., Smith, D. M., Kasper, M., Ämmälä, C. & Sandberg, R. Single-Cell Transcriptome Profiling of Human Pancreatic Islets in Health and Type 2 Diabetes. *Cell Metab.* **24,** 593–607 (2016).

48. Nauck, M. A., Bartels, E., Orskov, C., Ebert, R. & Creutzfeldt, W. Additive insulinotropic effects of exogenous synthetic human gastric inhibitory polypeptide and glucagon-like peptide-1-(7-36) amide infused at near-physiological insulinotropic hormone and glucose concentrations. *J. Clin. Endocrinol. Metab.* **76,** 912–917 (1993).

49. Ahrén, B. & Holst, J. J. The cephalic insulin response to meal ingestion in humans is dependent on both cholinergic and noncholinergic mechanisms and is important for postprandial glycemia. *Diabetes* **50,** 1030–1038 (2001).

50. Havel, P. J., Mundinger, T. O., Veith, R. C., Dunning, B. E. & Taborsky, G. J. Corelease of galanin and NE from pancreatic sympathetic nerves during severe hypoglycemia in dogs. *Am. J. Physiol.* **263,** E8-16 (1992).

51. Latour, M. G., Alquier, T., Oseid, E., Tremblay, C., Jetton, T. L., Luo, J., Lin, D. C.-H. & Poitout, V. GPR40 is necessary but not sufficient for fatty acid stimulation of insulin secretion in vivo. *Diabetes* **56,** 1087–1094 (2007).

52. Campbell, J. E. & Newgard, C. B. Mechanisms controlling pancreatic islet cell function in insulin secretion. *Nat. Rev. Mol. Cell Biol.* **22,** 142–158 (2021).

53. Trexler, A. J. & Taraska, J. W. Regulation of insulin exocytosis by calcium-dependent protein kinase C in beta cells. *Cell Calcium* **67,** 1–10 (2017).

54. Takeda, S., Kadowaki, S., Haga, T., Takaesu, H. & Mitaku, S. Identification of G protein-coupled receptor genes from the human genome sequence. *FEBS Lett.* **520,** 97–101 (2002).

55. LeBlanc, A. G., Gao, Y. J., McRae, L. & Pelletier, C. At-a-glance - Twenty years of diabetes surveillance using the Canadian Chronic Disease Surveillance System. *Health Promot. Chronic Dis. Prev. Can. Res. Policy Pract.* **39,** 306–309 (2019).

56. International Diabetes Federation Diabetes Atlas 10th edition. (2021).

57. Saeedi, P., Petersohn, I., Salpea, P., Malanda, B., Karuranga, S., Unwin, N., Colagiuri, S., Guariguata, L., Motala, A. A., Ogurtsova, K., Shaw, J. E., Bright, D. & Williams, R. Global and regional diabetes prevalence estimates for 2019 and projections for 2030 and 2045: Results from the International Diabetes Federation Diabetes Atlas, 9th edition. *Diabetes Res. Clin. Pract.* **157,** (2019).

58. Williams, R., Karuranga, S., Malanda, B., Saeedi, P., Basit, A., Besançon, S., Bommer, C., Esteghamati, A., Ogurtsova, K., Zhang, P. & Colagiuri, S. Global and regional estimates and projections of diabetes-related health expenditure: Results from the International Diabetes Federation Diabetes Atlas, 9th edition. *Diabetes Res. Clin. Pract.* **162,** (2020).

59. Butler, A. E., Janson, J., Bonner-Weir, S., Ritzel, R., Rizza, R. A. & Butler, P. C. β-Cell Deficit and Increased β-Cell Apoptosis in Humans With Type 2 Diabetes. *Diabetes* **52,** 102–110 (2003).

60. Mahajan, A., Taliun, D., Thurner, M., Robertson, N. R., Torres, J. M., Rayner, N. W., Payne, A. J., Steinthorsdottir, V., Scott, R. A., Grarup, N., Cook, J. P., Schmidt, E. M., Wuttke, M., Sarnowski, C., Mägi, R., Nano, J., Gieger, C., Trompet, S., Lecoeur, C., Preuss, M. H., Prins, B. P., Guo, X., Bielak, L. F., Below, J. E., Bowden, D. W., Chambers, J. C., Kim, Y. J., Ng, M. C. Y., Petty, L. E., Sim, X., Zhang, W., Bennett, A. J., Bork-Jensen, J., Brummett, C. M., Canouil, M., Ec Kardt, K.-U., Fischer, K., Kardia, S. L. R., Kronenberg, F., Läll, K., Liu, C.-T., Locke, A. E., Luan, J., Ntalla, I., Nylander, V.,

Schönherr, S., Schurmann, C., Yengo, L., Bottinger, E. P., Brandslund, I., Christensen, C., Dedoussis, G., Florez, J. C., Ford, I., Franco, O. H., Frayling, T. M., Giedraitis, V., Hackinger, S., Hattersley, A. T., Herder, C., Ikram, M. A., Ingelsson, M., Jørgensen, M. E., Jørgensen, T., Kriebel, J., Kuusisto, J., Ligthart, S., Lindgren, C. M., Linneberg, A., Lyssenko, V., Mamakou, V., Meitinger, T., Mohlke, K. L., Morris, A. D., Nadkarni, G., Pankow, J. S., Peters, A., Sattar, N., Stančáková, A., Strauch, K., Taylor, K. D., Thorand, B., Thorleifsson, G., Thorsteinsdottir, U., Tuomilehto, J., Witte, D. R., Dupuis, J., Peyser, P. A., Zeggini, E., Loos, R. J. F., Froguel, P., Ingelsson, E., Lind, L., Groop, L., Laakso, M., Collins, F. S., Jukema, J. W., Palmer, C. N. A., Grallert, H., Metspalu, A., Dehghan, A., Köttgen, A., Abecasis, G. R., Meigs, J. B., Rotter, J. I., Marchini, J., Pedersen, O., Hansen, T., Langenberg, C., Wareham, N. J., Stefansson, K., Gloyn, A. L., Morris, A. P., Boehnke, M. & McCarthy, M. I. Fine-mapping type 2 diabetes loci to single-variant resolution using high-density imputation and islet-specific epigenome maps. *Nat. Genet.* **50,** 1505–1513 (2018).

61. Kahn, S. E., Chen, Y.-C., Esser, N., Taylor, A. J., van Raalte, D. H., Zraika, S. & Verchere, C. B. The β Cell in Diabetes: Integrating Biomarkers With Functional Measures. *Endocr. Rev.* **42,** 528–583 (2021).

62. Kahn, S. E., Hull, R. L. & Utzschneider, K. M. Mechanisms linking obesity to insulin resistance and type 2 diabetes. *Nature* **444,** 840–846 (2006).

63. Patterson, R., McNamara, E., Tainio, M., de Sá, T. H., Smith, A. D., Sharp, S. J., Edwards, P., Woodcock, J., Brage, S. & Wijndaele, K. Sedentary behaviour and risk of all-cause, cardiovascular and cancer mortality, and incident type 2 diabetes: a systematic review and dose response meta-analysis. *Eur. J. Epidemiol.* **33,** 811–829 (2018).

64. Punthakee, Z., Goldenberg, R. & Katz, P. Definition, Classification and Diagnosis of Diabetes, Prediabetes and Metabolic Syndrome. *Can. J. Diabetes* **42,** S10–S15 (2018).

65. Panagiotopoulos, C., Hadjiyannakis, S. & Henderson, M. Type 2 Diabetes in Children and Adolescents. *Can. J. Diabetes* **42,** S247–S254 (2018).

66. Pugliese, A. Autoreactive T cells in type 1 diabetes. *J. Clin. Invest.* **127,** 2881–2891 (2017).

67. Sims, E. K., Bahnson, H. T., Nyalwidhe, J., Haataja, L., Davis, A. K., Speake, C., DiMeglio, L. A., Blum, J., Morris, M. A., Mirmira, R. G., Nadler, J., Mastracci, T. L., Marcovina, S., Qian, W.-J., Yi, L., Swensen, A. C., Yip-Schneider, M., Schmidt, C. M., Considine, R. V., Arvan, P., Greenbaum, C. J. & Evans-Molina, C. Proinsulin Secretion Is a Persistent Feature of Type 1 Diabetes. *Diabetes Care* **42,** 258–264 (2019).

68. Campbell-Thompson, M., Fu, A., Kaddis, J. S., Wasserfall, C., Schatz, D. A., Pugliese, A. & Atkinson, M. A. Insulitis and β-Cell Mass in the Natural History of Type 1 Diabetes. *Diabetes* **65,** 719–731 (2016).

69. von Herrath, M., Sanda, S. & Herold, K. Type 1 diabetes as a relapsing–remitting disease? *Nat. Rev. Immunol.* **7,** 988–994 (2007).

70. Ziegler, A. G., Rewers, M., Simell, O., Simell, T., Lempainen, J., Steck, A., Winkler, C., Ilonen, J., Veijola, R., Knip, M., Bonifacio, E. & Eisenbarth, G. S. Seroconversion to Multiple Islet Autoantibodies and Risk of Progression to Diabetes in Children. *JAMA* **309,** 2473–2479 (2013).

71. Barrett, J. C., Clayton, D., Concannon, P., Akolkar, B., Cooper, J. D., Erlich, H. A., Julier, C., Morahan, G., Nerup, J., Nierras, C., Plagnol, V., Pociot, F., Schuilenburg, H., Smyth, D. J., Stevens, H., Todd, J. A., Walker, N. M. & Rich, S. S. Genome-wide association study

and meta-analysis finds over 40 loci affect risk of type 1 diabetes. *Nat. Genet.* **41,** 703–707 (2009).

72. Erlich, H., Valdes, A. M., Noble, J., Carlson, J. A., Varney, M., Concannon, P., Mychaleckyj, J. C., Todd, J. A., Bonella, P., Fear, A. L., Lavant, E., Louey, A. & Moonsamy, P. HLA DR-DQ Haplotypes and Genotypes and Type 1 Diabetes Risk: Analysis of the Type 1 Diabetes Genetics Consortium Families. *Diabetes* **57,** 1084–1092 (2008).
73. Redondo, M. J., Jeffrey, J., Fain, P. R., Eisenbarth, G. S. & Orban, T. Concordance for Islet Autoimmunity among Monozygotic Twins. *N. Engl. J. Med.* **359,** 2849–2850 (2008).
74. Knip, M. & Simell, O. Environmental Triggers of Type 1 Diabetes. *Cold Spring Harb. Perspect. Med.* **2,** a007690 (2012).
75. Riddle, M. C., Philipson, L. H., Rich, S. S., Carlsson, A., Franks, P. W., Greeley, S. A. W., Nolan, J. J., Pearson, E. R., Zeitler, P. S. & Hattersley, A. T. Monogenic Diabetes: From Genetic Insights to Population-Based Precision in Care. Reflections From a Diabetes Care Editors' Expert Forum. *Diabetes Care* **43,** 3117–3128 (2020).
76. Feig, D. S., Hwee, J., Shah, B. R., Booth, G. L., Bierman, A. S. & Lipscombe, L. L. Trends in Incidence of Diabetes in Pregnancy and Serious Perinatal Outcomes: A Large, Population-Based Study in Ontario, Canada, 1996–2010. *Diabetes Care* **37,** 1590–1596 (2014).
77. Feig, D. S., Berger, H., Donovan, L., Godbout, A., Kader, T., Keely, E. & Sanghera, R. Diabetes and Pregnancy. *Can. J. Diabetes* **42,** S255–S282 (2018).
78. Feig, D. S., Zinman, B., Wang, X. & Hux, J. E. Risk of development of diabetes mellitus after diagnosis of gestational diabetes. *Can. Med. Assoc. J.* **179,** 229–234 (2008).

79. Buzzetti, R., Tuomi, T., Mauricio, D., Pietropaolo, M., Zhou, Z., Pozzilli, P. & Leslie, R. D. Management of Latent Autoimmune Diabetes in Adults: A Consensus Statement From an International Expert Panel. *Diabetes* **69,** 2037–2047 (2020).

80. Sosenko, J. M., Skyler, J. S., Beam, C. A., Krischer, J. P., Greenbaum, C. J., Mahon, J., Rafkin, L. E., Matheson, D., Herold, K. C. & Palmer, J. P. Acceleration of the Loss of the First-Phase Insulin Response During the Progression to Type 1 Diabetes in Diabetes Prevention Trial–Type 1 Participants. *Diabetes* **62,** 4179–4183 (2013).

81. Davies, M. J., Rayman, G., Grenfell, A., Gray, I. P., Day, J. L. & Hales, C. N. Loss of the first phase insulin response to intravenous glucose in subjects with persistent impaired glucose tolerance. *Diabetic Med.* **11,** 432–436 (1994).

82. Brown, R. J., Sinaii, N. & Rother, K. I. Too Much Glucagon, Too Little Insulin. *Diabetes Care* **31,** 1403–1404 (2008).

83. Butler, P. C. & Rizza, R. A. Contribution to Postprandial Hyperglycemia and Effect on Initial Splanchnic Glucose Clearance of Hepatic Glucose Cycling in Glucose-Intolerant or NIDDM Patients. *Diabetes* **40,** 73–81 (1991).

84. Uno, S., Imagawa, A., Okita, K., Sayama, K., Moriwaki, M., Iwahashi, H., Yamagata, K., Tamura, S., Matsuzawa, Y., Hanafusa, T., Miyagawa, J. & Shimomura, I. Macrophages and dendritic cells infiltrating islets with or without beta cells produce tumour necrosis factor-alpha in patients with recent-onset type 1 diabetes. *Diabetologia* **50,** 596–601 (2007).

85. Ehses, J. A., Perren, A., Eppler, E., Ribaux, P., Pospisilik, J. A., Maor-Cahn, R., Gueripel, X., Ellingsgaard, H., Schneider, M. K. J., Biollaz, G., Fontana, A., Reinecke, M., Homo-Delarche, F. & Donath, M. Y. Increased Number of Islet-Associated Macrophages in Type 2 Diabetes. *Diabetes* **56,** 2356–2370 (2007).

86. Courtade, J. A., Klimek-Abercrombie, A. M., Chen, Y.-C., Patel, N., Lu, P. Y. T., Speake, C., Orban, P. C., Najafian, B., Meneilly, G., Greenbaum, C. J., Warnock, G. L., Panagiotopoulos, C. & Verchere, C. B. Measurement of Pro-Islet Amyloid Polypeptide (1–48) in Diabetes and Islet Transplants. *J. Clin. Endocrinol. Metab.* **102,** 2595–2603 (2017).

87. Zheng, X., Ren, W., Zhang, S., Liu, J., Li, S., Li, J., Yang, P., He, J., Su, S. & Li, P. Serum levels of proamylin and amylin in normal subjects and patients with impaired glucose regulation and type 2 diabetes mellitus. *Acta Diabetol.* **47,** 265–270 (2010).

88. Zhao, H.-L., Lai, F. M. M., Tong, P. C. Y., Zhong, D.-R., Yang, D., Tomlinson, B. & Chan, J. C. N. Prevalence and clinicopathological characteristics of islet amyloid in chinese patients with type 2 diabetes. *Diabetes* **52,** 2759–2766 (2003).

89. Clark, A., Wells, C. A., Buley, I. D., Cruickshank, J. K., Vanhegan, R. I., Matthews, D. R., Cooper, G. J., Holman, R. R. & Turner, R. C. Islet amyloid, increased A-cells, reduced B-cells and exocrine fibrosis: quantitative changes in the pancreas in type 2 diabetes. *Diabetes Res. Edinb. Scotl.* **9,** 151–159 (1988).

90. Westermark, P. Quantitative Studies of Amyloid in the Islets of Langerhans. *Ups. J. Med. Sci.* **77,** 91–94 (1972).

91. Westermark, G. T., Krogvold, L., Dahl-Jørgensen, K. & Ludvigsson, J. Islet amyloid in recent-onset type 1 diabetes—the DiViD study. *Ups. J. Med. Sci.* **122,** 201–203 (2017).

92. Beery, M. L., Jacobsen, L. M., Atkinson, M. A., Butler, A. E. & Campbell-Thompson, M. Islet amyloidosis in a child with type 1 diabetes. *Islets* **11,** 44–49 (2019).

93. Marhfour, I., Lopez, X. M., Lefkaditis, D., Salmon, I., Allagnat, F., Richardson, S. J., Morgan, N. G. & Eizirik, D. L. Expression of endoplasmic reticulum stress markers in the islets of patients with type 1 diabetes. *Diabetologia* **55,** 2417–2420 (2012).

94. Laybutt, D. R., Preston, A. M., Akerfeldt, M. C., Kench, J. G., Busch, A. K., Biankin, A. V. & Biden, T. J. Endoplasmic reticulum stress contributes to beta cell apoptosis in type 2 diabetes. *Diabetologia* **50,** 752–763 (2007).

95. Moin, A. S. M. & Butler, A. E. Alterations in Beta Cell Identity in Type 1 and Type 2 Diabetes. *Curr. Diab. Rep.* **19,** 83 (2019).

96. Potter, K. J., Abedini, A., Marek, P., Klimek, A. M., Butterworth, S., Driscoll, M., Baker, R., Nilsson, M. R., Warnock, G. L., Oberholzer, J., Bertera, S., Trucco, M., Korbutt, G. S., Fraser, P. E., Raleigh, D. P. & Verchere, C. B. Islet amyloid deposition limits the viability of human islet grafts but not porcine islet grafts. *Proc. Natl. Acad. Sci. U. S. A.* **107,** 4305–4310 (2010).

97. van Raalte, D. H. & Verchere, C. B. Improving glycaemic control in type 2 diabetes: Stimulate insulin secretion or provide beta-cell rest? *Diabetes Obes. Metab.* **19,** 1205–1213 (2017).

98. Inzucchi, S. E. Oral Antihyperglycemic Therapy for Type 2 DiabetesScientific Review. *JAMA* **287,** 360–372 (2002).

99. Drucker, D. J., Habener, J. F. & Holst, J. J. Discovery, characterization, and clinical development of the glucagon-like peptides. *J. Clin. Invest.* **127,** 4217–4227 (2017).

100. Hsia, D. S., Grove, O. & Cefalu, W. T. An Update on SGLT2 Inhibitors for the Treatment of Diabetes Mellitus. *Curr. Opin. Endocrinol. Diabetes Obes.* **24,** 73–79 (2017).

101. American Diabetes Association. 4. Lifestyle Management. *Diabetes Care* **40,** S33–S43 (2017).

102. Beck, R. W., Riddlesworth, T., Ruedy, K., Ahmann, A., Bergenstal, R., Haller, S., Kollman, C., Kruger, D., McGill, J. B., Polonsky, W., Toschi, E., Wolpert, H., Price, D., &

DIAMOND Study Group. Effect of Continuous Glucose Monitoring on Glycemic Control in Adults With Type 1 Diabetes Using Insulin Injections: The DIAMOND Randomized Clinical Trial. *JAMA* **317,** 371–378 (2017).

103. Shapiro, A. M. J., Lakey, J. R. T., Ryan, E. A., Korbutt, G. S., Toth, E., Warnock, G. L., Kneteman, N. M. & Rajotte, R. V. Islet Transplantation in Seven Patients with Type 1 Diabetes Mellitus Using a Glucocorticoid-Free Immunosuppressive Regimen. *N. Engl. J. Med.* **343,** 230–238 (2000).

104. Barton, F. B., Rickels, M. R., Alejandro, R., Hering, B. J., Wease, S., Naziruddin, B., Oberholzer, J., Odorico, J. S., Garfinkel, M. R., Levy, M., Pattou, F., Berney, T., Secchi, A., Messinger, S., Senior, P. A., Maffi, P., Posselt, A., Stock, P. G., Kaufman, D. B., Luo, X., Kandeel, F., Cagliero, E., Turgeon, N. A., Witkowski, P., Naji, A., O'Connell, P. J., Greenbaum, C., Kudva, Y. C., Brayman, K. L., Aull, M. J., Larsen, C., Kay, T. W. H., Fernandez, L. A., Vantyghem, M.-C., Bellin, M. & Shapiro, A. M. J. Improvement in Outcomes of Clinical Islet Transplantation: 1999–2010. *Diabetes Care* **35,** 1436–1445 (2012).

105. Shapiro, A. M. J., Thompson, D., Donner, T. W., Bellin, M. D., Hsueh, W., Pettus, J., Wilensky, J., Daniels, M., Wang, R. M., Brandon, E. P., Jaiman, M. S., Kroon, E. J., D'Amour, K. A. & Foyt, H. L. Insulin expression and C-peptide in type 1 diabetes subjects implanted with stem cell-derived pancreatic endoderm cells in an encapsulation device. *Cell Rep. Med.* **2,** (2021).

106. Ramzy, A., Thompson, D. M., Ward-Hartstonge, K. A., Ivison, S., Cook, L., Garcia, R. V., Loyal, J., Kim, P. T. W., Warnock, G. L., Levings, M. K. & Kieffer, T. J. Implanted

pluripotent stem-cell-derived pancreatic endoderm cells secrete glucose-responsive C-peptide in patients with type 1 diabetes. *Cell Stem Cell* **28,** 2047-2061.e5 (2021).

107. Centers for Disease Control and Prevention (CDC). Prevalence of overweight and obesity among adults with diagnosed diabetes--United States, 1988-1994 and 1999-2002. *MMWR Morb. Mortal. Wkly. Rep.* **53,** 1066–1068 (2004).
108. Santomauro, A. T., Boden, G., Silva, M. E., Rocha, D. M., Santos, R. F., Ursich, M. J., Strassmann, P. G. & Wajchenberg, B. L. Overnight lowering of free fatty acids with Acipimox improves insulin resistance and glucose tolerance in obese diabetic and nondiabetic subjects. *Diabetes* **48,** 1836–1841 (1999).
109. Roden, M., Price, T. B., Perseghin, G., Petersen, K. F., Rothman, D. L., Cline, G. W. & Shulman, G. I. Mechanism of free fatty acid-induced insulin resistance in humans. *J. Clin. Invest.* **97,** 2859–2865 (1996).
110. El-Assaad, W., Buteau, J., Peyot, M.-L., Nolan, C., Roduit, R., Hardy, S., Joly, E., Dbaibo, G., Rosenberg, L. & Prentki, M. Saturated Fatty Acids Synergize with Elevated Glucose to Cause Pancreatic β-Cell Death. *Endocrinology* **144,** 4154–4163 (2003).
111. Bollheimer, L. C., Skelly, R. H., Chester, M. W., McGarry, J. D. & Rhodes, C. J. Chronic exposure to free fatty acid reduces pancreatic beta cell insulin content by increasing basal insulin secretion that is not compensated for by a corresponding increase in proinsulin biosynthesis translation. *J. Clin. Invest.* **101,** 1094–1101 (1998).
112. Tricò, D., Natali, A., Arslanian, S., Mari, A. & Ferrannini, E. Identification, pathophysiology, and clinical implications of primary insulin hypersecretion in nondiabetic adults and adolescents. *JCI Insight* **3,** (2018).

113. Vliet, S. van, Koh, H.-C. E., Patterson, B. W., Yoshino, M., LaForest, R., Gropler, R. J., Klein, S. & Mittendorfer, B. Obesity Is Associated With Increased Basal and Postprandial β-Cell Insulin Secretion Even in the Absence of Insulin Resistance. *Diabetes* **69,** 2112–2119 (2020).

114. Mehran, A. E., Templeman, N. M., Brigidi, G. S., Lim, G. E., Chu, K.-Y., Hu, X., Botezelli, J. D., Asadi, A., Hoffman, B. G., Kieffer, T. J., Bamji, S. X., Clee, S. M. & Johnson, J. D. Hyperinsulinemia Drives Diet-Induced Obesity Independently of Brain Insulin Production. *Cell Metab.* **16,** 723–737 (2012).

115. Hamza, S. M., Sung, M. M., Gao, F., Soltys, C.-L. M., Smith, N. P., MacDonald, P. E., Light, P. E. & Dyck, J. R. B. Chronic insulin infusion induces reversible glucose intolerance in lean rats yet ameliorates glucose intolerance in obese rats. *Biochim. Biophys. Acta BBA - Gen. Subj.* **1861,** 313–322 (2017).

116. Blüher, M., Kahn, B. B. & Kahn, C. R. Extended longevity in mice lacking the insulin receptor in adipose tissue. *Science* **299,** 572–574 (2003).

117. Pereira, M. J., Thombare, K., Sarsenbayeva, A., Kamble, P. G., Almby, K., Lundqvist, M. & Eriksson, J. W. Direct effects of glucagon on glucose uptake and lipolysis in human adipocytes. *Mol. Cell. Endocrinol.* **503,** 110696 (2020).

118. Kleinert, M., Sachs, S., Habegger, K. M., Hofmann, S. M. & Müller, T. D. Glucagon Regulation of Energy Expenditure. *Int. J. Mol. Sci.* **20,** 5407 (2019).

119. Hollander, P. A., Levy, P., Fineman, M. S., Maggs, D. G., Shen, L. Z., Strobel, S. A., Weyer, C. & Kolterman, O. G. Pramlintide as an Adjunct to Insulin Therapy Improves Long-Term Glycemic and Weight Control in Patients With Type 2 Diabetes: A 1-year randomized controlled trial. *Diabetes Care* **26,** 784–790 (2003).

120. Whitehouse, F., Kruger, D. F., Fineman, M., Shen, L., Ruggles, J. A., Maggs, D. G., Weyer, C. & Kolterman, O. G. A randomized study and open-label extension evaluating the long-term efficacy of pramlintide as an adjunct to insulin therapy in type 1 diabetes. *Diabetes Care* **25,** 724–730 (2002).

121. Ling, S., Brown, K., Miksza, J. K., Howells, L., Morrison, A., Issa, E., Yates, T., Khunti, K., Davies, M. J. & Zaccardi, F. Association of Type 2 Diabetes With Cancer: A Meta-analysis With Bias Analysis for Unmeasured Confounding in 151 Cohorts Comprising 32 Million People. *Diabetes Care* **43,** 2313–2322 (2020).

122. Gordon-Dseagu, V. L. Z., Shelton, N. & Mindell, J. S. Epidemiological evidence of a relationship between type-1 diabetes mellitus and cancer: a review of the existing literature. *Int. J. Cancer* **132,** 501–508 (2013).

123. Tsujimoto, T., Kajio, H. & Sugiyama, T. Association between hyperinsulinemia and increased risk of cancer death in nonobese and obese people: A population-based observational study. *Int. J. Cancer* **141,** 102–111 (2017).

124. Belfiore, A., Frasca, F., Pandini, G., Sciacca, L. & Vigneri, R. Insulin Receptor Isoforms and Insulin Receptor/Insulin-Like Growth Factor Receptor Hybrids in Physiology and Disease. *Endocr. Rev.* **30,** 586–623 (2009).

125. Sanchez-Vega, F., Mina, M., Armenia, J., Chatila, W. K., Luna, A., La, K. C., Dimitriadoy, S., Liu, D. L., Kantheti, H. S., Saghafinia, S., Chakravarty, D., Daian, F., Gao, Q., Bailey, M. H., Liang, W.-W., Foltz, S. M., Shmulevich, I., Ding, L., Heins, Z., Ochoa, A., Gross, B., Gao, J., Zhang, H., Kundra, R., Kandoth, C., Bahceci, I., Dervishi, L., Dogrusoz, U., Zhou, W., Shen, H., Laird, P. W., Way, G. P., Greene, C. S., Liang, H., Xiao, Y., Wang, C., Iavarone, A., Berger, A. H., Bivona, T. G., Lazar, A. J., Hammer, G. D., Giordano, T.,

Kwong, L. N., McArthur, G., Huang, C., Tward, A. D., Frederick, M. J., McCormick, F., Meyerson, M., Van Allen, E. M., Cherniack, A. D., Ciriello, G., Sander, C. & Schultz, N. Oncogenic Signaling Pathways in The Cancer Genome Atlas. *Cell* **173,** 321-337.e10 (2018).

126. Masur, K., Vetter, C., Hinz, A., Tomas, N., Henrich, H., Niggemann, B. & Zänker, K. S. Diabetogenic glucose and insulin concentrations modulate transcriptome and protein levels involved in tumour cell migration, adhesion and proliferation. *Br. J. Cancer* **104,** 345–352 (2011).
127. Venkatanarayan, A., Raulji, P., Norton, W., Chakravarti, D., Coarfa, C., Su, X., Sandur, S. K., Ramirez, M. S., Lee, J., Kingsley, C. V., Sananikone, E. F., Rajapakshe, K., Naff, K., Parker-Thornburg, J., Bankson, J. A., Tsai, K. Y., Gunaratne, P. H. & Flores, E. R. IAPP-driven metabolic reprogramming induces regression of *p53*-deficient tumours *in vivo*. *Nature* **517,** 626–630 (2015).
128. Bhaskaran, K., Douglas, I., Forbes, H., dos-Santos-Silva, I., Leon, D. A. & Smeeth, L. Body-mass index and risk of 22 specific cancers: a population-based cohort study of 5·24 million UK adults. *Lancet* **384,** 755–765 (2014).
129. Parker, E. D. & Folsom, A. R. Intentional weight loss and incidence of obesity-related cancers: the Iowa Women's Health Study. *Int. J. Obesity* **27,** 1447–1452 (2003).
130. Hopkins, B. D., Goncalves, M. D. & Cantley, L. C. Obesity and Cancer Mechanisms: Cancer Metabolism. *J. Clin. Oncol.* **34,** 4277–4283 (2016).
131. Iyengar, N. M., Gucalp, A., Dannenberg, A. J. & Hudis, C. A. Obesity and Cancer Mechanisms: Tumor Microenvironment and Inflammation. *J. Clin. Oncol.* **34,** 4270–4276 (2016).

132. Gebre-Medhin, S., Mulder, H., Pekny, M., Westermark, G., Törnell, J., Westermark, P., Sundler, F., Ahrén, B. & Betsholtz, C. Increased Insulin Secretion and Glucose Tolerance in Mice Lacking Islet Amyloid Polypeptide (Amylin). *Biochem. Biophys. Res. Commun.* **250,** 271–277 (1998).

133. Jackson, E. L., Willis, N., Mercer, K., Bronson, R. T., Crowley, D., Montoya, R., Jacks, T. & Tuveson, D. A. Analysis of lung tumor initiation and progression using conditional expression of oncogenic K-ras. *Genes Dev.* **15,** 3243–3248 (2001).

134. Marino, S., Vooijs, M., van Der Gulden, H., Jonkers, J. & Berns, A. Induction of medulloblastomas in p53-null mutant mice by somatic inactivation of Rb in the external granular layer cells of the cerebellum. *Genes Dev.* **14,** 994–1004 (2000).

135. Pan, F. C., Bankaitis, E. D., Boyer, D., Xu, X., Van de Casteele, M., Magnuson, M. A., Heimberg, H. & Wright, C. V. E. Spatiotemporal patterns of multipotentiality in Ptf1a-expressing cells during pancreas organogenesis and injury-induced facultative restoration. *Development* **140,** 751–764 (2013).

136. Skarnes, W. C., Rosen, B., West, A. P., Koutsourakis, M., Bushell, W., Iyer, V., Mujica, A. O., Thomas, M., Harrow, J., Cox, T., Jackson, D., Severin, J., Biggs, P., Fu, J., Nefedov, M., de Jong, P. J., Stewart, A. F. & Bradley, A. A conditional knockout resource for the genome-wide study of mouse gene function. *Nature* **474,** 337–342 (2011).

137. Kranz, A., Fu, J., Duerschke, K., Weidlich, S., Naumann, R., Stewart, A. F. & Anastassiadis, K. An improved Flp deleter mouse in C57Bl/6 based on Flpo recombinase. *Genesis* **48,** 512–520 (2010).

138. Thorens, B., Tarussio, D., Maestro, M. A., Rovira, M., Heikkilä, E. & Ferrer, J. Ins1Cre knock-in mice for beta cell-specific gene recombination. *Diabetologia* **58,** 558–565 (2015).

139. Muzumdar, M. D., Tasic, B., Miyamichi, K., Li, L. & Luo, L. A global double-fluorescent Cre reporter mouse. *Genesis* **45,** 593–605 (2007).

140. Courtade, J. Impaired pro-islet amyloid polypeptide processing promotes beta-cell dysfunction in diabetes and islet transplants. (2016). at <https://doi.library.ubc.ca/10.14288/1.0314119>

141. Couce, M., Kane, L. A., O'Brien, T. D., Charlesworth, J., Soeller, W., McNeish, J., Kreutter, D., Roche, P. & Butler, P. C. Treatment With Growth Hormone and Dexamethasone in Mice Transgenic for Human Islet Amyloid Polypeptide Causes Islet Amyloidosis and β-Cell Dysfunction. *Diabetes* **45,** 1094–1101 (1996).

142. Janson, J., Soeller, W. C., Roche, P. C., Nelson, R. T., Torchia, A. J., Kreutter, D. K. & Butler, P. C. Spontaneous diabetes mellitus in transgenic mice expressing human islet amyloid polypeptide. *Proc. Natl. Acad. Sci. U. S. A.* **93,** 7283–7288 (1996).

143. Ling, S., Brown, K., Miksza, J. K., Howells, L., Morrison, A., Issa, E., Yates, T., Khunti, K., Davies, M. J. & Zaccardi, F. Association of Type 2 Diabetes With Cancer: A Meta-analysis With Bias Analysis for Unmeasured Confounding in 151 Cohorts Comprising 32 Million People. *Diabetes Care* **43,** 2313–2322 (2020).

144. Gordon-Dseagu, V. L. Z., Shelton, N. & Mindell, J. S. Epidemiological evidence of a relationship between type-1 diabetes mellitus and cancer: a review of the existing literature. *Int. J. Cancer* **132,** 501–508 (2013).

145. Canadian Cancer Statistics Advisory Committee. Canadian Cancer Statistics 2019. Toronto, ON: Canadian Cancer Society; 2019. Available at: cancer.ca/Canadian-Cancer-Statistics-2019-EN (accessed [31 October 2021]). (2019).

146. Abbruzzese, J. L., Andersen, D. K., Borrebaeck, C. A. K., Chari, S. T., Costello, E., Cruz-Monserrate, Z., Eibl, G., Engleman, E. G., Fisher, W. E., Habtezion, A., Kim, S. K., Korc, M., Logsdon, C., Lyssiotis, C. A., Pandol, S. J., Rustgi, A., Wolfe, B. M., Zheng, L. & Powers, A. C. The Interface of Pancreatic Cancer With Diabetes, Obesity, and Inflammation: Research Gaps and Opportunities: Summary of a National Institute of Diabetes and Digestive and Kidney Diseases Workshop. *Pancreas* **47,** 516–525 (2018).

147. Preziosi, G., Oben, J. A. & Fusai, G. Obesity and pancreatic cancer. *Surg. Oncol.* **23,** 61–71 (2014).

148. Philip, B., Roland, C. L., Daniluk, J., Liu, Y., Chatterjee, D., Gomez, S. B., Ji, B., Huang, H., Wang, H., Fleming, J. B., Logsdon, C. D. & Cruz-Monserrate, Z. A high-fat diet activates oncogenic Kras and COX2 to induce development of pancreatic ductal adenocarcinoma in mice. *Gastroenterology* **145,** 1449–1458 (2013).

149. Wolpin, B. M., Bao, Y., Qian, Z. R., Wu, C., Kraft, P., Ogino, S., Stampfer, M. J., Sato, K., Ma, J., Buring, J. E., Sesso, H. D., Lee, I.-M., Gaziano, J. M., McTiernan, A., Phillips, L. S., Cochrane, B. B., Pollak, M. N., Manson, J. E., Giovannucci, E. L. & Fuchs, C. S. Hyperglycemia, insulin resistance, impaired pancreatic β-cell function, and risk of pancreatic cancer. *J. Natl. Cancer Inst.* **105,** 1027–1035 (2013).

150. Zhang, A. M. Y., Magrill, J., de Winter, T. J. J., Hu, X., Skovsø, S., Schaeffer, D. F., Kopp, J. L. & Johnson, J. D. Endogenous Hyperinsulinemia Contributes to Pancreatic Cancer Development. *Cell Metab.* **30,** 403–404 (2019).

151. Stevens, R. J., Roddam, A. W. & Beral, V. Pancreatic cancer in type 1 and young-onset diabetes: systematic review and meta-analysis. *Br. J. Cancer* **96,** 507–509 (2007).

152. Ryu, T. Y., Park, J. & Scherer, P. E. Hyperglycemia as a Risk Factor for Cancer Progression. *Diabetes Metab. J.* **38,** 330 (2014).

153. Liou, G.-Y., Döppler, H., Necela, B., Krishna, M., Crawford, H. C., Raimondo, M. & Storz, P. Macrophage-secreted cytokines drive pancreatic acinar-to-ductal metaplasia through NF-κB and MMPs. *J. Cell Biol.* **202,** 563–577 (2013).

154. Corcoran, R. B., Contino, G., Deshpande, V., Tzatsos, A., Conrad, C., Benes, C. H., Levy, D. E., Settleman, J., Engelman, J. A. & Bardeesy, N. STAT3 plays a critical role in KRAS-induced pancreatic tumorigenesis. *Cancer Res.* **71,** 5020–5029 (2011).

155. Xue, J., Sharma, V., Hsieh, M. H., Chawla, A., Murali, R., Pandol, S. J. & Habtezion, A. Alternatively activated macrophages promote pancreatic fibrosis in chronic pancreatitis. *Nat. Commun.* **6,** 7158 (2015).

156. Liou, G.-Y., Bastea, L., Fleming, A., Döppler, H., Edenfield, B. H., Dawson, D. W., Zhang, L., Bardeesy, N. & Storz, P. The Presence of Interleukin-13 at Pancreatic ADM/PanIN Lesions Alters Macrophage Populations and Mediates Pancreatic Tumorigenesis. *Cell Rep.* **19,** 1322–1333 (2017).

157. Venkatanarayan, A., Raulji, P., Norton, W. & Flores, E. R. Novel therapeutic interventions for p53-altered tumors through manipulation of its family members, p63 and p73. *Cell Cycle Georget. Tex* **15,** 164–171 (2016).

158. Bower, R. L. & Hay, D. L. Amylin structure-function relationships and receptor pharmacology: implications for amylin mimetic drug development. *Br. J. Pharmacol.* **173,** 1883–1898 (2016).

159. Christopoulos, G., Perry, K. J., Morfis, M., Tilakaratne, N., Gao, Y., Fraser, N. J., Main, M. J., Foord, S. M. & Sexton, P. M. Multiple Amylin Receptors Arise from Receptor Activity-

Modifying Protein Interaction with the Calcitonin Receptor Gene Product. *Mol. Pharmacol.* **56,** 235–242 (1999).

160. Gorn, A. H., Lin, H. Y., Yamin, M., Auron, P. E., Flannery, M. R., Tapp, D. R., Manning, C. A., Lodish, H. F., Krane, S. M. & Goldring, S. R. Cloning, characterization, and expression of a human calcitonin receptor from an ovarian carcinoma cell line. *J. Clin. Invest.* **90,** 1726–1735 (1992).
161. Morfis, M., Tilakaratne, N., Furness, S. G. B., Christopoulos, G., Werry, T. D., Christopoulos, A. & Sexton, P. M. Receptor Activity-Modifying Proteins Differentially Modulate the G Protein-Coupling Efficiency of Amylin Receptors. *Endocrinology* **149,** 5423–5431 (2008).
162. Cheng, X., Ji, Z., Tsalkova, T. & Mei, F. Epac and PKA: a tale of two intracellular cAMP receptors. *Acta Biochim. Biophys. Sin.* **40,** 651–662 (2008).
163. Walsh, D. A., Perkins, J. P. & Krebs, E. G. An adenosine 3',5'-monophosphate-dependant protein kinase from rabbit skeletal muscle. *J. Biol. Chem.* **243,** 3763–3765 (1968).
164. Kawasaki, H., Springett, G. M., Mochizuki, N., Toki, S., Nakaya, M., Matsuda, M., Housman, D. E. & Graybiel, A. M. A family of cAMP-binding proteins that directly activate Rap1. *Science* **282,** 2275–2279 (1998).
165. de Rooij, J., Zwartkruis, F. J., Verheijen, M. H., Cool, R. H., Nijman, S. M., Wittinghofer, A. & Bos, J. L. Epac is a Rap1 guanine-nucleotide-exchange factor directly activated by cyclic AMP. *Nature* **396,** 474–477 (1998).
166. Lorenz, R., Aleksic, T., Wagner, M., Adler, G. & Weber, C. K. The cAMP/Epac1/Rap1 Pathway in Pancreatic Carcinoma. *Pancreas* **37,** 102–103 (2008).

167. Patra, K. C., Kato, Y., Mizukami, Y., Widholz, S., Boukhali, M., Revenco, I., Grossman, E. A., Ji, F., Sadreyev, R. I., Liss, A. S., Screaton, R. A., Sakamoto, K., Ryan, D. P., Mino-Kenudson, M., Castillo, C. F.-D., Nomura, D. K., Haas, W. & Bardeesy, N. Mutant GNAS drives pancreatic tumourigenesis by inducing PKA-mediated SIK suppression and reprogramming lipid metabolism. *Nat. Cell Biol.* **20,** 811–822 (2018).

168. Mack, C. M., Soares, C. J., Wilson, J. K., Athanacio, J. R., Turek, V. F., Trevaskis, J. L., Roth, J. D., Smith, P. A., Gedulin, B., Jodka, C. M., Roland, B. L., Adams, S. H., Lwin, A., Herich, J., Laugero, K. D., Vu, C., Pittner, R., Paterniti, J. R., Hanley, M., Ghosh, S. & Parkes, D. G. Davalintide (AC2307), a novel amylin-mimetic peptide: enhanced pharmacological properties over native amylin to reduce food intake and body weight. *Int. J. Obes.* **34,** 385–395 (2010).

169. Mack, C. M., Smith, P. A., Athanacio, J. R., Xu, K., Wilson, J. K., Reynolds, J. M., Jodka, C. M., Lu, M. G. W. & Parkes, D. G. Glucoregulatory effects and prolonged duration of action of davalintide: a novel amylinomimetic peptide. *Diabetes Obes. Metab.* **13,** 1105–1113 (2011).

170. Hoare, S. Mechanisms of peptide and nonpeptide ligand binding to Class B G-protein-coupled receptors. *Drug Discov. Today* **10,** 417–427 (2005).

171. Bailey, R. J., Walker, C. S., Ferner, A. H., Loomes, K. M., Prijic, G., Halim, A., Whiting, L., Phillips, A. R. J. & Hay, D. L. Pharmacological characterization of rat amylin receptors: implications for the identification of amylin receptor subtypes. *Br. J. Pharmacol.* **166,** 151–167 (2012).

172. Wagner, K. W., Punnoose, E. A., Januario, T., Lawrence, D. A., Pitti, R. M., Lancaster, K., Lee, D., von Goetz, M., Yee, S. F., Totpal, K., Huw, L., Katta, V., Cavet, G., Hymowitz, S.

G., Amler, L. & Ashkenazi, A. Death-receptor O-glycosylation controls tumor-cell sensitivity to the proapoptotic ligand Apo2L/TRAIL. *Nat. Med.* **13,** 1070–1077 (2007).

173. Deer, E. L., González-Hernández, J., Coursen, J. D., Shea, J. E., Ngatia, J., Scaife, C. L., Firpo, M. A. & Mulvihill, S. J. Phenotype and genotype of pancreatic cancer cell lines. *Pancreas* **39,** 425–435 (2010).
174. Butz, J., Wickstrom, E. & Edwards, J. Characterization of mutations and loss of heterozygosity of p53 and K-ras2 in pancreatic cancer cell lines by immobilized polymerase chain reaction. *BMC Biotechnol.* **3,** 11 (2003).
175. Poyner, D. R. International Union of Pharmacology. XXXII. The Mammalian Calcitonin Gene-Related Peptides, Adrenomedullin, Amylin, and Calcitonin Receptors. *Pharmacol. Rev.* **54,** 233–246 (2002).
176. Bühlmann, N., Leuthäuser, K., Muff, R., Fischer, J. A. & Born, W. A receptor activity modifying protein (RAMP)2-dependent adrenomedullin receptor is a calcitonin gene-related peptide receptor when coexpressed with human RAMP1. *Endocrinology* **140,** 2883–2890 (1999).
177. Lu, T., Meng, F., Wei, Y., Li, Y., Wang, C. & Li, F. Exploring the relation between the oligomeric structure and membrane damage by a study on rat islet amyloid polypeptide. *Phys. Chem. Chem. Phys.* **20,** 8976–8983 (2018).
178. Young, L. M., Cao, P., Raleigh, D. P., Ashcroft, A. E. & Radford, S. E. Ion mobility spectrometry-mass spectrometry defines the oligomeric intermediates in amylin amyloid formation and the mode of action of inhibitors. *J. Am. Chem. Soc.* **136,** 660–670 (2014).

179. Evdokiou, A., Raggatt, L.-J., Atkins, G. J. & Findlay, D. M. Calcitonin receptor-mediated growth suppression of HEK-293 cells is accompanied by induction of p21WAF1/CIP1 and G2/M arrest. *Mol. Endocrinol.* **13,** 1738–1750 (1999).

180. Findlay, D., Raggatt, L., Bouralexis, S., Hay, S., Atkins, G. & Evdokiou, A. Calcitonin decreases the adherence and survival of HEK-293 cells by a caspase-independent mechanism. *J. Endocrinol.* **175,** 715–725 (2002).

181. Isobe, K., Jung, H. J., Yang, C.-R., Claxton, J., Sandoval, P., Burg, M. B., Raghuram, V. & Knepper, M. A. Systems-level identification of PKA-dependent signaling in epithelial cells. *Proc. Natl. Acad. Sci. U. S. A.* **114,** E8875–E8884 (2017).

182. Al-Keilani, M., Alsmadi, D., Darweesh, R. & Alzoubi, K. Pramlintide, an antidiabetic, is antineoplastic in colorectal cancer and synergizes with conventional chemotherapy. *Clin. Pharmacol. Adv. Appl.* **Volume 10,** 23–29 (2018).

183. Garnett, S., de Bruyns, A., Provencher-Tom, V., Dutchak, K., Shu, R. & Dankort, D. Metabolic Regulator IAPP (Amylin) Is Required for BRAF and RAS Oncogene-Induced Senescence. *Mol. Cancer Res.* **19,** 874–885 (2021).

184. Li, Y., Zhu, Y., Dai, G., Wu, D., Gao, Z., Zhang, L., Fan, Y., & Department of Oncology, The Second Affiliated Hospital of Jiaxing University, Jiaxing 314000, China. Screening and validating the core biomarkers in patients with pancreatic ductal adenocarcinoma. *Math. Biosci. Eng.* **17,** 910–927 (2020).

185. Mawla, A. M. & Huising, M. O. Navigating the Depths and Avoiding the Shallows of Pancreatic Islet Cell Transcriptomes. *Diabetes* **68,** 1380–1393 (2019).

186. Permert, J., Mogaki, M., Andrén-Sandberg, Å., Kazokoff, K. & Pouf, P. M. Pancreatic mixed Ductal-Islet tumors. *Int. J. Pancreatol.* **11,** 23–29 (1992).

187. Nakamura, M., Han, B., Nishishita, T., Bai, Y. & Kakudo, K. Calcitonin targets extracellular signal-regulated kinase signaling pathway in human cancers. *J. Mol. Endocrinol.* **39,** 375–384 (2007).

188. Ng, K. W., Livesey, S. A., Larkins, R. G. & Martin, T. J. Calcitonin Effects on Growth and on Selective Activation of Type II Isoenzyme of Cyclic Adenosine 3':5'-Monophosphate-dependent Protein Kinase in T 47D Human Breast Cancer Cells. **43,** 8 (1983).

189. Ritchie, C. K., Thomas, K. G., Andrews, L. R., Tindall, D. J. & Fitzpatrick, L. A. Effects of the calciotrophic peptides calcitonin and parathyroid hormone on prostate cancer growth and chemotaxis. *The Prostate* **30,** 183–187 (1997).

190. Mould, R. & Pondel, M. D. Calcitonin receptor gene expression in K562 chronic myelogenous leukemic cells. *Cancer Cell Int.* **3,** 6 (2003).

191. Ostrovskaya, A., Hick, C., Hutchinson, D. S., Stringer, B. W., Wookey, P. J., Wootten, D., Sexton, P. M. & Furness, S. G. B. Expression and activity of the calcitonin receptor family in a sample of primary human high-grade gliomas. *BMC Cancer* **19,** 157 (2019).

192. Wells, G., Chernoff, J., Gilligan, J. P. & Krause, D. S. Does salmon calcitonin cause cancer? A review and meta-analysis. *Osteoporosis Int.* **27,** 13–19 (2016).

193. Shah, G. V., Rayford, W., Noble, M. J., Austenfeld, M., Weigel, J., Vamos, S. & Mebust, W. K. Calcitonin stimulates growth of human prostate cancer cells through receptor-mediated increase in cyclic adenosine 3',5'-monophosphates and cytoplasmic Ca2+ transients. *Endocrinology* **134,** 596–602 (1994).

194. Thomas, S., Muralidharan, A. & Shah, G. Knock-down of calcitonin receptor expression induces apoptosis and growth arrest of prostate cancer cells. *Int. J. Oncol.* (2007). doi:10.3892/ijo.31.6.1425

195. Ramachandran, V., Arumugam, T., Hwang, R. F., Greenson, J. K., Simeone, D. M. & Logsdon, C. D. Adrenomedullin Is Expressed in Pancreatic Cancer and Stimulates Cell Proliferation and Invasion in an Autocrine Manner via the Adrenomedullin Receptor, ADMR. *Cancer Res.* **67,** 2666–2675 (2007).

196. Keleg, S., Kayed, H., Jiang, X., Penzel, R., Giese, T., Büchler, M. W., Friess, H. & Kleeff, J. Adrenomedullin is induced by hypoxia and enhances pancreatic cancer cell invasion. *Int. J. Cancer* **121,** 21–32 (2007).

197. Hollander, L. L., Guo, X., Salem, R. R. & Cha, C. H. The novel tumor angiogenic factor, adrenomedullin-2, predicts survival in pancreatic adenocarcinoma. *J. Surg. Res.* **197,** 219–224 (2015).

198. Insel, P. A., Zhang, L., Murray, F., Yokouchi, H. & Zambon, A. C. Cyclic AMP is both a pro-apoptotic and anti-apoptotic second messenger. *Acta Physiol. Oxf. Engl.* **204,** 277–287 (2012).

199. Hollander, P. A., Levy, P., Fineman, M. S., Maggs, D. G., Shen, L. Z., Strobel, S. A., Weyer, C. & Kolterman, O. G. Pramlintide as an Adjunct to Insulin Therapy Improves Long-Term Glycemic and Weight Control in Patients With Type 2 Diabetes: A 1-year randomized controlled trial. *Diabetes Care* **26,** 784–790 (2003).

200. Jurgens, C. A., Toukatly, M. N., Fligner, C. L., Udayasankar, J., Subramanian, S. L., Zraika, S., Aston-Mourney, K., Carr, D. B., Westermark, P., Westermark, G. T., Kahn, S. E. & Hull, R. L. β-cell loss and β-cell apoptosis in human type 2 diabetes are related to islet amyloid deposition. *Am. J. Pathol.* **178,** 2632–2640 (2011).

201. Permert, J., Larsson, J., Westermark, G. T., Herrington, M. K., Christmanson, L., Pour, P. M., Westermark, P. & Adrian, T. E. Islet amyloid polypeptide in patients with pancreatic cancer and diabetes. *N. Engl. J. Med.* **330,** 313–318 (1994).

202. Permert, J., Larsson, J., Fruin, A. B., Tatemoto, K., Herrington, M. K., von Schenck, H. & Adrian, T. E. Islet Hormone Secretion in Pancreatic Cancer Patients with Diabetes: *Pancreas* **15,** 60–68 (1997).

203. Chari, S. T., Klee, G. G., Miller, L. J., Raimondo, M. & DiMagno, E. P. Islet amyloid polypeptide is not a satisfactory marker for detecting pancreatic cancer. *Gastroenterology* **121,** 640–645 (2001).

204. Brand, R. E., Ding, X.-Z., Young, C. M. & Adrian, T. E. The Specificity of Amylin for the Diagnosis of Pancreatic Adenocarcinoma. *Int. J. Gastrointest. Cancer* **31,** 123–128 (2002).

205. Ding, X., Flatt, P. R., Permert, J. & Adrian, T. E. Pancreatic cancer cells selectively stimulate islet beta cells to secrete amylin. *Gastroenterology* **114,** 130–138 (1998).

206. Wang, F., Larsson, J., Abdiu, A., Gasslander, T., Westermark, P., Adrian, T. E. & Permert, J. Dissociated secretion of islet amyloid polypeptide and insulin in serum-free culture media conditioned by human pancreatic adenocarcinoma cell lines. *Int. J. Pancreatol.* **21,** 157–164 (1997).

207. Wang, F., Adrian, T. E., Westermark, G., Gasslander, T. & Permert, J. Dissociated Insulin and Islet Amyloid Polypeptide Secretion from Isolated Rat Pancreatic Islets Cocultured with Human Pancreatic Adenocarcinoma Cells: *Pancreas* **18,** 403–409 (1999).

208. Westwell-Roper, C. Y., Ehses, J. A. & Verchere, C. B. Resident Macrophages Mediate Islet Amyloid Polypeptide–Induced Islet IL-1β Production and β-Cell Dysfunction. *Diabetes* **63,** 1698–1711 (2014).

209. Westwell-Roper, C., Denroche, H. C., Ehses, J. A. & Verchere, C. B. Differential Activation of Innate Immune Pathways by Distinct Islet Amyloid Polypeptide (IAPP) Aggregates. *J. Biol. Chem.* **291,** 8908–8917 (2016).

210. Schludi, B., Moin, A. S. M., Montemurro, C., Gurlo, T., Matveyenko, A. V., Kirakossian, D., Dawson, D. W., Dry, S. M., Butler, P. C. & Butler, A. E. Islet inflammation and ductal proliferation may be linked to increased pancreatitis risk in type 2 diabetes. *JCI Insight* **2,** e92282 (2017).

211. Westermark, P., Wernstedt, C., Wilander, E. & Sletten, K. A novel peptide in the calcitonin gene related peptide family as an amyloid fibril protein in the endocrine pancreas. *Biochem. Biophys. Res. Commun.* **140,** 827–831 (1986).

212. DiGruccio, M. R., Mawla, A. M., Donaldson, C. J., Noguchi, G. M., Vaughan, J., Cowing-Zitron, C., van der Meulen, T. & Huising, M. O. Comprehensive alpha, beta and delta cell transcriptomes reveal that ghrelin selectively activates delta cells and promotes somatostatin release from pancreatic islets. *Mol. Metab.* **5,** 449–458 (2016).

213. Raleigh, D., Zhang, X., Hastoy, B. & Clark, A. The β-cell assassin: IAPP cytotoxicity. *J. Mol. Endocrinol.* **59,** R121–R140 (2017).

214. Young, A. in *Adv. Pharmacol.* **52,** 173–192 (Academic Press, 2005).

215. Miyazato, M., Nakazato, M., Shiomi, K., Aburaya, J., Toshimori, H., Kangawa, K., Matsuo, H. & Matsukura, S. Identification and characterization of islet amyloid polypeptide in mammalian gastrointestinal tract. *Biochem. Biophys. Res. Commun.* **181,** 293–300 (1991).

216. Mulder, H., Lindh, A.-C., Ekblad, E., Westermark, P. & Sundler, F. Islet amyloid polypeptide is expressed in endocrine cells of the gastric mucosa in the rat and mouse. *Gastroenterology* **107,** 712–719 (1994).

217. DeVroede, M., Foriers, A., Van De Winkel, M., Madsen, O. & Pipeleers, D. Presence of islet amyloid polypeptide in rat islet B and D cells determines parallelism and dissociation between rat pancreatic islet amyloid polypeptide and insulin content. *Biochem. Biophys. Res. Commun.* **182,** 886–893 (1992).

218. Mawla, A. M. & Huising, M. O. Navigating the Depths and Avoiding the Shallows of Pancreatic Islet Cell Transcriptomes. *Diabetes* **68,** 1380–1393 (2019).

219. Pontén, F., Jirström, K. & Uhlen, M. The Human Protein Atlas--a tool for pathology. *J. Pathol.* **216,** 387–393 (2008).

220. Chance, W. T., Balasubramaniam, A., Zhang, F. S., Wimalawansa, S. J. & Fischer, J. E. Anorexia following the intrahypothalamic administration of amylin. *Brain Res.* **539,** 352–354 (1991).

221. Morley, J. E. & Flood, J. F. Amylin decreases food intake in mice. *Peptides* **12,** 865–869 (1991).

222. Lutz, T. A., Geary, N., Szabady, M. M., Del Prete, E. & Scharrer, E. Amylin decreases meal size in rats. *Physiol. Behav.* **58,** 1197–1202 (1995).

223. Smith, S. R., Blundell, J. E., Burns, C., Ellero, C., Schroeder, B. E., Kesty, N. C., Chen, K. S., Halseth, A. E., Lush, C. W. & Weyer, C. Pramlintide treatment reduces 24-h caloric intake and meal sizes and improves control of eating in obese subjects: a 6-wk translational research study. *Am. J. Physiol. Endocrinol. Metab.* **293,** E620-627 (2007).

224. Roth, J. D., Roland, B. L., Cole, R. L., Trevaskis, J. L., Weyer, C., Koda, J. E., Anderson, C. M., Parkes, D. G. & Baron, A. D. Leptin responsiveness restored by amylin agonism in diet-induced obesity: Evidence from nonclinical and clinical studies. *Proc. Natl. Acad. Sci.* **105,** 7257–7262 (2008).

225. Clementi, G., Caruso, A., Cutuli, V. M., de Bernardis, E., Prato, A. & Amico-Roxas, M. Amylin given by central or peripheral routes decreases gastric emptying and intestinal transit in the rat. *Experientia* **52,** 677–679 (1996).

226. Young, A. A., Gedulin, B. R. & Rink, T. J. Dose-responses for the slowing of gastric emptying in a rodent model by glucagon-like peptide (7-36) NH2, amylin, cholecystokinin, and other possible regulators of nutrient uptake. *Metabolism.* **45,** 1–3 (1996).

227. Fineman, M. S., Koda, J. E., Shen, L. Z., Strobel, S. A., Maggs, D. G., Weyer, C. & Kolterman, O. G. The human amylin analog, pramlintide, corrects postprandial hyperglucagonemia in patients with type 1 diabetes. *Metabolism.* **51,** 636–641 (2002).

228. Kolterman, O. G., Gottlieb, A., Moyses, C. & Colburn, W. Reduction of postprandial hyperglycemia in subjects with IDDM by intravenous infusion of AC137, a human amylin analogue. *Diabetes Care* **18,** 1179–1182 (1995).

229. Osaka, T., Tsukamoto, A., Koyama, Y. & Inoue, S. Central and peripheral administration of amylin induces energy expenditure in anesthetized rats. *Peptides* **29,** 1028–1035 (2008).

230. Mather, K. J., Paradisi, G., Leaming, R., Hook, G., Steinberg, H. O., Fineberg, N., Hanley, R. & Baron, A. D. Role of amylin in insulin secretion and action in humans: antagonist studies across the spectrum of insulin sensitivity. *Diabetes Metab. Res. Rev.* **18,** 118–126 (2002).

231. Moreno, P., Acitores, A., Gutiérrez-Rojas, I., Nuche-Berenguer, B., El Assar, M., Rodriguez-Mañas, L., Gomis, R., Valverde, I., Visa, M., Malaisse, W. J., Novials, A., González, N. & Villanueva-Peñacarrillo, M. L. Amylin effect in extrapancreatic tissues participating in glucose homeostasis, in normal, insulin-resistant and type 2 diabetic state. *Peptides* **32,** 2077–2085 (2011).

232. Miegueu, P., St-Pierre, D. H., Munkonda, M. N., Lapointe, M. & Cianflone, K. Amylin stimulates fatty acid esterification in 3T3-L1 adipocytes. *Mol. Cell. Endocrinol.* **366,** 99–107 (2013).

233. Dacquin, R., Davey, R. A., Laplace, C., Levasseur, R., Morris, H. A., Goldring, S. R., Gebre-Medhin, S., Galson, D. L., Zajac, J. D. & Karsenty, G. Amylin inhibits bone resorption while the calcitonin receptor controls bone formation in vivo. *J. Cell Biol.* **164,** 509–514 (2004).

234. Carlsson, P. O., Karlsson, E., Mulder, H. & Gebre-Medhin, S. Unaltered pancreatic islet blood perfusion in islet amyloid polypeptide-deficient mice. *Eur. J. Endocrinol.* **146,** 107–112 (2002).

235. Brain, S. D., Wimalawansa, S., MacIntyre, I. & Williams, T. J. The demonstration of vasodilator activity of pancreatic amylin amide in the rabbit. *Am. J. Pathol.* **136,** 487–490 (1990).

236. Svensson, A. M., Sandler, S. & Jansson, L. Pancreatic islet blood flow in the rat after administration of islet amyloid polypeptide or calcitonin gene-related peptide. *Diabetes* **43,** 454–458 (1994).

237. Visa, M., Alcarraz-Vizán, G., Montane, J., Cadavez, L., Castaño, C., Villanueva-Peñacarrillo, M. L., Servitja, J.-M. & Novials, A. Islet amyloid polypeptide exerts a novel autocrine action in β-cell signaling and proliferation. *FASEB J. Off. Publ. Fed. Am. Soc. Exp. Biol.* **29,** 2970–2979 (2015).

238. Smith, S. R., Aronne, L. J., Burns, C. M., Kesty, N. C., Halseth, A. E. & Weyer, C. Sustained Weight Loss Following 12-Month Pramlintide Treatment as an Adjunct to Lifestyle Intervention in Obesity. *Diabetes Care* **31,** 1816–1823 (2008).

239. Hay, D. L., Chen, S., Lutz, T. A., Parkes, D. G. & Roth, J. D. Amylin: Pharmacology, Physiology, and Clinical Potential. *Pharmacol. Rev.* **67,** 564–600 (2015).

240. Lutz, T. A., Senn, M., Althaus, J., Del Prete, E., Ehrensperger, F. & Scharrer, E. Lesion of the area postrema/nucleus of the solitary tract (AP/NTS) attenuates the anorectic effects of amylin and calcitonin gene-related peptide (CGRP) in rats. *Peptides* **19,** 309–317 (1998).

241. Mollet, A., Gilg, S., Riediger, T. & Lutz, T. A. Infusion of the amylin antagonist AC 187 into the area postrema increases food intake in rats. *Physiol. Behav.* **81,** 149–155 (2004).

242. Li, Z., Kelly, L., Gergi, I., Vieweg, P., Heiman, M., Greengard, P. & Friedman, J. M. Hypothalamic Amylin Acts in Concert with Leptin to Regulate Food Intake. *Cell Metab.* **22,** 1059–1067 (2015).

243. Liberini, C. G., Boyle, C. N., Cifani, C., Venniro, M., Hope, B. T. & Lutz, T. A. Amylin receptor components and the leptin receptor are co-expressed in single rat area postrema neurons. *Eur. J. Neurosci.* **43,** 653–661 (2016).

244. Lutz, T. A., Coester, B., Whiting, L., Dunn-Meynell, A. A., Boyle, C. N., Bouret, S. G., Levin, B. E. & Le Foll, C. Amylin Selectively Signals Onto POMC Neurons in the Arcuate Nucleus of the Hypothalamus. *Diabetes* **67,** 805–817 (2018).

245. Coester, B., Koester-Hegmann, C., Lutz, T. A. & Le Foll, C. Amylin/Calcitonin Receptor-Mediated Signaling in POMC Neurons Influences Energy Balance and Locomotor Activity in Chow-Fed Male Mice. *Diabetes* **69,** 1110–1125 (2020).

246. Fernandes-Santos, C., Zhang, Z., Morgan, D. A., Guo, D.-F., Russo, A. F. & Rahmouni, K. Amylin Acts in the Central Nervous System to Increase Sympathetic Nerve Activity. *Endocrinology* **154,** 2481–2488 (2013).

247. Fehmann, H.-C., Weber, V., Göke, R., Göke, B., Eissele, R. & Arnold, R. Islet amyloid polypeptide (IAPP;Amylin) influences the endocrine but not the exocrine rat pancreas. *Biochem. Biophys. Res. Commun.* **167,** 1102–1108 (1990).

248. Bretherton-Watt, D., Gilbey, S. G., Ghatei, M. A., Beacham, J., Macrae, A. D. & Bloom, S. R. Very high concentrations of islet amyloid polypeptide are necessary to alter the insulin response to intravenous glucose in man. *J. Clin. Endocrinol. Metab.* **74,** 1032–1035 (1992).

249. Wang, F., Adrian, T. E., Westermark, G. T., Ding, X., Gasslander, T. & Permert, J. Islet amyloid polypeptide tonally inhibits β-, α-, and δ-cell secretion in isolated rat pancreatic islets. *Am. J. Physiol.-Endocrinol. Metab.* **276,** E19–E24 (1999).

250. Pittner, R. A. Lack of effect of calcitonin gene-related peptide and amylin on major markers of glucose metabolism in hepatocytes. *Eur. J. Pharmacol.* **325,** 189–197 (1997).

251. Zierath, J. R., Galuska, D., Engström, A., Johnson, K. H., Betsholtz, C., Westermark, P. & Wallberg-Henriksson, H. Human islet amyloid polypeptide at pharmacological levels inhibits insulin and phorbol ester-stimulated glucose transport in in vitro incubated human muscle strips. *Diabetologia* **35,** 26–31 (1992).

252. Young, A. A., Vine, W., Gedulin, B. R., Pittner, R., Janes, S., Gaeta, L. S. L., Percy, A., Moore, C. X., Koda, J. E., Rink, T. J. & Beaumont, K. Preclinical pharmacology of pramlintide in the rat: Comparisons with human and rat amylin. *Drug Dev. Res.* **37,** 231–248 (1996).

253. Leighton, B. & Cooper, G. J. S. Pancreatic amylin and calcitonin gene-related peptide cause resistance to insulin in skeletal muscle in vitro. *Nature* **335,** 632–635 (1988).

254. Pittner, R., Beaumont, K., Young, A. & Rink, T. Dose-dependent elevation of cyclic AMP, activation of glycogen phosphorylase, and release of lactate by amylin in rat skeletal muscle. *Biochim. Biophys. Acta BBA - Mol. Cell Res.* **1267,** 75–82 (1995).

255. Turek, V. F., Trevaskis, J. L., Levin, B. E., Dunn-Meynell, A. A., Irani, B., Gu, G., Wittmer, C., Griffin, P. S., Vu, C., Parkes, D. G. & Roth, J. D. Mechanisms of Amylin/Leptin Synergy in Rodent Models. *Endocrinology* **151,** 143–152 (2010).

256. Olsson, M., Herrington, M. K., Reidelberger, R. D., Permert, J., Gebre-Medhin, S. & Arnelo, U. Food intake and meal pattern in IAPP knockout mice with and without infusion of exogenous IAPP. *Scand. J. Gastroenterol.* **47,** 191–196 (2012).

257. Mollet, A., Meier, S., Grabler, V., Gilg, S., Scharrer, E. & Lutz, T. A. Endogenous amylin contributes to the anorectic effects of cholecystokinin and bombesin. *Peptides* **24,** 91–98 (2003).

258. Mulder, H., Gebre-Medhin, S., Betsholtz, C., Sundler, F. & Ahrén, B. Islet amyloid polypeptide (amylin)-deficient mice develop a more severe form of alloxan-induced diabetes. *Am. J. Physiol.-Endocrinol. Metab.* **278,** E684–E691 (2000).

259. Weyer, C., Gottlieb, A., Kim, D. D., Lutz, K., Schwartz, S., Gutierrez, M., Wang, Y., Ruggles, J. A., Kolterman, O. G. & Maggs, D. G. Pramlintide Reduces Postprandial Glucose Excursions When Added to Regular Insulin or Insulin Lispro in Subjects With Type 1 Diabetes: A dose-timing study. *Diabetes Care* **26,** 3074–3079 (2003).

260. Levetan, C., Want, L. L., Weyer, C., Strobel, S. A., Crean, J., Wang, Y., Maggs, D. G., Kolterman, O. G., Chandran, M., Mudaliar, S. R. & Henry, R. R. Impact of Pramlintide on Glucose Fluctuations and Postprandial Glucose, Glucagon, and Triglyceride Excursions

Among Patients With Type 1 Diabetes Intensively Treated With Insulin Pumps. *Diabetes Care* **26,** 1–8 (2003).

261. Maikawa, C. L., Smith, A. A. A., Zou, L., Roth, G. A., Gale, E. C., Stapleton, L. M., Baker, S. W., Mann, J. L., Yu, A. C., Correa, S., Grosskopf, A. K., Liong, C. S., Meis, C. M., Chan, D., Troxell, M., Maahs, D. M., Buckingham, B. A., Webber, M. J. & Appel, E. A. A co-formulation of supramolecularly stabilized insulin and pramlintide enhances mealtime glucagon suppression in diabetic pigs. *Nat. Biomed. Eng.* **4,** 507–517 (2020).
262. Gedulin, B. R., Jodka, C. M., Herrmann, K. & Young, A. A. Role of endogenous amylin in glucagon secretion and gastric emptying in rats demonstrated with the selective antagonist, AC187. *Regul. Pept.* **137,** 121–127 (2006).
263. Stridsberg, M., Sandler, S. & Wilander, E. Cosecretion of islet amylid polypeptide (IAPP) and insulin from isolated rat pancreatic islets following stimulation or inhibition of β-cell function. *Regul. Pept.* **45,** 363–370 (1993).
264. El-Haschimi, K., Pierroz, D. D., Hileman, S. M., Bjørbæk, C. & Flier, J. S. Two defects contribute to hypothalamic leptin resistance in mice with diet-induced obesity. *J. Clin. Invest.* **105,** 1827–1832 (2000).
265. Münzberg, H., Flier, J. S. & Bjørbæk, C. Region-Specific Leptin Resistance within the Hypothalamus of Diet-Induced Obese Mice. *Endocrinology* **145,** 4880–4889 (2004).
266. Kong, M. F., Stubbs, T. A., King, P., Macdonald, I. A., Lambourne, J. E., Blackshaw, P. E., Perkins, A. C. & Tattersall, R. B. The effect of single doses of pramlintide on gastric emptying of two meals in men with IDDM. *Diabetologia* **41,** 577–583 (1998).

267. Vella, A., Lee, J. S., Camilleri, M., Szarka, L. A., Burton, D. D., Zinsmeister, A. R., Rizza, R. A. & Klein, P. D. Effects of pramlintide, an amylin analogue, on gastric emptying in type 1 and 2 diabetes mellitus. *Neurogastroenterol. Motil.* **14,** 123–131 (2002).

268. Fineman, M., Weyer, C., Maggs, D. G., Strobel, S. & Kolterman, O. G. The human amylin analog, pramlintide, reduces postprandial hyperglucagonemia in patients with type 2 diabetes mellitus. *Horm. Metab. Res.* **34,** 504–508 (2002).

269. Silvestre, R. A., Rodríguez-Gallardo, J., Jodka, C., Parkes, D. G., Pittner, R. A., Young, A. A. & Marco, J. Selective amylin inhibition of the glucagon response to arginine is extrinsic to the pancreas. *Am. J. Physiol.-Endocrinol. Metab.* **280,** E443–E449 (2001).

270. Hauge-Evans, A. C., King, A. J., Carmignac, D., Richardson, C. C., Robinson, I. C. A. F., Low, M. J., Christie, M. R., Persaud, S. J. & Jones, P. M. Somatostatin Secreted by Islet δ-Cells Fulfills Multiple Roles as a Paracrine Regulator of Islet Function. *Diabetes* **58,** 403–411 (2009).

271. Kiba, T., Tanaka, K., Numata, K., Hoshino, M., Misugi, K. & Inoue, S. Ventromedial hypothalamic lesion-induced vagal hyperactivity stimulates rat pancreatic cell proliferation. *Gastroenterology* **110,** 885–893 (1996).

272. Cooper, G. J., Leighton, B., Dimitriadis, G. D., Parry-Billings, M., Kowalchuk, J. M., Howland, K., Rothbard, J. B., Willis, A. C. & Reid, K. B. Amylin found in amyloid deposits in human type 2 diabetes mellitus may be a hormone that regulates glycogen metabolism in skeletal muscle. *Proc. Natl. Acad. Sci. U. S. A.* **85,** 7763–7766 (1988).

273. Nyholm, B., Møller, N., Gravholt, C. H., Orskov, L., Mengel, A., Bryan, G., Moyses, C., Alberti, K. G. & Schmitz, O. Acute effects of the human amylin analog AC137 on basal

and insulin-stimulated euglycemic and hypoglycemic fuel metabolism in patients with insulin-dependent diabetes mellitus. *J. Clin. Endocrinol. Metab.* **81,** 1083–1089 (1996).

274. Kahn, S. E. & Halban, P. A. Release of Incompletely Processed Proinsulin Is the Cause of the Disproportionate Proinsulinemia of NIDDM. *Diabetes* **46,** 1725–1732 (1997).

275. Chen, Y.-C., Taylor, A. J. & Verchere, C. B. Islet prohormone processing in health and disease. *Diabetes Obes. Metab.* **20,** 64–76 (2018).

276. Schvartz, D., Brunner, Y., Couté, Y., Foti, M., Wollheim, C. B. & Sanchez, J.-C. Improved characterization of the insulin secretory granule proteomes. *J. Proteomics* **75,** 4620–4631 (2012).

277. Rhodes, C. J. & Halban, P. A. Newly synthesized proinsulin/insulin and stored insulin are released from pancreatic B cells predominantly via a regulated, rather than a constitutive, pathway. *J. Cell Biol.* **105,** 145–153 (1987).

278. Liu, M., Lara-Lemus, R., Shan, S., Wright, J., Haataja, L., Barbetti, F., Guo, H., Larkin, D. & Arvan, P. Impaired Cleavage of Preproinsulin Signal Peptide Linked to Autosomal-Dominant Diabetes. *Diabetes* **61,** 828–837 (2012).

279. Rhodes, C. J., Lucas, C. A., Mutkoski, R. L., Orci, L. & Halban, P. A. Stimulation by ATP of proinsulin to insulin conversion in isolated rat pancreatic islet secretory granules. Association with the ATP-dependent proton pump. *J. Biol. Chem.* **262,** 10712–10717 (1987).

280. Davidson, H. W., Wenzlau, J. M. & O'Brien, R. M. Zinc transporter 8 (ZnT8) and β cell function. *Trends Endocrinol. Metab. TEM* **25,** 415–424 (2014).

281. Mitchell, K. J., Pinton, P., Varadi, A., Tacchetti, C., Ainscow, E. K., Pozzan, T., Rizzuto, R. & Rutter, G. A. Dense core secretory vesicles revealed as a dynamic Ca2+ store in

neuroendocrine cells with a vesicle-associated membrane protein aequorin chimaera. *J. Cell Biol.* **155,** 41–52 (2001).

282. Germanos, M., Gao, A., Taper, M., Yau, B. & Kebede, M. A. Inside the Insulin Secretory Granule. *Metabolites* **11,** 515 (2021).
283. Wang, Z. & Thurmond, D. C. Mechanisms of biphasic insulin-granule exocytosis – roles of the cytoskeleton, small GTPases and SNARE proteins. *J. Cell Sci.* **122,** 893–903 (2009).
284. Steiner, D. F., Cunningham, D., Spigelman, L. & Aten, B. Insulin Biosynthesis: Evidence for a Precursor. *Science* **157,** 697–700 (1967).
285. Tran, D. T., Pottekat, A., Mir, S. A., Loguercio, S., Jang, I., Campos, A. R., Scully, K. M., Lahmy, R., Liu, M., Arvan, P., Balch, W. E., Kaufman, R. J. & Itkin-Ansari, P. Unbiased Profiling of the Human Proinsulin Biosynthetic Interaction Network Reveals a Role for Peroxiredoxin 4 in Proinsulin Folding. *Diabetes* **69,** 1723–1734 (2020).
286. Huang, X. F. & Arvan, P. Intracellular Transport of Proinsulin in Pancreatic β-Cells: Structural maturation probed by disulfide accessibility. *J. Biol. Chem.* **270,** 20417–20423 (1995).
287. Sizonenko, S., Irminger, J.-C., Buhler, L., Deng, S., Morel, P. & Halban, P. A. Kinetics of Proinsulin Conversion in Human Islets. *Diabetes* **42,** 933–936 (1993).
288. Hou, X., Ling, Z., Zambre, Y., Foriers, A., Houssa, P., Deberg, M., Sodoyez, J. C., Hales, C. N., Van der Auwera, B. J., Pipeleers, D. & Van Schravendijk, C. Proinsulin and its conversion intermediates in human pancreas and isolated islet tissue: kinetics and steady-state analysis. *Pancreas* **15,** 113–121 (1997).

289. Ramzy, A., Asadi, A. & Kieffer, T. J. Revisiting Proinsulin Processing: Evidence That Human β-Cells Process Proinsulin With Prohormone Convertase (PC) 1/3 but Not PC2. *Diabetes* **69,** 1451–1462 (2020).

290. Davalli, A. M., Perego, L., Bertuzzi, F., Finzi, G., La Rosa, S., Blau, A., Placidi, C., Nano, R., Gregorini, L., Perego, C., Capella, C. & Folli, F. Disproportionate Hyperproinsulinemia, β-Cell Restricted Prohormone Convertase 2 Deficiency, and Cell Cycle Inhibitors Expression by Human Islets Transplanted into Athymic Nude Mice: Insights into Nonimmune-Mediated Mechanisms of Delayed Islet Graft Failure. *Cell Transplant.* **17,** 1323–1336 (2008).

291. Itoh, Y., Tanaka, S., Takekoshi, S., Itoh, J. & Osamura, R. Y. Prohormone convertases (PC1/3 and PC2) in rat and human pancreas and islet cell tumors: Subcellular immunohistochemical analysis. *Pathol. Int.* **46,** 726–737 (1996).

292. Teitelman, G. Heterogeneous Expression of Proinsulin Processing Enzymes in Beta Cells of Non-diabetic and Type 2 Diabetic Humans. *J. Histochem. Cytochem.* **67,** 385–400 (2019).

293. Verchere, C. B., D'Alessio, D. A., Prigeon, R. L., Hull, R. L. & Kahn, S. E. The constitutive secretory pathway is a major route for islet amyloid polypeptide secretion in neonatal but not adult rat islet cells. *Diabetes* **49,** 1477–1484 (2000).

294. Marzban, L., Trigo-Gonzalez, G. & Verchere, C. B. Processing of pro-islet amyloid polypeptide in the constitutive and regulated secretory pathways of beta cells. *Mol. Endocrinol. Baltim. Md* **19,** 2154–2163 (2005).

295. Marzban, L., Trigo-Gonzalez, G., Zhu, X., Rhodes, C. J., Halban, P. A., Steiner, D. F. & Verchere, C. B. Role of β-Cell Prohormone Convertase (PC)1/3 in Processing of Pro-Islet Amyloid Polypeptide. *Diabetes* **53,** 141–148 (2004).

296. Marzban, L., Soukhatcheva, G. & Verchere, C. B. Role of Carboxypeptidase E in Processing of Pro-Islet Amyloid Polypeptide in β-Cells. *Endocrinology* **146,** 1808–1817 (2005).

297. Chen, Y.-C., Mains, R. E., Eipper, B. A., Hoffman, B. G., Czyzyk, T. A., Pintar, J. E. & Verchere, C. B. PAM haploinsufficiency does not accelerate the development of diet- and human IAPP-induced diabetes in mice. *Diabetologia* **63,** 561–576 (2020).

298. Marzban, L., Rhodes, C. J., Steiner, D. F., Haataja, L., Halban, P. A. & Verchere, C. B. Impaired NH2-terminal processing of human proislet amyloid polypeptide by the prohormone convertase PC2 leads to amyloid formation and cell death. *Diabetes* **55,** 2192–2201 (2006).

299. Wang, J., Xu, J., Finnerty, J., Furuta, M., Steiner, D. F. & Verchere, C. B. The Prohormone Convertase Enzyme 2 (PC2) Is Essential for Processing Pro-Islet Amyloid Polypeptide at the NH2-Terminal Cleavage Site. *Diabetes* **50,** 534–539 (2001).

300. Fugère, M., Limperis, P. C., Beaulieu-Audy, V., Gagnon, F., Lavigne, P., Klarskov, K., Leduc, R. & Day, R. Inhibitory potency and specificity of subtilase-like pro-protein convertase (SPC) prodomains. *J. Biol. Chem.* **277,** 7648–7656 (2002).

301. Muller, L., Cameron, A., Fortenberry, Y., Apletalina, E. V. & Lindberg, I. Processing and Sorting of the Prohormone Convertase 2 Propeptide. *J. Biol. Chem.* **275,** 39213–39222 (2000).

302. Zhou, Y. & Lindberg, I. Enzymatic properties of carboxyl-terminally truncated prohormone convertase 1 (PC1/SPC3) and evidence for autocatalytic conversion. *J. Biol. Chem.* **269,** 18408–18413 (1994).

303. Lamango, N. S., Apletalina, E., Liu, J. & Lindberg, I. The Proteolytic Maturation of Prohormone Convertase 2 (PC2) is a pH-Driven Process. *Arch. Biochem. Biophys.* **362,** 275–282 (1999).

304. Li, Q.-L., Naqvi, S., Shen, X., Liu, Y.-J., Lindberg, I. & Friedman, T. C. Prohormone convertase 2 enzymatic activity and its regulation in neuro-endocrine cells and tissues. *Regul. Pept.* **110,** 197–205 (2003).

305. Zhu, X., Orci, L., Carroll, R., Norrbom, C., Ravazzola, M. & Steiner, D. F. Severe block in processing of proinsulin to insulin accompanied by elevation of des-64,65 proinsulin intermediates in islets of mice lacking prohormone convertase 1/3. *Proc. Natl. Acad. Sci. U. S. A.* **99,** 10299–10304 (2002).

306. Rhodes, C. J., Lincoln, B. & Shoelson, S. E. Preferential cleavage of des-31,32-proinsulin over intact proinsulin by the insulin secretory granule type II endopeptidase. Implication of a favored route for prohormone processing. *J. Biol. Chem.* **267,** 22719–22727 (1992).

307. Keenan, H. A., Sun, J. K., Levine, J., Doria, A., Aiello, L. P., Eisenbarth, G., Bonner-Weir, S. & King, G. L. Residual Insulin Production and Pancreatic β-Cell Turnover After 50 Years of Diabetes: Joslin Medalist Study. *Diabetes* **59,** 2846–2853 (2010).

308. Sims, E. K., Chaudhry, Z., Watkins, R., Syed, F., Blum, J., Ouyang, F., Perkins, S. M., Mirmira, R. G., Sosenko, J., DiMeglio, L. A. & Evans-Molina, C. Elevations in the Fasting Serum Proinsulin–to–C-Peptide Ratio Precede the Onset of Type 1 Diabetes. *Diabetes Care* **39,** 1519–1526 (2016).

309. Rodriguez-Calvo, T., Zapardiel-Gonzalo, J., Amirian, N., Castillo, E., Lajevardi, Y., Krogvold, L., Dahl-Jørgensen, K. & von Herrath, M. G. Increase in Pancreatic Proinsulin

and Preservation of β-Cell Mass in Autoantibody-Positive Donors Prior to Type 1 Diabetes Onset. *Diabetes* **66,** 1334–1345 (2017).

310. Wasserfall, C., Nick, H. S., Campbell-Thompson, M., Beachy, D., Haataja, L., Kusmartseva, I., Posgai, A., Beery, M., Rhodes, C., Bonifacio, E., Arvan, P. & Atkinson, M. Persistence of Pancreatic Insulin mRNA Expression and Proinsulin Protein in Type 1 Diabetes Pancreata. *Cell Metab.* **26,** 568-575.e3 (2017).
311. Sims, E. K., Syed, F., Nyalwidhe, J., Bahnson, H. T., Haataja, L., Speake, C., Morris, M. A., Balamurugan, A. N., Mirmira, R. G., Nadler, J., Mastracci, T. L., Arvan, P., Greenbaum, C. J. & Evans-Molina, C. Abnormalities in proinsulin processing in islets from individuals with longstanding T1D. *Transl. Res.* **213,** 90–99 (2019).
312. Hostens, K., Pavlovic, D., Zambre, Y., Ling, Z., Van Schravendijk, C., Eizirik, D. L. & Pipeleers, D. G. Exposure of human islets to cytokines can result in disproportionately elevated proinsulin release. *J. Clin. Invest.* **104,** 67–72 (1999).
313. Schölin, A., Nyström, L., Arnqvist, H., Bolinder, J., Björk, E., Berne, C., Karlsson, F. A. & Sweden (DISS), the D. I. S. G. in. Proinsulin/C-peptide ratio, glucagon and remission in new-onset Type 1 diabetes mellitus in young adults. *Diabet. Med.* **28,** 156–161 (2011).
314. Klimek, A. M., Soukhatcheva, G., Thompson, D. M., Warnock, G. L., Salehi, M., Rilo, H., D'Alessio, D., Meneilly, G. S., Panagiotopoulos, C. & Verchere, C. B. Impaired Proinsulin Processing is a Characteristic of Transplanted Islets. *Am. J. Transplant.* **9,** 2119–2125 (2009).
315. Larsson, H. & Ahrén, B. Relative Hyperproinsulinemia as a Sign of Islet Dysfunction in Women with Impaired Glucose Tolerance1. *J. Clin. Endocrinol. Metab.* **84,** 2068–2074 (1999).

316. Røder, M. E., Porte, D., Schwartz, R. S. & Kahn, S. E. Disproportionately elevated proinsulin levels reflect the degree of impaired B cell secretory capacity in patients with noninsulin-dependent diabetes mellitus. *J. Clin. Endocrinol. Metab.* **83,** 604–608 (1998).

317. Saad, M. F., Kahn, S. E., Nelson, R. G., Pettitt, D. J., Knowler, W. C., Schwartz, M. W., Kowalyk, S., Bennett, P. H. & Porte, D. Disproportionately elevated proinsulin in Pima Indians with noninsulin-dependent diabetes mellitus. *J. Clin. Endocrinol. Metab.* **70,** 1247–1253 (1990).

318. Ullsten, S., Bohman, S., Oskarsson, M. E., Nilsson, K. P. R., Westermark, G. T. & Carlsson, P.-O. Islet amyloid deposits preferentially in the highly functional and most blood-perfused islets. *Endocr. Connect.* **6,** 458–468 (2017).

319. Sönksen, P. H., Tompkins, C. V., Srivastava, M. C. & Nabarro, J. D. A comparative study on the metabolism of human insulin and porcine proinsulin in man. *Clin. Sci. Mol. Med.* **45,** 633–654 (1973).

320. Kuzuya, T. & Matsuda, A. Disappearance rate of endogenous human C-peptide from blood. *Diabetologia* **12,** 519–521 (1976).

321. Furuta, M., Carroll, R., Martin, S., Swift, H. H., Ravazzola, M., Orci, L. & Steiner, D. F. Incomplete Processing of Proinsulin to Insulin Accompanied by Elevation of Des-31,32 Proinsulin Intermediates in Islets of Mice Lacking Active PC2. *J. Biol. Chem.* **273,** 3431–3437 (1998).

322. O'Rahilly, S., Gray, H., Humphreys, P. J., Krook, A., Polonsky, K. S., White, A., Gibson, S., Taylor, K. & Carr, C. Brief report: impaired processing of prohormones associated with abnormalities of glucose homeostasis and adrenal function. *N. Engl. J. Med.* **333,** 1386–1390 (1995).

323. Martín, M. G., Lindberg, I., Solorzano-Vargas, R. S., Wang, J., Avitzur, Y., Bandsma, R., Sokollik, C., Lawrence, S., Pickett, L. A., Chen, Z., Egritas, O., Dalgic, B., Albornoz, V., de Ridder, L., Hulst, J., Gok, F., Aydoğan, A., Al-Hussaini, A., Gok, D. E., Yourshaw, M., Wu, S. V., Cortina, G., Stanford, S. & Georgia, S. Congenital proprotein convertase 1/3 deficiency causes malabsorptive diarrhea and other endocrinopathies in a pediatric cohort. *Gastroenterology* **145,** 138–148 (2013).

324. Burnett, L. C., LeDuc, C. A., Sulsona, C. R., Paull, D., Rausch, R., Eddiry, S., Carli, J. F. M., Morabito, M. V., Skowronski, A. A., Hubner, G., Zimmer, M., Wang, L., Day, R., Levy, B., Fennoy, I., Dubern, B., Poitou, C., Clement, K., Butler, M. G., Rosenbaum, M., Salles, J. P., Tauber, M., Driscoll, D. J., Egli, D. & Leibel, R. L. Deficiency in prohormone convertase PC1 impairs prohormone processing in Prader-Willi syndrome. *J. Clin. Invest.* **127,** 293–305 (2017).

325. Angulo, M. A., Butler, M. G. & Cataletto, M. E. Prader-Willi syndrome: a review of clinical, genetic, and endocrine findings. *J. Endocrinol. Invest.* **38,** 1249–1263 (2015).

326. Revers, R. R., Henry, R., Schmeiser, L., Kolterman, O., Cohen, R., Bergenstal, R., Polonsky, K., Jaspan, J., Rubenstein, A. & Frank, B. The effects of biosynthetic human proinsulin on carbohydrate metabolism. *Diabetes* **33,** 762–770 (1984).

327. Yu, S. S. & Kitbachi, A. E. Biological activity of proinsulin and related polypeptides in the fat tissue. *J. Biol. Chem.* **248,** 3753–3761 (1973).

328. Ahlqvist, E., Turrini, F., Lang, S. T., Taneera, J., Zhou, Y., Almgren, P., Hansson, O., Isomaa, B., Tuomi, T., Eriksson, K., Eriksson, J. G., Lyssenko, V. & Groop, L. A common variant upstream of the PAX6 gene influences islet function in man. *Diabetologia* **55,** 94–104 (2012).

329. Ugleholdt, R., Zhu, X., Deacon, C. F., Ørskov, C., Steiner, D. F. & Holst, J. J. Impaired Intestinal Proglucagon Processing in Mice Lacking Prohormone Convertase 1. *Endocrinology* **145,** 1349–1355 (2004).

330. Ugleholdt, R., Poulsen, M.-L. H., Holst, P. J., Irminger, J.-C., Orskov, C., Pedersen, J., Rosenkilde, M. M., Zhu, X., Steiner, D. F. & Holst, J. J. Prohormone Convertase 1/3 Is Essential for Processing of the Glucose-dependent Insulinotropic Polypeptide Precursor. *J. Biol. Chem.* **281,** 11050–11057 (2006).

331. Yoshida, H., Ohagi, S., Sanke, T., Furuta, H., Furuta, M. & Nanjo, K. Association of the prohormone convertase 2 gene (PCSK2) on chromosome 20 with NIDDM in Japanese subjects. *Diabetes* **44,** 389–393 (1995).

332. Winters, A., Ramos-Molina, B., Jarvela, T. S., Yerges-Armstrong, L., Pollin, T. & Lindberg, I. Functional analysis of PCSK2 coding variants: a founder effect in the Old Order Amish population. *Diabetes Res. Clin. Pract.* **131,** 82–90 (2017).

333. Type 2 Diabetes Knowledge Portal. at <t2d.hugeamp.org>

334. Webb, G. C., Akbar, M. S., Zhao, C., Swift, H. H. & Steiner, D. F. Glucagon Replacement via Micro-Osmotic Pump Corrects Hypoglycemia and α-Cell Hyperplasia in Prohormone Convertase 2 Knockout Mice. *Diabetes* **51,** 398–405 (2002).

335. Jackson, R. S., Creemers, J. W. M., Ohagi, S., Raffin-Sanson, M.-L., Sanders, L., Montague, C. T., Hutton, J. C. & O'Rahilly, S. Obesity and impaired prohormone processing associated with mutations in the human prohormone convertase 1 gene. *Nat. Genet.* **16,** 303–306 (1997).

336. Frank, G. R., Fox, J., Candela, N., Jovanovic, Z., Bochukova, E., Levine, J., Papenhausen, P. R., O'Rahilly, S. & Farooqi, I. S. Severe obesity and diabetes insipidus in a patient with PCSK1 deficiency. *Mol. Genet. Metab.* **110,** 191–194 (2013).

337. Benzinou, M., Creemers, J. W. M., Choquet, H., Lobbens, S., Dina, C., Durand, E., Guerardel, A., Boutin, P., Jouret, B., Heude, B., Balkau, B., Tichet, J., Marre, M., Potoczna, N., Horber, F., Le Stunff, C., Czernichow, S., Sandbaek, A., Lauritzen, T., Borch-Johnsen, K., Andersen, G., Kiess, W., Körner, A., Kovacs, P., Jacobson, P., Carlsson, L. M. S., Walley, A. J., Jørgensen, T., Hansen, T., Pedersen, O., Meyre, D. & Froguel, P. Common nonsynonymous variants in PCSK1 confer risk of obesity. *Nat. Genet.* **40,** 943–945

338. Heni, M., Haupt, A., Schäfer, S. A., Ketterer, C., Thamer, C., Machicao, F., Stefan, N., Staiger, H., Häring, H.-U. & Fritsche, A. Association of obesity risk SNPs in PCSK1with insulin sensitivity and proinsulin conversion. *BMC Med. Genet.* **11,** 86 (2010).

339. Stijnen, P., Tuand, K., Varga, T. V., Franks, P. W., Aertgeerts, B. & Creemers, J. W. M. The association of common variants in PCSK1 with obesity: a HuGE review and meta-analysis. *Am. J. Epidemiol.* **180,** 1051–1065 (2014).

340. Nead, K. T., Li, A., Wehner, M. R., Neupane, B., Gustafsson, S., Butterworth, A., Engert, J. C., Davis, A. D., Hegele, R. A., Miller, R., den Hoed, M., Khaw, K.-T., Kilpeläinen, T. O., Wareham, N., Edwards, T. L., Hallmans, G., Varga, T. V., Kardia, S. L. R., Smith, J. A., Zhao, W., Faul, J. D., Weir, D., Mi, J., Xi, B., Quinteros, S. C., Cooper, C., Sayer, A. A., Jameson, K., Grøntved, A., Fornage, M., Sidney, S., Hanis, C. L., Highland, H. M., Häring, H.-U., Heni, M., Lasky-Su, J., Weiss, S. T., Gerhard, G. S., Still, C., Melka, M. M., Pausova, Z., Paus, T., Grant, S. F. A., Hakonarson, H., Price, R. A., Wang, K., Scherag, A., Hebebrand, J., Hinney, A., BioBank Japan, AGEN-BMI, GIANT Consortium, Franks, P.

W., Frayling, T. M., McCarthy, M. I., Hirschhorn, J. N., Loos, R. J., Ingelsson, E., Gerstein, H. C., Yusuf, S., Beyene, J., Anand, S. S. & Meyre, D. Contribution of common non-synonymous variants in PCSK1 to body mass index variation and risk of obesity: a systematic review and meta-analysis with evidence from up to 331 175 individuals. *Hum. Mol. Genet.* **24,** 3582–3594 (2015).

341. Strawbridge, R. J., Dupuis, J., Prokopenko, I., Barker, A., Ahlqvist, E., Rybin, D., Petrie, J. R., Travers, M. E., Bouatia-Naji, N., Dimas, A. S., Nica, A., Wheeler, E., Chen, H., Voight, B. F., Taneera, J., Kanoni, S., Peden, J. F., Turrini, F., Gustafsson, S., Zabena, C., Almgren, P., Barker, D. J. P., Barnes, D., Dennison, E. M., Eriksson, J. G., Eriksson, P., Eury, E., Folkersen, L., Fox, C. S., Frayling, T. M., Goel, A., Gu, H. F., Horikoshi, M., Isomaa, B., Jackson, A. U., Jameson, K. A., Kajantie, E., Kerr-Conte, J., Kuulasmaa, T., Kuusisto, J., Loos, R. J. F., Luan, J., Makrilakis, K., Manning, A. K., Martínez-Larrad, M. T., Narisu, N., Nastase Mannila, M., Ohrvik, J., Osmond, C., Pascoe, L., Payne, F., Sayer, A. A., Sennblad, B., Silveira, A., Stancáková, A., Stirrups, K., Swift, A. J., Syvänen, A.-C., Tuomi, T., van ’t Hooft, F. M., Walker, M., Weedon, M. N., Xie, W., Zethelius, B., DIAGRAM Consortium, GIANT Consortium, MuTHER Consortium, CARDIoGRAM Consortium, C4D Consortium, Ongen, H., Mälarstig, A., Hopewell, J. C., Saleheen, D., Chambers, J., Parish, S., Danesh, J., Kooner, J., Ostenson, C.-G., Lind, L., Cooper, C. C., Serrano-Ríos, M., Ferrannini, E., Forsen, T. J., Clarke, R., Franzosi, M. G., Seedorf, U., Watkins, H., Froguel, P., Johnson, P., Deloukas, P., Collins, F. S., Laakso, M., Dermitzakis, E. T., Boehnke, M., McCarthy, M. I., Wareham, N. J., Groop, L., Pattou, F., Gloyn, A. L., Dedoussis, G. V., Lyssenko, V., Meigs, J. B., Barroso, I., Watanabe, R. M., Ingelsson, E., Langenberg, C., Hamsten, A. & Florez, J. C. Genome-wide association identifies nine

common variants associated with fasting proinsulin levels and provides new insights into the pathophysiology of type 2 diabetes. *Diabetes* **60,** 2624–2634 (2011).

342. Leak, T. S., Keene, K. L., Langefeld, C. D., Gallagher, C. J., Mychaleckyj, J. C., Freedman, B. I., Bowden, D. W., Rich, S. S. & Sale, M. M. Association of the proprotein convertase subtilisin/kexin-type 2 (PCSK2) gene with type 2 diabetes in an African American population. *Mol. Genet. Metab.* **92,** 145–150 (2007).
343. Jonsson, A., Isomaa, B., Tuomi, T., Eriksson, J. G., Groop, L. & Lyssenko, V. Effect of a common variant of the PCSK2 gene on reduced insulin secretion. *Diabetologia* **55,** 3245–3251 (2012).
344. Chang, T.-J., Chiu, Y.-F., Sheu, W. H.-H., Shih, K.-C., Hwu, C.-M., Quertermous, T., Jou, Y.-S., Kuo, S.-S., Chang, Y.-C. & Chuang, L.-M. Genetic polymorphisms of PCSK2 are associated with glucose homeostasis and progression to type 2 diabetes in a Chinese population. *Sci. Rep.* **5,** 14380 (2015).
345. Zhu, X., Zhou, A., Dey, A., Norrbom, C., Carroll, R., Zhang, C., Laurent, V., Lindberg, I., Ugleholdt, R., Holst, J. J. & Steiner, D. F. Disruption of PC1/3 expression in mice causes dwarfism and multiple neuroendocrine peptide processing defects. *Proc. Natl. Acad. Sci. U. S. A.* **99,** 10293–10298 (2002).
346. Lloyd, D. J., Bohan, S. & Gekakis, N. Obesity, hyperphagia and increased metabolic efficiency in Pc1 mutant mice. *Hum. Mol. Genet.* **15,** 1884–1893 (2006).
347. Stijnen, P., Brouwers, B., Dirkx, E., Ramos-Molina, B., Van Lommel, L., Schuit, F., Thorrez, L., Declercq, J. & Creemers, J. W. M. Endoplasmic reticulum-associated degradation of the mouse PC1/3-N222D hypomorph and human PCSK1 mutations contributes to obesity. *Int. J. Obes.* **40,** 973–981 (2016).

348. Muhsin, N. I. A., Bentley, L., Bai, Y., Goldsworthy, M. & Cox, R. D. A novel mutation in the mouse Pcsk1 gene showing obesity and diabetes. *Mamm. Genome* **31,** 17–29 (2020).

349. Furuta, M., Yano, H., Zhou, A., Rouillé, Y., Holst, J. J., Carroll, R., Ravazzola, M., Orci, L., Furuta, H. & Steiner, D. F. Defective prohormone processing and altered pancreatic islet morphology in mice lacking active SPC2. *Proc. Natl. Acad. Sci.* **94,** 6646–6651 (1997).

350. Fox, D. L. & Good, D. J. Nescient Helix-Loop-Helix 2 Interacts with Signal Transducer and Activator of Transcription 3 to Regulate Transcription of Prohormone Convertase 1/3. *Mol. Endocrinol.* **22,** 1438–1448 (2008).

351. Gosmain, Y., Katz, L. S., Masson, M. H., Cheyssac, C., Poisson, C. & Philippe, J. Pax6 Is Crucial for β-Cell Function, Insulin Biosynthesis, and Glucose-Induced Insulin Secretion. *Mol. Endocrinol.* **26,** 696–709 (2012).

352. Wen, J. H., Chen, Y. Y., Song, S. J., Ding, J., Gao, Y., Hu, Q. K., Feng, R. P., Liu, Y. Z., Ren, G. C., Zhang, C. Y., Hong, T. P., Gao, X. & Li, L. S. Paired box 6 (PAX6) regulates glucose metabolism via proinsulin processing mediated by prohormone convertase 1/3 (PC1/3). *Diabetologia* **52,** 504–513 (2009).

353. Swisa, A., Avrahami, D., Eden, N., Zhang, J., Feleke, E., Dahan, T., Cohen-Tayar, Y., Stolovich-Rain, M., Kaestner, K. H., Glaser, B., Ashery-Padan, R. & Dor, Y. PAX6 maintains **β** cell identity by repressing genes of alternative islet cell types. *J. Clin. Invest.* **127,** 230–243 (2017).

354. Wang, H., Brun, T., Kataoka, K., Sharma, A. J. & Wollheim, C. B. MAFA controls genes implicated in insulin biosynthesis and secretion. *Diabetologia* **50,** 348–358 (2007).

355. Katz, L. S., Gosmain, Y., Marthinet, E. & Philippe, J. Pax6 Regulates the Proglucagon Processing Enzyme PC2 and Its Chaperone 7B2. *Mol. Cell. Biol.* **29,** 2322–2334 (2009).

356. Jing, E., Nillni, E. A., Sanchez, V. C., Stuart, R. C. & Good, D. J. Deletion of the Nhlh2 Transcription Factor Decreases the Levels of the Anorexigenic Peptides α Melanocyte-Stimulating Hormone and Thyrotropin-Releasing Hormone and Implicates Prohormone Convertases I and II in Obesity. *Endocrinology* **145,** 1503–1513 (2004).

357. Stijnen, P., Ramos-Molina, B., O'Rahilly, S. & Creemers, J. W. M. PCSK1 Mutations and Human Endocrinopathies: From Obesity to Gastrointestinal Disorders. *Endocr. Rev.* **37,** 347–371 (2016).

358. Benjannet, S., Rondeau, N., Paquet, L., Boudreault, A., Lazure, C., Chrétien, M. & Seidah, N. G. Comparative biosynthesis, covalent post-translational modifications and efficiency of prosegment cleavage of the prohormone convertases PC1 and PC2: glycosylation, sulphation and identification of the intracellular site of prosegment cleavage of PC1 and PC2. *Biochem. J.* **294,** 735–743 (1993).

359. Garcia-Ocaña, A. Glucose Mediated Regulation of Beta Cell Proliferation. *Open Endocrinol. J.* **4,** 55–65 (2010).

360. Kim-Muller, J. Y., Fan, J., Kim, Y. J. R., Lee, S.-A., Ishida, E., Blaner, W. S. & Accili, D. Aldehyde dehydrogenase 1a3 defines a subset of failing pancreatic β cells in diabetic mice. *Nat. Commun.* **7,** 12631 (2016).

361. Bone, R. N., Oyebamiji, O., Talware, S., Selvaraj, S., Krishnan, P., Syed, F., Wu, H. & Evans-Molina, C. A Computational Approach for Defining a Signature of β-Cell Golgi Stress in Diabetes. *Diabetes* **69,** 2364–2376 (2020).

362. Omar, B., Pacini, G. & Ahrén, B. Differential Development of Glucose Intolerance and Pancreatic Islet Adaptation in Multiple Diet Induced Obesity Models. *Nutrients* **4,** 1367–1381 (2012).

363. Xu, B., Allard, C., Alvarez-Mercado, A. I., Fuselier, T., Kim, J. H., Coons, L. A., Hewitt, S. C., Urano, F., Korach, K. S., Levin, E. R., Arvan, P., Floyd, Z. E. & Mauvais-Jarvis, F. Estrogens Promote Misfolded Proinsulin Degradation to Protect Insulin Production and Delay Diabetes. *Cell Rep.* **24,** 181–196 (2018).

364. Minn, A. H., Hafele, C. & Shalev, A. Thioredoxin-interacting protein is stimulated by glucose through a carbohydrate response element and induces beta-cell apoptosis. *Endocrinology* **146,** 2397–2405 (2005).

365. Yanagisawa, H., Miyashita, T., Nakano, Y. & Yamamoto, D. HSpin1, a transmembrane protein interacting with Bcl-2/Bcl-xL, induces a caspase-independent autophagic cell death. *Cell Death Differ.* **10,** 798–807 (2003).

366. Kao, C.-J., Chiang, Y.-J., Chen, P.-H., Lin, K.-R., Hwang, P.-I., Yang-Yen, H.-F. & Yen, J. J.-Y. CBAP interacts with the un-liganded common β-subunit of the GM-CSF/IL-3/IL-5 receptor and induces apoptosis via mitochondrial dysfunction. *Oncogene* **27,** 1397–1403 (2008).

367. Rondas, D., Tomas, A. & Halban, P. A. Focal Adhesion Remodeling Is Crucial for Glucose-Stimulated Insulin Secretion and Involves Activation of Focal Adhesion Kinase and Paxillin. *Diabetes* **60,** 1146–1157 (2011).

368. Yeo, R. W. Y., Yang, K., Li, G. & Lim, S. K. High Glucose Predisposes Gene Expression and ERK Phosphorylation to Apoptosis and Impaired Glucose-Stimulated Insulin Secretion via the Cytoskeleton. *PLOS ONE* **7,** e44988 (2012).

369. Arous, C. & Halban, P. A. The skeleton in the closet: actin cytoskeletal remodeling in β-cell function. *Am. J. Physiol. Endocrinol. Metab.* **309,** E611-620 (2015).

370. Kalwat, M. A. & Thurmond, D. C. Signaling mechanisms of glucose-induced F-actin remodeling in pancreatic islet β cells. *Exp. Mol. Med.* **45,** e37 (2013).

371. Wang, Y., Thiele1, C. & Huttner, W. B. Cholesterol is Required for the Formation of Regulated and Constitutive Secretory Vesicles from the trans-Golgi Network. *Traffic* **1,** 952–962 (2000).

372. Kruit, J. K., Wijesekara, N., Fox, J. E. M., Dai, X.-Q., Brunham, L. R., Searle, G. J., Morgan, G. P., Costin, A. J., Tang, R., Bhattacharjee, A., Johnson, J. D., Light, P. E., Marsh, B. J., Macdonald, P. E., Verchere, C. B. & Hayden, M. R. Islet cholesterol accumulation due to loss of ABCA1 leads to impaired exocytosis of insulin granules. *Diabetes* **60,** 3186–3196 (2011).

373. Cinti, F., Bouchi, R., Kim-Muller, J. Y., Ohmura, Y., Sandoval, P. R., Masini, M., Marselli, L., Suleiman, M., Ratner, L. E., Marchetti, P. & Accili, D. Evidence of β-Cell Dedifferentiation in Human Type 2 Diabetes. *J. Clin. Endocrinol. Metab.* **101,** 1044–1054 (2016).

374. Hunter, C. S. & Stein, R. W. Evidence for Loss in Identity, De-Differentiation, and Trans-Differentiation of Islet β-Cells in Type 2 Diabetes. *Front. Genet.* **8,** 35 (2017).

375. Salinno, Cota, Bastidas-Ponce, Tarquis-Medina, Lickert, & Bakhti. β-Cell Maturation and Identity in Health and Disease. *Int. J. Mol. Sci.* **20,** 5417 (2019).

376. Krentz, N. A. J., Lee, M. Y. Y., Xu, E. E., Sproul, S. L. J., Maslova, A., Sasaki, S. & Lynn, F. C. Single-Cell Transcriptome Profiling of Mouse and hESC-Derived Pancreatic Progenitors. *Stem Cell Rep.* **11,** 1551–1564 (2018).

377. Nishimura, W., Takahashi, S. & Yasuda, K. MafA is critical for maintenance of the mature beta cell phenotype in mice. *Diabetologia* **58,** 566–574 (2015).

378. Hang, Y. & Stein, R. MafA and MafB activity in pancreatic β cells. *Trends Endocrinol. Metab. TEM* **22,** 364–373 (2011).

379. Talchai, C., Xuan, S., Lin, H. V., Sussel, L. & Accili, D. Pancreatic β Cell Dedifferentiation as a Mechanism of Diabetic β Cell Failure. *Cell* **150,** 1223–1234 (2012).

380. Blum, B., Hrvatin, S., Schutz, C., Bonal, C., Rezaniaand, A. & Melton, D. A. Functional β-cells maturation is marked by an increase in the glucose threshold for insulin secretion and by expression of urocortin3. *Nat. Biotechnol.* **30,** 261–264 (2012).

381. Puri, S., Roy, N., Russ, H. A., Leonhardt, L., French, E. K., Roy, R., Bengtsson, H., Scott, D. K., Stewart, A. F. & Hebrok, M. Replication confers β cell immaturity. *Nat. Commun.* **9,** 485 (2018).

382. Kitamura, Y. I., Kitamura, T., Kruse, J.-P., Raum, J. C., Stein, R., Gu, W. & Accili, D. FoxO1 protects against pancreatic β cell failure through NeuroD and MafA induction. *Cell Metab.* **2,** 153–163 (2005).

383. Johnson, J. H., Newgard, C. B., Milburn, J. L., Lodish, H. F. & Thorens, B. The high Km glucose transporter of islets of Langerhans is functionally similar to the low affinity transporter of liver and has an identical primary sequence. *J. Biol. Chem.* **265,** 6548–6551 (1990).

384. Kailey, B., van de Bunt, M., Cheley, S., Johnson, P. R., MacDonald, P. E., Gloyn, A. L., Rorsman, P. & Braun, M. SSTR2 is the functionally dominant somatostatin receptor in human pancreatic β- and α-cells. *Am. J. Physiol. - Endocrinol. Metab.* **303,** E1107–E1116 (2012).

385. Renström, E., Ding, W.-G., Bokvist, K. & Rorsman, P. Neurotransmitter-Induced Inhibition of Exocytosis in Insulin-Secreting β Cells by Activation of Calcineurin. *Neuron* **17,** 513–522 (1996).

386. Cooper, G. J., Willis, A. C., Clark, A., Turner, R. C., Sim, R. B. & Reid, K. B. Purification and characterization of a peptide from amyloid-rich pancreases of type 2 diabetic patients. *Proc. Natl. Acad. Sci. U. S. A.* **84,** 8628–8632 (1987).

387. Opie, E. L. The Relation of Diabetes Mellitus to Lesions of the Pancreas. Hyaline Degeneration of the Islands of Langerhans. *J. Exp. Med.* **5,** 527–540 (1901).

388. Weichselbaum, A. & Stangl, E. Zur Kenntnis der feineren Veränderungen des Pankreas bei Diabetes mellitus. *Wien. Klin. Wochenschr.* **14,** 968–972 (1901).

389. Hull, R. L., Westermark, G. T., Westermark, P. & Kahn, S. E. Islet Amyloid: A Critical Entity in the Pathogenesis of Type 2 Diabetes. *J. Clin. Endocrinol. Metab.* **89,** 3629–3643 (2004).

390. Kahn, S. E., Templin, A. T., Hull, R. L. & Verchere, C. B. Probing the Meaning of Persistent Propeptide Release in Type 1 Diabetes. *Diabetes Care* **42,** 183–185 (2019).

391. Masters, S. L., Dunne, A., Subramanian, S. L., Hull, R. L., Tannahill, G. M., Sharp, F. A., Becker, C., Franchi, L., Yoshihara, E., Chen, Z., Mullooly, N., Mielke, L. A., Harris, J., Coll, R. C., Mills, K. H. G., Mok, K. H., Newsholme, P., Nuñez, G., Yodoi, J., Kahn, S. E., Lavelle, E. C. & O'Neill, L. A. J. Activation of the NLRP3 inflammasome by islet amyloid polypeptide provides a mechanism for enhanced IL-1β in type 2 diabetes. *Nat. Immunol.* **11,** 897–904 (2010).

392. Westwell-Roper, C., Dai, D. L., Soukhatcheva, G., Potter, K. J., Rooijen, N. van, Ehses, J. A. & Verchere, C. B. IL-1 Blockade Attenuates Islet Amyloid Polypeptide-Induced

Proinflammatory Cytokine Release and Pancreatic Islet Graft Dysfunction. *J. Immunol.* **187,** 2755–2765 (2011).

393. Westwell-Roper, C. Y., Ehses, J. A. & Verchere, C. B. Resident Macrophages Mediate Islet Amyloid Polypeptide–Induced Islet IL-1β Production and β-Cell Dysfunction. *Diabetes* **63,** 1698–1711 (2014).

394. Knight, J. D., Hebda, J. A. & Miranker, A. D. Conserved and Cooperative Assembly of Membrane-Bound α-Helical States of Islet Amyloid Polypeptide. *Biochemistry* **45,** 9496–9508 (2006).

395. Engel, M. F. M., Khemtemourian, L., Kleijer, C. C., Meeldijk, H. J. D., Jacobs, J., Verkleij, A. J., de Kruijff, B., Killian, J. A. & Hoppener, J. W. M. Membrane damage by human islet amyloid polypeptide through fibril growth at the membrane. *Proc. Natl. Acad. Sci.* **105,** 6033–6038 (2008).

396. Abedini, A., Plesner, A., Cao, P., Ridgway, Z., Zhang, J., Tu, L.-H., Middleton, C. T., Chao, B., Sartori, D. J., Meng, F., Wang, H., Wong, A. G., Zanni, M. T., Verchere, C. B., Raleigh, D. P. & Schmidt, A. M. Time-resolved studies define the nature of toxic IAPP intermediates, providing insight for anti-amyloidosis therapeutics. *eLife* **5,** e12977 (2016).

397. Janson, J., Ashley, R. H., Harrison, D., McIntyre, S. & Butler, P. C. The mechanism of islet amyloid polypeptide toxicity is membrane disruption by intermediate-sized toxic amyloid particles. *Diabetes* **48,** 491–498 (1999).

398. Casas, S., Novials, A., Reimann, F., Gomis, R. & Gribble, F. M. Calcium elevation in mouse pancreatic beta cells evoked by extracellular human islet amyloid polypeptide involves activation of the mechanosensitive ion channel TRPV4. *Diabetologia* **51,** 2252–2262 (2008).

399. Zraika, S., Hull, R. L., Verchere, C. B., Clark, A., Potter, K. J., Fraser, P. E., Raleigh, D. P. & Kahn, S. E. Toxic oligomers and islet beta cell death: guilty by association or convicted by circumstantial evidence? *Diabetologia* **53,** 1046–1056 (2010).

400. Ridgway, Z., Lee, K.-H., Zhyvoloup, A., Wong, A., Eldrid, C., Hannaberry, E., Thalassinos, K., Abedini, A. & Raleigh, D. P. Analysis of Baboon IAPP Provides Insight into Amyloidogenicity and Cytotoxicity of Human IAPP. *Biophys. J.* **118,** 1142–1151 (2020).

401. Howard, C. F. Longitudinal studies on the development of diabetes in individual Macaca nigra. *Diabetologia* **29,** 301–306 (1986).

402. Westermark, P., Eizirik, D. L., Pipeleers, D. G., Hellerström, C. & Andersson, A. Rapid deposition of amyloid in human islets transplanted into nude mice. *Diabetologia* **38,** 543–549 (1995).

403. Westermark, G. T., Westermark, P., Berne, C. & Korsgren, O. Widespread Amyloid Deposition in Transplanted Human Pancreatic Islets. *N. Engl. J. Med.* **359,** 977–979 (2008).

404. Van Hulle, F., De Groot, K., Stangé, G., Suenens, K., De Mesmaeker, I., De Paep, D. L., Ling, Z., Hilbrands, R., Gillard, P., Keymeulen, B., Kroon, E., Westermark, G. T., Jacobs-Tulleneers-Thevissen, D. & Pipeleers, D. Formation of amyloid in encapsulated human pancreatic and human stem cell-generated beta cell implants. *Am. J. Transplant.* **21,** 2090–2099 (2021).

405. Höppener, J. W. M., Verbeek, J. S., de Koning, E. J. P., Oosterwijk, C., van Hulst, K. L., Visser-Vernooy, H. J., Hofhuis, F. M. A., van Gaalen, S., Berends, M. J. H., Hackeng, W. H. L., Jansz, H. S., Morris, J. F., Clark, A., Capel, P. J. A. & Lips, C. J. M. Chronic overproduction of islet amyloid polypeptide/amylin in transgenic mice: lysosomal

localization of human islet amyloid polypeptide and lack of marked hyperglycaemia or hyperinsulinaemia. *Diabetologia* **36,** 1258–1265 (1993).

406. D'Alessio, D. A., Verchere, C. B., Kahn, S. E., Hoagland, V., Baskin, D. G., Palmiter, R. D. & Ensinck, J. W. Pancreatic Expression and Secretion of Human Islet Amyloid Polypeptide in a Transgenic Mouse. *Diabetes* **43,** 1457–1461 (1994).
407. Fox, N., Schrementi, J., Nishi, M., Ohagi, S., Chan, S. J., Heisserman, J. A., Westermark, G. T., Leckström, A., Westermark, P. & Steiner, D. F. Human islet amyloid polypeptide transgenic mice as a model of non-insulin-dependent diabetes mellitus (NIDDM). *FEBS Lett.* **323,** 40–44 (1993).
408. Yagui, K., Yamaguchi, T., Kanatsuka, A., Shimada, F., Huang, C. I., Tokuyama, Y., Ohsawa, H., Yamamura, K., Miyazaki, J. & Mikata, A. Formation of islet amyloid fibrils in beta-secretory granules of transgenic mice expressing human islet amyloid polypeptide/amylin. *Eur. J. Endocrinol.* **132,** 487–496 (1995).
409. Koning, E. J. P. de, Höppener, J. W. M., Verbeek, J. S., Oosterwijk, C., Hulst, K. L. van, Baker, C. A., Lips, C. J. M., Morris, J. F. & Clark, A. Human Islet Amyloid Polypeptide Accumulates at Similar Sites in Islets of Transgenic Mice and Humans. *Diabetes* **43,** 640–644 (1994).
410. Verchere, C. B., D'Alessio, D. A., Palmiter, R. D., Weir, G. C., Bonner-Weir, S., Baskin, D. G. & Kahn, S. E. Islet amyloid formation associated with hyperglycemia in transgenic mice with pancreatic beta cell expression of human islet amyloid polypeptide. *Proc. Natl. Acad. Sci. U. S. A.* **93,** 3492–3496 (1996).

411. Soeller, W. C., Janson, J., Hart, S. E., Parker, J. C., Carty, M. D., Stevenson, R. W., Kreutter, D. K. & Butler, P. C. Islet amyloid-associated diabetes in obese A(vy)/a mice expressing human islet amyloid polypeptide. *Diabetes* **47,** 743–750 (1998).

412. Höppener, J. W., Oosterwijk, C., Nieuwenhuis, M. G., Posthuma, G., Thijssen, J. H., Vroom, T. M., Ahrén, B. & Lips, C. J. Extensive islet amyloid formation is induced by development of Type II diabetes mellitus and contributes to its progression: pathogenesis of diabetes in a mouse model. *Diabetologia* **42,** 427–434 (1999).

413. Hull, R. L., Andrikopoulos, S., Verchere, C. B., Vidal, J., Wang, F., Cnop, M., Prigeon, R. L. & Kahn, S. E. Increased Dietary Fat Promotes Islet Amyloid Formation and β-Cell Secretory Dysfunction in a Transgenic Mouse Model of Islet Amyloid. *Diabetes* **52,** 372–379 (2003).

414. Hull, R. L., Shen, Z.-P., Watts, M. R., Kodama, K., Carr, D. B., Utzschneider, K. M., Zraika, S., Wang, F. & Kahn, S. E. Long-term treatment with rosiglitazone and metformin reduces the extent of, but does not prevent, islet amyloid deposition in mice expressing the gene for human islet amyloid polypeptide. *Diabetes* **54,** 2235–2244 (2005).

415. Hiddinga, H. J., Sakagashira, S., Ishigame, M., Madde, P., Sanke, T., Nanjo, K., Kudva, Y. C., Lee, J. J., van Deursen, J. & Eberhardt, N. L. Expression of wild-type and mutant S20G hIAPP in physiologic knock-in mouse models fails to induce islet amyloid formation, but induces mild glucose intolerance. *J. Diabetes Investig.* **3,** 138–147 (2012).

416. Potter, K. J., Scrocchi, L. A., Warnock, G. L., Ao, Z., Younker, M. A., Rosenberg, L., Lipsett, M., Verchere, C. B. & Fraser, P. E. Amyloid inhibitors enhance survival of cultured human islets. *Biochim. Biophys. Acta* **1790,** 566–574 (2009).

417. Marzban, L., Tomas, A., Becker, T. C., Rosenberg, L., Oberholzer, J., Fraser, P. E., Halban, P. A. & Verchere, C. B. Small interfering RNA-mediated suppression of proislet amyloid polypeptide expression inhibits islet amyloid formation and enhances survival of human islets in culture. *Diabetes* **57,** 3045–3055 (2008).

418. Huang, C., Haataja, L., Gurlo, T., Butler, A. E., Wu, X., Soeller, W. C. & Butler, P. C. Induction of endoplasmic reticulum stress-induced β-cell apoptosis and accumulation of polyubiquitinated proteins by human islet amyloid polypeptide. *Am. J. Physiol.-Endocrinol. Metab.* **293,** E1656–E1662 (2007).

419. Hull, R. L., Zraika, S., Udayasankar, J., Aston-Mourney, K., Subramanian, S. L. & Kahn, S. E. Amyloid formation in human IAPP transgenic mouse islets and pancreas, and human pancreas, is not associated with endoplasmic reticulum stress. *Diabetologia* **52,** 1102–1111 (2009).

420. Montane, J., de Pablo, S., Obach, M., Cadavez, L., Castaño, C., Alcarraz-Vizán, G., Visa, M., Rodríguez-Comas, J., Parrizas, M., Servitja, J. M. & Novials, A. Protein disulfide isomerase ameliorates β-cell dysfunction in pancreatic islets overexpressing human islet amyloid polypeptide. *Mol. Cell. Endocrinol.* **420,** 57–65 (2016).

421. Westwell-Roper, C., Denroche, H. C., Ehses, J. A. & Verchere, C. B. Differential Activation of Innate Immune Pathways by Distinct Islet Amyloid Polypeptide (IAPP) Aggregates. *J. Biol. Chem.* **291,** 8908–8917 (2016).

422. Templin, A. T., Mellati, M., Meier, D. T., Esser, N., Hogan, M. F., Castillo, J. J., Akter, R., Raleigh, D. P., Zraika, S., Hull, R. L. & Kahn, S. E. Low concentration IL-1β promotes islet amyloid formation by increasing hIAPP release from humanised mouse islets in vitro. *Diabetologia* **63,** 2385–2395 (2020).

423. Badman, M. K., Pryce, R. A., Chargé, S. B., Morris, J. F. & Clark, A. Fibrillar islet amyloid polypeptide (amylin) is internalised by macrophages but resists proteolytic degradation. *Cell Tissue Res.* **291,** 285–294 (1998).

424. Westwell-Roper, C. Y., Chehroudi, C. A., Denroche, H. C., Courtade, J. A., Ehses, J. A. & Verchere, C. B. IL-1 mediates amyloid-associated islet dysfunction and inflammation in human islet amyloid polypeptide transgenic mice. *Diabetologia* **58,** 575–585 (2015).

425. Ma, Z. & Westermark, G. T. Effects of free fatty acid on polymerization of islet amyloid polypeptide (IAPP) in vitro and on amyloid fibril formation in cultivated isolated islets of transgenic mice overexpressing human IAPP. *Mol. Med.* **8,** 863–868 (2002).

426. Wijesekara, N., Kaur, A., Westwell-Roper, C., Nackiewicz, D., Soukhatcheva, G., Hayden, M. R. & Verchere, C. B. ABCA1 deficiency and cellular cholesterol accumulation increases islet amyloidogenesis in mice. *Diabetologia* **59,** 1242–1246 (2016).

427. Sciacca, M. F. M., Lolicato, F., Di Mauro, G., Milardi, D., D'Urso, L., Satriano, C., Ramamoorthy, A. & La Rosa, C. The Role of Cholesterol in Driving IAPP-Membrane Interactions. *Biophys. J.* **111,** 140–151 (2016).

428. Young, I. D., Ailles, L., Narindrasorasak, S., Tan, R. & Kisilevsky, R. Localization of the basement membrane heparan sulfate proteoglycan in islet amyloid deposits in type II diabetes mellitus. *Arch. Pathol. Lab. Med.* **116,** 951–954 (1992).

429. Meng, F., Abedini, A., Song, B. & Raleigh, D. P. Amyloid formation by pro-islet amyloid polypeptide processing intermediates: examination of the role of protein heparan sulfate interactions and implications for islet amyloid formation in type 2 diabetes. *Biochemistry* **46,** 12091–12099 (2007).

430. Park, K. & Verchere, C. B. Identification of a Heparin Binding Domain in the N-terminal Cleavage Site of Pro-islet Amyloid Polypeptide. *J. Biol. Chem.* **276,** 16611–16616 (2001).

431. Potter, K. J., Werner, I., Denroche, H. C., Montane, J., Plesner, A., Chen, Y., Lei, D., Soukhatcheva, G., Warnock, G. L., Oberholzer, J., Fraser, P. E. & Verchere, C. B. Amyloid Formation in Human Islets Is Enhanced by Heparin and Inhibited by Heparinase. *Am. J. Transplant.* **15,** 1519–1530 (2015).

432. Templin, A. T., Mellati, M., Soininen, R., Hogan, M. F., Esser, N., Castillo, J. J., Zraika, S., Kahn, S. E. & Hull, R. L. Loss of perlecan heparan sulfate glycosaminoglycans lowers body weight and decreases islet amyloid deposition in human islet amyloid polypeptide transgenic mice. *Protein Eng. Des. Sel.* **32,** 95–102 (2019).

433. Paulsson, J. F., Andersson, A., Westermark, P. & Westermark, G. T. Intracellular amyloid-like deposits contain unprocessed pro-islet amyloid polypeptide (proIAPP) in beta cells of transgenic mice overexpressing the gene for human IAPP and transplanted human islets. *Diabetologia* **49,** 1237–1246 (2006).

434. Westermark, G. T., Steiner, D. F., Gebre-Medhin, S., Engström, U. & Westermark, P. Pro islet amyloid polypeptide (ProIAPP) immunoreactivity in the islets of Langerhans. *Ups. J. Med. Sci.* **105,** 97–106 (2000).

435. Westermark, P., Engström, U., Westermark, G. T., Johnson, K. H., Permerth, J. & Betsholtz, C. Islet amyloid polypeptide (IAPP) and pro-IAPP immunoreactivity in human islets of Langerhans. *Diabetes Res. Clin. Pract.* **7,** 219–226 (1989).

436. Krampert, M., Bernhagen, J., Schmucker, J., Horn, A., Schmauder, A., Brunner, H., Voelter, W. & Kapurniotu, A. Amyloidogenicity of recombinant human pro-islet amyloid polypeptide (ProIAPP). *Chem. Biol.* **7,** 855–871 (2000).

437. Yonemoto, I. T., Kroon, G. J. A., Dyson, H. J., Balch, W. E. & Kelly, J. W. Amylin proprotein processing generates progressively more amyloidogenic peptides that initially sample the helical state. *Biochemistry* **47,** 9900–9910 (2008).

438. Khemtémourian, L., Lahoz Casarramona, G., Suylen, D. P. L., Hackeng, T. M., Meeldijk, J. D., de Kruijff, B., Höppener, J. W. M. & Killian, J. A. Impaired Processing of Human Pro-Islet Amyloid Polypeptide Is Not a Causative Factor for Fibril Formation or Membrane Damage in Vitro. *Biochemistry* **48,** 10918–10925 (2009).

439. Jha, S., Sellin, D., Seidel, R. & Winter, R. Amyloidogenic Propensities and Conformational Properties of ProIAPP and IAPP in the Presence of Lipid Bilayer Membranes. *J. Mol. Biol.* **389,** 907–920 (2009).

440. Knight, J. D. & Miranker, A. D. Phospholipid Catalysis of Diabetic Amyloid Assembly. *J. Mol. Biol.* **341,** 1175–1187 (2004).

441. Paulsson, J. F. & Westermark, G. T. Aberrant Processing of Human Proislet Amyloid Polypeptide Results in Increased Amyloid Formation. *Diabetes* **54,** 2117–2125 (2005).

442. Courtade, J. A., Wang, E. Y., Yen, P., Dai, D. L., Soukhatcheva, G., Orban, P. C. & Verchere, C. B. Loss of prohormone convertase 2 promotes beta cell dysfunction in a rodent transplant model expressing human pro-islet amyloid polypeptide. *Diabetologia* **60,** 453–463 (2017).

443. Westermark, P., Li, Z.-C., Westermark, G. T., Leckström, A. & Steiner, D. F. Effects of beta cell granule components on human islet amyloid polypeptide fibril formation. *FEBS Lett.* **379,** 203–206 (1996).

444. Jaikaran, E. T. A. S., Nilsson, M. R. & Clark, A. Pancreatic beta-cell granule peptides form heteromolecular complexes which inhibit islet amyloid polypeptide fibril formation. *Biochem. J.* **377,** 709–716 (2004).

445. Wang, F., Hull, R. L., Vidal, J., Cnop, M. & Kahn, S. E. Islet Amyloid Develops Diffusely Throughout the Pancreas Before Becoming Severe and Replacing Endocrine Cells. *Diabetes* **50,** 2514–2520 (2001).

446. Rivera, J. F., Gurlo, T., Daval, M., Huang, C. J., Matveyenko, A. V., Butler, P. C. & Costes, S. Human-IAPP disrupts the autophagy/lysosomal pathway in pancreatic β-cells: protective role of p62-positive cytoplasmic inclusions. *Cell Death Differ.* **18,** 415–426 (2011).

447. Shigihara, N., Fukunaka, A., Hara, A., Komiya, K., Honda, A., Uchida, T., Abe, H., Toyofuku, Y., Tamaki, M., Ogihara, T., Miyatsuka, T., Hiddinga, H. J., Sakagashira, S., Koike, M., Uchiyama, Y., Yoshimori, T., Eberhardt, N. L., Fujitani, Y. & Watada, H. Human IAPP–induced pancreatic β cell toxicity and its regulation by autophagy. *J. Clin. Invest.* **124,** 3634–3644 (2014).

448. Kim, J., Cheon, H., Jeong, Y. T., Quan, W., Kim, K. H., Cho, J. M., Lim, Y.-M., Oh, S. H., Jin, S.-M., Kim, J. H., Lee, M.-K., Kim, S., Komatsu, M., Kang, S.-W. & Lee, M.-S. Amyloidogenic peptide oligomer accumulation in autophagy-deficient β cells induces diabetes. *J. Clin. Invest.* **124,** 3311–3324 (2014).

449. Rivera, J. F., Costes, S., Gurlo, T., Glabe, C. G. & Butler, P. C. Autophagy defends pancreatic β cells from human islet amyloid polypeptide-induced toxicity. *J. Clin. Invest.* **124,** 3489–3500 (2014).

450. Kim, J., Park, K., Kim, M. J., Lim, H., Kim, K. H., Kim, S.-W., Lee, E.-S., Kim, H. (Henry), Kim, S. J., Hur, K. Y., Kim, J. H., Ahn, J. H., Yoon, K.-H., Kim, J.-W. & Lee, M.-

S. An autophagy enhancer ameliorates diabetes of human IAPP-transgenic mice through clearance of amyloidogenic oligomer. *Nat. Commun.* **12,** 183 (2021).

451. Barbetti, F., Colombo, C., Haataja, L., Cras-Méneur, C., Bernardini, S. & Arvan, P. Hyperglucagonemia in an animal model of insulin- deficient diabetes: what therapy can improve it? *Clin. Diabetes Endocrinol.* **2,** 11 (2016).
452. Michael, M. D., Kulkarni, R. N., Postic, C., Previs, S. F., Shulman, G. I., Magnuson, M. A. & Kahn, C. R. Loss of Insulin Signaling in Hepatocytes Leads to Severe Insulin Resistance and Progressive Hepatic Dysfunction. *Mol. Cell* **6,** 87–97 (2000).

Appendix: Mouse illness scoring chart for survival endpoint

Clinical Signs	Clinical Health Score					
	0	1	2	3*	4	5**
	(not actively monitored)	(begin active monitoring til resolved)				
Body Weight (Loss)	No loss	<5%	5-9%	10-14%	15-19%	≥20%
Attitude/Activity	BAR (Bright/alert/ responsive)	QAR (quiet/alert/ responsive)	Decreased activity and alertness or hyperactivity	Huddled, obvious activity decrease, vocalization when handled	inactive, shaking or increased aggression	Inactive, Non-responsive to handling,
Appearance	Normal	--	Mild piloerection (hair stands up slightly)	Noticeable/ moderate piloerection, (head/ shoulders), light jaundice	Moderate piloerection/ pale or cool extremities; easily noticeable jaundice	Marked piloerection (all over) or Pale/cold to touch; dark jaundice
Posture/Gait	Normal	Mild infrequent/ possible hunching	Mild persistent hunching	Moderate hunching,some limb weakness	Obvious hunching or head tilt, tip toe gait or obvious weakness	Severe hunching, immobile, falling over
Hydration	Normal	--	-	dehydration (dull eyes, slightly sunken)	Significant dehydration (sunken, pale eyes, skin tent -1s	Severe dehydration (obvious skin tent (>1-2sec), sunken/pale eyes and tail)
Breathing	Normal	--	mild increase in rate, normal effort	Rapid/ increased effort (chest expansion)	Laboured (obvious increase in effort)/ Irregular	Gasping or cyanosis
Tumor Scores	none	none	none	palpable tumor	palpable tumor	palpable tumor
Facial/Behavioural signs of Pain (score 1-occasional-2 persistent 3-severe) per category)	ears back	eyes squinted	nose bulge/whiskers tightened	vocalizations	flinching, twitching	writhing, pressing

* A score of 2 in any category or a cumulative score of 3 or higher results in increased monitoring, including: daily weighing, supportive care (e.g. supplemental heat, SQ fluids, additional analgesia, gel food or food treats/moistened pellets on cage floor)

** A score of 3 in any category, more than one score of 2 or a cumulative score of >6 after appropriate analgesia or supportive care requires immediate euthanasia or Veterinary consultation